Ultrasound Imaging Analysis for Diagnostics of Functional Muscle Status and Evaluation of Rehabilitation Techniques in Spinal Cord Injury (SCI)

Jennifer Miller

Submitted in fulfilment of the requirements for the
Degree of Doctor of Philosophy

School of Engineering
College of Science and Engineering
University of Glasgow

October 2020

Abstract

The spinal cord connects the brain and the rest of the body through the transmission of sensory and motor signals. A spinal cord injury (SCI) disrupts this flow of information, resulting in loss of sensation and muscle paralysis. Although the muscles are not directly affected, a lack of activation leads to structural changes in the weeks and even years after the injury has occurred. These changes include muscle atrophy, an increased accumulation of intramuscular fat, and a fibre type transformation that makes muscles more susceptible to fatigue. In order to assess muscle function to provide an accurate prognosis and monitor recovery, quantitative and sensitive assessment methods are required. Current methods have limited sensitivity and are not able to differentiate between different muscles or assess deep muscles.

Ultrasound imaging (USI) provides a potential additional tool to assess muscles. This non-invasive imaging technique uses the behaviour of sound waves travelling through tissue to allow internal structures such as muscles to be visualised. USI of skeletal muscle is a well-established technique, which can make accurate measurements of muscle size, and describe muscle activity through changes in architectural parameters. It has also been widely used as a screening tool in the diagnosis of neuromuscular disorders. In addition, USI could also improve understanding of muscle behaviour during the application of neuromuscular electrical stimulation (NMES), which is widely used in the rehabilitation of paralysed muscles. NMES uses low amplitude current to artificially generate a contraction, allowing exercise or functional movements to be achieved, however, it is limited by the early onset of muscle fatigue. The underlying mechanisms of fibre recruitment during NMES are unclear and USI has the potential to provide a greater insight.

The main aim of this PhD project is to investigate the suitability of USI as a diagnostic tool for assessing muscles following a spinal cord injury, by establishing if it can differentiate between measurements of structure at different times post-injury, and correlate measurements of muscle movement with different levels of muscle function. Its suitability to monitor recovery is also investigated by establishing if it can detect changes in these measurements at different times post-injury. A secondary aim of the project is to demonstrate the potential of USI to provide insight into muscle behaviour during the application of NMES.

The first study presented in this thesis involved recording USI videos of muscles in SCI patients and able-bodied controls under different conditions. USI videos of the muscle at rest provided measurements of muscle structure through the use of tracking software to measure the

thickness of the muscle, and greyscale analysis to measure echogenicity and echotexture. USI videos of the muscle during attempted voluntary contractions provided measurements of muscle movement. Tracking software was used to measure muscle deformation and regional displacement, which were compared between groups of SCI participants with different levels of muscle function. A simpler analysis method based on the changes in pixel intensity values, referred to throughout this thesis as the pixel difference method, was also compared to the results obtained from the tracking software. Recordings were repeated at monthly intervals for the SCI participants, allowing these measurements of structure and function to be compared over time for individual participants. USI videos were also recorded during the application of NMES, allowing measurements of muscle movement to be compared between healthy muscles and those affected by a SCI. The second study involved recording USI videos of muscles in the lower limbs of acute SCI participants during attempted isotonic contractions, and using the pixel difference method to detect very small muscle movements. The USI measurements were compared to the results of a manual muscle test (MMT), a physical exam performed by a trained physiotherapist. Finally, a further two studies are presented where USI videos were recorded in able-bodied participants during the application of NMES and measurements of muscle movement were compared between different conditions. The first of these studies compared changes in stimulation parameters, as well as time-varying patterns of these parameters; and the second investigated the effect of spatially distributed patterns of stimulation using a multi-electrode configuration.

USI measurements of muscle thickness, echogenicity and echotexture described changes in muscle structure after a SCI, and could differentiate between different times post-injury. USI measurements of muscle movement could also describe the functional status of muscles, with measurements of regional displacement found to be far more successful than measurements of deformation. Furthermore, the simpler pixel difference method provided similar results without the limitations of the tracking software. These measurements of muscle structure and function also showed changes over time for individual participants, highlighting the potential of USI to monitor recovery. The most successful results were seen in acute SCI patients, where the pixel difference method was able to detect very small muscle movements. Differences were also seen in USI measurements under different conditions of NMES, differentiating between different levels of stimulation intensity; different patterns of stimulation, as the result of variations in the stimulation parameters themselves and different spatially distributed patterns created through a multi-electrode configuration; finally, differences in muscle fibre recruitment and the amount of muscle movement produced during the application of NMES could be seen between healthy muscles and those affected by a SCI.

In conclusion, USI has been shown to be a useful tool for the assessment of muscle structure and function following a SCI, and for monitoring recovery. Furthermore, it can also provide greater insight into muscle behaviour during the application of NMES, demonstrating its potential for optimising its use in rehabilitation.

Acknowledgements

First and foremost, I would like to express my gratitude towards my supervisor Dr Henrik Gollee, for his mentorship throughout this project. His continuous guidance and support were not only vital to the completion of this work, but allowed me to develop my skills as a researcher. My warmest thanks for your ongoing help. I would also like to acknowledge Dr Helen Mulvana for her input on the project.

I would like to take this opportunity to recognise all the participants who took part in each study. This work would not have been possible without you. I must express my gratitude to Dr Mariel Purcell and the staff at the Queen Elizabeth National Spinal Injuries Unit who supported this research, and Dr Aleksandra Dybus and Dr Colm Craven for their assistance. Furthermore, I would like to acknowledge Prof Ian Loram and his research group from the Manchester Metropolitan University for sharing the ultrasound processing algorithms with us.

My time during this PhD project would not have been the same without my colleagues from the Centre for Rehabilitation Engineering research group at the University of Glasgow. I would like to thank Margaret, for her invaluable advice and encouragement at the start of my PhD, and Linda, who was not only a valuable colleague with whom I was able to collaborate, but also a friend. I wish to thank Alberto, Anna, Radha, Ciaran, Ioana, Keri, Tao, Aimin and Thomas for their companionship, and Dr Aleksandra Vuckovic for encouraging us all to be the best version of ourselves. I would especially like to thank Nina and Finda, who became great friends that I could always rely on for advice and support. I wish them both every success. My biggest thanks must go to Ania, who has not only become a dear friend that was always there to listen and support me, but who also offered practical advice and was kind enough to proofread my writing.

I am extremely grateful to my family who have been so encouraging throughout my studies. I would especially like to thank my mum and dad wholeheartedly for supporting me in every way, including turning their living room into an office for me to work over these final months. I must also thank my sister Eilidh, with whom I shared this office and who provided both encouragement and a welcomed distraction while writing this thesis. I am also very lucky to have incredibly supportive friends. I would particularly like to thank Hannah and Judith for always believing in me. A very special thanks must go to Jan, who was always there to offer support and encouragement, and kept me sane over the years. I would not be writing my acknowledgements without you all.

Declaration

I declare that, except where explicit reference is made to the contribution of others, this thesis is the result of my own work and has not been submitted for any other degree at the University of Glasgow or any other institution.

All of the methods and experimental results presented in this thesis were generated by the author.

Jennifer Miller

October 2020

Publications

R. Ruslee, J. Miller and H. Gollee, "Investigation of different stimulation patterns with doublet pulses to reduce muscle fatigue", *In Proceedings of 21st IFESS Conference*, London, United Kingdom, 2017.

J. Miller and H. Gollee, "Ultrasound imaging analysis for the optimisation of functional electrical stimulation", *In Proceedings of 22nd IFESS Conference*, Nottwil, Switzerland, 2018.

R. Ruslee, J. Miller and H. Gollee, "Investigation of different stimulation patterns with doublet pulses to reduce muscle fatigue", *Journal of Rehabilitation and Assistive Technologies Engineering*, vol. 6, doi: 10.1177/2055668319825808, 2019.

J. Miller, H. Gollee and M. Purcell, "Ultrasound imaging as a diagnostic tool to assess the functional status of muscles following a spinal cord injury", *Ultrasound in Medicine and Biology*, vol. 47, no. 3, pp 386-397, 2021.

Contents

List of Tables

List of Figures

List of Abbreviations

AB:	Able-bodied
AIS:	ASIA Impairment Scale
ASIA:	American Spinal Injury Association
ASM:	Active Shape Model
AsynR:	Asynchronous Random stimulation
AsynS:	Asynchronous Sequential stimulation
CFT:	Constant Frequency Train
CNS:	Central Nervous System
CSA:	Cross-sectional Area
CSS:	Conventional Synchronous Stimulation
DAQ:	Data Acquisition
DFT:	Doublet Frequency Train
DOMS:	Delayed Onset of Muscle Soreness
DXA:	Dual-energy X-ray Absorptiometry
EMG:	Electromyography
FES:	Functional Electrical Stimulation
FIM:	Functional Independence Measure
GLCM:	Grey-level Co-occurrence Matrix
GLNU:	Grey-level Non-uniformity
GM:	Gastrocnemius Medialis
Hz:	Hertz
I:	Current
IMCL:	Intramyocellular lipid
IMF:	Intramuscular fat
IOD:	Integrated Optical Density
IPI:	Inter-pulse Interval
KLT:	Kanade-Lucas-Tomasi (tracking algorithm)
LBP:	Local Binary Pattern
LRE:	Long Run Emphasis
MANOVA:	Multivariate Analysis of Variance

MEP:	Motor-evoked Potential
MHC:	Myosin Heavy Chain
MMT:	Manual Muscle Testing
MRI:	Magnetic Resonance Imaging
MVC:	Maximum Voluntary Contraction
NMES:	Neuromuscular Electrical Stimulation
NMJ:	Neuromuscular Junction
NPD:	Normalised Pixel Difference
PDM:	Point Distribution Model
PNS:	Peripheral Nervous System
pQCT:	Peripheral Quantitative Computed Tomography
PW:	Pulsewidth
Q:	Charge
QST:	Quantitative Sensory Testing
REC:	Research Ethics Committee
RF:	Rectus Femoris
RLM:	Run Length Matrix
RLNU:	Run Length Non-uniformity
RMS:	Root Mean Square
ROI:	Region of Interest
ROM:	Range of Motion
RP:	Run Percentage
SCI:	Spinal Cord Injury
SCIM:	Spinal Cord Independence Measure
SD:	Standard Deviation
SDSS:	Spatially Distributed Sequential Stimulation
SRE:	Short Run Emphasis
TA:	Tibialis Anterior
TMS:	Transcranial Magnetic Stimulation
TVD:	Telemed Video Data (file type)
US(I):	Ultrasound (Imaging)
VFT:	Variable Frequency Train
VL:	Vastus Lateralis
VM:	Vastus Medialis
WISCI:	Walking Index for Spinal Cord Injury

Chapter 1

Introduction

1.1 Summary

In this chapter, the main concepts and background information relevant to the investigation are presented. Firstly, an overview of the basic physiology of the neuromuscular system is provided, describing how the nervous system communicates with skeletal muscles to bring about movement. This is followed by a brief introduction to the effects of a spinal cord injury (SCI). An injury to this major component of the nervous system disrupts communication with the muscular system, resulting in muscle paralysis. Next, the basic principles of ultrasound imaging (USI) are described. This imaging tool allows skeletal muscle to be visualised, making it a potential tool for assessing the effects of a spinal cord injury on muscle function. A commonly used rehabilitation technique known as neuromuscular electrical stimulation (NMES) is also introduced. NMES can be used to produce muscle contractions artificially, making it particularly useful for muscles affected by a SCI which can no longer contract voluntarily. Finally, the aims and objectives of the project are presented along with the contributions of this work.

1.2 Neuromusculoskeletal system

The neuromuscular system refers to two organ systems of the body, the nervous system and muscular system, working together to produce and control movement.

1.2.1 Nervous system

The nervous system is composed of billions of highly organised nerve cells, called neurons, that transmit information within the body by conducting electrical signals known as action potentials. Neurons are composed of a cell body, which contains the nucleus and controls cell functions; dendrites, which are short projections of the cell that receive electrical signals; and an axon, which is a long projection that conducts electrical signals away from the cell body.

The nervous system can be divided into two parts, the **central nervous system (CNS)**, which consists of the brain and the spinal cord, and the **peripheral nervous system (PNS)**, which consists of all nervous tissue outside the CNS [2, 9, 10].

1.2.1.1 Central nervous system (CNS)

The brain is located within the skull and the spinal cord is located within the vertebral column formed by the vertebrae of the spine. The brain and spinal cord connect at an opening in the skull called the foramen magnum. The brain is the control centre of the entire body. It contains over 100 billion neurons and consists of several specialised areas which work together to process the sensory inputs and generate command signals which control body movements [2, 9].

The spinal cord is a cylindrical bundle of nervous tissue which forms the main connection between the brain and the rest of the body. The centre of the spinal cord consists of grey matter containing neurons. This is surrounded by white matter which contains pathways that carry information to (ascending tracts) and away from (descending tracts) the brain. The spinal cord is divided into cervical, thoracic, lumbar and sacral segments, corresponding to the vertebrae through which the spinal nerves (part of the PNS) enter and exit the vertebral column [2, 9, 11].

1.2.1.2 Peripheral nervous system (PNS)

There are 31 pairs of spinal nerves: 8 cervical, 12 thoracic, 5 lumbar, 5 sacral and 1 coccygeal. Each spinal nerve is designated a number and a letter corresponding to its position. For example, the first cervical nerve is designated "C1". Each spinal nerve consists of a dorsal root, containing a sensory neuron, and a ventral root, containing a motor neuron [2, 9].

Each pair of spinal nerves supply specific areas of the body. A dermatome is the area of skin supplied by the sensory neuron of a particular spinal nerve. Similarly, the motor neuron of each spinal nerve supplies muscles in a particular area of the body. The cervical nerves are responsible for movement of the head, neck, diaphragm and upper limbs; thoracic nerves control the chest and abdominal muscles; lumbar nerves control the lower limbs; and sacral nerves are responsible for bladder, bowels and sexual function [2, 9].

An overview of the neuromuscular system is shown in Figure 1.1, illustrating the connections between the different systems. This includes the spinal cord (CNS), the spinal nerves which arise from it (PNS), with particular emphasis on the motor neurons which innervate skeletal muscles (muscular system).

1.2.2 Motor units

1.2.2.1 Nerve supply to muscles

Motor neurons are nerve cells with the specific purpose of stimulating muscles to contract. The cell bodies of motor neurons are found in the brain and spinal cord, while their axons extend

to muscle fibres. Axons of motor neurons branch off, innervating several individual muscle fibres. All fibres are innervated by one of these branches from the axon of a motor unit, however muscles are usually supplied by several different motor neurons [2, 10].

1.2.2.2 Motor units

A motor unit is the smallest functional unit of muscle contraction. It consists of a motor neuron and all the muscle fibres that it innervates [12]. An action potential in the motor neuron generates an action potential in all muscle fibres in a single motor unit. Different motor units contain different numbers of muscle fibres and also vary in their sensitivity to stimuli. Small motor units have small diameter axons and innervate a small number of slow-twitch, fatigue resistant fibres, whereas large motor units have large diameter axons and innervate a large number of fast-twitch muscle fibres which are easily fatigued. These properties of the motor unit dictate the order in which they are recruited [13, 14], which is discussed further in Section 2.4.2 of Chapter 2.

1.2.2.3 Neuromuscular junction

The neuromuscular junction (NMJ) is a chemical synapse between the motor neuron and the muscle fibre that it innervates, allowing the transmission of a signal from the brain or spinal cord and causing the muscle to contract. The presynaptic terminal is the axon terminal and the postsynaptic membrane is the plasma membrane of the muscle fibre, called the sarcolemma. The presynaptic terminal releases neurotransmitters that bind to the postsynaptic membrane, also known as the motor end-plate [2, 9, 10].

1.2.3 Skeletal muscle

Muscle tissue is characterised by its ability to contract with force in order to generate movement. Skeletal muscle is attached to the skeleton, allowing movement of the body, and is under voluntary control, allowing specific movements to be achieved.

1.2.3.1 Structure

Skeletal muscles are composed of skeletal muscle cells, known as muscle fibres, which are surrounded by a thin layer of connective tissue called endomysium. These muscle fibres are arranged in bundles known as fascicles, each of which are surrounded by a thicker layer of connective tissue called perimysium. The muscle is composed of several fascicles and is encased in a dense collagenous connective tissue known as epimysium. A further sheet of connective tissue called the muscle fascia encases and separates individual muscles. The connective tissue around the muscle and each internal component extends to the end of the muscle to form tendons, allowing muscles to connect to bone. Blood vessels and nerves associated with the muscle also run together through the layers of connective tissue [2].

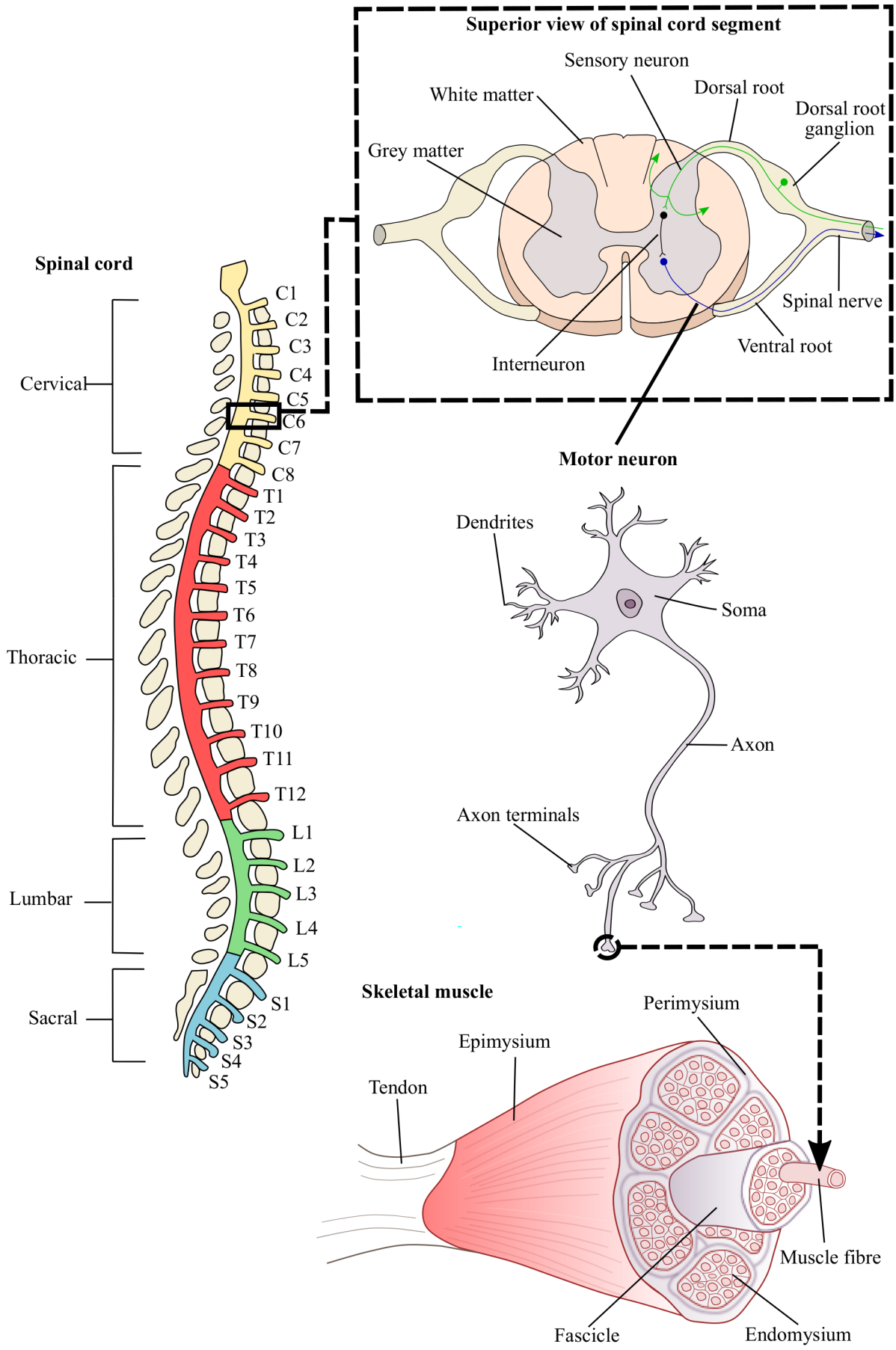

Figure 1.1: Overview of neuromuscular system showing the different regions of the spinal cord, a superior view of a segment of the spinal cord, the structure of a motor neuron and the skeletal muscle it innervates at the neuromuscular junction. Adapted from [2].

1.2.3.2 Muscle fibres

Muscle fibres consist of bundles of protein filaments called myofibrils, which contain proteins actin and myosin that are essential for muscle contraction. Myosin is composed of two protein chains wound around each other to form a thick spiral while actin is a thin filament. Together the actin and myosin proteins form the structural unit of the myofibril called a sarcomere [2, 10].

Depending on their composition, muscle fibres can be classified as slow-twitch or fast-twitch. Slow-twitch fibres, also known as type I fibres, contract more slowly and are more resistant to muscle fatigue. These muscle fibres are adapted to aerobic respiration and most often used for prolonged muscle contractions at lower velocities. In contrast, fast-twitch fibres, or type II fibres, contract very quickly but also fatigue quickly, making them more suited to short muscle contractions which produce a large force very quickly. Fast-twitch fibres can be further categorised as type IIa, which rely on aerobic and anaerobic respiration, or type IIb, which rely almost entirely on anaerobic respiration. Muscles consist of a mixture of these fibre types, and the proportion of different fibre types varies between different muscles [2, 10].

1.2.3.3 Muscle contraction

A muscle contraction is the overall shortening of muscle fibres, resulting from the shortening of several sarcomeres which repeat along the length of the myofibril and join end to end. The sliding filament model describes the mechanism of the sarcomere shortening as the actin and myosin filaments themselves do not shorten but instead slide past one another [15]. This is caused by a cross-bridge cycle, whereby a series of molecular events cause the heads of the myosin filament to slide over the actin filament [2, 9, 16].

1.2.3.4 Muscle action

When a stimulus is applied to a muscle in the form of an action potential, the contractile elements of the muscle fibres attempt to shorten as described above. This can result in the following types of muscle contractions [17]:

- **Isometric:** a force is generated but the muscle cannot shorten as it cannot overcome external resistance. Isometric contractions are defined as having no change in muscle length, however, it has been shown that shortening of the muscle itself does occur and it is the entire muscle-tendon complex which shows no change in length.
- **Isotonic:** a force is generated by changing the length of the muscle. This can be:
  - **Concentric:** the muscle shortens, generating force and resulting in movement of the joint.
  - **Eccentric:** the muscle is elongated in response to an external force exceeding that produced by the muscle.

1.2.3.5 Muscle shape

The orientation of the muscle fascicles determines the shape of the muscle [18]. There are three classes of muscle shape [2, 17]:

- **Pennate:** muscle fascicles attach to a tendon at an angle. Pennate muscles can be further subdivided into
  - **semipennate/unipennate:** all muscle fascicles attach on one side of the tendon.
  - **bipennate:** muscle fascicles attach on two sides of a common tendon.
  - **multipennate:** muscle fascicles attach at many places around a central tendon.
- **Straight:** fascicles are parallel to the long axis of the muscle.
- **Orbicular:** fascicles are arranged in a circle around an opening.

Muscles investigated throughout this PhD project are pennate, the different forms of which are shown in Figure 1.2.

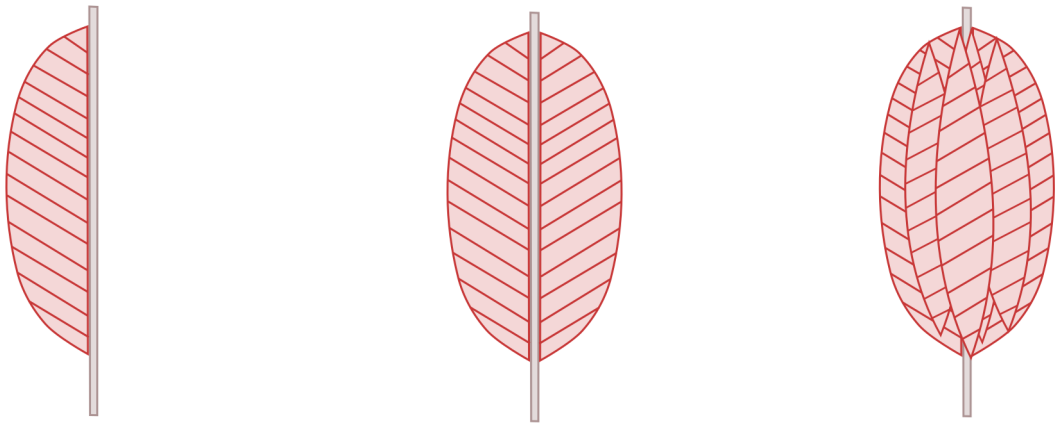

(a) Unipennate (b) Bipennate (c) Multipennate

Figure 1.2: Different type of pennate muscle shapes. Adapted from [2].

The shape of the muscle determines how much force it can generate. Muscle fibres in an individual fascicle are parallel and exert force along the longitudinal axis. In a straight muscle where all fascicles run in parallel, the total force exerted by the muscle is simply the sum of the force exerted by all fascicles. Pennate muscles on the other hand connect to the tendon at an angle (θ), determining the total force exerted on the muscle [17]:

$$F_{tendon} = F_{fascicle} \times \cos\theta \tag{1.1}$$

1.3 Spinal cord injury

As discussed in Section 1.2.1, the spinal cord is the main pathway for communication between the brain and the rest of the body. When an injury occurs, this flow of information is disrupted.

1.3.1 Introduction

Spinal cord injuries (SCI) affect more than 12,000 people in the United Kingdom every year. They are the result of compulsion, contusion or incision damaging the spinal cord. This is most often due to traumatic events such as a traffic accident or sports injury, however it can also be caused by disease such as tumours [19, 20]. As a result of the injury, normal functions of the spinal cord are disrupted, leading to lack of sensation and muscle paralysis. This can be extremely debilitating and greatly limit a person's ability to perform everyday tasks.

The neurological damage which occurs immediately as a direct result of the mechanical injury to the spinal cord is called **primary injury**. This then leads to a series of biological responses known as the **secondary injury**, which can begin minutes after the initial injury and continue for weeks, leading to further neurological damage. Finally, the **chronic phase** occurs and can last for years after the injury took place [11, 21].

The extent of the injury and the areas of the body which are affected depend on the nature of the injury. An injury is defined as **complete** or **incomplete** depending on whether or not the spinal cord is totally severed. Complete injuries result in a complete loss of sensory and motor function, whereas varying degrees of function can be preserved when the injury is incomplete.

In general, loss of function occurs below the level of injury, however, the neurological damage can be higher than the physical injury and this is the level which is used to classify it. **Tetraplegia** refers to an injury in the cervical segments of the spinal cord, resulting in loss of sensory and/or motor function in the upper limbs, trunk and lower limbs. **Paraplegia** is an injury in the thoracic, lumbar or sacral region which affects the trunk and lower limbs [20, 22].

1.3.2 Assessment of SCI

Accurate assessment of the injury is essential for obtaining a reliable prognosis, monitoring recovery and assessing the effectiveness of rehabilitation interventions [20]. Moreover, there is a recognised need for a standardised measure of injury severity to allow comparison of research outcomes.

In order to meet this need, the American Spinal Injury Association (ASIA) developed the ASIA impairment scale (AIS) [23], which was last revised in 2011 [3]. Key sensory and motor points were identified to accurately determine the neurological level of injury, and a standardised grading system was put in place.

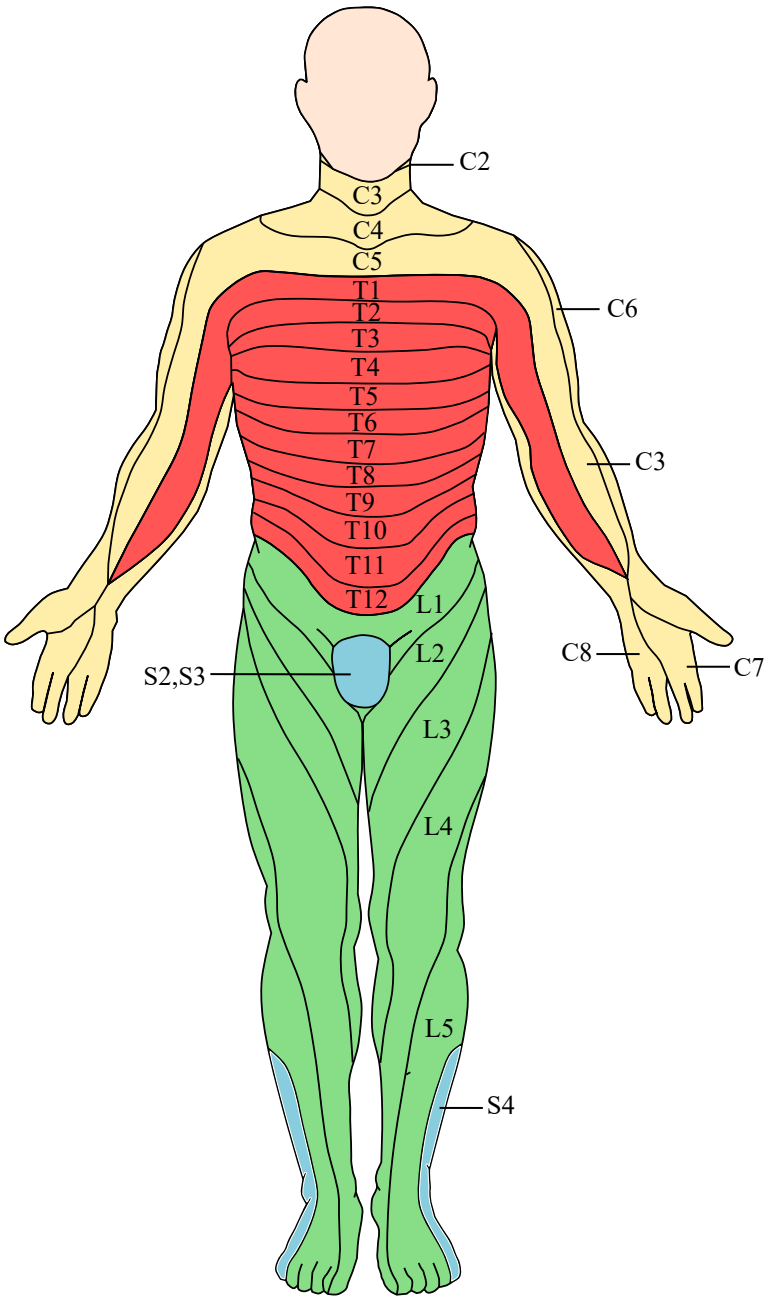

Figure 1.3: Map of dermatomes showing areas of the body innervated by sensory nerves originating at different levels of the spinal cord. Adapted from [3].

Each key sensory point (dermatome) is graded based on sensitivity to a pin prick and light touch, while each key motor point (myotome) is graded on the muscles ability to generate a contraction. These scores are then combined to give an overall score:

- **A =** Complete: no sensory or motor function is preserved.
- **B =** Incomplete: sensory function is preserved but there is no motor function below injury level.

- **C =** Incomplete: sensory and motor function are preserved, with most key muscles producing a muscle grade less than 3 (out of 5).
- **D =** Incomplete: sensory and motor function are preserved, with most key muscle producing a muscle grade of more than 3 (out of 5).
- **E =** Normal: both motor and sensory function are normal.

1.4 Ultrasound imaging

Ultrasound imaging (USI) is a commonly used diagnostic tool based on the behaviour of sound waves travelling through tissue to produce an image. The unique structure of skeletal muscle, described in Section 1.2.3, allows for it to be easily visualised. As a result, USI has been widely used as a screening tool for neuromuscular disorders [24], and has potential as a diagnostic tool for assessing muscles following a SCI.

1.4.1 Basic principles

Ultrasound is defined as sound waves with a frequency greater than 20 kHz, however diagnostic USI generally uses sound waves with a frequency between 3.5 and 15 MHz. Ultrasound waves are fundamentally mechanical waves that propagate through the vibration of particles in the surrounding medium. As a result, they follow the principles of penetration and attenuation. Penetration refers to the depth the ultrasound wave can reach and is dependent on three factors:

- **Intensity:** the rate at which energy is delivered per unit of area i.e. $power/area$ of the probe. Depth of penetration increases with intensity.
- **Frequency:** the number of oscillations per second. Higher frequency sound waves diverge less, but in general, the lower the frequency the farther it will penetrate.
- **Speed:** the speed of an ultrasound wave travelling through a medium is determined by density and stiffness. The speed will be higher in dense, rigid mediums.

Attenuation is the loss of energy which occurs at the boundaries between different media. This is mostly as a result of absorption into the surrounding tissue in the form of heat, however, some sound waves are scattered, refracted or reflected back to the source [25].

Ultrasound waves are emitted by a probe and travel into the body, coming into contact with different tissues. All tissues have an intrinsic property called the acoustic impedance (Z), which describes the tissues resistance to the sound waves and is defined as:

$$Z = \rho c \tag{1.2}$$

where ρ is the density of the tissue and c is the speed at which the sound waves propagate through the tissue. The speed at which the ultrasound wave travels is determined by the elastic modulus (E) and the density (ρ) of the tissue it is travelling through:

$$c = \sqrt{\frac{E}{\rho}} \tag{1.3}$$

Typical values of acoustic impedance for different body tissues are shown in Table 1.1. There is clearly a difference in acoustic impedance between muscles and the surrounding tissues in the body. It should also be noted that the value of acoustic impedance for skeletal muscle is based on its heterogeneous structure which includes a mixture of muscle fibres and connective tissue. When an ultrasound wave comes into contact with the boundary between two tissues with different acoustic impedances, attenuation occurs. This results in some sound waves being reflected back to the probe, while others travel further and are reflected by other boundaries [25, 26].

These sound waves form the basis of image formation. The strength of the reflected signal determines the brightness of the image. This information is combined with the time taken for the signal to return and the position from which they were returned to reconstruct an image of the tissue.

Table 1.1: Typical values of acoustic impedance for tissues within the body [1].

Body tissue	**Acoustic impedance** ($kgm^{-2}s^{-1}$)
Air	0.0004
Fat	1.34×10^6
Tendon [27]	1.40×10^6
Water	1.48×10^6
Muscle	1.71×10^6
Bone	7.80×10^6

1.4.2 Instrumentation

USI devices typically consist of a transducer assembly and an imaging system. The transducer emits ultrasound waves which travel into the body. It also collects those ultrasound waves which return as an echo and converts them to an electrical signal. The imaging system then processes this electrical signal to create a digital image which represents the signal from the returned echo.

1.4.2.1 Transducer assembly

The transducer assembly (also known as the "probe") contains an array of piezoelectric crystals (also referred to as "elements") which convert energy from one form to another. The acoustic

energy of the returning echo applies pressure to the element, causing it to deform and produce a voltage (electrical signal).

Elements within a probe can be arranged in a linear or curved format. Linear probes contain elements which are arranged side by side in a straight line and triggered sequentially. This allows a rectangular image to be formed from several vertical scan lines. This type of probe is most suited to imaging small superficial structures due to its wide near field. A curved probe is similar except that the elements form a curved shape instead of a straight line. As a result, the image produced is a diverging sector shape. This probe is more suitable for imaging deep structures as it has wide far field [25].

1.4.2.2 Imaging system

The imaging system typically consists of a beam former, signal processor, image processor and visual display. The beam former generates an electrical signal which drives the transducer assembly and ultimately causes the elements to emit an ultrasound wave. It also amplifies and digitises the electrical signal returned from the transducer assembly as a result of the ultrasound echo. This electrical signal is then filtered and compressed by the signal processor. Finally, the image processor converts the signal into an image which then appears on the visual display [25].

1.4.3 Modes of imaging

There are several possible modes to display the signal of the returned echo, as shown in Figure 1.4. The most commonly used are:

- Amplitude mode (A-mode): the intensity of the returned echo is displayed along a single line with respect to depth.
- Brightness mode (B-mode): displayed as a greyscale image, the returned echo is plotted as a 2D map. The x-axis consists of scan lines generated from pulses sent by different elements along the length of the probe. For each scan line, pixels represent the location and characteristics of the tissue. The brightness of the pixel represents the strength of the echo and the location is determined from the direction of the sound wave, the time taken for it to return and the speed at which sound waves travel through tissue.
- Motion mode (M-mode): greyscale levels are used to represent the intensity of the echo, however in this case a single scan line describing the depth is plotted over time [25].

1.4.4 Identifying tissue types

Echogenicity is a property describing the interaction of ultrasound waves in tissue, in other words, whether the tissue reflects or transmits the sound wave. Tissues which reflect a high

number of sound waves have high echogenicity and will appear bright in the ultrasound image, whereas tissues which absorb most of the sound waves have low echogenicity and appear dark. Based on echogenicity, tissues can be classified as:

- hyperechoic: appear white in US image e.g. connective tissue.
- hypoechoic: appear grey in US image e.g. cartilage.
- anechoic: appear black in US e.g. bone.

The difference in echogenicity between different tissue types makes identification of these tissues in an ultrasound image relatively easy as each tissue has a characteristic appearance [26, 28].

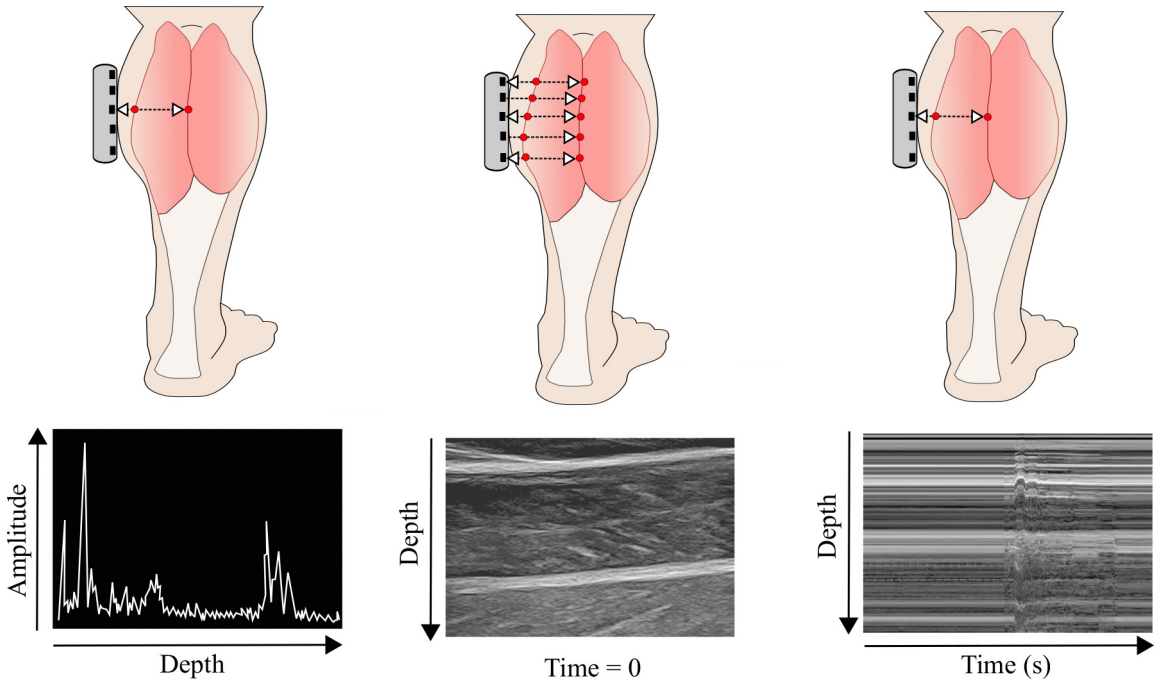

(a) A-mode (b) B-mode (c) M-mode

Figure 1.4: Different modes of ultrasound imaging.

1.4.5 Imaging of skeletal muscle

The structure of skeletal muscles, discussed in Section 1.2.3.1, gives them a distinct appearance and allows them to be easily discriminated from surrounding tissue. The muscle tissue itself has low echogenicity and therefore appears dark in an US image. The connective tissue surrounding the muscle (epimysium) however is highly reflective, resulting in bright hyperechoic boundaries that are clearly visible. Furthermore, in the longitudinal plane, the connective tissue around individual muscle fascicles (perimysium) is also hyperechoic, resulting in a striated appearance [24, 26, 29, 30].

1.5 Neuromuscular electrical stimulation (NMES)

Neuromuscular electrical stimulation (NMES) involves the application of low levels of current to artificially elicit a muscle contraction by activating the innervating nerves. For people affected by paralysis as the result of a spinal cord injury, who are limited in their ability to voluntarily contract their muscles, this holds great potential as a rehabilitation technique [13, 31–33].

1.5.1 Basic principles

NMES delivers pulses of low amplitude current through electrodes, which can either be placed on the surface of the skin or implanted. The current flows between the two electrodes, generating an electric field. When the electric field reaches a motor neuron, an action potential is generated which in turn causes innervated muscle fibres to contract [33, 34].

Stimulation can be delivered to specific muscles, controlling the timing and order of stimulation to produce functional movements such as stepping or grasping. In the case where stimulation is applied to produce a functional movement, the term functional electrical stimulation (FES) is used. This is particularly useful for people with a SCI who are unable to voluntarily produce functional movements. The injury to the spinal cord blocks the signals sent from the brain to produce movement, however, in most cases the peripheral nerves remain intact. NMES is therefore able to provide an artificial stimulus, initiating an action potential to excite the nerves and ultimately produce movements which are not possible voluntarily [32, 35].

1.5.2 Stimulation parameters

In order to achieve the desired stimulation, there are several parameters which can be controlled. **Amplitude** is the intensity of the current delivered. During transcutaneous electrical stimulation, this is usually in the range of 10 to 100 mA. The current can be delivered in monophasic or biphasic waveforms. If the waveform is monophasic, only positive or negative charges are delivered, whereas a biphasic waveform delivers both positive and negative charges. Biphasic waveforms balance the charges entering the body and are therefore generally the preferred choice. The waveforms can also be applied in different shapes such as triangular waves, however rectangular waveforms are most common [34]. **Pulsewidth**, also known as pulse duration, is the time a single pulse is delivered for. Typically values between 100 and 500 μs are used [36]. The total charge (Q) delivered to the muscle is dependent on the amplitude of the current (I) and the pulsewidth (PW).

$$Q = I \times PW \tag{1.4}$$

The higher the current and pulsewidth, the higher the charge delivered to the muscle. This results in a larger electric field which spreads further and activates more motor neurons, which

in turn leads to increased recruitment of muscle fibres and a greater overall force is produced.

Frequency is the number of pulses produced per second and is given in units of Hertz (Hz). Similarly, the **inter-pulse interval (IPI)** also describes how often pulses are delivered, however it is a measure of the time between pulses. A frequency of 40 Hz is therefore equivalent to an IPI of 25 ms. Frequency varies greatly depending on the application but is generally between 20 to 50 Hz [36]. A diagram of these stimulation parameters is shown in Figure1.5.

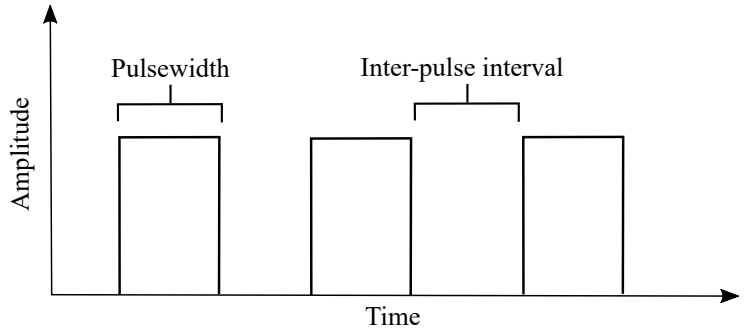

Figure 1.5: Diagram of the electrical stimulation parameters amplitude, pulsewidth and inter-pulse interval.

1.6 Aims and objectives

A spinal cord injury (SCI) disrupts the flow of information between the brain and the rest of the body, resulting in varying degrees of muscle paralysis and structural changes which occur over time and are dependent on the severity of the injury. Ultrasound imaging (USI) is a potential diagnostic tool, which has been used extensively to screen for several other neuromuscular disorders, and can provide additional insight.

The main aim of this PhD project is to investigate the suitability of USI as a diagnostic tool for the assessment of muscles following a spinal cord injury, by establishing whether or not it can differentiate measurements of structure over time and correlate measurements of muscle movement with different levels of muscle activity. Its ability to detect changes in these measurements over time for individual participants also allows us to investigate its potential for monitoring recovery. A secondary aim of the project is to improve the use of neuromuscular electrical stimulation (NMES) during the rehabilitation of SCI patients by gaining further insight into muscle behaviour during its application. The corresponding objectives are:

1. Comparison of USI measurements of muscle structure in able-bodied participants and SCI participants at different times post-injury (addressed in Chapter 4).

2. Comparison of USI measurements of muscle movement in able-bodied participants and SCI participants with different levels of muscle function (addressed in Chapter 5).

3. Feasibility of monitoring and predicting recovery from acute to chronic injury based on USI measurements (addressed in Chapter 6).

4. Evaluation of various NMES conditions with respect to muscle contraction characteristics (addressed in Chapter 7).

1.7 Thesis outline

Chapter 2: In this chapter, atrophy and increased fatiguability of skeletal muscles following a SCI are discussed, highlighting the need for accurate assessment of muscle function, with current methods and their limitations being discussed. USI of skeletal muscle is then explored, with particular emphasis on its use for screening neuromuscular disorders. The use of NMES as a rehabilitation technique is also introduced and the differences in muscle fibre recruitment which limit its use are discussed.

Chapter 3: This chapter presents the experimental methods used throughout this project. Firstly, techniques used repeatedly throughout experiments are explained, followed by a detailed description of the experimental methods for each study, including the participants, setup, data acquisition and experimental protocol. The methodology of ultrasound analysis and statistical methods used throughout this thesis are also provided.

Chapter 4: Changes in muscle structure over time following a SCI and the suitability of USI to detect these changes are investigated in this chapter. The analysis methods used to obtain measurements of resting muscle thickness and several features describing muscle echogenicity and echotexture are provided. These measurements are then compared between a group of able-bodied participants and SCI participants at different times post-injury.

Chapter 5: In this chapter, USI measurements describe the amount of muscle movement that participants are able to produce. This includes measurements of muscle deformation and displacement obtained from tracking software, and changes in pixel greyscale values. These measurements are compared between able-bodied participants and SCI participants with various levels of muscle function, determined by torque and EMG. The suitability of USI as a diagnostic tool for assessing muscle function is investigated by establishing if it can differentiate between various levels of muscle activity.

Chapter 6: The measurements of muscle structure and movement described in the previous chapters are compared over time for individual participants. The ability of USI to detect changes over time and its suitability for monitoring recovery is explored here. In this chapter, there is particular emphasis on the ability of USI to detect small movements which might not be seen by current assessment methods.

Chapter 7: This chapter compares measurements of muscle movement during electrical stimulation under different conditions to gain further insight into muscle behaviour. Different combinations of the basic stimulation parameters are compared, as well as different patterns of stimulation parameters and electrode configurations. Finally, the behaviour of healthy muscles is compared to muscles affected by a SCI, to better understand the application of electrical stimulation as a rehabilitation technique.

Chapter 8: The main results are discussed in this chapter.

Chapter 9: This chapter summarises the main conclusions and outlines suggestions for future work.

1.8 Contributions

The main clinical contributions of this research project are as follows:

- The suitability of USI to detect structural changes which occur in the muscle following a SCI is demonstrated in Chapter 4. This involved the implementation and development of novel greyscale analysis techniques to show changes in echogenicity and echotexture, and the implementation of tracking software to show a reduction in muscle size.
- The suitability of USI to describe the functional status of muscles following a SCI is demonstrated in Chapter 5. Tracking software was implemented to measure movement of the whole muscle and at the regional level, which enabled us to differentiate between different levels of torque. A pixel difference method based on the brightness of the individual pixels was also implemented to measure the total movement within the muscle, which was associated with the electrical activity of the muscle. This is a new method for assessing the functional status of muscles after a SCI.
- The potential of USI to monitor recovery following a SCI is demonstrated in Chapter 6. USI was able to detect changes over time, providing additional information to the currently used methods. Furthermore, the protocol was performed bedside, demonstrating the potential for clinical use.

The main technological contributions of this research project are as follows:

- A novel method for detecting small muscle movements in acute SCI was implemented (Chapter 6). This method, which is based on the difference in pixel greyscale values between frames of an USI video, was found to detect muscle movements which could not be detected by EMG or manual muscle testing at an earlier stage in recovery

- Tracking software was implemented to provide additional information on muscle behaviour under different conditions during the application of NMES. This included different intensities of stimulation by changing the parameters (current, pulsewidth and frequency); different patterns of stimulation by varying these parameters; and different spatially distributed patterns through a multi-electrode configuration. It also showed differences in muscle behaviour between able-bodied and SCI participants.

Chapter 2

Literature Review

2.1 Summary

An injury to the spinal cord has implications for the entire body, particularly skeletal muscles. In this chapter, the different structural and functional changes which occur in the muscle over time following an injury are discussed, along with the currently used assessment methods.

Ultrasound imaging (USI) has been widely used to image skeletal muscle, making accurate measurements of morphology and movement. Its value has also been proven as a screening tool for several neuromuscular disorders. The main findings from past studies are reviewed in this chapter, highlighting the potential of USI as a diagnostic tool for assessing muscles affected by a spinal cord injury (SCI).

Finally, the role of neuromuscular electrical stimulation (NMES) in the rehabilitation of people with a SCI is discussed. There is particular emphasis on the differences between voluntary and NMES-induced contractions, which make NMES less efficient, and attempts which have been made to overcome these limitations.

2.2 Spinal cord injury

A traumatic spinal cord injury is the result of applied force causing mechanical damage to neurological tissue, disrupting the flow of information between the brain and the rest of the body. In 1911 it was suggested for the first time that secondary events occur after the initial injury that cause further damage [37]. This led to the classification of the initial neurological damage as the primary injury, followed by a series of complex biological events referred to as secondary injury. This phase includes vascular changes, inflammatory responses and cell death, and can last for weeks after the injury has occurred. Finally, a chronic phase, which can last for years, consists of structural changes in the spinal cord and the formation of scar tissue [11, 38]. Each phase of the injury has implications for the entire body, not just the spinal cord and surrounding nerves. This review focuses on the effect on skeletal muscles and how this is assessed.

2.2.1 Effect on skeletal muscle

2.2.1.1 Atrophy

A widely accepted effect of a SCI is the occurrence of muscle atrophy, which is defined as a reduction in the size and number of muscle fibres [39–41]. Several studies have demonstrated a significant reduction in muscle size in both complete [42] and incomplete [43] SCI populations when compared to matched able-bodied controls as early as 6 weeks post-injury. Muscle biopsies have shown a reduction in the cross-sectional area of the muscle fibres themselves [42], while imaging techniques such as magnetic resonance imaging (MRI) [43], peripheral quantitative computed tomography (pQCT) [44], and dual-energy X-ray absorptiometry (DXA) [45] show a reduction in the cross-sectional area of the entire muscle.

Two possible causes of muscle atrophy have been identified and their differences investigated in an early study by Solandt and Magladery [46]. **Denervation atrophy** is the result of damaged motor neurons at the level of injury, occurring in the spinal cord itself or in the ventral root of the spinal nerve. Atrophy is severe in muscles which completely lose all innervation from motor neurons. This usually only occurs in a small number of muscles, with most muscles only suffering partial denervation [47]. Surviving motor neurons have the capacity to sprout and supply additional muscle fibres, allowing the reinnervation of some denervated fibres [48]. Nevertheless, this capacity is limited and motor neurons generally only reinnervate muscle fibres which are in close proximity, therefore denervation atrophy can be a contributing factor in muscles ability to generate force [39].

Disuse atrophy, on the other hand is attributed to a lack of muscle activation below the level of injury [35, 39, 46, 49]. This concept that disuse leads to muscle atrophy is generally accepted, however, it has been suggested that "altered neuronal discharge" may be a more accurate definition as activity is not always reduced and other factors such as weight-bearing and muscle length also occur in models of disuse [40, 50]. Several studies have suggested that loading and muscle length are perhaps even more significant factors, and account for much of the atrophy accredited to disuse [39]. Indeed, disuse atrophy has been shown to be more pronounced in weight bearing muscles, particularly those that cross a single joint [39–41, 51]. Muscles which are immobilised at a shortened length have shown a similar pattern of preferential atrophy [52–54], even when muscle activity was not necessarily reduced [55]. It has also been suggested that preferential atrophy occurs in type II muscle fibres [42, 56]. This could explain why atrophy appears to affect different muscles to varying degrees [51, 57].

Moore et al. has shown that several factors are associated with the amount of atrophy that occurs including body mass, level of injury, motor-score, spasticity and wheelchair use [44]. A study by Cha et al. not only demonstrated a correlation between spasticity and muscle index (based on mass and height), but also suggested that there is a causal relationship, where spasticity preserves muscle mass by maintaining contractions [58].

2.2.1.2 Fibre transformation

Muscles affected by a SCI have also been shown to be less resistant to fatigue [40, 41, 49, 59], which is widely believed to be the result of a transformation from slow-twitch to fast-twitch fibres [39, 51, 60]. Fast-twitch muscle fibres have less resistance to fatigue than slow-twitch fibres due to their limited oxidative capacity and high metabolic demands. As discussed in Section 1.2.3 of Chapter 1, muscle fibres consist of contractile proteins actin and myosin. The myosin heavy chain (MHC) molecule determines the properties of muscle fibres and is expressed differently on different muscle fibre types (type I, IIa and IIx) [61]. The different versions are referred to as isoforms throughout the literature.

Although it is generally accepted that a fibre change does occur, the timing is less clear [60]. A study by Burnham et al. suggested that the isoform composition of fibres remains stable within the first month after injury, with a transitional period occurring between 1 and 20 months post-injury where fibres co-express both fast and slow MHC [62]. By 70 months, a steady state has been reached and isoform expression is almost exclusively fast MHC. It should however be noted that there were a limited number of subjects at each time period in this study and no measurements taken between the time periods stated. Similarly, another study found that there was no fibre transformation within the first 6 months following a SCI, but instead a transition from type IIa to type IIa+IIx [42]. This coincided with reduced fatigue resistance in SCI participants compared to able-bodied which did not change between 6 weeks and 24 weeks post-injury.

2.2.1.3 Intramuscular fat

A further adaptation which results from a SCI is the infiltration of adipose tissue leading to an increase in intramuscular fat (IMF) [45]. Similarly to disuse muscle atrophy, it is attributed to the loss of activation and unloading of skeletal muscle and associated changes in metabolism. A recent study by Graham et al. has suggested that the shift in fibre type from oxidative to glycolytic alters glucose metabolism [63].

IMF has been shown to increase as early as 6 weeks post-injury and continue for up to 3 months [43]. There are a number of factors which are thought to be associated with the amount of IMF, including motor-score, spasticity, wheelchair use, age and waist circumference [44]. IMF should be considered when making measurements of muscle size, as studies have shown that atrophy can be underestimated without correction [43]. It can also alter the mechanical properties of the muscle, with infiltration of fat leading to an increase in the stiffness of the tissue. This resists the shortening of muscle fibres during a contraction leading to a reduction in force production [64]. Furthermore, increased IMF can lead to secondary health problems including cardiovascular disease and type II diabetes [44]. A study by Shah et al. used proton spectroscopy to demonstrate a large increase in the intramyocellular lipid (IMCL) content of the soleus muscle and suggested this could potentially lead to the development of insulin resistance [65].

2.2.1.4 Contractile properties

As a result of these structural changes which occur following a SCI, the contractile properties of the muscle are also altered [61]. Animal studies have shown that a transected spinal cord leads to decreased excitability of motor neurons. Furthermore, contraction speed is also reduced due to a reduction in the overall tension in the motor unit [66].

Although there are variations between studies in the time post-injury at which measurements were taken, there is overwhelming evidence that there is a progressive decline in fatigue resistance [67–70] and the force which can be generated through electrical stimulation [68, 71–76], which is not seen during the acute phase of the injury. Häger-Ross et al. also found the force produced during a tetanic contraction to be weak, however, muscles were able to produce a strong twitch [77]. This could be explained by the findings of several studies [39, 48, 74] which suggest that as the number of motor units decreases, the size increases as motor neurons sprout to reinnervate fibres which have lost their innervation. This leads to an increase in strength of single motor units. The force-frequency relationship is also altered, showing a shift to the left, therefore forces can be achieved at a lower frequency [74–78].

There are also changes in the speed of muscle contractions. Häger-Ross et al. demonstrated a reduction in contraction speeds with a slower twitch contraction time [77]. However, it should be noted that this study focused on activation of individual motor units, not the muscle as a whole. Shields et al. showed similar results, but only as the effects of a fatigue protocol [71]. Several other studies have demonstrated faster contraction times [68, 76, 78] with a higher maximal rate of force rise and a faster rise time for both twitch and tetanic contractions [72]. Similarly there are differences in relaxation times reported, with some studies suggesting relaxation time is unchanged [76, 77] and others contradicting this with faster relaxation [68, 72, 78]. This variability may be explained by differences between the muscles studied or the time post-injury.

The onset of fatigue also has implications for the speed of force production. Rinaldin et al. has recently shown that during the application of electrical stimulation, not only does the peak torque decrease as the muscle fatigues, but there is also an increase in the delay between the electrical activation and the production of force [79]. This delay can occur during electrochemical or mechanical events depending on the type of muscle fibres and the fatigue process.

2.2.1.5 Underlying mechanisms

Much recent research has focused on the underlying mechanisms which contribute to muscle atrophy and fibre transformation. Lundell et al. investigated the imbalance of protein synthesis and breakdown which results in muscle atrophy [80], while a similar study from the same group focused on the role of oxidative stress and cell signalling [81]. A review by Hyatt et al. also provides evidence that damaged or dysfunctional mitochondria could be responsible for changes in the rate of protein synthesis [82]. The review in this chapter focuses on the structural changes and ability of muscles to generate a contraction as this is most relevant to the work of this project.

2.2.2 Methods for assessing muscle function

Rehabilitation following a SCI is an ongoing process which begins in the acute stage and can continue for years. The main aims of rehabilitation adjust over the course of recovery, therefore an accurate assessment of the injury is important for developing a unique rehabilitation plan [20]. As discussed in Section 1.3.2 of Chapter 1, in a clinical setting a spinal cord injury is routinely assessed through the ASIA impairment scale (AIS) [3, 22, 23], often combined with an MRI of the spinal cord [21]. The AIS is the most widely accepted outcome measure in spinal cord injury research. It has helped to improve the understanding of natural recovery which is essential for evaluating the implications of an intervention and early examinations have been shown to be useful for providing a prognosis. However, several factors can make the examination unreliable, particularly as it is subjective [83].

This has led to the development of several functional capacity scales, such as the functional independence measure (FIM), walking index for SCI (WISCI) and spinal cord independence measure (SCIM). These scales provide a measurement of a person's ability to perform everyday tasks such as feeding, dressing and grooming as well as walking [83]. The advantage of using these functional capacity scales as outcome measures is that they clearly demonstrate whether or not an intervention will have a meaningful impact on a person's day to day life. The downside is that it may not be sensitive enough to detect small improvements.

Alternative methods for obtaining quantitative measurements of muscle function include electromyography (EMG), which is the gold standard for measuring the electrical activity of muscle, and transcranial magnetic stimulation (TMS) to elicit motor-evoked potentials (MEPs) [84]. These techniques are limited by their ability to discriminate between different muscles or make measurements from deep muscles. Furthermore, they may not detect low level muscle activity below the noise threshold. As previously mentioned, several studies have used different imaging modalities such as MRI [43], pQCT [44], and DXA [45] for measurements of the cross-sectional area (CSA) of muscle tissue and fat, and proton spectroscopy has been shown to detect lipid content [65]. However, due to cost and accessibility, these techniques are limited to research and are not often used in a clinical setting.

One recent study by Ghatas et al. has investigated the potential use of near-infrared spectroscopy to assess mitochondrial capacity following a SCI in an attempt to provide an alternative to expensive MRI measurements and invasive biopsies [85], but to our knowledge only one study has investigated the use of USI. Bjerkefors et al. assessed abdominal muscle function in motor complete SCI participants, comparing USI with the standard techniques of EMG and manual examination [86]. The results of this study showed that ultrasound was less sensitive than EMG and manual examination but was highly specific.

2.3 Ultrasound imaging (USI)

The first report of musculoskeletal ultrasonography was in 1958 [87], demonstrating the ability of ultrasound to differentiate between different tissue types within a joint. However, it was not until 1980 that the first B-mode ultrasound scan was applied to skeletal muscle, investigating the decrease in muscle mass of the quadriceps as the result of immobilisation [88]. This study found that anthropometric measurements were severely underestimating the muscle wasting and highlighted the importance of techniques such as ultrasound imaging (USI) for accurate evaluation of muscles. This was the beginning of a myriad of studies investigating the potential uses of ultrasound imaging to assess skeletal muscle.

2.3.1 Measurements of muscle architecture

Muscle architecture is the arrangement of muscle fibres, determining not only the size and shape of the muscle, but the direction of force generation during a contraction. Typical measurements of muscle architecture obtained through USI include thickness, cross-sectional area (CSA), fibre length, and pennation angle in pennate muscles. Not only does USI allow these measurements to be obtained at rest, it also allows dynamic measurements during muscle movement.

2.3.1.1 Measurements of muscle size and fibre arrangement

The most common measurement obtained from the muscle while at rest is size, in the form of thickness or CSA. MRI is widely considered the gold standard for measurements of muscle size, limited only by its cost and accessibility. As a result, measurements obtained from MRI are often used for comparison to validate the use of USI. The vastus lateralis [89], trapezius [90], anterior hip [91] and hamstring [92] muscles have all shown high similarity between USI and MRI measurements. A further study by Scott et al. has shown USI measurements of the cross-sectional area and volume of vastus lateralis, rectus femoris, medial gastrocnemius and lateral gastrocnemius muscles have high agreement with MRI, demonstrating the suitability of USI to make accurate measurements of muscle size [93]. A sensor attached to the transducer, which records the position of the transducer as two-dimensional images are recorded, has been used to create a three-dimensional freehand ultrasound system. This allows measurements of muscle volume to be calculated which also show high agreement with MRI measurements [94]. Thickness of the rectus femoris muscle has also been validated against dual X-ray densitometry (DXA) [95] and a study by Rosenberg et al. made simultaneous measurements of muscle CSA and echo intensity as a measure of muscle quality [96].

The reliability of measurements of muscle size made with USI has also been investigated by comparing repeated measurements [91], often taken on different days [89, 96, 97]. Jenkins et al. found that measurements obtained from a single transverse scan were just as reliable as those from panoramic USI, which are simpler to obtain [97]. Tanaka et al. also demonstrated

reproducibility of CSA measurements with extended field of view USI [98]. USI has also been shown to provide reliable measurements even with different operators, showing high intra- and inter-operator reliability [93, 99], although it should be noted that a standardised protocol is necessary to achieve reliable measurements [91, 92].

Despite the overwhelming evidence that USI is capable of accurately measuring muscle size, there are some studies which show moderate or poor agreement with MRI measurements. This could be caused by differences in imaging planes between modalities [90], or the position of the muscle being imaged, for example the upper portion of the anterior thigh best reflects the size of adductor muscle [100].

In pennate muscles, another important measurement is the pennation angle, which describes the arrangement of the muscle fibres. This measurement can also be obtained with good intra- and inter-operator reliability [101]. Recently, similarly consistent results have been seen for measurements of echo intensity both between operators and measurements made on different days [98, 102].

2.3.1.2 Changes in muscle architecture related to muscle activity

During muscle movement, changes occur in architectural parameters that can be captured by USI. As the muscle contracts, fibre length decreases and the pennation angle increases in the gastrocnemius [103], soleus [104] and tibialis anterior [105] muscles, leading to an increase in CSA [103] or thickness [104]. This occurs both as the result of an isometric contraction at a fixed joint angle and a passive change in joint angle while the muscle is at rest [103]. However, there are also differences between passive and active movements [106, 107]. This is due to the behaviour of the muscle-tendon complex which consists of both muscle fibres, which are considered to be the contractile components, and the tendon, which is often equated to series elastic components. The tensile response of the tendon is also thought to be responsible for changes in muscle behaviour during repeated isometric contractions [108].

USI has been used to evaluate muscle behaviour during treadmill walking, demonstrating the muscle's ability to conserve energy and the ability of the tendon to store and release energy [109]. Imaging of the gastrocnemius medialis muscle at proximal, distal and midbelly sites showed that the same actions are performed along the length of the muscle, however, the distal fascicles shorten more and act at a greater pennation angle than the more proximal fascicles [110]. While the muscle fascicles behave relatively isometrically during the stance phase of walking [109, 110], they shorten during this phase when running, most likely due to increased strain on the series elastic elements [110].

Dynamic measurements of these parameters allow for the contraction velocity to be calculated. The shortening velocity of fascicles appears to be dependent on the force applied, which is thought to be a result of elongation of the tendon [111]. During isokinetic concentric contractions of the tibialis anterior muscle, the fascicle length increases and pennation angle decreases

curvilinearly with angular velocity, reflecting the degree of stretch applied to the series elastic component. In contrast, during eccentric contraction, fascicles contract quasi-isometrically regardless of velocity, suggesting the series elastic components act as a mechanical buffer during active lengthening [105].

Dynamic changes in muscle architecture have been shown to be related to the electrical activity of the muscle, as measured by EMG. During low level isometric contractions, a small increase in muscle activity shows a large change in architectural parameters including thickness, fascicle length and pennation angle. However, at higher levels of contraction there is very little further change in muscle architecture. This non-linear relationship with muscle activity means that architectural parameters can provide a measure of activity for low-level contractions but are not able to distinguish between moderate and high levels. Changes in these parameters also appear to be more sensitive to changes in activity in the limb muscles compared to abdominal muscles [112].

The onset of a muscle contraction detected by M-mode USI has been found to be closely related to EMG-measured onset, allowing measurements from deep muscles non-invasively [113, 114]. However, there is some variation which may be caused by heterogenous motor unit recruitment with immediate motion transmission [115]. A more recent study by Tweedell et al. has advised caution and it has shown USI detected muscle onsets before surface or fine wire EMG methods, possibly due to movement in adjacent muscles [116].

The force generated by a muscle is regulated by the recruitment of motor units and varying the firing rate. Motor unit recruitment is non-uniform in terms of spatial distribution, however, different parts of the muscle are dominantly active depending on force level, and can also vary over time during sustained contractions. This has been found from electromyography, however, a similar result can be obtained by recording ultrasound and estimating M-mode strain from the velocity of the tissue [117]. Chen et al. showed that a different relationship exists between torque and changes in muscle CSA recorded by USI than that which exists between torque and electrical activity of the muscle, as recorded by EMG [118].

A study by Shi et al. demonstrated the feasibility of continuous signals from USI and EMG to provide a more comprehensive assessment of muscle activity [119]. This led to the use of USI to measure changes in muscle thickness as the result of fatigue during a sustained isometric contraction [120–122]. Changes in fascicle length and pennation angle suggested tendon creep could be a potential mechanism during fatigue [121], however a follow up study did not find any changes in tendon compliance [122].

In addition to muscle activity, USI has also been used to investigate the transmission of force between different muscles [123]. The curvature of fascicles can be measured as an indication of internal pressure within the muscles. A study by Wakeling et al. found that in the gastrocnemius muscle, fascicles followed an S-shape trajectory in the superficial-to-deep direction, with positive curvatures in the superficial region, negative curvatures in the deep region and intermediate

values in the central portion of the muscle [124]. The application of pressure was associated with greater negative curvatures in the distal and central regions of the middle layer but did not seem to affect the superficial and deep layers.

A factor which is not well reported in the literature but should also be considered is the effect of a muscle contraction on acoustic impedance compared to when the muscle is in a relaxed state. As discussed in Section 1.4 of Chapter 1, the entire basis of image formation using ultrasound is dependent on differences in acoustic impedance between different tissues resulting in soundwaves being reflected back to the transducer. It therefore follows that when the muscle contracts, changes in the stiffness of the muscle could have an effect on the acoustic impedance and consequently the image obtained. A study that applied shear acoustic waves to a phantom mimicking skeletal muscle found that increasing the fibre tension resulted in the increased velocity of shear wave propagation along the fibres. However, in the case of wave propagation across fibres, the effects of increased tension were negligible [125]. It is also possible that any changes in acoustic impedance due to muscle contraction are small compared to the difference in acoustic impedance between the muscle and the surrounding tissue. Overall, the wide range of studies demonstrating the ability of USI to visualise changes in muscle morphology during a contraction suggest that any changes in acoustic impedance are not sufficient to limit its use.

2.3.2 Detection of neuromuscular disorders

The use of USI to detect neuromuscular disorders began in 1980 with the pioneering work of Heckmatt [126], who demonstrated an increase in muscle echogenicity in children with muscular dystrophy and developed a widely adopted semi-quantitative scale for grading echo intensity. Soon after, USI was shown to be a useful screening tool for detecting muscle abnormalities in a range of neuromuscular disorders [127].

Advances in technology led to more complex qualitative assessment methods based on pattern recognition to differentiate between myopathic and neurogenic changes [128], as well as the development of quantitative approaches based on digital image analysis [129, 130]. This ranges from simple histogram plots that quantify the overall brightness of the image [131], to more recent measurements of texture, which have been shown to provide an estimate of muscle quality [132].

Quantitative analysis of muscle echogenicity based on a histogram plot has been shown to improve sensitivity and interobserver agreement [131] when compared to the traditional Heckmatt criteria [126]. Muscles have a speckled or striated appearance in USI and the signal strength is highly variable depending on the arrangement of muscle fascicles which can make visual inspection difficult. In contrast, there are also some disadvantages to quantitative analysis, namely it has been found to decrease specificity. Furthermore, quantitative analysis is often more-time consuming and relies on normal values for the particular ultrasound device. This makes it more suitable for research purposes and potentially limits its use in a clinical setting [131].

The increase in muscle echogenicity is the result of an increase in reflective surfaces, generally attributed to a combination of factors including an increase in fibrous connective tissue, infiltration of fat, as well as swelling and odema. The contribution of each of these factors to the overall increase in echogenicity is largely unknown, however, one study has shown that an increase in fibrosis, where the amount of interstitial fat was negligible, is sufficient to increase echogenicity [133].

While changes in muscle echogenicity and thickness occur in neuropathies [134] just as with myopathies, they are also often associated with spontaneous muscle activity. The dynamic nature of USI combined with recent improvements in resolution make it well-suited to detect such disorders. Several studies have demonstrated the ability of USI to detect these extremely small muscle movements known as fasculations, or fibrillations when referring to single fibres. Overall it is agreed that USI is able to visualise the spontaneous movements, however, there are some differences in sensitivity and specificity when compared with EMG and it is possible that each methodology is detecting different events. This has led to the conclusion that USI and EMG provide complementary information and their integration could improve detection of small muscle movements associated with neuropathic disorders [135–137].

Although not as the direct result of a neuromuscular disorder, a similar increase in muscle echogenicity is seen in people who are hospitalised for prolonged periods [138–140]. This has been shown to be accompanied by increased homogeneity, indicative of a breakdown in muscle structure [138], increased thickness of subcutaneous tissue [138] and detection of spontaneous muscle activity [139]. In one case, the increase in echogenicity was strongly correlated with measurements of muscle strength [140], suggesting this may be an alternative for assessing muscle weakness in patients who are unable to perform voluntary strength testing. USI has also been validated against MRI as a suitable tool to measure the reduction in muscle cross-sectional area due to bed rest over a longer time period [141]. Similarly, measurements of muscle architecture including thickness and pennation angle have been shown to be related to functional capacity in hospitalised older adults [142].

Another early application of USI which began in the 1980s is measuring the decline of muscle mass associated with muscle weakness in older people, also known as sarcopenia [143]. Sarcopenia is commonly diagnosed by DXA and MRI measurements of muscle mass, however USI could provide a suitable alternative which is low cost, portable and does not involve radiation [144]. Over the years several studies have demonstrated its ability to detect changes in muscle architecture, including a reduction in muscle thickness [145–147] and fascicle length [145]. These changes in architecture have even been shown to be associated with strength and functional capacity [146, 148]. Echo intensity has also been shown to increase with age [149] and is thought to reflect the strength of the muscle [147, 150], but not the endurance [150]. USI has been shown to be a reliable method for assessing muscles in sarcopenia, with high test-retest reliability [151], however results are more reliable if corrected for subcutaneous fat [152].

2.3.3 Skeletal muscle ultrasound in rehabilitation

Since USI was first used to visualise skeletal muscles, it has been utilised to assess the effects of exercise in able-bodied people. Training of muscles leads to an increase in muscle size [111, 153, 154], which is often underestimated by measurements of limb circumference, highlighting the importance of direct measurements of muscle size [153]. In pennate muscles, an increase in pennation angle is also seen [111, 153], which has been shown to have a strong correlation with muscle thickness [111].

Following this demonstration of USI's ability to detect changes induced by exercise in the able-bodied population, its applications were extended to the rehabilitation interventions of sarcopenia [155], stroke [156] and spinal cord injury [157]. It was also used to demonstrate the use of electrical stimulation to preserve the thickness of chest and abdominal muscles in ventilated patients in an intensive care unit [158].

In addition to measurements of muscle size, USI provides a unique tool that allows muscle contractions to be visualised in real time by both patients and therapists. This could allow therapists to incorporate a physical demonstration into their explanations of subtle changes in motor control and function, as well as offering a biofeedback tool which provides information on performance [25]. USI has been used to assess muscle movement in lateral epicondylalgia [159] and the activation of trunk muscles during exercise [160].

2.4 Neuromuscular Electrical Stimulation

2.4.1 Rehabilitation

There are several clinical applications of neuromuscular electrical stimulation (NMES) for neurological rehabilitation. Electrical stimulation can be used to perform a functional task, often referred to as functional electrical stimulation (FES). It can also be used to provide therapeutic benefits such as motor relearning or cardiovascular conditioning, which can enhance function indirectly [31, 32, 36].

2.4.1.1 NMES for functional movements

Following a SCI, the loss of volitional motor control can greatly affect a person's ability to perform everyday tasks. This affects their ability to live independently and can have a huge impact on their overall quality of life. NMES artificially excites the motor neurons, causing paralysed muscles to contract. By activating specific muscles in a particular sequence and with precise control over the timing and magnitude of stimulation, functional movements can be produced [32].

In applications involving the upper limb this generally involves facilitating reaching and grasping motions. This allows essential daily tasks such as feeding and grooming to be per-

formed, which can greatly improve independence. Lower limb systems are used to produce standing and stepping motions, allowing ambulation over short distances and gait training. Implantable systems can be used to stimulate the bladder, and pacing of the phrenic nerve or diaphragm allows for respiratory control [32, 36].

2.4.1.2 NMES for exercise

Neuromuscular diseases are characterised by progressive muscle weakness and loss of function. In such cases the primary clinical goal is to maintain or improve strength and functional capacity in order to maintain independence and quality of life. This can often be achieved through exercise, with strength training to increase the size and strength of the muscle, and aerobic exercise to improve endurance and cardiopulmonary function [161, 162]. This is particularly important in the SCI population as the limited ability to perform volitional movement leads to an overall decline in the level of activity. As previously discussed, SCI greatly affects skeletal muscles, however the lack of physical activity leads to a number of secondary complications, such as diabetes, hypertension and cardiovascular disease. Exercise has been shown to be effective in slowing or in some cases even reversing many of these secondary complications, therefore regular exercise is essential for maintaining a healthy lifestyle following a SCI. Depending on the level and completeness of the injury, electrical stimulation may be required to perform exercise [163, 164].

Strength training performed through the use of NMES has been shown to reverse some of the effects of atrophy including the fibre type transformation from type I to type II [32]. An increase in muscle mass, strength and endurance occurs as the result of resistance training [165]. NMES can also be used to perform aerobic exercises, for example stimulation of the quadriceps and hamstrings to produce sub-tetanic contractions was shown to increase oxygen consumption and heart rate [166]. NMES is often used to perform cycling, which can be achieved through stimulation of the quadriceps, gluteus maximus and hamstring muscles. This has been shown to improve cardiopulmonary function [32], with increased endurance after 3 months of training [167]. Body composition also improved after 10 weeks, showing increased lean muscle mass, lower blood glucose and insulin levels and even improved ASIA motor and sensory scores in the lower limbs [168].

2.4.1.3 Limitations

Despite the wide range of applications for NMES, there are limitations to its use. The most important of these limitations is the early onset of muscle fatigue, which occurs due to alterations in muscle fibre recruitment [36]. NMES-induced contractions are not as efficient as voluntary movements and the differences between the two are discussed in detail in Section 2.4.2.

NMES is also limited by the spatial recruitment of motor units, only recruiting those that lie within the electric field. Moreover, current must travel through subcutaneous tissue to activate

motor units. This limits the depth of penetration, resulting in the activation of superficial motor units which are in close proximity to the electrodes. Increasing the current amplitude or the pulsewidth can increase the depth of penetration and therefore recruit motor units which are further away, however, this is limited by discomfort and early onset of fatigue. Conversely, the depth of penetration can also be a limiting factor if it is so great that it results in co-activation of antagonist muscles [31, 36].

2.4.2 Voluntary vs. NMES contractions

During voluntary movement, motor units are recruited according to the size principle [169], whereby motor units are recruited in progressive order of size, i.e. smaller motor units are recruited first, before larger ones. As smaller motor units are more resistant to fatigue, this delays the onset of fatigue for the overall muscle. This is not the case during NMES-induced contractions. It has been reported that NMES causes a reversal of the size principle, where the larger more fatigable motor units are recruited first. This conclusion is based on the fact that large diameter axons have a lower excitation threshold, and would therefore be recruited first [13, 31, 170]. Since large motor units are generally thought to innervate fast-twitch fibres which are more fatigable, this would explain the excessive fatigue observed during electrical stimulation [13, 170]. However, it is now more widely accepted that recruitment is random and non-selective, rather than an exact reversal [31, 36].

During voluntary contractions, there is a highly efficient system of recruitment and derecruitment. The firing rate of motor units can be increased to offset fatigue. Furthermore, motor units which are fatigued can be derecruited and replaced by different motor units. In contrast, electrical stimulation simultaneously recruits the same motor units over and over again, not allowing for the replacement of fatigued motor units [36].

2.4.3 Modulation of stimulation parameters

Attempts to overcome the limitations of NMES and produce optimal results have focused on the modulation of parameters which control stimulation. The higher the current amplitude, the stronger the depolarising effect on structures below the electrodes. This in turn activates more motor units and leads to stronger contraction with a higher force. When higher pulsewidth values are used, less current is required to activate nerves and achieve the desired force. Muscle fibre recruitment also increases with pulsewidth due to an increase in the depth of penetration [13,36]. An increase in pulsewidth is thought to increase the force produced up to approximately 600 μs, at which point a plateau is reached [13]. Increasing the current amplitude and pulsewidth effectively increase the spatial distribution, a limitation which is previously discussed in Section 2.4.1.3. Other strategies include moving electrodes to recruit different motor units and manipulating the joint angle to change the length of the muscle and consequently changing the position

of the muscle fibres [31].

Higher values of current and pulsewidth may be effective for initially activating motor units and producing a strong contraction, however, this must be balanced against the onset of fatigue, which is reduced with lower values of current and pulsewidth. Comfort also has to be considered, with high current and pulsewidth values less likely to be tolerated. Furthermore, lower current amplitudes result in more central activation as higher current values produce antidromic transmission which blocks motor and sensory impulses [36].

An increase in frequency also leads to an increase in force production. If the frequency of stimulation is too high, the muscle will fatigue quickly, however if it is too low it can also be limited by the phenomenon known as low frequency fatigue. Frequency must also be above a certain level to produce a smooth fused contraction. This is also reported to be more comfortable, with low frequencies often described as a "tapping" sensation. Frequency values which are aligned with the physiological rates of motor discharge are generally successful [13, 36]. It has been suggested that the combination of low frequency and high pulsewidth are effective in reducing fatigue and optimising muscle performance [171], however high frequency trains have been shown to be more effective for repetitive non-isometric tasks [172].

During the application of stimulation, frequency usually remains constant. However, several studies have investigated the use of variable frequency trains (VFT), which begin with an initial doublet, and doublet frequency trains (DFT) which use doublet pulses throughout, in order to exploit the catchlike property of the muscle [36]. Furthermore, it has been shown that switching between different patterns could be a useful strategy for reducing fatigue. A train of constant frequency trains (CFTs) followed by a train of DFTs has been shown to be more effective than either train alone [173]. The effect of stimulation patterns has even been extended to the SCI population, investigating the effectiveness during a strength training application. VFT was found to be less fatiguing than CFT, and when combining stimulation trains it is more effective to use VFT followed by CFT [174].

A study by Graham et al. investigated the effect of randomly modulating stimulation parameters on muscle fatigue [175]. Frequency, current and pulsewidth were all randomised separately, whereby the parameter was altered every 100ms within 15% of a mean value. This did not appear to have an effect on muscle fatigue, however this could be due to insufficient rest time between different modes of stimulation. Another potential strategy is to modulate the frequency by gradually increasing it over time. A stepwise increase in frequency was shown to improve performance by producing higher forces without increasing the rate of fatigue [176]. By varying the stimulation parameters, this is thought to more closely mimic voluntary muscle contractions by activating different motor units.

Another way to activate different motor units is through electrodes placed over different muscles or different areas of the muscle. In an attempt to activate the motor units of the quadriceps asynchronously, Binder-Macleod and McLaughlin used two pairs of electrodes placed over

different areas of the muscle group (vastus lateralis and vastus medialis) [177]. This highlighted that asynchronous activation can be less efficient under certain conditions. A similar strategy was later applied to FES cycling for persons with a SCI. By alternately stimulating the rectus femoris (RF) and the vastus lateralis (VL) and medialis (VM), the performance can be improved [178]. Another method for activating different motor units is the use of multipad electrodes instead of a single pair of electrodes. In this case several smaller electrodes are placed over the same area that a single electrode would normally cover and are activated asynchronously. This was found to reduce fatigue in the quadricep muscle of six SCI participants [179]. Similarly, Sayenko et al. developed a method called spatially distributed sequential stimulation (SDSS), which distributes the centre of the electrical field over a wide area within a stimulation site [180]. By activating subcompartments of muscles, fatigue tolerance was improved, allowing stimulation to be applied for longer.

Careful consideration of the stimulation parameters is key for obtaining the best results from NMES, however it must also be considered that some optimisation is related to the anatomy of the individual [31]. MRI has been used to map the areas of the muscle which are activated during electrical stimulation, demonstrating an increase in the area of muscle which is activated with increased levels of current, as well as different patterns of activation between voluntary and NMES-induced contractions [181, 182]. USI has been used during the application of NMES [123], however, the purpose of using electrical stimulation was to isolate muscle movements from the effect of synergistic muscles. Overall, little has been done in terms of imaging to understand muscle behaviour during NMES to optimise its use in rehabilitation applications.

2.5 Conclusion

An injury to the spinal cord has a huge impact on skeletal muscles. Not only does it result in reduced muscle movement due to paralysis, but there are also structural changes which occur. Muscle atrophy occurs due to damaged motor neurons or lack of activation; a fibre type transformation occurs making muscles less resistant to fatigue; and there is an increase in intramuscular fat. These structural changes can further impact the contractile properties of the muscle. These changes occur with time after the injury has taken place, therefore accurate assessment of muscles is important for providing an accurate prognosis and monitoring recovery.

Currently muscles are assessed by manual muscle testing as part of the ASIA impairment scale. As this is a subjective test with limited sensitivity, a need for more sensitive and quantitative tests is recognised, however, other methods such as EMG are also limited in their ability to distinguish between different muscles or obtain measurements from deeper muscles non-invasively. Several imaging techniques, particularly MRI, have been investigated. These methods are capable of detecting a reduction in muscle size due to atrophy and an increased fat content, however, cost and accessibility often limit their use to research.

USI is a potential additional tool which has been shown to be useful for assessing skeletal muscles. Not only can it provide accurate measurements of muscle morphology, but its dynamic nature also allows muscle movement to be measured. As a result, it is widely used as a screening tool for the detection of various neuromuscular disorders, however, to our knowledge its use for assessing muscles following a SCI is limited to a single study [86].

A further potential use of USI is to gain a better understanding of muscle behaviour during the application of NMES, which is a useful technique in the rehabilitation of paralysed muscles. It can improve muscle strength and allow functional movements to be performed, however, its use is limited due to the early onset of fatigue. This is attributed to differences between voluntary and NMES-induced activation, however, the exact mechanisms are still not fully understood. Several attempts have been made to reduce fatigue and improve performance, however the use of imaging to better understand the effects on the muscle are limited.

Chapter 3

Experimental Methods

3.1 Summary

This chapter introduces the main methods used throughout this PhD project. First, the techniques which are most commonly used throughout all studies are explained, providing general information on the equipment. Following that, experimental methods for all studies are presented, describing the participants involved, the experimental setup, and the details of data acquisition and procedures specific to each study. Detailed analysis methods are presented in the Methods section of the relevant chapters. Data from each study is analysed in the following chapters:

- **Study 1** describes how ultrasound imaging (USI) videos of the gastrocnemius medialis muscles are obtained from a group of spinal cord injury (SCI) patients and a group of able-bodied age and gender matched controls. Data obtained while the muscle is at rest is analysed in **Chapter 4**, data obtained during attempted voluntary movement is analysed in **Chapter 5**, and data obtained during the application of neuromuscular electrical stimulation (NMES) is analysed in **Chapter 7**. Repeated measurements from the SCI participants are analysed in **Chapter 6**.

- In **Study 2**, USI videos of muscles in the lower limbs of SCI patients were recorded to capture small movements in the acute stage after injury, and are analysed in **Chapter 6**.

- **Studies 3A** and **3B** describe how USI videos were recorded during the application of NMES, investigating the effect of different stimulation parameters and patterns respectively in able-bodied participants. Data from these studies is analysed in **Chapter 7**.

Finally, the general methods used in this investigation but not developed by the researcher are presented here. This includes the operation of an algorithm used to detect and track features in ultrasound videos, greyscale analysis of ultrasound videos to measure muscle echogenicity and statistical considerations used throughout the study.

3.2 Commonly used methods

This section introduces the common methods used throughout this project, including the application of NMES, data acquisition techniques, and synchronisation of the data.

3.2.1 Application of neuromuscular electrical stimulation

Neuromuscular electrical stimulation was delivered by a stimulator (Rehastim v1, GmbH, Germany) through electrodes (PALS, Axelgaard, USA), 5 ×9 cm in size, placed on the skin over the muscle belly in order to induce muscle contractions. This is shown in Figure 3.1a.

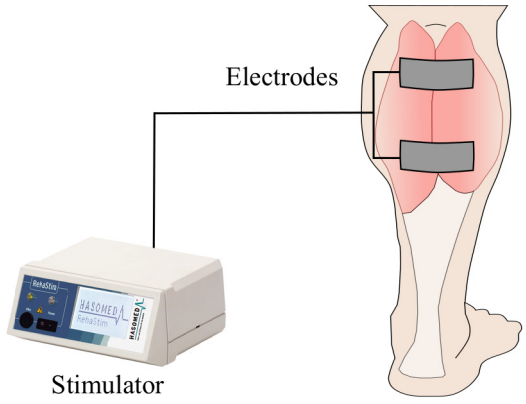

(a) Diagram of setup for application of NMES

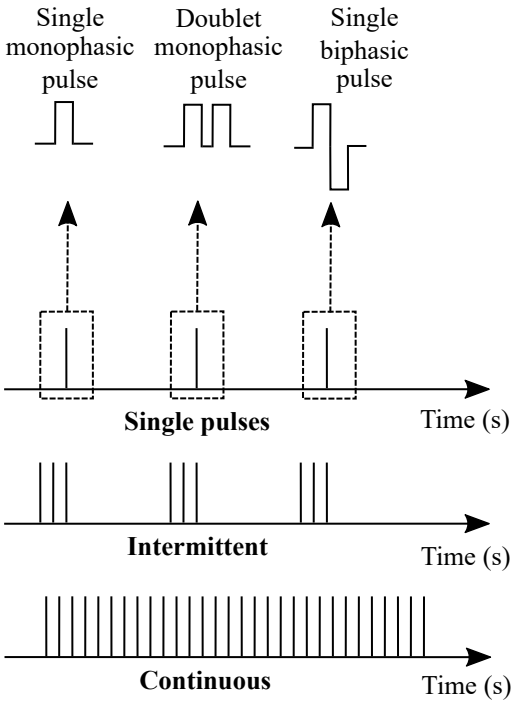

(b) Types of stimulation

Figure 3.1: Overview of the application of neuromuscular electrical stimulation (NMES), including the setup and the different types of stimulation.

Stimulation was controlled through custom-written Simulink models (Mathworks, USA) which allowed stimulation parameters such as the current amplitude, pulsewidth and frequency to be controlled. Throughout the PhD project, these parameters were varied to deliver the desired level of electrical stimulation, details of which are given in the relevant sections of this chapter. Figure 3.1b illustrates how the timing of these parameters can be used to deliver electrical stimulation in single pulses (one pulse per second), intermittently, or continuously.

3.2.2 Data acquisition

3.2.2.1 Ultrasound imaging

Ultrasound videos were recorded using an ultrasound probe (LV7.5/60/96Z - a linear probe with a maximum operating frequency of 7.5 MHz, a field of view of 60 mm and an array of 96 elements), connected to an Echo Blaster 128 ultrasound device (Telemed, Lithuania). Ultrasound videos were recorded in B-mode using Echo Wave II version 3.5.2 software (Telemed, Lithuania). Ultrasound images were recorded at an average rate of 40 fps with a central frequency of 6 MHz and a scanning depth of 50 mm. The exception to this is Study 3B which was recorded with a frame rate of 20 fps to allow longer recordings. A dynamic range of 80 dB, power of 100% and gain of 94% were used to obtain optimal images while avoiding saturation. These values are based on the "automatic adjustment" feature within the software and visual inspection of the image as parameters were adjusted. All scanning parameters were kept constant throughout each study.

The probe was positioned over the belly of the muscle being evaluated. For each muscle the probe was aligned to the mediolateral midline of the muscle at the mid-belly level. Hypoallergenic water-based ultrasound gel was applied between the skin and the ultrasound probe to reduce acoustic impedance mismatch between the probe and tissue.

3.2.2.2 Electromyography (EMG)

The electrical activity of the muscle was recorded by a Bagnoli EMG system (Delsys, USA). A single differential surface EMG sensor was placed over the muscle being evaluated using adhesive sensor interfaces. Alcohol swabs were used to remove oils and surface residue from the skin, ensuring the sensor adhesive interfaces sufficiently bonded to the skin. The sensor houses two bar contacts 10 mm apart which were positioned perpendicular to the longitudinal midline of the muscle for optimal signal detection. A reference electrode was placed over the knee or ankle to provide a neutral site away from the EMG sources. A gain of 1000 was chosen on the main amplifier unit as this is optimal for typical EMG signals in the range of ± 100 μV to ± 5 mV [183].

3.2.2.3 Torque

Ankle torque was recorded using one of two devices:

1. Custom-built force platform

   The platform consists of a single load cell which measures the ground reaction force. It also measures the distance between the edge of the platform and location where force was applied, providing a torque output. The platform housed a custom amplifier which converted the sensor signal into a voltage proportional to the force applied. The gain of the device was calibrated using three weights (0.5kg, 1kg and 5kg). During each experiment the offset was also adjusted for the weight of the foot when the participant was seated. This meant that when the participant was resting their foot on the force platform without pushing on it, the torque output was zero.

2. Dynamometer system

   Biodex System 3-PRO (Biodex Medical Systems Inc., USA) is a commercial dynamometer system. This device has an analogue signal range of -5 to +5 volts i.e. 10 V and a maximum torque range of -512 ft-lbs to +512 ft-lbs i.e. 1024 ft-lbs. This results in an output resolution scale factor of 9.8 mV per ft-lb, however, this is less than the signal to noise ratio (15-35 mV). A range of $\pm$ 64 ft-lbs is therefore used instead, resulting in a resolution scale factor of 78.1 mV, to allow small torque values to be readily seen [184]. The torque accuracy is $\pm$1% of the full scale (512 ft-lbs).

   Again the offset was adjusted for the weight of the foot resting on the foot plate so when the participant was not pushing against it, the torque was zero.

3.2.2.4 Joint angle

A twin axis goniometer (Biometrics, USA) was used to measure changes in joint angle in two planes. The sensors were attached on either side of the joint using double-sided medical adhesive tape. As movement of the joint occurs, measurements from strain gauges mounted between the two endblocks are equated to the angle. This device has range of $\pm 150^\circ$ and a resolution of 0.1°. It also has an accuracy of $\pm 2^\circ$ over a range of $\pm 90^\circ$ and repeatability of 1° measured over over a range of 90° [185].

3.2.2.5 Synchronisation of data

Throughout this investigation, torque, EMG and joint angle were recorded synchronously through the same data acquisition method (DAQ). Ultrasound on the other hand was recorded using the custom software Echo Wave II, as discussed in Section 3.2.2.1. This is shown in Figure 3.2.

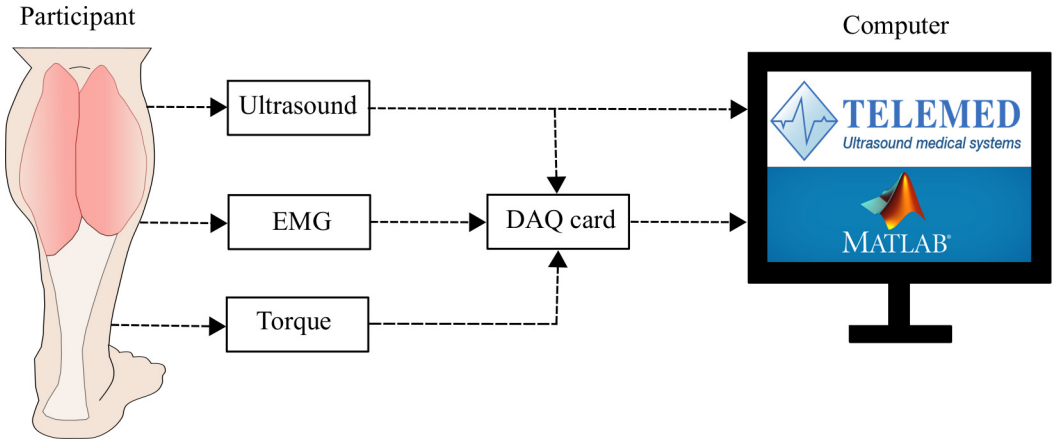

Figure 3.2: Diagram of data acquisition. Torque, electromyography (EMG) and a 5 volt signal from the ultrasound device are recorded through a data acquisition (DAQ) card and the ultrasound video is recorded separately through Echo Wave software.

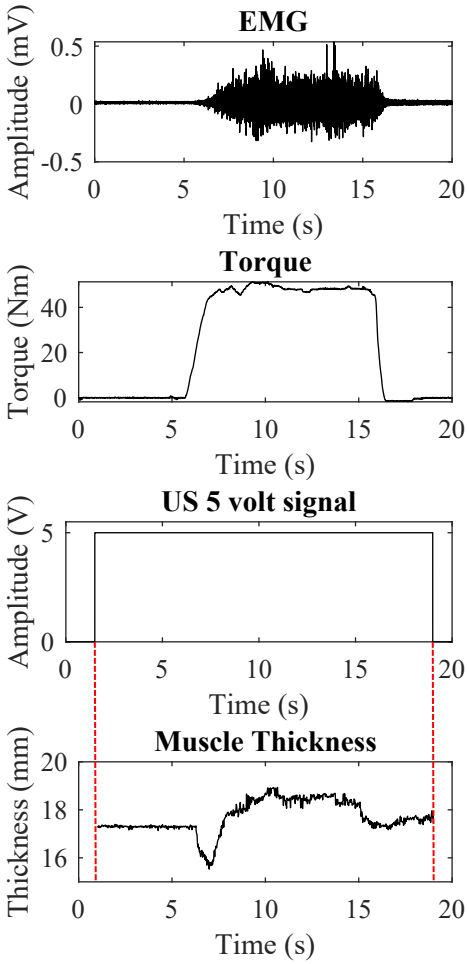

Figure 3.3: An example of the electromyography (EMG), torque and 5 volt ultrasound (US) signal recorded through the data acquisition card and the muscle thickness calculated from the video recorded with Echo Wave software.

To enable the ultrasound videos to be aligned with recordings of these other signals, a digital output from the ultrasound system was also recorded with the same data acquisition method. This provided a signal which showed whether the ultrasound was recording (5 volts) or not (0 volts). As this signal is already aligned with the other signals, it allows measurements from the ultrasound videos to be synchronised with measurements of torque, EMG and joint angle as shown in Figure 3.3.

The open source B to Lines 1.1.2 package (Telemed, Lithuania) was used to obtain binary files containing time stamped data. This is used to account for the variable frame rate of ultrasound imaging.

3.3 Experimental methods for Study 1

During this study, the USI measurements from the gastrocnemius muscle were obtained under different conditions from a group of able-bodied and a group of SCI participants. The data obtained was analysed in three different ways:

- **Cohort study:** comparison of able-bodied and SCI participants
- **Cross-sectional study:** comparison of different groups of SCI participants based on time post-injury or muscle function
- **Longitudinal study:** changes in SCI participants over time

3.3.1 Participants

Fifteen participants with a spinal cord injury (9 male, 6 female, 55 $\pm$ 18 years (mean $\pm$ SD)) and fifteen able-bodied participants of the same gender and comparable age (54 $\pm$ 16 years (mean $\pm$ SD)) were recruited for this study. SCI participants were inpatients at the Queen Elizabeth National Spinal Injuries Unit, Queen Elizabeth University Hospital who had an incomplete spinal cord injury affecting their lower limbs and were expected to remain inpatients for at least 3 months. Able-bodied participants were in self-reported good health with no known neuromuscular disorders.

3.3.2 Experimental setup

The experimental setup for this study is shown in Figure 3.4. Participants were seated comfortably on the chair of a dynamometer in an upright position. The right leg was elevated with a limb support under the thigh. The hip was flexed at an angle of approximately 135°and the knee was extended, allowing the lower leg to be positioned parallel to the ground. The foot rested on

the foot plate of the dynamometer with the heel supported and the ankle in the neutral position. A Velcro strap was wrapped around the foot to minimise ankle movements.

An ultrasound probe was positioned over the belly of the medial gastrocnemius muscle. Surface EMG electrodes were also placed over the medial gastrocnemius alongside the ultrasound probe, with a reference electrode placed over the ankle. A pair of NMES electrodes were placed over the back of the calf, covering both the medial and lateral gastrocnemius.

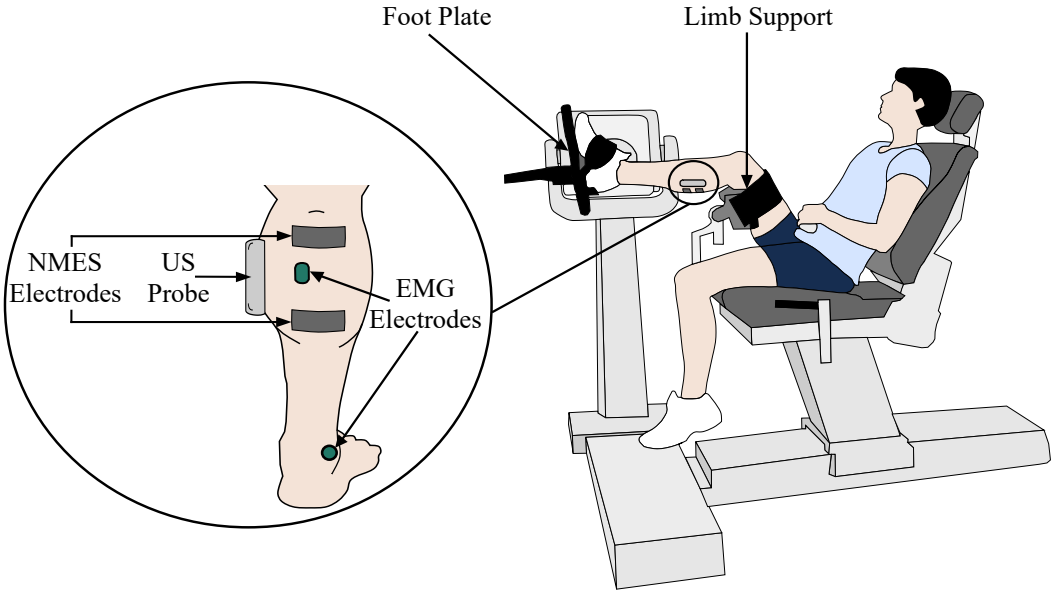

Figure 3.4: Experimental setup for Study 1 showing the participant seated on the chair of a dynamometer with their foot resting on the foot plate. A pair of NMES electrodes are positioned over the gastrocnemius muscle with the ultrasound probe and EMG electrode placed on the medial side.

3.3.3 Data acquisition

An ultrasound device was used to record videos of the medial gastrocnemius muscle, ankle torque was recorded using a dynamometer system and EMG recorded the electrical activity of the muscle, as described in Section 3.2.2. The dynamometer, the EMG device and the ultrasound were connected to a data acquisition board (DAQcard-6036E, National Instruments, USA) which digitised the signal at a frequency of 1000 Hz. The custom-written MATLAB scripts and Simulink models (R2014b, The Mathworks, USA) used to run this experiment are provided in Appendix A.1.

3.3.4 Experimental protocol

3.3.4.1 Overview

During each session, measurements were taken while the muscle was in the resting state, during NMES, and during attempted voluntary activation. An overview of a single session is shown in Figure 3.5. Participants in the SCI group completed monthly sessions until they were discharged, all completing at least three sessions except for one participant, who withdrew from the study after only two sessions. Each of the able-bodied participants completed a single session.

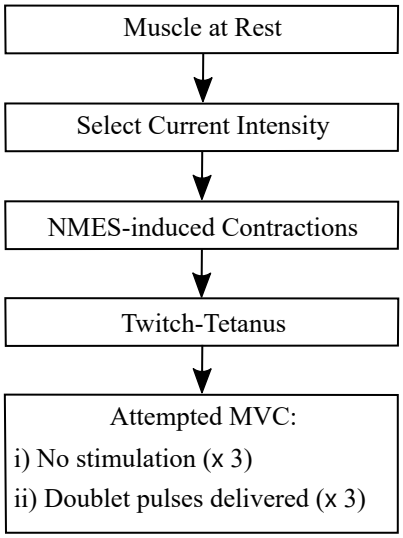

Figure 3.5: Flowchart showing the organisation of Study 1: First measurements were made while the muscle was at rest; then the current intensity was selected, followed by the application of neuromuscular electrical stimulation (NMES) to produce smooth contractions and a twitch-tetanus; finally, maximum voluntary contractions (MVCs) were attempted.

3.3.4.2 Muscle in resting state

Ultrasound videos were recorded for 30 seconds while the muscle was in a resting state. Participants were not required to do anything but were instructed to remain as still as possible.

3.3.4.3 Muscle during NMES-induced contractions

1. **Current selection:** A series of doublet pulses were delivered at 5 second intervals. The first pulse had a current of 2mA and each subsequent pulse increased by 2mA until the torque produced no longer increased or the maximum level that was tolerable to the participant was reached, as demonstrated in Figure 3.6.

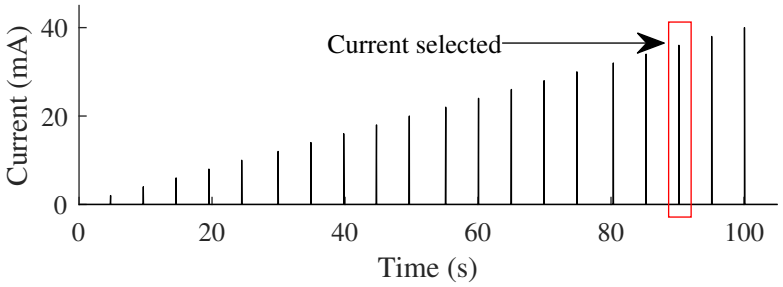

(a) Current

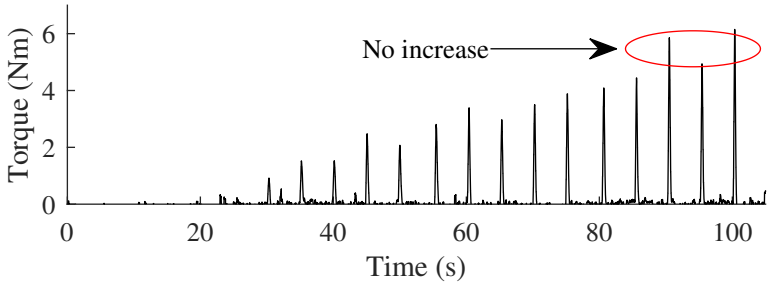

(b) Torque

Figure 3.6: An example of the current applied and the torque produced during the current selection process.

2. **NMES-induced contractions:** Electrical stimulation was delivered to produce four muscle contractions as shown in Figure 3.7. The current value selected for the participant was used with a standard frequency value of 40 Hz and pulsewidth value of 300 μs. Each train of stimulation consisted of a ramp up (lasting 2.5s), constant (lasting 5s) and ramp down phase (lasting 2.5s), with the entire contraction lasting 10 seconds in total. Each train of stimulation was separated by a 5 second rest period.

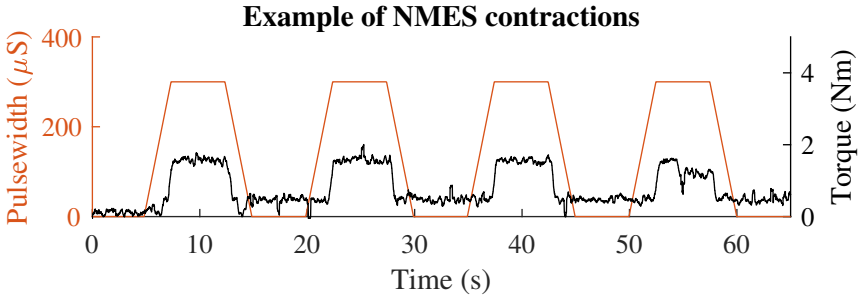

Figure 3.7: An example of the pulsewidth and the torque produced during four contractions induced by electrical stimulation at the selected current value.

3. **Twitch-tetanus:** Three single pulses were delivered 5 seconds apart, each producing a single twitch. This was followed 10 seconds later by a 0.5 second train of pulses, delivered at a frequency of 20 Hz to produce a low frequency tetanic contraction. A further 10 seconds later another 0.5 second train of pulses was delivered at a frequency of 80 Hz

to produce a high frequency tetanic contraction. A diagram of the stimulation and an example of the torque produced is shown in Figure 3.8.

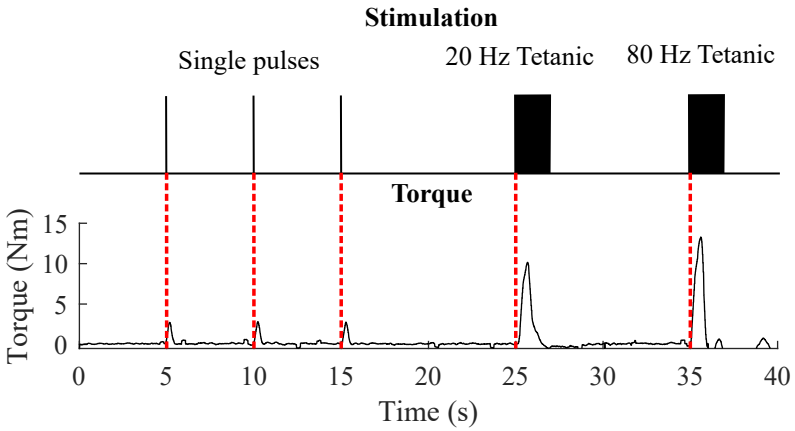

Figure 3.8: Diagram of the stimulation applied and an example of the torque produced during a twitch-tetanus.

3.3.4.4 Muscle during attempted maximum voluntary contraction

Participants attempted to perform an isometric maximal voluntary contraction (MVC) in this part of the protocol. These attempted contractions lasted approximately 10 seconds with verbal cues instructing the participants when to start and when to stop. This was done three times each under two conditions:

- No electrical stimulation is applied.
- A doublet pulse of stimulation is delivered before the MVC is attempted, while the muscle is at rest, followed by a second doublet pulse during the attempted MVC.

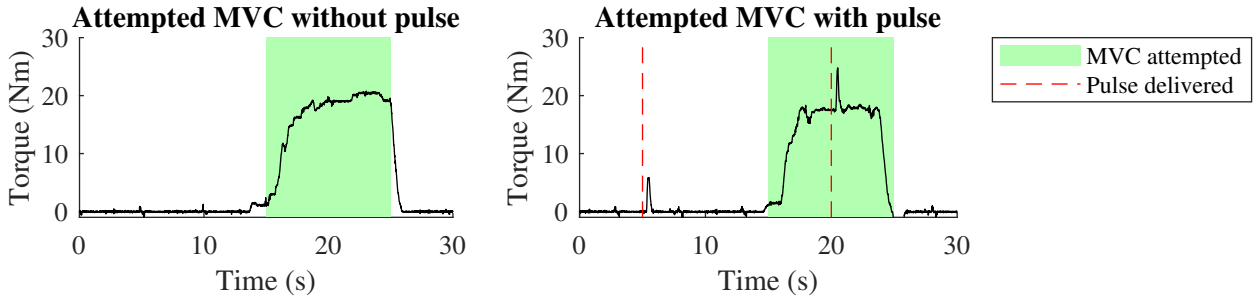

(a) No electrical stimulation

(b) Pulses of electrical stimulation delivered at t=5s and t=20s

Figure 3.9: An example of the torque produced during an attempted maximum voluntary contraction (MVC) with and without electrical stimulation (shown by the dashed red line).

3.4 Experimental methods for Study 2

The main focus of this study was the detection of small muscle movements in the acute stage of a SCI. USI was compared to other techniques including EMG, manual muscle testing (MMT) and changes in joint angle during attempted movement. These measurements were repeated over time and related to recovery.

3.4.1 Participants

Six participants with a spinal cord injury (3 male, 3 female, 41 $\pm$ 17 years (mean $\pm$ SD)) participated in this study. Participants were inpatients at the Queen Elizabeth National Spinal Injuries Unit, Queen Elizabeth University Hospital who were less than 1 month post-injury and had no visible movement in at least one of the key muscles in the lower limbs (gastrocnemius medialis, tibialis anterior and rectus femoris).

3.4.2 Experimental setup

Figure 3.10 shows the experimental setup for this study. Participants were in the supine position while three muscles on both the right and left leg were examined: gastrocnemius medialis (GM), tibialis anterior (TA) and rectus femoris (RF). The position of the leg was dependent on the muscle being examined:

- GM: Hip in external rotation and approximately 45 degrees of flexion. Knee is flexed.
- TA: Hip in neutral rotation, knee fully extended and the ankle slightly plantarflexed.
- RF: Hip in neutral rotation, natural flexion of the hip and knee at approximately 15 degrees.

During examination of each muscle, an ultrasound probe and surface EMG electrodes were positioned over the belly of the muscle, with an EMG reference electrode placed over the knee. A goniometer was also placed across the ankle joint during examination of the GM and TA muscles, and across the knee during examination of the RF muscle.

3.4.3 Data acquisition

Ultrasound videos and EMG were recorded for the medial gastrocnemius, tibialis anterior and rectus femoris muscles on both legs, and the angle of the knee and ankle joints were also recorded using a goniometer as described in Section 3.2.2. A handheld button was used to deliver a 5 volt trigger signal by pressing the button when participants attempted to perform the muscle movement. This allowed the timing of the attempted movements to be recorded.

The trigger signal along with the signal from the ultrasound, EMG and goniometer devices was recorded using a USB analogue input module (USB-6216, National Instruments, USA) which digitised the signal at a frequency of 2000 Hz. The MATLAB scripts and application created in the Matlab App Designer (R2019a, The Mathworks, USA) used to run this experiment are provided in Appendix A.2.

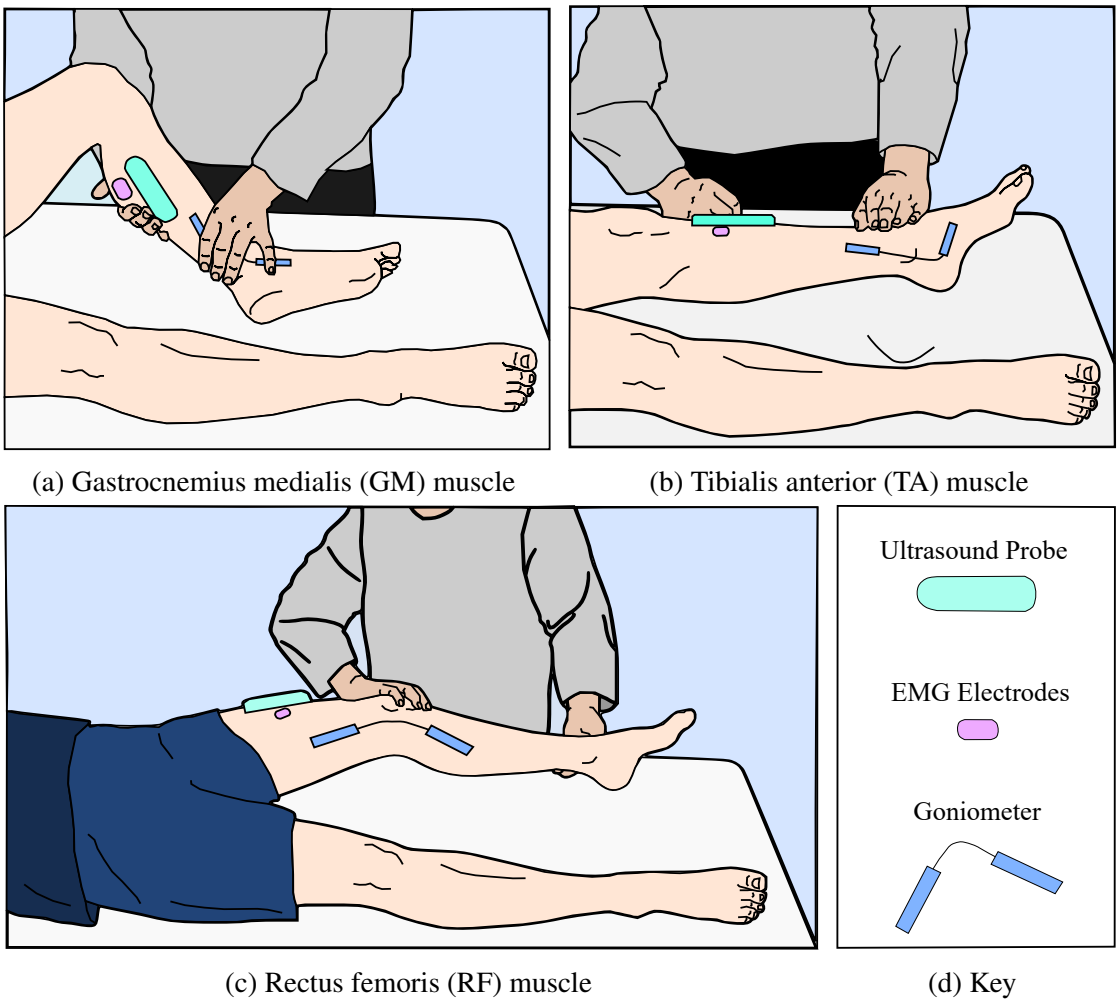

(a) Gastrocnemius medialis (GM) muscle

(b) Tibialis anterior (TA) muscle

(c) Rectus femoris (RF) muscle

(d) Key

Figure 3.10: Experimental setup for Study 2 showing the different positions of the participant's leg and the placement of the ultrasound probe, EMG electrodes and goniometer sensors for each muscle. Adapted from [4].

3.4.4 Experimental protocol

3.4.4.1 Overview

Manual muscle testing was performed by a trained physiotherapist. Following this, ultrasound videos, EMG and joint ankle were recorded for each of the three muscles on the right leg, and then the left leg.

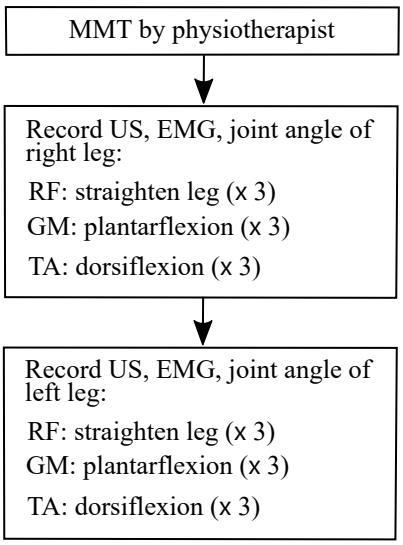

Figure 3.11: Flowchart of the organisation of Study 2. Manual muscle testing (MMT) was performed by a physiotherapist before recording ultrasound (US), electromyography (EMG) and joint angle in the rectus femoris (RF), gastrocnemius medialis (GM), and tibialis anterior (TA) muscles of each leg.

3.4.4.2 Manual muscle testing

Manual muscle testing [3, 4, 83] was performed separately by a trained physiotherapist. The ability of the muscle to generate a contraction was graded as follows:

- 0 = no muscle movement is detected i.e. total paralysis
- 1 = a small contraction is detected either visually or by palpating the muscle
- 2 = active movement can be detected in the form of a full range of motion performed with gravity eliminated
- 3 = active movement can be detected in the form of a full range of motion against gravity
- 4 = active movement can be detected in the form of a full range of motion against gravity and moderate resistance in a muscle specific position
- 5 = active movement expected from an otherwise unimpaired person, with a full range of motion performed against gravity and full resistance in a functional muscle position.

The position of the participants described in Section 3.4.2 was the same as the position used during manual muscle testing for distinguishing between grades 0 and 1. This was chosen because participants were only recruited to the study if at least one of the muscles being examined had no visible or palpable movement i.e. a grade 0. However, some participants may have had higher grades in other muscles being examined and as patients recover there is potential for MMT scores to increase. In this case, the position would be adapted as necessary, following the standard procedures to incorporate the effects of gravity and resistance.

3.4.4.3 Description of attempted movement task

Ultrasound videos, EMG and changes in joint angle were recorded while the muscle was in a relaxed state and during an attempted movement specific to each muscle. The GM muscle was evaluated during attempted plantarflexion of the foot, where participants were instructed to point their toes downwards. To assess the TA muscle, participants attempted dorsiflexion of the ankle, following instructions to point their toes upwards towards their head, letting their ankle bend. During evaluation of the RF muscle, participants were asked to straighten their leg from a bent knee position.

Each movement was carefully explained to the participants to ensure the muscle which was being evaluated was used to attempt the movement. EMG was recorded on three channels, one for each of the muscles on one leg. This allowed compensatory movements performed by other muscles to be identified.

Participants were given a verbal cue when to start and stop attempting the movement. The attempted movement of each muscle was performed three times for approximately 10 seconds each. There were rest periods of approximately 10 seconds between each attempted movement and participants were also given the opportunity to rest between assessment of different muscles.

3.4.4.4 Timing of assessment sessions

Participants took part in 5 assessment sessions over 12 weeks. As shown by the timeline in Figure 3.12, there were 2 weeks between each of the first three sessions and 4 weeks between the last two sessions. The first three sessions were carried out at intervals of 2 weeks to obtain data from those who may recover quickly within the first month after injury. During each session muscle movement was assessed by the traditional qualitative technique of manual muscle testing (MMT) and measured quantitatively by recording ultrasound videos, EMG and changes in joint angle.

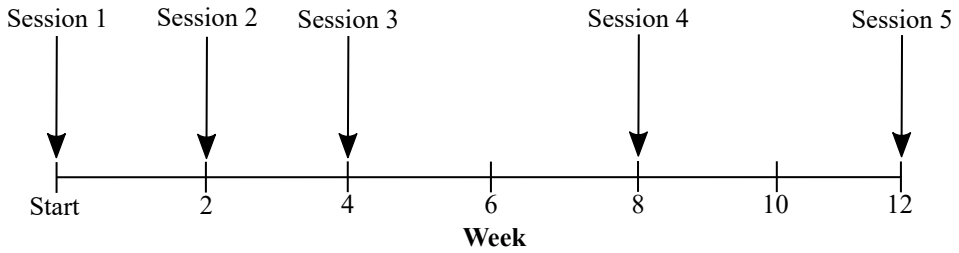

Figure 3.12: Timeline of assessment sessions for Study 2.

3.5 Experimental methods for Study 3A

This study was designed to investigate the effect of different stimulation parameters on muscle behaviour by applying different combinations of current, pulsewidth and inter-pulse interval. It also compared the application of constant stimulation parameters and patterns of variable pulsewidth and inter-pulse interval.

3.5.1 Participants

Eleven able-bodied participants (1male, 10 female, age 34 $\pm$ 12 years (mean $\pm$ SD)) in self-reported good health with no known neuromuscular disorders took part in this study.

3.5.2 Experimental setup

The experimental setup for this study is shown in Figure 3.13. Participants were seated comfortably on the chair of a dynamometer in an upright position. The right leg was elevated with a limb support under the thigh. The hip was flexed at an angle of approximately 135°and the knee was extended, allowing the lower leg to be positioned parallel to the ground. The foot rested on the foot plate of the dynamometer with the heel supported and the ankle in the neutral position. A Velcro strap was wrapped around the foot to minimise ankle movements.

An ultrasound probe was positioned over the belly of the right medial gastrocnemius muscle. A pair of NMES electrodes was also placed over the back of the calf, covering both the medial and lateral gastrocnemius.

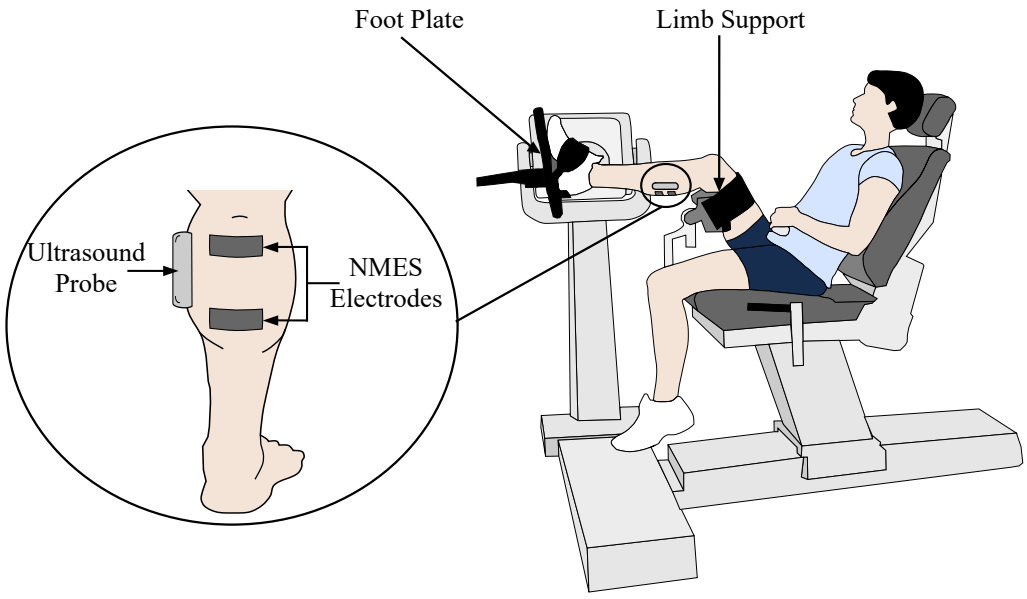

Figure 3.13: Experimental setup for Study 3A showing the participant seated on the chair of a dynamometer with their foot resting on the foot plate. A pair of NMES electrodes are positioned over the belly of the gastrocnemius muscle with the ultrasound probe placed on the medial side.

3.5.3 Data acquisition

An ultrasound device was used to record videos of the medial gastrocnemius muscle and ankle torque was recorded using a dynamometer as described in Section 3.2.2. The signal from the dynamometer and ultrasound trigger were digitised by a data acquisition board (DAQcard-6024E, National Instruments, USA) at a frequency of 50 Hz. The MATLAB scripts and Simulink models (R2014b, The Mathworks, USA) used to run this experiment are provided in Appendix A.3.

3.5.4 Experimental protocol

3.5.4.1 Overview

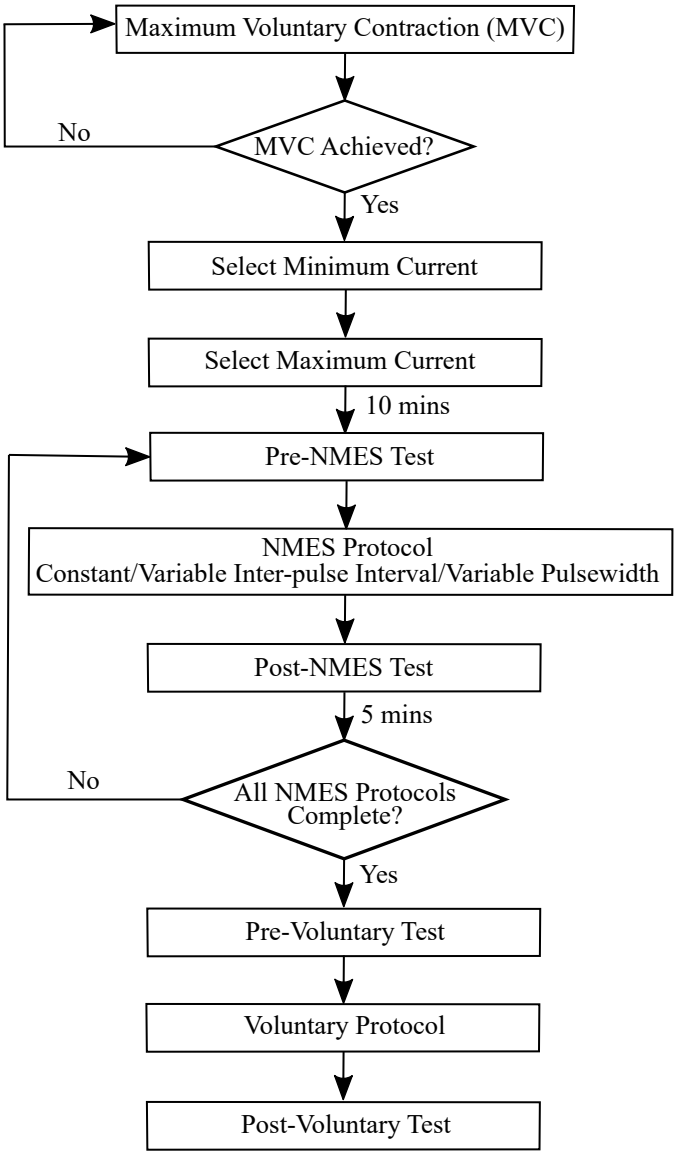

Figure 3.14: Flowchart showing the organisation of Study 3A. A maximum voluntary contraction (MVC) is performed, followed by selection of current values. Three patterns of neuromuscular electrical stimulation (NMES) are delivered and then voluntary contractions are performed.

An overview of the session is shown in Figure 3.14. The maximum voluntary contraction was performed and the stimulation parameters were selected. Participants were then given a rest period of 10 minutes before the NMES protocol. A twitch-tetanus was delivered before and after each variation of the NMES protocol and 5 minute rest periods were also provided between each cycle. The voluntary protocol follows a similar structure, with a twitch-tetanus delivered before and after the main voluntary protocol.

3.5.4.2 Maximum voluntary contraction

The burst superimposition technique was used to determine a participants maximum voluntary contraction (MVC). Participants performed a maximum voluntary isometric contraction during which a short burst of electrical stimulation was delivered. The stimulation train consisted of 10 pulses at a frequency of 100 Hz with a pulsewidth of 500 μs and a current of 20 mA.

The muscle contraction was deemed to be a true MVC if the burst of electrical stimulation did not cause a further increase in ankle torque of more than 10%. If this criteria was not met, participants were given a short rest before repeating the test up to three times. An example of the torque produced during an MVC is shown in Figure 3.15.

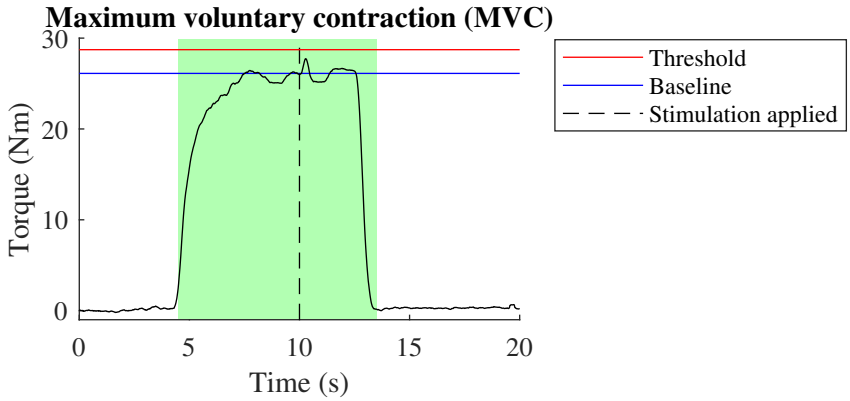

Figure 3.15: An example of the torque produced during a successful maximum voluntary contraction (MVC). When the stimulation is applied (t=10s), the torque produced does not exceed the threshold shown in red which is a 10% increase in the baseline value shown in blue.

3.5.4.3 Defining stimulation intensity

Different values of current, pulsewidth and inter-pulse interval were chosen to compare the effect of stimulation parameters. Three values of pulsewidth and two values of inter-pulse interval were predefined and were the same for all participants:

- Pulsewidth 1 (PW_1) = 300 μs
- Pulsewidth 2 (PW_2) = 350 μs

- Pulsewidth 3 (PW_3) = 400 μs
- Inter-pulse interval 1 (IPI_1) = 50 ms
- Inter-pulse interval 2 (IPI_2) = 25 ms

Two current values, minimum and maximum (I_{min} and I_{max}), were set for each participant in the following way:

- I_{min}: the lowest value of current required to produce a muscle contraction which registers a torque output on the dynamometer. A pattern of stimulation trains was applied where for each value of current being tested, the pulsewidth consisted of a ramp up phase (2.5s), a constant phase (5s) and a ramp down phase (2.5s). The current during the first train of pulses was 2mA and increased in increments of 2mA until the minimum current was found. To ensure that a measurable torque was produced during the combination of the lowest stimulation parameters, the pulsewidth reached during the constant phase was 300μs and an inter-pulse interval of 50ms was used throughout. An example of the current applied and the torque produced during this process is shown in Figure 3.16.

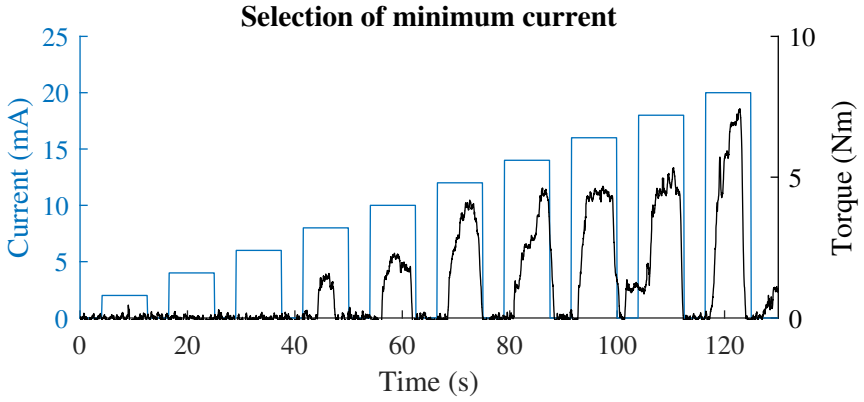

Figure 3.16: An example of current values and the torque produced during selection of the minimum current value. Current is chosen when a measurable torque is produced (8 mA).

- I_{max}: the lowest value of current required to produce an activation curve that gradually increases to a plateau and does not reach a higher torque value than that produced by the previous current value tested. A current activation curve is the torque produced when a single value of current is tested and the pulsewidth is slowly increased over 10 seconds and then remains constant for a further 5 seconds. To ensure the stimulation is tolerable for the participant during the combination of maximum stimulation parameters, the pulsewidth reached during the constant phase was 400μs and an inter-pulse interval of 25ms was used throughout. An example of the torque produced for each current value applied in this process is shown in Figure 3.17.

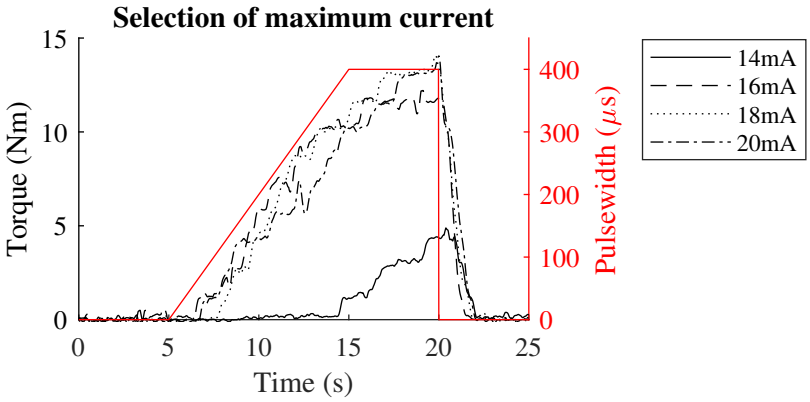

Figure 3.17: An example of the torque values produced during selection of the maximum current value (18 mA).

Overall this yields 12 different combinations of stimulation parameters as shown in Table 3.1.

Table 3.1: All combinations of stimulation parameters based on three values of pulsewidth (PW), two values of inter-pulse interval (IPI) and two values of current (I).

$\mathbf{I}_{min}$	$\mathbf{I}_{max}$
$PW_1 = 300\mu s$, $IPI_1 = 50ms$	$PW_1 = 300\mu s$, $IPI_1 = 50ms$
$PW_2 = 350\mu s$, $IPI_1 = 50ms$	$PW_2 = 350\mu s$, $IPI_1 = 50ms$
$PW_3 = 400\mu s$, $IPI_1 = 50ms$	$PW_3 = 400\mu s$, $IPI_1 = 50ms$
$PW_1 = 300\mu s$, $IPI_2 = 25ms$	$PW_1 = 300\mu s$, $IPI_2 = 25ms$
$PW_2 = 350\mu s$, $IPI_2 = 25ms$	$PW_2 = 350\mu s$, $IPI_2 = 25ms$
$PW_3 = 400\mu s$, $IPI_2 = 25ms$	$PW_3 = 400\mu s$, $IPI_2 = 25ms$

3.5.4.4 Twitch-tetanus

A single pulse of electrical stimulation was delivered causing the muscle to produce a twitch. This was followed 10 seconds later by a burst of stimulation lasting 1 second to produce a fused tetanic contraction. The maximum current value determined for the particpant (I_{max}) was used along with a pulsewidth value of $400\mu s$ and a 25ms inter-pulse interval.

3.5.4.5 NMES protocol

Twelve trains of stimulation lasting 10 seconds each were delivered with 5 second rest periods in between (3 minutes in total). A single stimulation train consisted of a ramp up phase lasting 2.5 seconds, a constant phase lasting 5 seconds and a ramp down phase lasting 2.5 seconds. Each train had a different combination of stimulation parameters from Table 3.1, resulting in short muscle contractions of different intesities. An example of the 12 different stimulation parameters delivered is shown in Figure 3.18.

There were three variations of the NMES protocol i) constant NMES, where all stimulation parameters remained constant for a single contraction, ii) variable inter-pulse interval, where the current and pulsewidth remained constant but the inter-pulse interval varied around a mean value ($IPI_1 = 50 \pm 5$ms, $IPI_2 = 25 \pm 5$ms), and iii) variable pulsewidth, where current and inter-pulse interval remained constant but the pulsewidth varied around a mean value ($PW_1 = 300\mu s \pm 20\mu s$, $PW_2 = 350\mu s \pm 20\mu s$, $PW_3 = 400\mu s \pm 20\mu s$). Stimulation was applied as described in Section 3.2.1, with the addition of a single-board computer (Raspberry Pi, UK) to allow the variation in stimulation parameters.

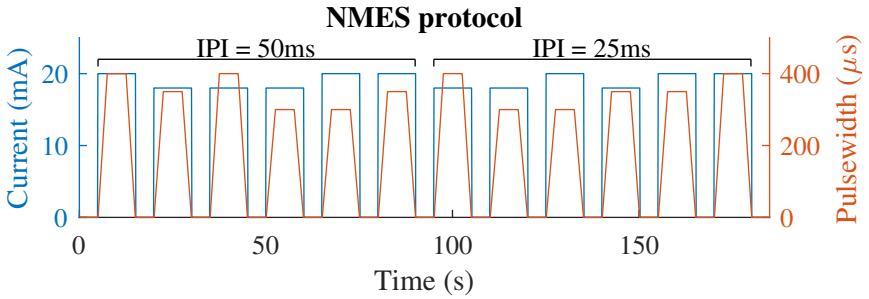

Figure 3.18: An example of the 12 combinations of stimulation parameters: three values of pulsewidth, two values of current and two values of inter-pulse interval.

3.5.4.6 Voluntary protocol

The participants were asked to perform 12 voluntary muscle contractions, each producing a specified torque level based on the torque produced during the NMES protocol. Visual feedback was provided on a computer screen which showed the target participants were expected to reach and the torque they were currently exerting in real time. A warning signal showed the target 1 second before participants were expected to perform the movement, as shown in Figure 3.19. Similarly to the NMES protocol, each contraction lasted 10 seconds with 5 second rest periods, taking a total of 3 minutes to complete.

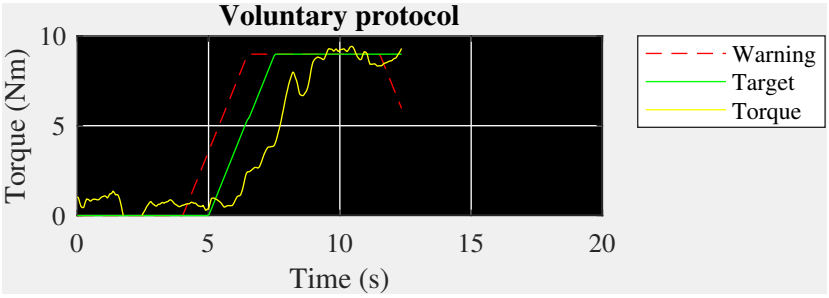

Figure 3.19: An example of the voluntary protocol showing the warning signal (red), the target torque (green) and the torque produced by the participant (yellow).

3.6 Experimental methods for Study 3B

This study was designed to investigate the effects of different multi-electrode patterns of stimulation. Conventional synchronous stimulation was compared to random and sequential patterns of asynchronous stimulation. This work was carried out in collaboration with Ruslinda Binti Ruslee [5], who was responsible for the design of the experimental setup and protocol. Ultrasound videos were recorded, pre-processed and analysed independently.

3.6.1 Participants

Eleven able-bodied participants (3 male, 8 female, age 28.3 $\pm$ 3.2 years (mean $\pm$ SD)) in self-reported good health with no known neuromuscular disorders were recruited for this study. Ten participants completed the study and one withdrew due to hyper-sensitivity to the electrical stimulation.

3.6.2 Experimental setup

Participants were comfortably seated on a chair in an upright position, with their hip and knee at an angle of approximately 90°and their foot resting on a custom built force platform. Velcro straps were wrapped around the foot to restrict ankle movements.

An ultrasound probe was placed over the belly of the medial gastrocnemius muscle. Four pairs of NMES electrodes were also placed over the calf, covering both the medial and lateral gastrocnemius. Four small electrodes covered the same area as one large electrode (5 $\times$ 9 cm), used in all other studies. Figure 3.20 shows the experimental setup for this study, including the position of the four pairs of NMES electrodes.

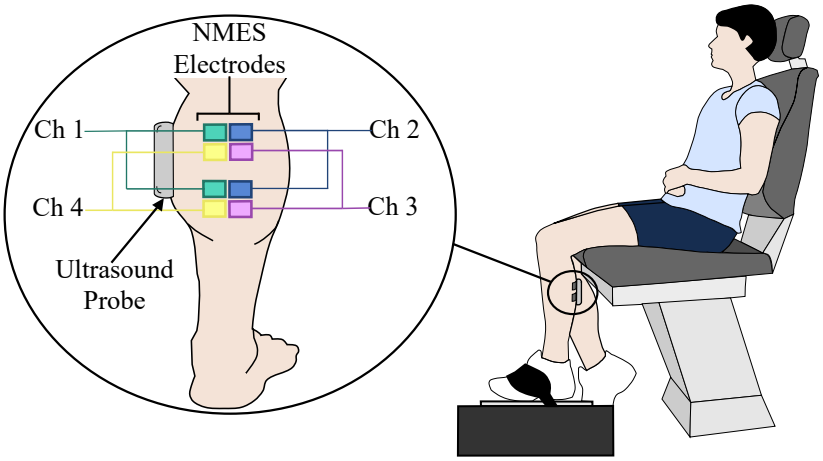

Figure 3.20: Experimental setup for Study 3B showing the participant seated on a chair with their foot resting on the force platform. Four pairs of NMES electrodes are positioned over the gastrocnemius muscle with the ultrasound probe placed on the medial side. Adapted from [5].

3.6.3 Data acquisition

An ultrasound device was used to record videos of the medial gastrocnemius muscle and ankle torque was recorded using a custom-built force platform as described in Section 3.2.2. The force platform and the ultrasound were connected to a data acquisition board (DAQcard-6024E, National Instruments, USA) which digitised the signal at a frequency of 50 Hz.

3.6.4 Experimental protocol

3.6.4.1 Overview

Participants completed three separate sessions during which the current was selected, a twitch-tetanus was applied as a pre-fatigue test, one of the stimulation patterns was delivered in the form of a 600 second fatigue protocol and a twitch-tetanus was delivered a further three times for post-fatigue testing. An overview of a single session is shown in Figure 3.21. Each session was carried out on a different day and the order of these sessions was random.

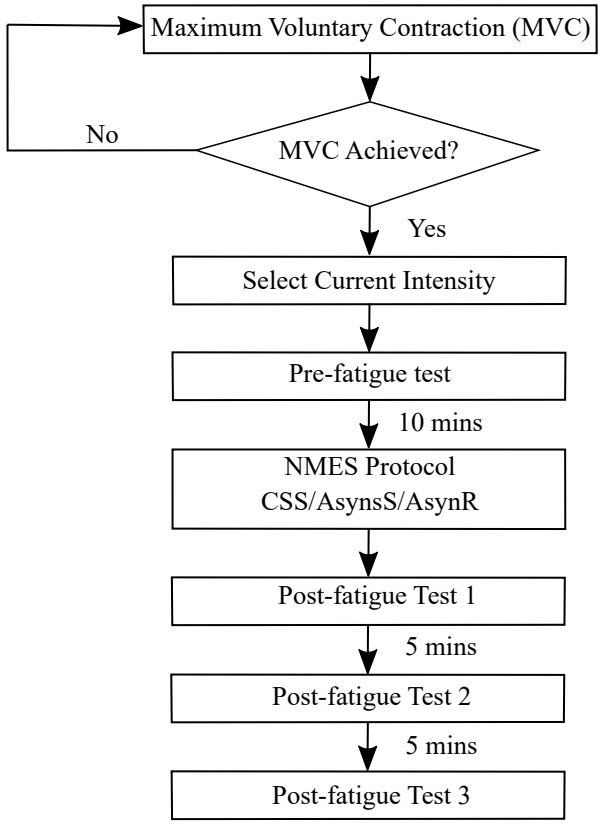

Figure 3.21: Flowchart showing the organisation of Study 3B. A maximum voluntary contraction (MVC) is performed, current is selected and one pattern of neuromuscular electrical stimulation (NMES) is delivered, with pre- and post-fatigue tests before and after.

3.6.4.2 Defining stimulation intensity

Pulsewidth values of 300 μs and a frequency of 40 Hz were used throughout this study. Current values were selected for each participant using a current activation curve, as discussed in section 3.5.4.3. A current value of 10 mA was tested first, and increased in increments of 2 mA until the torque no longer increased or the maximum intensity tolerable to the participant was reached.

3.6.4.3 Twitch-tetanus

A single pulse of stimulation was delivered to elicit a muscle twitch muscle, followed 10 seconds later by a short burst of stimulation, 5 seconds in duration, to produce a tetanic contraction.

3.6.4.4 Fatigue protocol

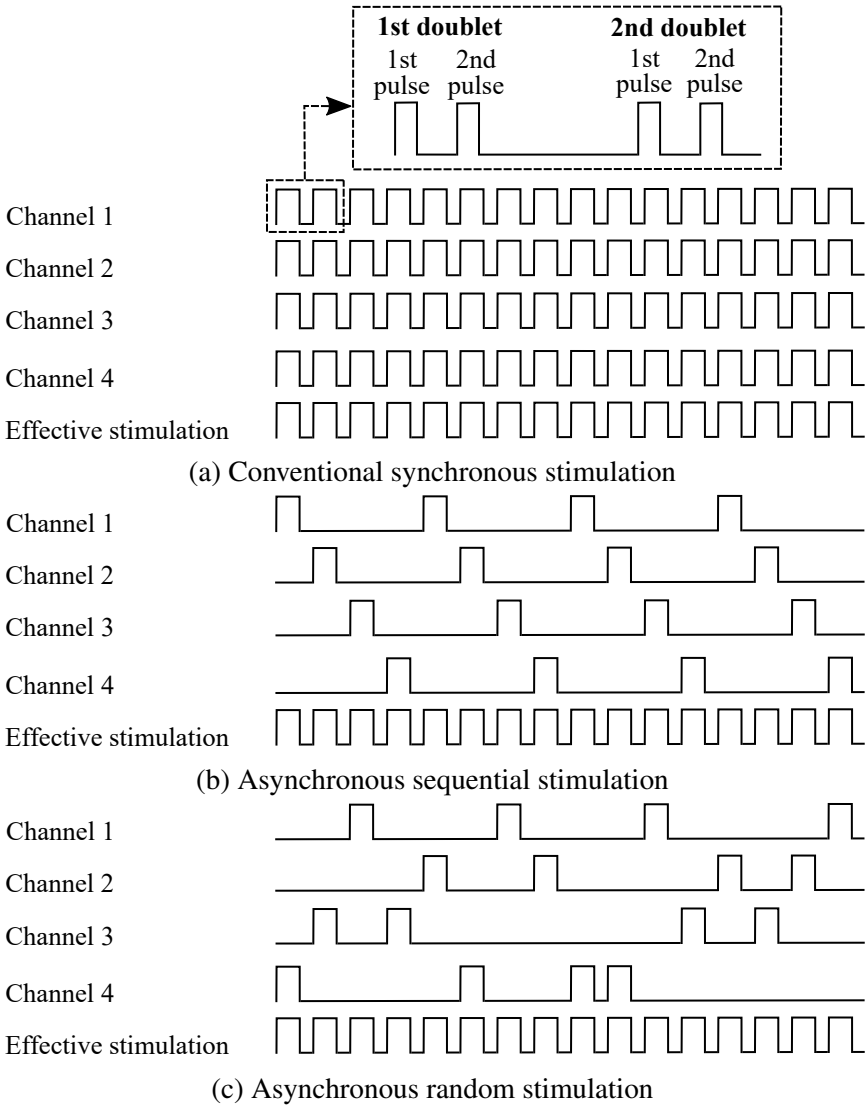

Figure 3.22: Overview of different multi-electrode spatially distributed stimulation patterns. Adapted from [5].

A fatigue protocol lasting 600 seconds was delivered through a series of stimulation trains using four different channels. Trains were 300 ms in duration applied intermittently at 1 s intervals and consisted of doublet pulses with a 6 ms inter-pulse interval. There are three variations of this fatigue protocol, each with a different pattern of stimulation:

1. Conventional synchronous stimulation (CSS): all four pairs of electrodes are activated at the same time i.e. synchronously, just like one pair of electrodes
2. Asynchronous sequential stimulation (AsynS): each of the four pairs of electrodes are activated one at a time, i.e. asynchronously, in a particular order
3. Asynchronous random stimulation (AsynR): each of the four pairs of electrodes are activated one at a time, i.e. asynchronously, in a random order

All patterns had an effective stimulation frequency of 40 Hz. During synchronous stimulation all four channels were activated every 25 ms whereas during the synchronous stimulation patterns one channel was activated every 25 ms. Figure 3.22 shows the three different stimulation patterns.

3.7 Ethical approval

All studies involving human participants were performed in accordance with the Declaration of Helsinki. For each study, all participants had the study explained to them and received the relevant information sheet before giving written informed consent. Studies which involved spinal cord injury participants took place at the Queen Elizabeth National Spinal Injuries Unit, Queen Elizabeth University Hospital, Glasgow. These studies were approved by NHS Greater Glasgow and Clyde:

- **Study 1**

  REC reference: 17/WM/0461 R&D reference: GN17NE660

- **Study 2**

  REC reference: 19/YH/0148 R&D reference: GN19NE102

Studies which only included able-bodied participants were approved by the Ethics Committee at the College of Science and Engineering, University of Glasgow:

- **Study 3A**

  Approval number: 300160169 (extension of 300160043)

- **Study 3B**

  Approval number: 300150028

3.8 Ultrasound analysis methods

Ultrasound videos were analysed to obtain quantitative measurements of muscle morphology and movement. Tracking software was used to segment the image into different anatomical regions, and track the movement of features within the muscle. This not only allowed measurements of muscle size, in the form of thickness, but also measurements of movement, both of the entire muscle and at the regional level. Greyscale analysis describes the brightness of the image through values assigned to each pixel in the ultrasound image.

3.8.1 Tracking of muscle shape

Throughout this project, information about muscle architectural parameters was obtained using an algorithm that tracked features in ultrasound videos. The algorithm was developed by Professor Ian Loram's research group at Manchester Metropolitan University [186]. It uses an active shape model (ASM) to automatically segment the image and the Kanade-Lucas-Tomasi (KLT) algorithm to track features between different frames.

3.8.1.1 Automatic segmentation

The first step performed by the algorithm is segmentation of the image, separating anatomically distinct regions of the muscle: the upper aponeurosis, the muscle tissue itself and the lower aponeurosis. This is done by an active shape model (ASM), a commonly used algorithm for shape detection that performs a probabilistic search for known shapes in new images [187]. It is constrained by a point distribution model (PDM) which uses training images to provide a model of shape variation.

The PDM is used to capture variations in the shape of the muscle during contractions. Several frames of an ultrasound video are manually labelled to create a model for that particular video. This involves placing markers along the boundaries of the muscle, identifying the upper and lower aponeuroses and the muscle itself. Throughout this thesis, training images were manually labelled to create seperate PDM's for each participant during each session, i.e. a PDM was created which could be used for all videos recorded during a particular session provided the position of the ultrasound probe did not change. In most cases, approximately 40 training images containing frames where the largest muscle movements occurred was sufficient to allow accurate segmentation, which was verified by visual inspection. If necessary, up to an additional 100 training images from different ultrasound videos recorded during the same session were added, allowing particularly large or fast muscle movement to be tracked. Principal component analysis is then applied to the spatial distributions resulting from these training images to recover a model of shape variation. Images from different participants can be used to create a general model for a particular muscle that would be capable of recognising the muscle in a new participant without having to provide additional training images.

The ASM then uses the PDM, along with Gaussian models of image intensity at each landmark within the PDM, to accurately describe the shape of the muscle in every image. The process of fitting the ASM to a new image is initialised from the mean shape of the PDM, before allowing each landmark to move along a fixed straight line to either side of its current location and perpendicular to its neighbours. As each landmark is moved pixel by pixel, the image intensity is sampled. This allows the most likely location to be determined by minimising the likelihood of a new normalised sample for each landmark. The new shape is projected into the PDM to find the closest conceivable shape. This segmentation process is shown in Figure 3.23.

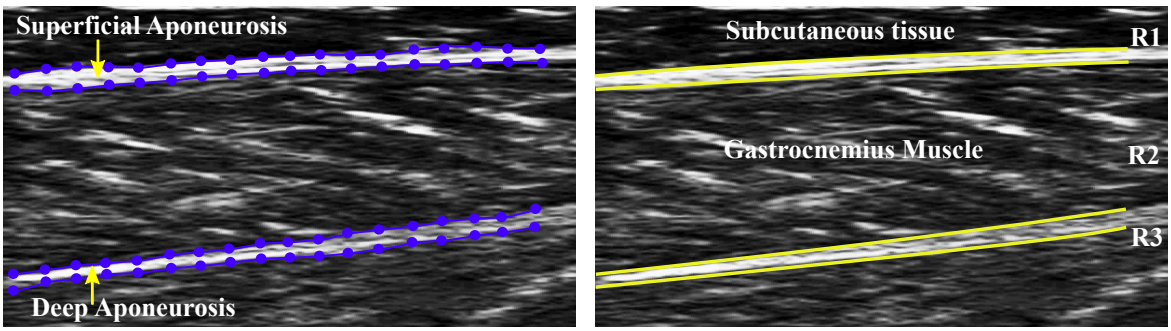

(a) Markers placed on muscle boundaries (b) Anatomical regions identified by segmentation

Figure 3.23: Segmentation process showing the markers manually placed on the boundaries of the muscle to create the point distribution model (PDM) and the anatomically distinct regions of the muscle identified by the active shape model (ASM). Adapted from [6].

3.8.1.2 Feature tracking

The second step of the algorithm is the tracking of features within the relevant image segment. A square template is used to identify suitable features based on the Hessian matrix, which uses pixel intensity to describe local curvature. Both eigenvalues for a potential feature window are set to exceed a minimum threshold as the presence of two large values is indicative of corners, which are especially good for tracking. This allows feature templates to be replaced with new features, which are good for tracking, if the features identified in the first frame disappear.

Once features have been identified, they are tracked frame to frame by the Kanade-Lucas-Tomasi (KLT) feature tracking algorithm [188]. The feature template is aligned with the new image by minimising some measure of the difference between the two regions. Features being tracked can disappear and new features can appear between frames. To make the tracking more robust to the lack of persistent features, test points known as probes are placed across the image. A total of 80 probes (8×10 matrix) are placed, with their initial position on the first frame based on the segmentation performed by the ASM; four probes are placed at the corners of the muscle segment and linear interpolation is used to place the remaining probes between these extreme points. For each frame, finite differencing of all persisting feature templates from the previous frame allows a displacement field to be estimated for each segment. Triangular interpolation

(Voroni or Delaunay) of the resultant vector fields is used to update the position of the probes [189]. The feature tracking process is shown in Figure 3.24.

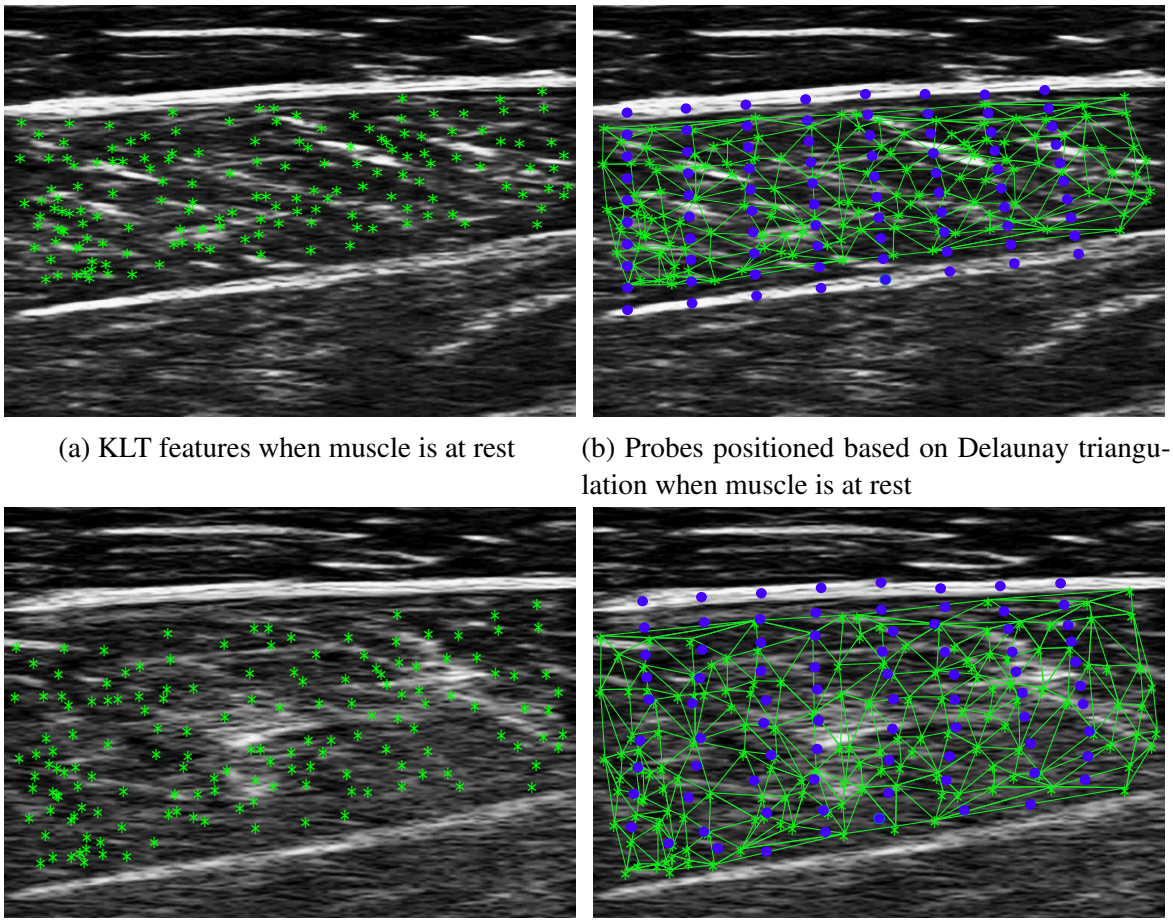

(a) KLT features when muscle is at rest

(b) Probes positioned based on Delaunay triangulation when muscle is at rest

(c) KLT features during muscle contraction

(d) Probes positioned based on Delaunay triangulation during muscle contraction

Figure 3.24: Feature tracking process showing the Kanade-Lucas-Tomasi (KLT) features and the probes placed over the muscle based on Delaunay triangulation. Adapted from [6].

3.8.2 Greyscale analysis

3.8.2.1 Pixel values

The echogenicity of a muscle can be described quantitatively though greyscale analysis. Ultrasound images are composed of pixels, each of which correspond to an element in the ultrasound transducer as discussed in Section 1.4.1 of Chapter 1. The brightness of each pixel is represented by a single value known as a *pixel value*. In greyscale images, these values of intensity range from 0, which represents black, to 255, which represents white. All values inbetween represent a shade of grey. This is demonstrated in Figure 3.25, which shows pixels within a small region of the image, with variations in brightness, along with the pixel values which represent them.

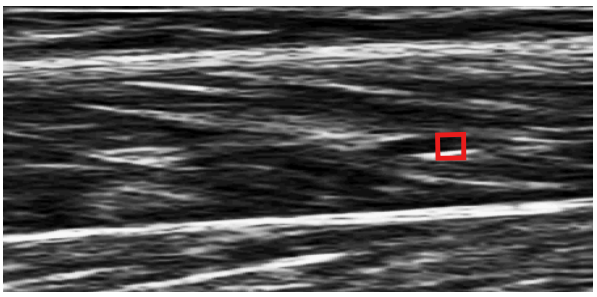

(a) US image with ROI selected

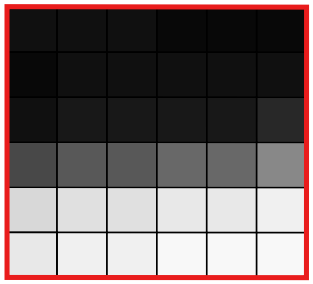

(b) Pixels within ROI

16	16	16	8	8	8
8	16	16	16	16	16
16	24	24	24	24	40
72	88	88	104	104	136
216	224	224	232	232	240
232	240	240	248	248	248

(c) Pixel values within ROI

Figure 3.25: Visual representation of the greyscale composition of a region of interest (ROI) within an ultrasound (US) image.

3.8.2.2 Histograms

Histograms display the number of pixels in an image at each intensity value (from 0 to 255), providing information on the central tendency, spread and shape of the distribution of pixel values. Histograms with a lower central tendency have more pixels with a low value, i.e. more dark pixels, than those with a higher central tendency, describing the brightness of the image. The width of the histogram describes the spread of the data. A narrow histogram indicates a smaller standard deviation in pixel values than a wide histogram. The shape of the histogram describes the distribution of pixel values. A symmetrical histogram suggests pixel values are evenly distributed around the mean, whereas one which is skewed to the left indicates more pixels with higher values and vice versa. Figure 3.26 shows an ultrasound image and a histogram of the pixel values found within the highlighted region of interest (ROI).

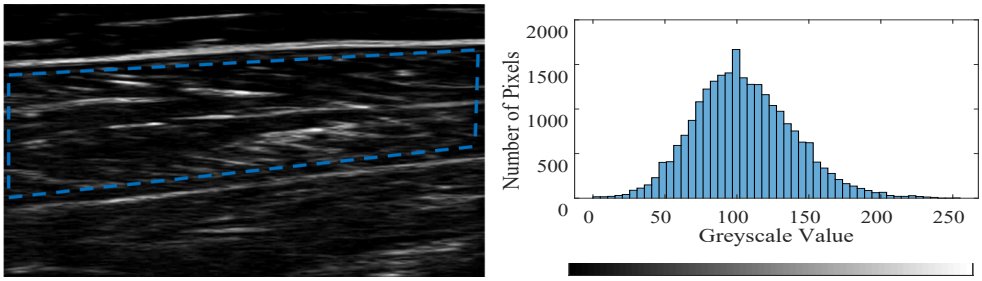

(a) US image with ROI selected

(b) Histogram of pixel values

Figure 3.26: Ultrasound (US) image of gastrocnemius medialis muscle with a region of interest (ROI) selected and the corresponding histogram of pixel values.

3.9 Statistical analysis methods

In this section, an overview of the statistical analysis methods used throughout this thesis is provided. First, the use of the Shapiro-Wilk test to assess normality is discussed; followed by an overview of the different statistical tests used for determining if a statistically significant difference exists, depending on the distribution of the data and whether the samples are paired or independent; and the use of the Bonferroni correction for multiple comparisons. Cohen's D effect size is then presented as an additional test to describe the magnitude of the difference between groups independent of sample size. Finally, multivariate analysis of variance (MANOVA) is described. All statistical analysis was performed using the statistics toolbox in MATLAB (R2019a, The Mathworks, USA).

3.9.1 Shapiro-Wilk test for normality

The Shapiro-Wilk test is used throughout this thesis to test the normality of the data when the sample size is sufficient ($n \geq 10$). It tests the null hypothesis that the sample is from a normally distributed population. If the null hypothesis is rejected, the data cannot be assumed to have a normal distribution and non-parametric tests are used, however, if the null hypothesis cannot be rejected then the assumption of normality is valid and parametric tests are used. The test statistic (W) is calculated as follows,

$$W = \frac{(\sum_{i=1}^{n} a_i x_{(i)})^2}{\sum_{i=1}^{n} (x_i - \bar{x})^2}, \tag{3.1}$$

where $x_{(i)}$ is the i^{th} smallest number in the sample, $\bar{x}$ is the sample mean and a_i is a weighted coefficient based on the number of samples. This W value is used to calculate the p-value, and the null hypothesis is rejected if it is less than the chosen significance level. When using the Shapiro-Wilk test, a significance level of 0.05 was used throughout this thesis [190].

3.9.2 Statistical tests

The choice of statistical test used is based on whether or not the data is normally distributed, and whether the samples are paired or independent [191].

1. **Distribution:** As discussed above, the normality of the data is assessed using the Shapiro-Wilk test. If the data is normally distributed, it is suitable to use a parametric test. If the assumption of normality cannot be met, alternative non-parametric tests are used.

2. **Paired vs independent samples:** Samples are paired when natural or matched couplings occur, i.e. each data point in one sample is uniquely paired to a data point in the second

sample. This occurs when measurements are obtained from the same participant under different conditions or at different points in time. Different participants who are matched according to age or gender are also considered to be paired. Samples are deemed to be unpaired or independent if measurements are compared between two separate groups of participants.

Throughout this thesis if data is normally distributed a t-test is used, paired or unpaired depending on whether or not the samples are paired or independent. If the assumption of normality cannot be met then the Wilcoxon signed rank test is used when samples are paired, and the Mann-Whitney U test is used when samples are independent. Further details on each of these tests are provided below.

3.9.2.1 Parametric tests

Parametric tests are used when the data is normally distributed as discussed above. The student t-test is a hypothesis statistical test which compares the mean of two samples, to evaluate whether or not there is a statistically significant difference between them. The null hypothesis states that there is no significant difference between the means of the two groups, and the alternative hypothesis states that there is a significant difference between the two population means. There are two variations of this test used throughout this thesis. The **paired t-test** is used to compare the means between two related samples and is calculated as follows,

$$t_{paired} = \frac{\bar{x}_D}{\frac{\sigma_D}{\sqrt{n}}}, \tag{3.2}$$

where $\bar{x_D}$ and σ_D are the mean and standard deviation of the difference (D) between the two groups and n is the number of paired samples. In this case the variance between the two groups is not assumed to be equal. The **unpaired t-test** is used to compare the means of two independent samples and is calculated as follows,

$$t_{ind.} = \frac{\bar{x}_A - \bar{x}_b}{\sqrt{\frac{\sigma^2}{n_A} + \frac{\sigma^2}{n_B}}}, \tag{3.3}$$

where $\bar{x}_A$ and $\bar{x}_B$ are the means of groups A and B, n_A and n_B are the size of groups of A and B, and σ^2 is the pooled variance. In this case, the variance between the two groups is assumed to be equal [191, 192].

3.9.2.2 Non-parametric tests

Non-parametric tests are used when the data cannot be assumed to be normally distributed. There are two non-parametric tests used throughout this thesis. The **Wilcoxon signed rank test** is used to compare the medians of the two groups based on the difference between each

matched pair [193]. The **Mann-Whitney U test** is used to compare data from two independent samples based on the order of the observations from the two samples. The null hypothesis states that it is equally likely that a randomly selected value from one population will be less than or greater than a randomly selected value from a second population, i.e. it tests whether there is a difference between the distributions of the two groups rather than differences between the medians [191, 194].

3.9.3 Bonferroni correction for multiple comparisons

The Bonferroni correction is used to negate the problem of multiple comparisons. The statistical tests discussed above are based on the rejection of the null hypothesis when the likelihood that the data is observed under the null hypothesis is low. When the hypothesis is tested multiple times, it increases the chance of incorrectly rejecting the null hypothesis. The Bonferroni correction compensates for this by reducing the accepted significance level of p to,

$$p \leq \frac{\alpha}{n}, \tag{3.4}$$

where α is the original significance level (0.05) and n is the number of comparisons being made [195].

The Bonferroni correction is used to reduce type I errors i.e. rejecting a true null hypothesis and reporting a significant difference when the result has occurred by chance. However, it must also be considered that such adjustments of the signifcance level can also be problematic, mostly because the number of tests perfomed determines how the results are interpreted. Furthermore, the Bonferroni correction is concerned with the general null hypothesis, i.e. that all null hypotheses are true simultaneously, which is often considered irrelevant. There is also an increase in type II errors, i.e. accepting a false null hypothesis and therefore rejecting meaningful differences as non-significant [196]. It is therefore of the utmost importance that the Bonferroni correction is used with caution, and with an understanding of its implications. In this thesis, results are reported as significant based on the Bonferroni correction to provide more rigorous testing, however, results are not dimissed solely on this basis but are considered in conjunction with calculations of the effect size (see Section 3.9.4).

3.9.4 Cohen's d effect size

Cohen's d effect size provides a measurement of the magnitude of the difference between two groups. While the p-value obtained from the hypothesis tests above tell us if the findings are due to chance, Cohen's d tells us how big the effect is. Unlike the hypothesis tests detailed in the previous sections, the effect size is unaffected by sample size. In order to provide a better understanding of the results, both the p-value and Cohen's d effect size are reported throughout this thesis.

For independent samples, Cohen's d effect size is calculated as follows,

$$d = \frac{\bar{x}_1 - \bar{x}_2}{\sigma} \tag{3.5}$$

where $\bar{x}$ is the group mean and σ is the standard deviation of the data [197]. When the samples are paired, Cohen's d effect size can also be calculated in line with a paired test as follows,

$$d = \frac{\bar{x}_D}{\sigma_D} \tag{3.6}$$

where $\bar{x}_D$ is the mean and σ_D is the standard deviation of the difference (D) between the two groups [198]. The general "rule of thumb" guidelines which are used to interpret these results are shown in Table 3.2. A d value of 1 indicates the two groups differ by 1 standard deviation, a d value of 2 indicates a difference of 2 standard deviations and so on.

Table 3.2: Interpretation of Cohen's d effect size.

Cohen's d value	Effect size
0.01	very small
0.20	small
0.50	medium
0.80	large
1.20	very large
2.00	huge

3.9.5 Multivariate analysis of variance (MANOVA)

Multivariate analysis of variance (MANOVA) is used to determine if there are differences between independent groups on more than one continuous dependent variable. It is an extension of the ANOVA, which determines if the mean of a variable is significantly different between groups. In the case of the MANOVA, there are multiple response variables and it determines if the entire set of means differs from one group to the next [199, 200].

3.9.5.1 Canonical analysis

Canonical analysis is a technique within multivariate analysis which determines the relationship between groups of variables in a data set. It looks for the linear combination of the original variables with the largest separation between groups. This is the first canonical variable. Next, the combination with the second highest separation is found, and so on. Plotting the first two canonical variables shows the biggest separation between groups than any other pair of original variables [199, 200].

Chapter 4

Detection of Changes in Muscle Structure

4.1 Summary

The aim of this work is to use ultrasound imaging (USI) to evaluate changes in muscle structure following a spinal cord injury (SCI). This chapter investigates the use of several different USI analysis measurements to describe the structural changes that occur in the months after injury. The use of tracking software to obtain measurements of muscle size, and greyscale analysis to extract information on the echogenicity and echotexture of the muscle are fully explained. The measurements are compared between able-bodied participants and SCI participants at different times post-injury. Measurements of muscle size, echogenicity and echotexture, and how these relate to structural changes that occur following a SCI are discussed. Furthermore, the suitability of USI parameters to distinguish between SCI at different times post-injury is examined. This chapter includes work that has been submitted to the journal *"Ultrasound in Medicine and Biology"* and is currently under review (see Publications section).

4.2 Introduction

An injury to the spinal cord commonly causes paralysis of muscles, as the motor signals from the brain can no longer reach the target muscle. Muscles affected by paralysis undergo atrophy which can either be a result of denervation, where the motor neurons themselves are damaged, or disuse, where damage to the spinal cord blocks synaptic input from higher segments and results in a lack of activation [39, 42, 61]. This leads to structural changes which occur in the muscle weeks, months or even years after the injury has occurred. Atrophy by definition is a reduction in the size and number of muscle fibres. There is also thought to be a transformation in fibre type which is responsible for the increased fatigability of muscles [39, 62, 201]. In addition, SCI has also been shown to be associated with an increase in intramuscular fat [43]. The changes in muscle fibres and infiltration of fat cause major structural changes within the muscle which could affect its ability to produce a contraction. Furthermore, the change in composition of

contractile and non-contractile elements could limit functional movements even after recovery from the original injury restores the pathway to the muscles.

As discussed in Section 1.3.2 of Chapter 1, assessment of muscles is an important part of evaluating a SCI, however, this focuses on the ability of muscles to generate a contraction (the use of USI to assess muscle function through measurements of movement is discussed in Chapter 5). While this provides useful information on the functional status of the muscle, it does not take into account the structure of the muscle. Measurements of structure could provide additional insight into the amount of atrophy the muscle has undergone, making rehabilitation interventions more successful. USI provides a potential non-invasive method to visualise internal structures such as muscles and therefore obtain measurements of muscle structure. Previous studies have found USI to be a reliable tool for making accurate measurements of muscle morphology, including thickness, cross-sectional area [89], fibre length and pennation angle [202].

Following the work of Heckmatt et al. [126], USI has been used to screen for a wide range of neuromuscular disorders [24, 128, 135, 203]. Neuromuscular disorders such as muscular dystrophy and motor neuron disease cause changes in the muscle structure which can be detected through USI measurements. Muscle thickness can be used to detect a reduction in muscle size and greyscale analysis of pixel values allows the echogenicity of the muscle, i.e. how bright it appears, to be quantified. Many of these neuromuscular disorders cause changes in the muscle structure which are similar to those caused by atrophy. Other studies [138, 139] also show that USI can detect changes in muscle echogenicity as a result of hospitalisation, where the changes in muscle structure are a result of immobilisation rather than a disorder which directly affects the neuromuscular system. It therefore follows that USI could detect changes in muscle structure as a result of atrophy following a SCI.

In this chapter, two analysis methods are used to make USI measurements which describe muscle structure. Firstly, tracking software developed by Loram and colleagues at Manchester Metropolitan University [186] (described in Section 3.8.1 of Chapter 3), is used to make measurements of muscle thickness. Secondly, pixel intensity values are extracted from the ultrasound image and greyscale analysis is performed to obtain statistical descriptors of echogenicity and echotexture. This includes first-order statistical descriptors, Haralick features based on the grey-level co-occurrence matrix (GLCM), Galloway features based on the run length matrix (RLM) and local binary pattern (LBP) features. These measurements are compared between a group of able-bodied participants and a group of SCI participants at different times post-injury. The aim of this study was to evaluate the ability of USI to provide measurements of muscle structure and detect these changes over time following a SCI by investigating:

- which features were most suitable for describing muscle structure.
- whether these parameters could be used to differentiate between able-bodied participants and SCI participants at different times post-injury

It was hypothesised that differences in muscle structure would occur over time following a SCI which could be detected by USI.

4.3 Methods

4.3.1 Overview of data used

The data analysed in this Chapter was obtained during Study 1 while the muscle was in the resting state (see Section 3.3.4.2 in Chapter 3 for details). This includes US videos of the gastrocnemius medialis (GM) muscle recorded from 15 participants with a SCI at different times post-injury and 15 able-bodied age and gender matched controls.

4.3.2 Pre-processing of USI videos for automatic segmentation

Ultrasound videos were recorded and saved as telemed video data (TVD) files, which is the default video file format for the software provided with the ultrasound scanner. To enable the use of the tracking software described in Section 3.8.1, the TVD files were converted to AVI file format. The videos were then cropped, showing only the area containing the US image of the GM muscle, and individual frames were extracted and saved in the form of a PGM file.

4.3.3 Calculation of muscle thickness through automatic segmentation

As shown in Figure 3.23 on page 59 and Figure 4.1, the active shape model (ASM) segments the US image into three regions: the superficial aponeurosis, the GM muscle and the deep aponeurosis. These regions are defined for every frame over the entire US video. The final output obtained from this segmentation process is the x and y component for the position of each marker located on the aponeuroses expressed in pixels. In this case, 19 markers were placed along the upper and lower boundaries of both the deep and superficial aponeuroses to create the point distribution model (PDM), resulting in the positioning of 76 markers.

Muscle thickness (Θ) is defined as the average distance between the superficial and deep aponeurosis. The distance between each pair of markers on the lower side of the superficial aponeurosis and upper side of the deep aponeurosis can be calculated based on position. By averaging the distance for each of these 19 pairs of markers, a single value for muscle thickness can be found:

$$\Theta = \frac{\sum_{i=1}^{n_{markers}} \sqrt{(x_{(U,i)} - x_{(L,i)})^2 + (y_{(U,i)} - y_{(L,i)})^2}}{n_{markers}} \tag{4.1}$$

where $x_{(U,i)}$ and $y_{(L,i)}$ are the x and y coordinates on the upper and lower aponeuroses respectively for the i^{th} marker. This is demonstrated in Figure 4.1.

This single value of thickness can be calculated for each frame of the US video. When averaged across frames where the muscle is in a relaxed state, this provides a value of resting muscle thickness, which is a useful measurement for describing the size of the muscle.

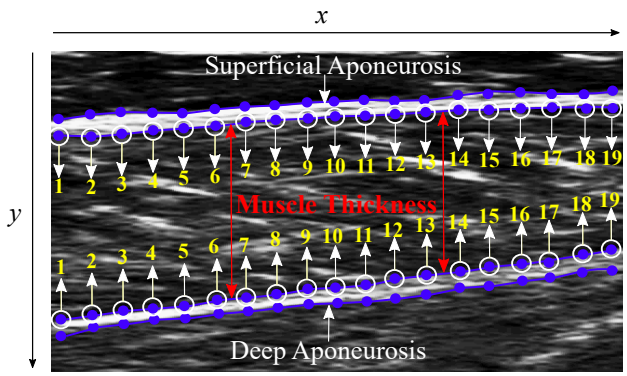

Figure 4.1: Annotation of the segmentation process used for calculating muscle thickness. Markers are placed along the boundaries of the aponeuroses (shown in blue). Their position is used to calculate the thickness of the muscle (represented by the red arrows).

4.3.4 Pre-processing of USI videos for greyscale analysis

4.3.4.1 Extraction of pixel intensity values

Each frame within the TVD file contained information about the pixel intensity of each scan line at a specific depth. The linear scanning probe had 96 transducers resulting in 96 scan lines and a scanning depth of 50 mm was used, corresponding to 884 pixels.

During offline analysis, the TVD files were converted to BIN file format containing the information about pixel intensity for each frame. This was done using an open source B to Lines 1.1.2 package (Telemed, Lithuania) supported in C++, which was then modified by Ania Sosnowska [8]. The program was controlled through MATLAB (R2019a, The Mathworks, USA), allowing the correct file to be converted with minimum effort. The BIN file could then be loaded in MATLAB, expressing pixel intensity data as a 96 $\times$ 884 matrix (width $\times$ height) containing values between 0 and 255.

4.3.4.2 Selection of region of interest

In order to only consider the intensity of the pixels within the muscle of interest, a region of interest (ROI) was selected, as shown in Figure 4.2. A rectangular ROI (75 $\times$ 115 pixels), different from that of the segmented muscle, was used to allow analysis of as much of the muscle as possible while keeping the size of the ROI consistent across all videos. This ensures the results of the greyscale analysis are not dependent on the size of the ROI. The ROI was selected so as not to include the aponeuroses of the muscle which are naturally very bright and therefore would affect the results. In this way, only the muscle tissue itself is analysed.

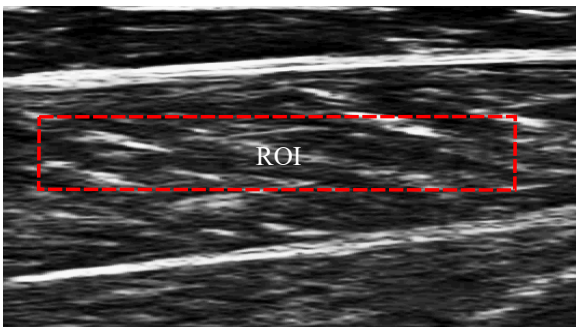

Figure 4.2: Annotation of the region of interest (ROI) selected for greyscale analysis.

4.3.5 Greyscale analysis

The pixel intensity values within the selected ROI were used to perform greyscale analysis on the ultrasound image of the muscle. This included first-order statistical descriptors to describe the echogenicity of the muscle and second-order statistical descriptors to describe the echotexture of the muscle by analysing the spatial arrangement of the pixels.

First-order statistical descriptors describe the histogram of pixel intensity values, providing measurements of the brightness of the image and therefore quantifying echogenicity. This provides information on the amount of non-contractile tissue within the muscle. Second-order statistical descriptors describe the spatial arrangement of light and dark pixels. They allow the echotexture of the muscle to be quantified and therefore provide a greater insight into the composition of the muscle. This includes Haralick features, which are calculated based on the grey-level co-occurrence matrix (GLCM), Galloway features that describe the run length matrix (RLM), and local binary pattern (LBP) features [7]. All features were calculated using functions in the image processing toolbox in MATLAB (R2019a, The Mathworks, USA).

The information these features provide can be split into two categories. The Haralick features and the LBP features describe the homogeneity of the muscle texture, while the Galloway features describe the coarseness. Homogeneity describes how equally distributed the pixel greyscale values are, i.e. how evenly black and white pixels are mixed. Coarseness describes the size of repeated elements within the image. Images with a rough texture are thought of as being more coarse than images with a finer, smoother texture.

4.3.5.1 First-order statistical descriptors

First-order statistics were used to describe the histogram of the pixel intensity values. Based on this, the following seven features were extracted from the pixel intensity values (I) within the selected ROI with width M and height N, denoted by $I(x,y)$:

1. **Integrated Optical Density (IOD)**: the sum of pixel intensity values within the area that is being measured.

$$IOD = \sum_{x=1}^{M} \sum_{y=1}^{N} I(x,y) \tag{4.2}$$

2. **Mean**: the average of the intensity values for all pixels within the ROI, representing the central tendency of the histogram.

$$m = \sum_{x=1}^{M} \sum_{y=1}^{N} \frac{I(x,y)}{M \times N} \tag{4.3}$$

3. **Energy**: describes the brightness of the image.

$$E_1 = \sum_{x=1}^{M} \sum_{y=1}^{N} I(x,y)^2 \tag{4.4}$$

4. **Variance**: the average degree to which each point differs from the central tendency.

$$\sigma^2 = \frac{\sum_{x=1}^{M} \sum_{y=1}^{N} \{I(x,y) - m\}^2}{M \times N} \tag{4.5}$$

5. **Standard deviation**: how far a group of numbers spreads from the central tendency, based on the square root of the variance (σ)

6. **Skewness**: the asymmetry of the probability distribution, i.e. how much the pixel intensity values vary from a normal distribution, where the histogram would be symmetrical.

$$S = \frac{1}{M \times N} \frac{\sum_{x=1}^{M} \sum_{y=1}^{N} \{I(x,y) - m\}^3}{\sigma^3} \tag{4.6}$$

7. **Kurtosis**: the combined sizes of the two tails i.e. a measure of the amount of probability in the tails. In terms of a histogram, the width of the central area of the curve compared to the tails.

$$K = \frac{1}{M \times N} \frac{\sum_{x=1}^{M} \sum_{y=1}^{N} \{I(x,y) - m\}^4}{\sigma^4} \tag{4.7}$$

4.3.5.2 Grey-level co-occurrence matrix (GLCM)

The grey-level co-occurrence matrix (GLCM) is a statistical method of measuring the texture of a greyscale image by considering the spatial relationship between pixels [7, 204]. It is a square matrix with dimensions equal to the number of grey levels. In this case pixel intensity values ranging from 0 to 255 were scaled to 8 levels, as this is the default for computational efficiency [7, 205]. The GLCM is created by calculating how often pairs of pixels with specific values occur in an image. Element $M(i, j)$ in the matrix measures the number of times a pixel with grey level i is found adjacent to a pixel with grey level j.

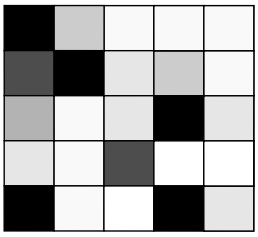

(a) Greyscale image

1	5	7	7	7
2	1	6	5	7
4	7	6	1	6
6	7	2	8	8
1	7	8	1	6

(b) Pixel values

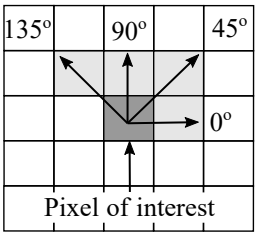

(c) Directions

	1	2	3	4	5	6	7	8
1	0	1	0	0	1	4	1	1
2	1	0	0	0	0	0	1	1
3	0	0	0	0	0	0	0	0
4	0	0	0	0	0	0	1	0
5	1	0	0	0	0	1	2	0
6	4	0	0	0	1	0	2	0
7	1	1	0	1	2	2	4	1
8	1	1	0	0	0	0	1	2

(d) GLCM (0°)

	1	2	3	4	5	6	7	8
1	0	1	0	1	0	0	3	1
2	1	0	0	0	1	0	1	0
3	0	0	0	0	0	0	0	0
4	1	0	0	0	0	0	0	0
5	0	1	0	0	0	1	1	0
6	0	0	0	0	1	0	4	1
7	3	1	0	0	1	4	0	0
8	1	0	0	0	0	1	0	2

(e) GLCM (45°)

	1	2	3	4	5	6	7	8
1	0	1	0	0	2	1	1	2
2	1	0	0	1	0	1	0	1
3	0	0	0	0	0	0	0	0
4	0	1	0	0	0	1	0	0
5	2	0	0	0	0	0	1	0
6	1	1	0	1	0	2	2	2
7	1	0	0	0	1	2	6	0
8	2	1	0	0	0	2	0	0

(f) GLCM (90°)

	1	2	3	4	5	6	7	8
1	2	1	0	0	0	2	0	1
2	1	0	0	0	0	0	2	0
3	0	0	0	0	0	0	0	0
4	0	0	0	0	0	0	1	0
5	0	0	0	0	0	2	1	0
6	2	0	0	0	2	0	1	2
7	0	2	0	1	1	1	2	1
8	1	0	0	0	0	2	1	0

(g) GLCM (135°)

Figure 4.3: Representation of the calculation of the grey-level co-occurrence matrix (GLCM) including a greyscale representation of the image, the corresponding pixel values and associated GLCMs in four directions (0°, 45°, 90° and 135°). Adapted from [7].

Two pixels can be adjacent in the horizontal, vertical or diagonal directions, therefore the GLCM was calculated for four angles 0°, 45°, 90° and 135°, as shown in Figures 4.3b and 4.3c. For all directions pairings were symmetric, counting both i,j and j,i pairings when calculating the number of times a pixel with grey level i is found adjacent to a pixel with grey level j. An example of this is highlighted by the red dashed line in Figure 4.3b, where a 6,1 pairing is counted in the number of times a pixel with grey level 1 is adjacent to a pixel with grey level 6.

Statistical measures known as the Haralick features were then extracted from this matrix to characterise the texture of the muscle (see Section 4.3.5.3). Figure 4.3 illustrates the calculation of a GLCM, showing an example of a small greyscale image, the corresponding pixel values, the four directions in which the GLCM is calculated and the four resultant GLCMs.

4.3.5.3 Haralick features

Haralick features are second-order statistics which describe the texture of an image and are calculated based on the GLCM. The GLCM was calculated as described in Section 4.3.5.2 and has dimensions $N \times N$, where N is the number of grey levels. $P(i,j)$ represents the probability that a pixel of grey level i is at a distance $(\Delta x, \Delta y)$ away from a pixel of grey level j. From this, the following features were extracted in each of the four directions in which the GLCM is calculated (0°, 45°, 90°, 135°):

1. **Contrast**: measures variations between the reference pixel and its neighbour.

$$H_{con} = \sum_{n=0}^{N-1} n^2 \{ \sum_{i=0}^{N} \sum_{j=0}^{N} P(i,j) \} \tag{4.8}$$

2. **Correlation**: shows the linear dependency of grey level values in the GLCM,

$$H_{corr} = \frac{\sum_{i=0}^{N-1} \sum_{j=0}^{N-1} (i,j) P(i,j) - \mu_x \mu_y}{\sigma_x \sigma_y} \tag{4.9}$$

   where σ_x and σ_y are the standard deviations, and μ_x and μ_y are the means of the partial probability density functions P_x and P_y. P_x and P_y describe the individual components of $P(i,j)$, i.e. the probability that a pixel of grey level i is at a distance of Δx and Δy respectively. $p_x(i) = i^{th}$ entry in the marginal probability matrix obtained by summing the rows of $P(i,j)$.

3. **Energy**: represents the local uniformity of the grey levels

$$H_{enrg} = \sum_{i=0}^{N-1} \sum_{j=0}^{N-1} P(i,j)^2 \tag{4.10}$$

4. **Entropy**: the randomness or degree of disorder present in the image.

$$H_{entr} = -\sum_{i=0}^{N-1}\sum_{j=0}^{N-1} P(i,j)log(P(i,j)) \tag{4.11}$$

5. **Homogeneity**: measures how close the distribution of elements in the GLCM is to the diagonal of the GLCM.

$$H_{hmg} = \sum_{i=0}^{N-1}\sum_{j=0}^{N-1} \frac{1}{1+(i-j)^2} P(i,j) \tag{4.12}$$

4.3.5.4 Run length matrix (RLM)

Element $R(i,j)$ in the run length matrix (RLM) contains the number of pixels with run length j and intensity i in a given direction. The number of rows in the RLM is equal to the number of grey levels in the image.

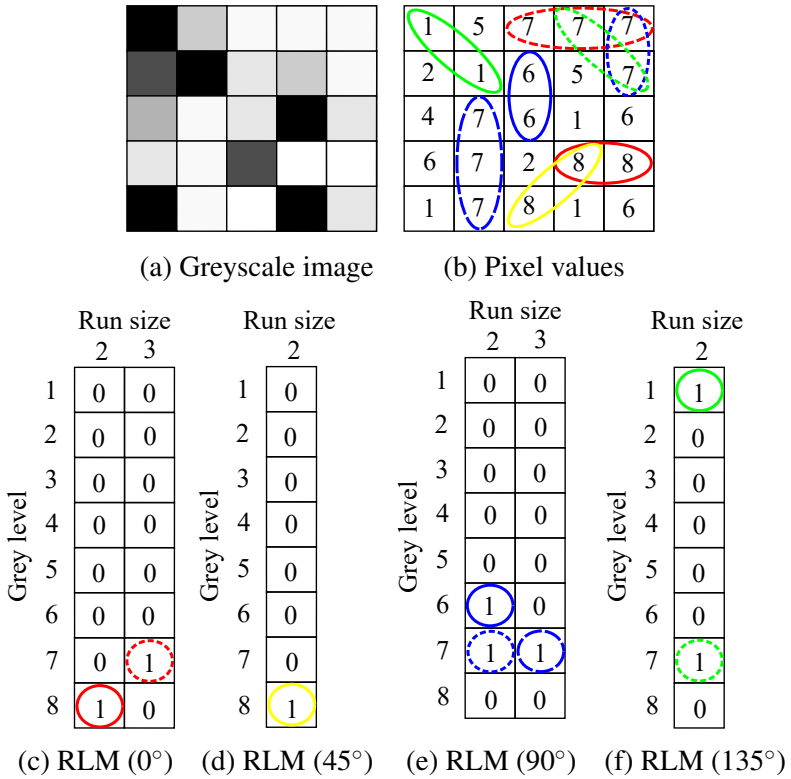

Figure 4.4: Representation of the calculation of the run length matrix (RLM) including a greyscale representation of the image, the corresponding pixel values and associated RLM for each of the four directions (0°,45°,90° and 135°). Adapted from [7].

Just as with the calculation of the GLCM (Section 4.3.5.2), pixels with values between 0 and 255 were scaled to 8 grey levels, resulting in a RLM with 8 rows. The number of columns is based on the maximum run length. Also similar to the calculation of the GLCM, the RLM was calculated in four directions (0°, 45°, 90° and 135°) as this is the maximum possible for a two-dimensional image.

An illustration of the calculation of the RLM in all four directions is shown in Figure 4.4. For the run length matrix in each of the four directions, features can be extracted to characterise the texture of the image (see Galloway features in section 4.3.5.5).

4.3.5.5 Galloway features

Galloway features are calculated from the RLM described in Section 4.3.5.4. Based on this RLM, $R(i,j)$, with N_g grey levels and N_r runs, the following features were calculated:

1. **Short run emphasis (SRE)**: measures the distribution of short runs, i.e. low numbers of pixels with the same grey level next to each other.

$$G_{SRE} = \frac{\sum_{i=1}^{N_g}\sum_{j=1}^{N_r}\frac{R(i,j)}{j^2}}{\sum_{i=1}^{N_g}\sum_{j=1}^{N_r}R(i,j)} \tag{4.13}$$

2. **Long run emphasis (LRE)**: measures the distribution of long runs, i.e. high numbers of pixels with the same grey level next to each other.

$$G_{LRE} = \frac{\sum_{i=1}^{N_g}\sum_{j=1}^{N_r}j^2R(i,j)}{\sum_{i=1}^{N_g}\sum_{j=1}^{N_r}R(i,j)} \tag{4.14}$$

3. **Grey-level non-uniformity (GLNU)**: measure the distribution of runs over the grey values.

$$G_{GLNU} = \frac{\sum_{i=1}^{N_g}(\sum_{j=1}^{N_r}R(i,j))^2}{\sum_{i=1}^{N_g}\sum_{j=1}^{N_r}R(i,j)} \tag{4.15}$$

4. **Run length non-uniformity (RLNU)**: measures the distribution of runs over the run lengths.

$$G_{RLNU} = \frac{\sum_{i=1}^{N_r}(\sum_{j=1}^{N_g}R(i,j))^2}{\sum_{i=1}^{N_g}\sum_{j=1}^{N_r}R(i,j)} \tag{4.16}$$

5. **Run percentage (RP)**: the fraction of the number of actual runs and the maximum number of potential runs.

$$G_{RP} = \frac{\sum_{i=1}^{N_g} \sum_{j=1}^{N_r} R(i,j)}{N_g \times M_r}, \tag{4.17}$$

where M_r is the maximum number of runs which is possible, i.e. size of the image in the direction the RLM is being calculated.

4.3.5.6 Local binary pattern (LBP)

The local binary pattern (LBP) assigns a value to a pixel neighbourhood based on the intensity of the pixels in comparison to the intensity of the central pixel. An example of a 3 × 3 pixel neighbourhood and the calculation of the resultant LBP is shown in Figure 4.5. This includes the pixel intensities of the 3 × 3 pixel neighbourhood; the binarisation of the image where pixels with an intensity value less than that of the central pixel are assigned the value 0 and those with a higher intensity are assigned the value 1; and the power-of two weights which are then multiplied with this binarised image to give the final LBP neighbourhood. The overall LBP value assigned to the central pixel is the sum of the numbers in the LBP neighbourhood, so in the case of Figure 4.5, the LBP is equal to 216.

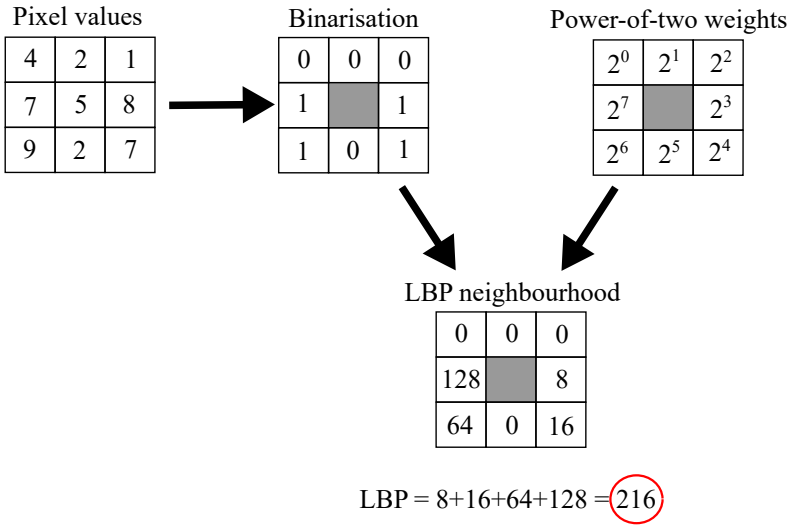

Figure 4.5: Representation of the calculation of the local binary pattern (LBP) including pixel values corresponding to greyscale intensity, binarisation by threshold, power-of-two weights and the resulting LBP neighbourhood. Adapted from [7].

The LBP was calculated with a radius of 4 pixels, taking into account 32 neighbouring pixels as shown in Figure 4.6. This allows the consideration of a relatively large neighbourhood as recommended in the literature [7].

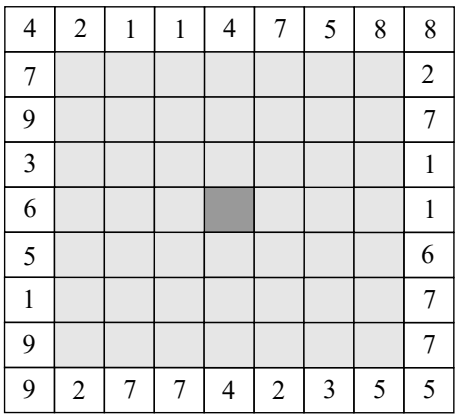

Figure 4.6: Local binary pattern (LBP) neighbourhood with a radius of 4 pixels.

Based on the relative frequency of the histogram derived from the LBP values of all the image pixels (f_i), the following features were extracted:

1. **Energy**: represents the local uniformity

$$LBP_{enrg} = \sum_{i}^{N_p} f_i^2 \tag{4.18}$$

2. **Entropy**: represents the randomness or degree of disorder

$$LBP_{entr} = -\sum_{i}^{N_p} f_i \times log_2(f_i), \tag{4.19}$$

where N_p is the total number of pixels.

4.3.6 Statistical analysis

4.3.6.1 Grouping of data

Fifteen able-bodied participants completed one session each, resulting in fifteen data points for each measurement. SCI participants on the other hand, each completed several sessions, resulting in a total of 63 data points for each measurement. These 63 data points are separated into three groups according to the time post-injury when it was obtained: 0-3, 3-6 and 6-9 months. The time post-injury at which SCI participants completed the first session varied between participants. Following this, each participant completed monthly sessions until they were discharged or withdrew from the study. As a result, there are participants with two or more data points from different sessions which fall into the same group. When this occurred, data points from the same participant within a group were averaged. There are also participants with no data points in at

least one group, resulting in different numbers of matched pairs for each comparison made. The number of data points used for each comparison is shown in Table 4.1

Table 4.1: Number of matched pairs being compared between groups.

Groups compared	Number of matched pairs
AB and SCI 0-3 months	12
AB and SCI 3-6 months	14
AB and SCI 6-9 months	7
SCI 0-3 months and SCI 3-6 months	11
SCI 0-3 months and SCI 6-9 months	5
SCI 3-6 months and SCI 6-9 months	7

4.3.6.2 Calculation of statistically significant differences

When the sample size was ten or more, the Shapiro-Wilk test was used to assess the normality of the data as described in Section 3.9.1. When data was found to be normally distributed, a paired t-test was used (see Section 3.9.2.1). When data was not normally distributed or the sample size was less than ten, the non-parametric Wilcoxon signed rank test was used as an alternative (see Section 3.9.2.2).

Both tests were performed using a significance level of p=0.05, however as comparisons were carried out in a pairwise manner this was adjusted using the Bonferroni correction for multiple comparisons, as described in Section 3.9.3. One group of able-bodied participants is compared to three SCI groups at different times post-injury. The SCI groups are also compared to each other, resulting in a total of six statistical tests. The adjusted significance value used is therefore p=0.008 (0.05/6).

4.3.6.3 Calculation of Cohen's d effect size

Cohen's d effect size was also calculated in line with a paired test using equation 3.6. Further details on Cohen's d effect size and how to interpret it are provided in Section 3.9.4.

4.3.6.4 Multivariate analysis of variance (MANOVA) to calculate canonical variables

Multivariate analysis of variance (MANOVA), described in Section 3.9.5, was performed on the texture features with respect to the time since a SCI had occurred. Three independent groups were compared, each containing five different SCI participants at 0-3, 3-6 and 6-9 months post-injury, and the texture features were considered as the dependent variables. There were 49 texture features in total: 7 first-order features; 20 Haralick features calculated from the GLCM; 20 Galloway features calculated from the RLM; and 2 LBP features. There were therefore 49 dependent variables before collinear variables were removed by computing Wilks' lambda in order to avoid singularities in the observation matrix. Wilks' lambda is the proportion the

total variance in the discriminant scores not explained by differences among groups, with lower values suggesting the associated variable is more discriminant between groups. Variables were removed if the lambda value calculated was more than 0.62 as a higher threshold was insufficient and a lower threshold removed more variables than was necessary.

After the removal of the collinear variables, 12 variables remained: first-order variables standard deviation and variance; Haralick contrast (0° and 45°), energy (90°) and homogeneity (0°, 45°); Galloway GLNU (45°, 90°), RLNU (90°) and RP (45°, 90°). MANOVA was used to test the equality of means among groups of SCI participants at different times post-injury based on these 12 variables. This allowed the calculation of the first and second canonical variables as described in Section 3.9.5.1.

4.4 Results

The results in this section are based on USI videos recorded while the muscle is at rest. Measurements of muscle structure are compared between SCI participants at different times post-injury, and with an age and gender matched able-bodied control group. Firstly, an example of the raw US images are shown. Then the thickness of the muscle, obtained from tracking software, quantitatively describes the size of the muscle. This is followed by the results of the greyscale analysis: histograms describe the distribution of the pixel values; first-order statistical descriptors are used to describe the echogenicity of the muscle; and second-order statistical descriptors are used to describe the echotexture of the muscle, with Haralick features describing the homogeneity of the muscle and Galloway features describing the coarseness.

4.4.1 Example of raw ultrasound images

An example of the US images obtained from one SCI participant at different times post-injury and an age and gender matched able-bodied participant are shown in Figure 4.7. The thickness of the muscle is smaller for the SCI participant, but there is little change between the different times post-injury. The echogenicity increases with time since injury and the striated appearance of the muscle, representing the arrangement of the fascicles, becomes less clearly defined.

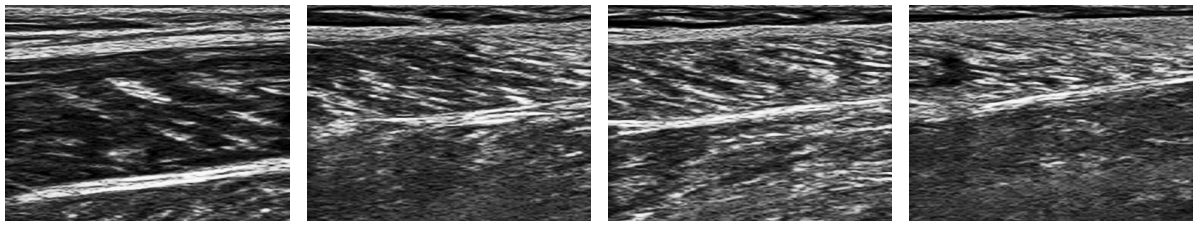

(a) Able-bodied (b) SCI: 8 weeks (c) SCI: 20 weeks (d) SCI: 28 weeks

Figure 4.7: Examples of ultrasound images of the gastrocnemius muscle for a spinal cord injury (SCI) participant at different times post-injury and a matched able-bodied control.

4.4.2 Resting muscle thickness

The resting thickness of the muscle, calculated from equation 4.1 (see Section 4.3.3), decreases following a SCI as shown in Figure 4.8. The p-values and effect sizes for the resting muscle thickness are shown in Table 4.2. There are large and very large effect sizes between the able-bodied participants and all SCI groups, however after the Bonferonni correction for multiple comparisons, a significant difference is only seen between able-bodied and SCI at 0-3 and 3-6 months post-injury. SCI participants show a similar muscle thickness across all times post-injury, with no significant differences and only very small to medium effect sizes.

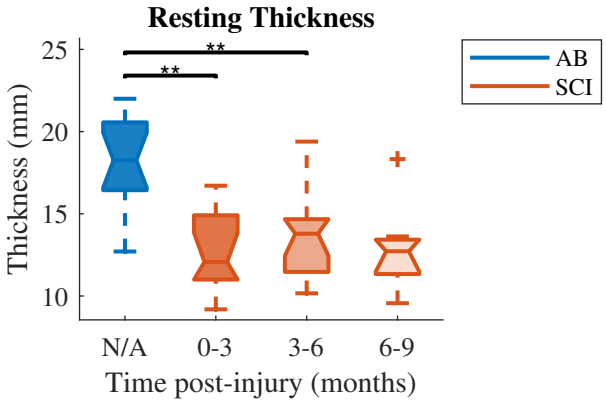

Figure 4.8: Boxplot of the resting muscle thickness for able-bodied participants and SCI participants at different times post-injury ($** - p < 0.01$).

Table 4.2: P-values and effect sizes for resting muscle thickness of able-bodied participants and SCI participants at different times post-injury. Values indicating a significant difference or a greater than medium effect size are shown in bold.

	P-Value	**Effect Size**
AB vs. $SCI_{0\text{-}3}$	**0.001**	**1.24**
AB vs. $SCI_{3\text{-}6}$	**0.002**	**1.07**
AB vs. $SCI_{6\text{-}9}$	0.03	**1.30**
$SCI_{0\text{-}3}$ vs. $SCI_{3\text{-}6}$	0.07	0.22
$SCI_{0\text{-}3}$ vs. $SCI_{6\text{-}9}$	0.63	0.38
$SCI_{3\text{-}6}$ vs. $SCI_{6\text{-}9}$	0.69	0.17

4.4.3 Greyscale analysis

4.4.3.1 Histogram of pixel greyscale values

Figure 4.9 shows histograms of the greyscale values of all pixels for able-bodied participants and SCI participants at different times post-injury, allowing the distribution of pixel intensity to be visualised. SCI participants at 0-3 months post-injury show a small shift to the right compared to the able-bodied group. This shift towards higher greyscale values continues to increase with time

after injury, suggesting that the brightness of the ROI increases following a SCI and continues to increase with time. There is also a difference in the shape of the histograms. The able-bodied histogram is skewed to the right, while the histograms of SCI participants become progressively more skewed to the left with time since injury. The p-values and effect sizes are shown in Table 4.3. Significant differences are seen between each group, however, as all pixel values within the ROI for all participants in each group (able-bodied: $n = 321,602$; SCI 0-3 months: $n = 264,421$; SCI 3-6 months: $n = 523,910$; SCI 6-9 months: $n = 181,505$) are included this should be interpreted with caution. The effect size increases from medium to large with time since injury compared to the able-bodied group, but are small between all SCI groups.

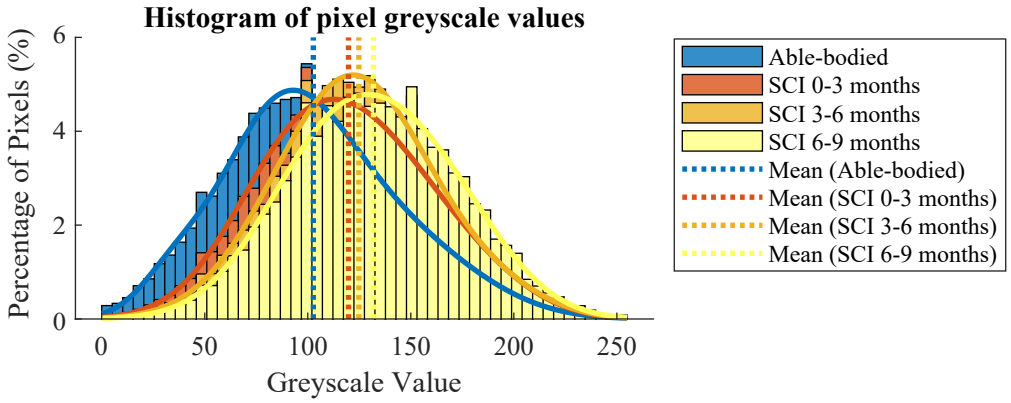

Figure 4.9: Histograms of the pixel greyscale values for able-bodied participants and SCI participants at different times post-injury. Higher greyscale values represent brighter pixels.

Table 4.3: P-values and effect sizes for all pixel intensity values within the selected region of interest for able-bodied participants and SCI participants at different times post-injury. Values indicating a significant difference or a greater than medium effect size are shown in bold.

	P-Value	**Effect Size**
AB vs. $SCI_{0\text{-}3}$	**< 0.001**	0.56
AB vs. $SCI_{3\text{-}6}$	**< 0.001**	0.77
AB vs. $SCI_{6\text{-}9}$	**< 0.001**	**0.87**
$SCI_{0\text{-}3}$ vs. $SCI_{3\text{-}6}$	**< 0.001**	0.62
$SCI_{0\text{-}3}$ vs. $SCI_{6\text{-}9}$	**< 0.001**	0.29
$SCI_{3\text{-}6}$ vs. $SCI_{6\text{-}9}$	**< 0.001**	0.19

4.4.3.2 First-order statistical descriptors

First-order descriptors are quantitative measurements, calculated from equations 4.2 to 4.7 in Section 4.3.5.1, that describe the histograms shown in Figure 4.9 as a single value. The p-values and effect sizes for the first-order statistical descriptors are shown in Table 4.4. Integrated optical density (Figure 4.10a), the mean greyscale value (Figure 4.10b), and energy (Figure 4.10c) all show a similar increase following a SCI. The 0-3 and 3-6 months post-injury groups are

significantly higher than the able-bodied group, however after the Bonferroni correction the 6-9 months post-injury group does not reach statistical significance. Despite this, the effect size increases from large between able-bodied and SCI at 0-3 months to huge at 6-9 months post-injury. There are no significant differences between SCI groups, however, a medium effect size is seen between 0-3 and 3-6 months post-injury groups, and a large effect size is seen between 3-6 and 6-9 months post-injury. There is an even bigger effect size, still classified as large, between 0-3 and 6-9 months post-injury.

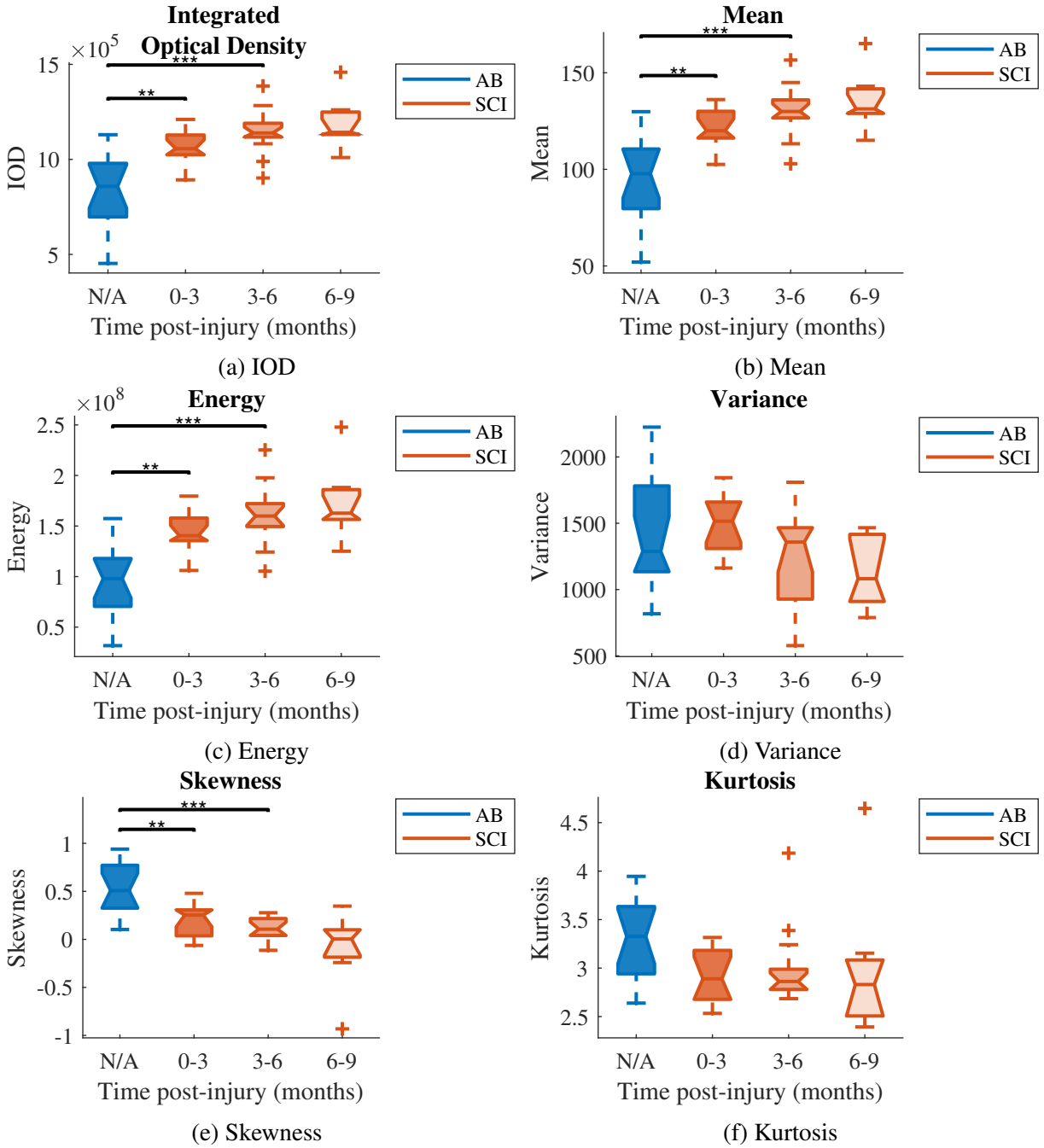

Figure 4.10: Boxplots of the first-order measurements of muscle echogenicity for able-bodied participants and SCI participants at different times post-injury ($**-p<0.01, ***-p<0.001$).

Variance (Figure 4.10d) shows a similar value between able-bodied and SCI at 0-3 months post-injury, and then decreases. There are no significant differences between any of the groups, however there are medium effect sizes between the able-bodied group, and the 3-6 and 6-9 months post-injury groups. There are also medium effect sizes between SCI participants at 0-3 months and those at 3-6 and 6-9 months post-injury, and very large effect sizes between 3-6 and 6-9 months post-injury. Standard deviation is not shown in this section as it showed the same results as variance.

Figure 4.10e shows that skewness decreases with SCI and continues to decrease with time since injury. There are significant differences between the able-bodied group and all SCI groups except at 6-9 months post-injury after the Bonferroni correction. The effect size between the able-bodied group and all SCI groups is large to very large. There is also a medium effect size between SCI groups at 3-6 and 6-9 months post-injury and a large effect size between 0-3 and 6-9 months post-injury. Figure 4.10f shows a decrease in kurtosis between able-bodied and SCI participants, however, this difference does not reach statistical significance and only small to medium effect sizes are seen. Kurtosis appears to be similar between SCI at different times post-injury.

Table 4.4: P-values and effect sizes for first-order statistical descriptors of echogenicity for able-bodied participants and SCI participants at different times post-injury. Values indicating a significant difference or a greater than medium effect size are shown in bold.

P-Value						
	IOD	*Mean*	*Energy*	*Variance*	*Skewness*	*Kurtosis*
AB vs. SCI_{0-3}	**0.004**	**0.004**	**0.002**	0.52	**0.002**	0.04
AB vs. SCI_{3-6}	**< 0.001**	**< 0.001**	**< 0.001**	0.04	**< 0.001**	0.08
AB vs. SCI_{6-9}	0.02	0.02	0.02	0.16	0.02	0.58
SCI_{0-3} vs. SCI_{3-6}	0.06	0.09	0.10	0.10	0.16	0.32
SCI_{0-3} vs. SCI_{6-9}	0.19	0.19	0.19	0.31	0.13	0.63
SCI_{3-6} vs. SCI_{6-9}	0.08	0.08	0.11	0.02	0.08	0.81
Effect Size						
	IOD	*Mean*	*Energy*	*Variance*	*Skewness*	*Kurtosis*
AB vs. SCI_{0-3}	**1.05**	**1.06**	**1.15**	0.19	**1.15**	0.67
AB vs. SCI_{3-6}	**1.52**	**1.52**	**1.57**	0.63	**1.91**	0.51
AB vs. SCI_{6-9}	**2.75**	**2.76**	**2.64**	0.69	**1.83**	0.26
SCI_{0-3} vs. SCI_{3-6}	0.64	0.57	0.55	0.55	0.46	0.13
SCI_{0-3} vs. SCI_{6-9}	**1.04**	**0.98**	**0.95**	**0.72**	**0.84**	0.17
SCI_{3-6} vs. SCI_{6-9}	**0.88**	**0.89**	**0.78**	**1.37**	0.57	0.20

4.4.3.3 Haralick features

The GLCM describes the spatial distribution of pixel greyscale values as described in Section 4.3.5.2. From this the Haralick features are calculated using equations 4.8 to 4.12, as described in Section 4.3.5.3. The p-values and effect sizes for the Haralick features are shown in Table 4.5.

Figure 4.11a shows that contrast initially increases after a spinal cord injury, with a statistically significant increase and very large to huge effect size seen between the able-bodied group and SCI participants at 0-3 months post-injury in the 0° and 45° directions. The large effect sizes in the 90° and 135° directions do not reach statistical significance after the Bonferroni correction. Contrast then decreases back to a similar level to the able-bodied group for SCI participants by 6-9 months post-injury. No further significant differences are seen, however, effect sizes ranging from large to huge are seen between SCI participants at 6-9 months and the other SCI groups. Contrast also appears to be lower in the 90° direction compared to all other directions.

Correlation decreases over time following a SCI as shown in Figure 4.11b. SCI participants at 0-3 months show a similar correlation to able-bodied participants, however a significant decrease can be seen between able-bodied participants and SCI at 3-6 months post-injury in all directions, coinciding with large effect sizes. This does not reach statistical significance at 6-9 months post-injury, however large effect sizes are seen in the 45° and 90° directions. The only difference seen between SCI groups are large effect sizes between 3-6 and 6-9 months post-injury in the 90° direction, which is slightly higher compared to the other directions.

Figure 4.11c shows that energy decreases immediately following a SCI and then increases over time until it reaches a similar level to the able-bodied group. There are medium to large effect sizes between the able-bodied and SCI at 0-3 months post-injury groups, and only very small to small effect sizes between the able-bodied group and all other SCI groups. There are medium to large effect sizes between SCI participants at 6-9 months and all other SCI groups. None of these differences reach statistical significance.

Entropy decreases immediately following a SCI, before increasing with time in the 0°,45° and 135° directions (Figure 4.11d). Large to huge effect sizes are seen between able-bodied and SCI at 0-3 months, however, after the Bonferroni correction statistical significance is only reached in the 0° and 45° directions. Large to huge effect sizes are also seen between SCI at 6-9 months post-injury and all other SCI groups. Conversely, in the 90° direction, entropy appears to increase immediately after injury and then decrease with time. A large effect size is seen between able-bodied and SCI at 0-3 months post-injury, as well as between SCI participants at 3-6 and 6-9 months, however, no statistically significant differences are seen.

Similar to energy, homogeneity (Figure 4.11e) initially decreases following a SCI and then increases with time since injury to a similar level to that of the able-bodied group. No statistically significant differences are seen after the Bonferroni correction, however, a medium effect size is seen between the able-bodied group and SCI participants at 0-3 months in the 45° direction. Furthermore, large to very large effect sizes are seen between SCI at 0-3 and 6-9 months post-injury in all directions, and large to huge effect sizes are seen between SCI at 3-6 and 6-9 months in the 0° and 45° directions. A medium effect size is also seen between SCI participants at 0-3 and 3-6 months in the 45° direction. Homogeneity is higher in the 90° direction compared to all other directions.

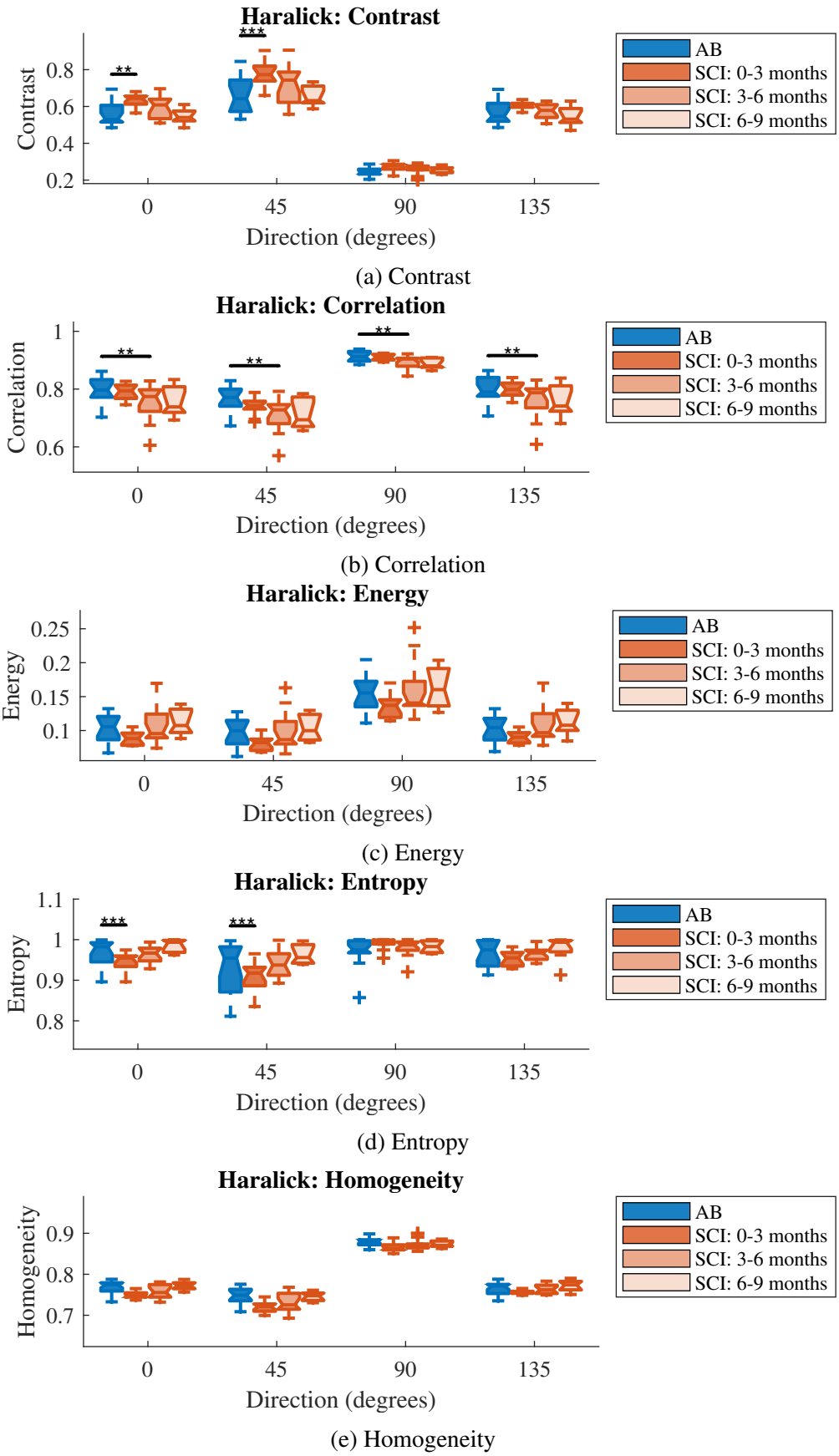

(a) Contrast

(b) Correlation

(c) Energy

(d) Entropy

(e) Homogeneity

Figure 4.11: Boxplots of Haralick features describing muscle echotexture for able-bodied participants and SCI participants at different times post-injury ($**-p<0.01, ***-p<0.001$).

Table 4.5: P-values and effect sizes for Haralick features for able-bodied participants and SCI participants at different times post-injury. Values indicating a significant difference or a greater than medium effect size are shown in bold.

Contrast								
	P-Value				*Effect Size*			
	0°	*45°*	*90°*	*135°*	*0°*	*45°*	*90°*	*135°*
AB vs. SCI_{0-3}	**0.002**	**< 0.001**	0.01	0.03	**1.38**	**2.46**	**0.87**	**0.82**
AB vs. SCI_{3-6}	0.14	0.03	0.19	0.63	0.43	0.64	0.34	0.13
AB vs. SCI_{6-9}	0.81	0.47	0.58	0.16	0.23	0.31	0.38	0.52
SCI_{0-3} vs. SCI_{3-6}	0.10	0.16	0.23	0.05	0.55	0.45	0.39	0.66
SCI_{0-3} vs. SCI_{6-9}	0.06	0.06	0.19	0.06	**2.10**	**1.57**	0.77	**1.64**
SCI_{3-6} vs. SCI_{6-9}	0.03	0.03	0.08	0.30	**1.03**	**1.21**	**0.89**	0.59
Correlation								
	P-Value				*Effect Size*			
	0°	*45°*	*90°*	*135°*	*0°*	*45°*	*90°*	*135°*
AB vs. SCI_{0-3}	0.64	0.17	0.77	0.93	0.14	0.42	0.09	0.03
AB vs. SCI_{3-6}	**0.01**	**0.001**	**0.003**	**0.01**	**0.86**	**1.08**	**0.98**	0.78
AB vs. SCI_{6-9}	0.16	0.08	0.05	0.16	0.69	**0.95**	**0.97**	0.65
SCI_{0-3} vs. SCI_{3-6}	0.21	0.17	0.08	0.15	0.43	0.43	0.53	0.43
SCI_{0-3} vs. SCI_{6-9}	0.63	0.63	0.44	0.63	0.26	0.25	0.54	0.27
SCI_{3-6} vs. SCI_{6-9}	0.22	0.22	0.11	0.16	0.70	0.72	**0.89**	0.67
Energy								
	P-Value				*Effect Size*			
	0°	*45°*	*90°*	*135°*	*0°*	*45°*	*90°*	*135°*
AB vs. SCI_{0-3}	0.02	0.01	0.04	0.03	**0.82**	**0.92**	0.67	0.70
AB vs. SCI_{3-6}	0.81	0.86	0.50	0.50	0.12	0.05	0.17	0.19
AB vs. SCI_{6-9}	0.58	0.69	0.58	0.47	0.32	0.19	0.25	0.36
SCI_{0-3} vs. SCI_{3-6}	0.07	0.07	0.08	0.07	0.49	0.49	0.46	0.49
SCI_{0-3} vs. SCI_{6-9}	0.06	0.31	0.31	0.06	**0.90**	**0.82**	0.69	**0.95**
SCI_{3-6} vs. SCI_{6-9}	0.02	0.05	0.08	0.02	**1.07**	**1.03**	**1.05**	**1.06**
Entropy								
	P-Value				*Effect Size*			
	0°	*45°*	*90°*	*135°*	*0°*	*45°*	*90°*	*135°*
AB vs. SCI_{0-3}	**< 0.001**	**< 0.001**	0.01	0.03	**1.33**	**2.41**	**0.87**	0.73
AB vs. SCI_{3-6}	0.13	0.02	0.24	0.74	0.43	0.68	0.33	0.09
AB vs. SCI_{6-9}	0.69	0.30	0.59	0.08	0.30	0.41	0.34	0.63
SCI_{0-3} vs. SCI_{3-6}	0.20	0.22	0.23	0.12	0.41	0.39	0.38	0.51
SCI_{0-3} vs. SCI_{6-9}	0.06	0.06	0.19	0.06	**2.50**	**2.17**	0.78	**1.80**
SCI_{3-6} vs. SCI_{6-9}	0.03	0.03	0.08	0.22	**1.15**	**1.33**	**0.96**	0.71
Homogeneity								
	P-Value				*Effect Size*			
	0°	*45°*	*90°*	*135°*	*0°*	*45°*	*90°*	*135°*
AB vs. SCI_{0-3}	0.06	0.03	0.05	0.15	0.61	0.71	0.53	0.45
AB vs. SCI_{3-6}	0.90	0.34	0.95	0.84	0.04	0.26	0.17	0.06
AB vs. SCI_{6-9}	0.22	0.69	0.22	0.38	0.39	0.23	0.48	0.45
SCI_{0-3} vs. SCI_{3-6}	0.21	0.03	0.32	0.27	0.46	0.78	0.34	0.35
SCI_{0-3} vs. SCI_{6-9}	0.06	0.13	0.06	0.06	**1.87**	**0.96**	**1.21**	**1.37**
SCI_{3-6} vs. SCI_{6-9}	0.02	0.05	0.58	0.16	**2.39**	**0.94**	0.40	0.67

4.4.3.4 Galloway features

The Galloway features are second-order statistical descriptors based on the run length matrix (RLM), which was calculated as described in Section 4.3.5.4. They are calculated from equations 4.13 to 4.17, as shown in Section 4.3.5.5. P-values and effect sizes for all Galloway features are shown in Table 4.6.

The short run emphasis (SRE) decreases following a SCI and continues to decrease over time, as can be seen in Figure 4.12a. After the Bonferroni correction the only significant difference is between the able-bodied group and SCI participants at 3-6 months, however, large effect sizes are seen between able-bodied participants and all SCI groups except 0-3 post-injury. There are also medium to large effect sizes seen between all SCI groups in all directions.

The long run emphasis (LRE) on the other hand increases following a SCI and continues to increase with time since the injury occurred, as shown in Figure 4.12b. Significant differences are seen and accompanied by large to very large effect sizes between the able-bodied group and SCI participants at 0-3 and 3-6 months post-injury. After the Bonferroni correction, the differences between able-bodied and SCI participants at 6-9 months post-injury do not reach statistical significance, however, huge effect sizes are seen in all directions. There are medium effect sizes seen between SCI participants at 6-9 months and all other SCI groups, although these also did not reach statistical significance.

Grey-level non-uniformity (GLNU) initially shows an increase following a SCI and then decreases with time as shown in Figure 4.12c. The only significant difference is between able-bodied participants and SCI participants at 0-3 months in the 45° direction, however, a large effect size is also seen in the 0° direction. Large to huge effect sizes are also seen between SCI participants at 6-9 months post-injury and all other SCI groups except in the 135° direction.

Run length non-uniformity (RLNU), shown in Figure 4.12d, increases over time following a SCI. Again, the only significant difference is in the 45° direction, this time between the able-bodied and SCI at 3-6 months injury groups. There are, however, large effect sizes in the 0° and 90° directions. There are also medium and large effect sizes between SCI participants at 3-6 and 6-9 months post-injury in the 45° and 90° directions respectively.

Figure 4.12e shows that the run percentage (RP) yields the same results as the GLNU, initially increasing after a SCI and then decreasing back to the same level as the able-bodied participants. Statistical significance is seen between the able-bodied participants and SCI participants at 0-3 months post-injury in the 0° and 45° directions, coinciding with large to huge effect sizes. Large to huge effect sizes are also seen between SCI participants at 6-9 months post-injury and all other SCI groups.

The GLNU, RLNU and RP all appear to be much lower in the 90° direction compared to all other directions. Despite this, each measurement follows the same trend in the 90° direction as is seen in the other three directions.

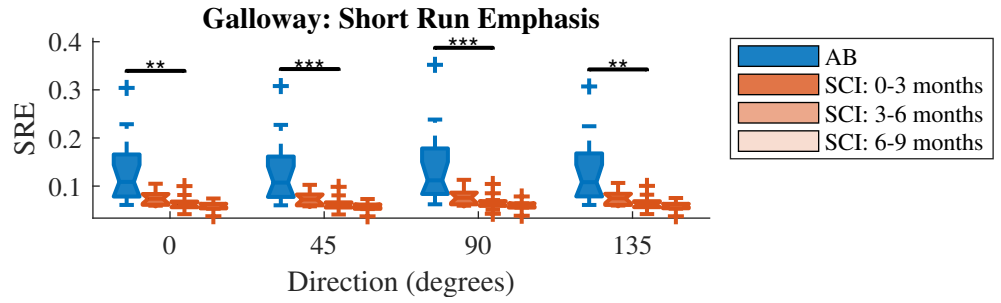

(a) Short run emphasis (SRE)

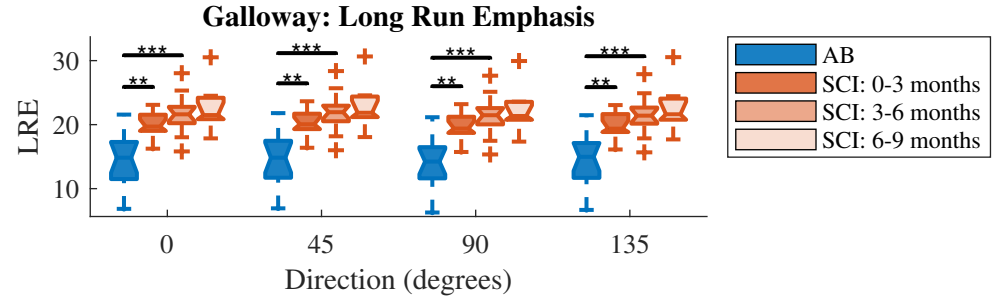

(b) Long run emphasis (LRE)

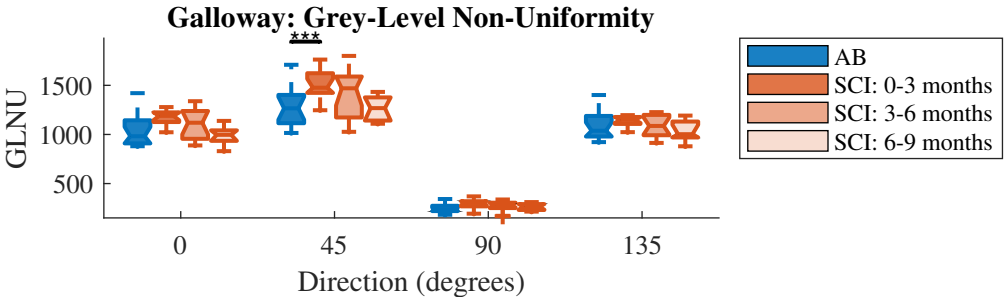

(c) Grey-level non-uniformity (GLNU)

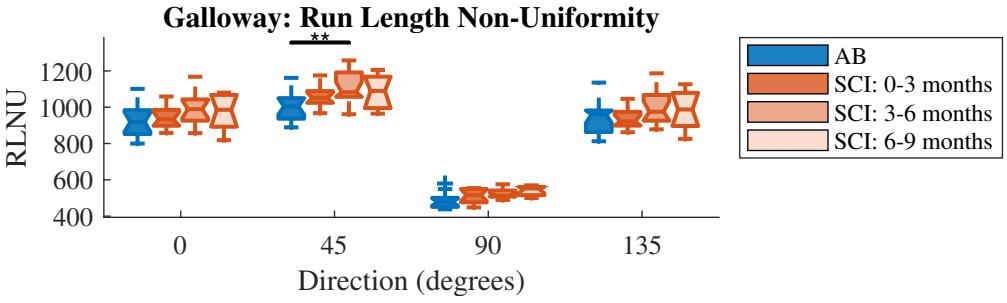

(d) Run length non-uniformity (RLNU)

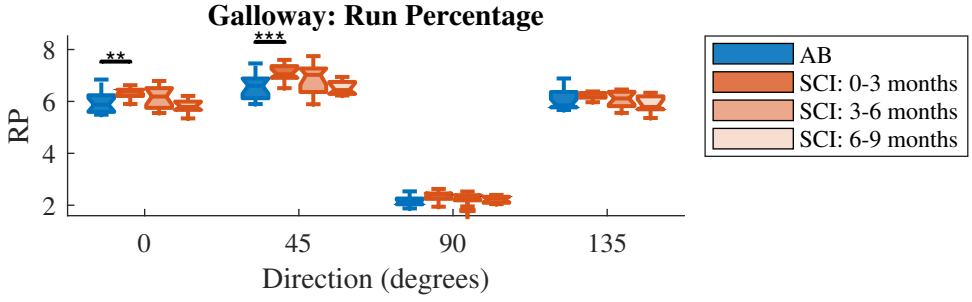

(e) Run Percentage (RP)

Figure 4.12: Boxplots of Galloway features describing muscle echotexture for able-bodied participants and SCI participants at different times post-injury ($**-p<0.01, ***-p<0.001$).

Table 4.6: P-values and effect sizes for Galloway features for able-bodied participants and SCI participants at different times post-injury. Values indicating a significant difference or a greater than medium effect size are shown in bold.

Short Run Emphasis (SRE)								
	P-Value				*Effect Size*			
	0°	*45°*	*90°*	*135°*	*0°*	*45°*	*90°*	*135°*
AB vs. SCI_{0-3}	0.01	0.01	0.01	0.01	0.77	0.76	0.73	0.76
AB vs. SCI_{3-6}	**0.002**	**< 0.001**	**< 0.001**	**0.002**	**1.04**	**1.02**	**0.99**	**1.03**
AB vs. SCI_{6-9}	0.02	0.02	0.02	0.02	**1.42**	**1.38**	**1.31**	**1.40**
SCI_{0-3} vs. SCI_{3-6}	0.04	0.07	0.07	0.04	0.70	0.67	0.69	0.70
SCI_{0-3} vs. SCI_{6-9}	0.19	0.19	0.19	0.19	0.74	0.74	0.70	0.74
SCI_{3-6} vs. SCI_{6-9}	0.03	0.03	0.03	0.05	**0.90**	**0.92**	**0.92**	**0.91**
Long Run Emphasis (LRE)								
	P-Value				*Effect Size*			
	0°	*45°*	*90°*	*135°*	*0°*	*45°*	*90°*	*135°*
AB vs. SCI_{0-3}	**0.002**	**0.002**	**0.003**	**0.002**	**1.15**	**1.16**	**1.12**	**1.13**
AB vs. SCI_{3-6}	**< 0.001**	**< 0.001**	**< 0.001**	**< 0.001**	**1.52**	**1.52**	**1.50**	**1.49**
AB vs. SCI_{6-9}	0.02	0.02	0.02	0.02	**2.71**	**2.69**	**2.58**	**2.64**
SCI_{0-3} vs. SCI_{3-6}	0.14	0.16	0.17	0.15	0.48	0.46	0.44	0.46
SCI_{0-3} vs. SCI_{6-9}	0.19	0.19	0.19	0.19	0.73	0.68	0.64	0.71
SCI_{3-6} vs. SCI_{6-9}	0.16	0.11	0.11	0.22	0.63	0.66	0.66	0.64
Grey-Level Non-Uniformity (GLNU)								
	P-Value				*Effect Size*			
	0°	*45°*	*90°*	*135°*	*0°*	*45°*	*90°*	*135°*
AB vs. SCI_{0-3}	0.03	**< 0.001**	0.03	0.27	**0.88**	**1.98**	0.73	0.42
AB vs. SCI_{3-6}	0.39	0.04	0.37	0.85	0.30	0.60	0.25	0.05
AB vs. SCI_{6-9}	0.69	0.58	0.94	1.00	0.28	0.33	0.09	0.20
SCI_{0-3} vs. SCI_{3-6}	0.47	0.42	0.25	0.28	0.23	0.26	0.37	0.34
SCI_{0-3} vs. SCI_{6-9}	0.06	0.06	0.19	0.06	**2.28**	**1.91**	0.72	**1.79**
SCI_{3-6} vs. SCI_{6-9}	0.05	0.03	0.08	0.30	**0.94**	**1.26**	**0.87**	0.52
Run Length Non-Uniformity (RLNU)								
	P-Value				*Effect Size*			
	0°	*45°*	*90°*	*135°*	*0°*	*45°*	*90°*	*135°*
AB vs. SCI_{0-3}	0.64	0.14	0.17	0.76	0.14	0.46	0.41	0.09
AB vs. SCI_{3-6}	0.01	**0.003**	0.02	0.02	0.77	**0.99**	0.76	0.69
AB vs. SCI_{6-9}	0.30	0.11	0.16	0.38	0.39	0.66	0.60	0.35
SCI_{0-3} vs. SCI_{3-6}	0.14	0.19	0.41	0.17	0.48	0.43	0.26	0.44
SCI_{0-3} vs. SCI_{6-9}	1.00	1.00	0.63	1.00	0.05	0.07	0.32	0.03
SCI_{3-6} vs. SCI_{6-9}	0.69	0.11	0.16	0.16	0.29	0.68	0.70	0.40
Run Percentage (RP)								
	P-Value				*Effect Size*			
	0°	*45°*	*90°*	*135°*	*0°*	*45°*	*90°*	*135°*
AB vs. SCI_{0-3}	**0.01**	**< 0.001**	0.02	0.11	**1.06**	**2.17**	0.76	0.55
AB vs. SCI_{3-6}	0.20	0.04	0.41	0.76	0.36	0.61	0.23	0.09
AB vs. SCI_{6-9}	0.81	0.58	0.81	0.47	0.29	0.32	0.12	0.40
SCI_{0-3} vs. SCI_{3-6}	0.48	0.37	0.21	0.30	0.22	0.29	0.40	0.33
SCI_{0-3} vs. SCI_{6-9}	0.06	0.06	0.19	0.06	**2.45**	**2.34**	0.76	**1.73**
SCI_{3-6} vs. SCI_{6-9}	0.05	0.02	0.08	0.16	**0.99**	**1.33**	**1.12**	0.57

4.4.3.5 Local binary pattern (LBP) features

Features were calculated from the local binary pattern (LBP) using equations 4.18 and 4.19 as described in Section 4.3.5.6. P-values and effect sizes for LBP features are provided in Table 4.7. Figure 4.13a shows that the energy increases following a SCI. There is a medium effect size between the able-bodied group and SCI participants at 0-3 months post-injury, which increases to a large effect size by 3-6 months post-injury and then further increase to a very large effect size at 6-9 months post-injury. Despite this, the only difference that reaches statistical significance is between the able-bodied and SCI participants at 3-6 months post-injury. There is also a large effect size between SCI participants at 3-6 and 6-9 months. The variation also decreases with a SCI and by 6-9 months all participants have a value of 1 which is the maximum possible.

Conversely, the entropy of the LBP, shown in Figure 4.13b, decreases after a SCI. Again there are increasingly large effect sizes between able-bodied and SCI participants with time since injury, however, the only significant difference exists between able-bodied and SCI at 3-6 months post-injury. A large effect size also exists between SCI participants at 3-6 and 6-9 months. Again the variation in values decrease with a SCI and approaches 0 by 6-9 months.

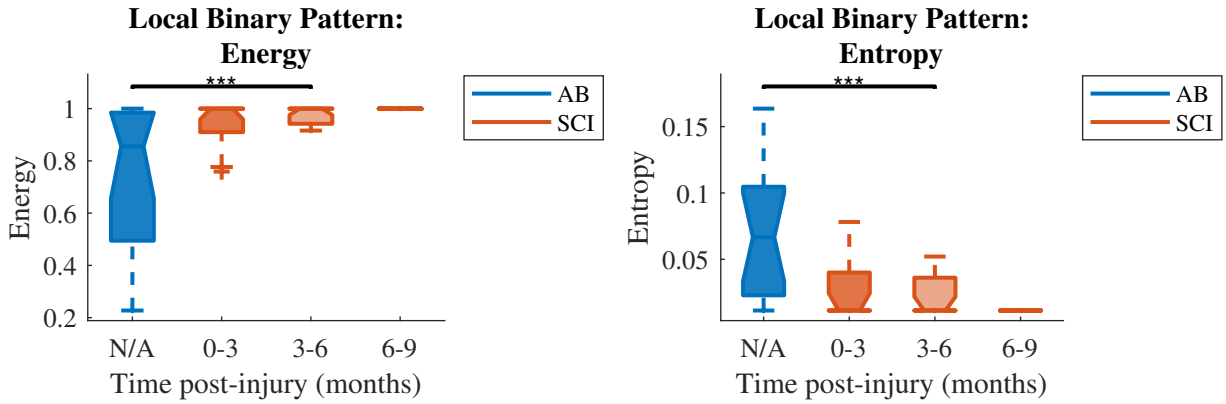

(a) Energy (b) Entropy

Figure 4.13: Boxplots of LBP features describing muscle echotexture for able-bodied participants and SCI participants at different times post-injury ($***-p<0.001$).

Table 4.7: P-values and effect sizes for LBP features for able-bodied participants and SCI participants at different times post-injury. Values indicating a significant difference or a greater than medium effect size are shown in bold.

	Energy		**Entropy**	
	P-value	*Effect Size*	*P-value*	*Effect Size*
AB vs. SCI_{0-3}	0.05	0.66	0.03	0.70
AB vs. SCI_{3-6}	**<0.001**	**0.97**	**< 0.001**	**1.28**
AB vs. SCI_{6-9}	0.02	**1.41**	0.02	**2.05**
SCI_{0-3} vs. SCI_{3-6}	0.43	0.44	0.44	0.28
SCI_{0-3} vs. SCI_{6-9}	1.00	0.44	1.00	0.45
SCI_{3-6} vs. SCI_{6-9}	0.13	**0.89**	0.13	**0.97**

4.4.3.6 Canonical variables

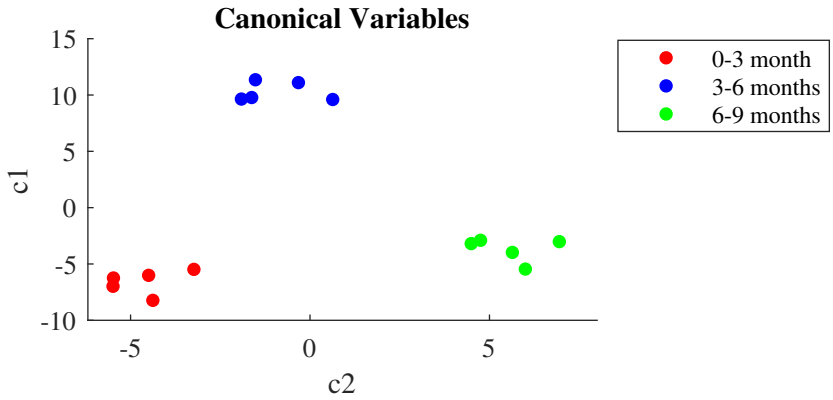

Figure 4.14: Scatter plot of the first two canonical variables showing the separation of SCI participants at different times post-injury based on 12 texture features.

A total of 12 out of a possible 49 texture features (2 first-order, 5 Haralick and 5 Galloway) are used to represent each participant during one assessment session as discussed in Section 4.3.6. Figure 4.14 shows SCI participants at different times post-injury in the plane of the first two canonical variables. The first canonical (c1) variable appears to separate those who are 3-6 months post-injury from the other SCI participants, while the second canonical variable (c2) separates each group of SCI participants at all three time periods.

4.5 Discussion

It was hypothesised that changes in muscle structure occur over time following a SCI that could be detected by USI. The results section of this chapter presents measurements of muscle thickness, obtained from tracking software, and measurements of muscle echogenicity and echotexture obtained from greyscale analysis. Differences in these measurements were seen between able-bodied participants and SCI participants at different times post-injury, supporting this hypothesis.

4.5.1 Changes in muscle structure following a SCI

4.5.1.1 Resting muscle thickness

The reduction in resting muscle thickness seen between able-bodied and SCI participants is characteristic of atrophy. Muscle atrophy is defined as a reduction in the size and number of muscle fibres, therefore it follows that as the muscle undergoes this process the overall size would decrease [39, 42].

However, there is no difference between SCI participants at different times post-injury, suggesting that there is an initial decrease in muscle thickness following the injury that does not

continue to change over time. The initial decline could be explained by rapid muscle atrophy during the first month following a SCI before data collection began. This would be expected as even patients with incomplete injuries would be completely immobile. It is less clear why no further changes in muscle thickness are seen over time. It is possible that after this initial phase patients receive physiotherapy which stops muscle atrophy progressing so quickly. Patients are grouped according to time since injury, therefore there is a wide variation in the amount of recovery participants have undergone within each group.

As well as a reduction in muscle fibres, skeletal muscle atrophy has also been shown to be related to the accumulation of intramuscular fat [43]. It is therefore also likely that muscle atrophy is still progressing over time and the number of muscle fibres is continuing to decrease, but the infiltration of fat is maintaining muscle bulk and therefore the overall size of the muscle is not decreasing any further.

4.5.1.2 Muscle echogenicity

Muscle echogenicity describes how bright the muscle appears on an ultrasound image i.e. how many white pixels and how many darks pixels there are, as images with a higher proportion of white pixels appear brighter. As discussed in Section 1.4.5 of Chapter 1, muscle tissue normally appears dark on an US image with a striated appearance due to the reflections from connective tissue surrounding the muscle fascicles. Section 2.3.2 of Chapter 2 explains how certain neuromuscular disorders lead to an increase in fat and fibrous tissue and as a result the muscle appears brighter on an ultrasound image due to an increase in reflective surfaces.

As discussed above (Section 4.5.1.1), following a SCI there is a reduction in muscle fibres as a result of atrophy [39, 42]. This could lead to a change in the proportion of fibrous connective tissue (epimysium and perimysium) compared to actual muscle fibres. This change in muscle composition, combined with the infiltration of fat discussed in Section 4.5.1.1, could lead to an increase in reflective surfaces and therefore a SCI could cause an increase in muscle echogenicity similar to that seen in other neuromuscular disorders [24].

This increase in echogenicity is seen in the histograms of pixel greyscale values shown in Figure 4.9. There is a clear shift to the right, towards higher greyscale values, seen between the able-bodied and SCI participants. Furthermore, there is also a shift between participants 0-3 and 6-9 months following a SCI. This suggests that muscle echogenicity not only increases following a SCI but continues to increase over time. Significant differences between able-bodied and SCI groups as well as between SCI participants at different times post injury further reinforce this idea. The integrated optical density, mean and energy of the pixel greyscale values within the ROI are all measurements of the brightness of the image and all show an increase between able-bodied and SCI participants as well as over time within the SCI group. Skewness also confirms the shift in the histograms towards higher greyscale values are statistically significant. The histogram of the able-bodied participants is skewed to the right, with a positive skewness value.

When the histogram is skewed towards the lower greyscale values, there are more black pixels indicating a higher proportion of muscle tissue. After a SCI, the histograms shift towards higher greyscale values. In the early stages following a SCI the histogram is normally distributed, with a skewness value close to zero. This suggests an equal distribution of black and white pixels, therefore an increase in the amount of non-contractile elements such as fat and fibrous tissue. By 6-9 months post-injury, the histogram is skewed to the left, with a negative skewness value, suggesting an even higher proportion of fat and fibrous tissue compared to muscle tissue.

Standard deviation and variance decrease over time following a SCI, indicating less variation in echo intensity, with more pixels having a value that is close to the mean value. However, these differences do not reach statistical significance. Kurtosis also shows a decrease between able-bodied and SCI participants, although there does not appear to be any changes over time within the SCI group. A decrease in kurtosis means the tails of the histograms are small, indicating a wider, flatter histogram. This suggests that there is a more even distribution of pixel greyscale values. Overall the first-order statistical descriptors suggest less variation in pixel values and therefore muscles appear to be more homogeneous.

This increase in the homogeneity of muscle echotexture was previously observed by Cartwright et al. [138] in patients with acquired weakness due to hospitalisation in an intensive care unit. A reduction in the standard deviation of pixel intensity values indicated that pixels became more uniform. It was thought that this could be the result of muscle breakdown and therefore a loss of the structure of muscle architecture which is normally well organised.

4.5.1.3 Muscle echotexture

While the echogenicity describes the amount of non-contractile tissue within the muscle, echotexture describes the distribution of light and dark pixels, providing further insight into muscle composition. The Haralick features and local binary pattern (LBP) measurements describe the homogeneity of the muscle i.e. how equally distributed light and dark pixels are, while the Galloway features describe the coarseness of the muscle, i.e. the size of repeated elements.

Homogeneity of the muscle

Haralick features appear to show muscles becoming more homogenous over time within the SCI group. There is a decrease in contrast and correlation which represent the variation between a pixel and its neighbour, and the linear dependency on the GLCM, respectively. Energy increases over time, representing the local uniformity of pixel greyscale values and therefore indicates an increase in local homogeneity. Finally, the feature of homogeneity itself, which is based on how closely the distribution of the GLCM lies to the diagonal, is shown to increase with time post-injury.

Correlation informs that SCI participants at 0-3 months post-injury show similar values to able-bodied participants and then decrease with increased time since injury occurred. On the

other hand, there is an increase in contrast between the able-bodied group and SCI participants at 0-3 months post-injury, which then decreases back to a similar value to that of the able-bodied participants. Similarly, homogeneity appears to decrease within 0-3 months post-injury compared to able-bodied participants and then increase, returning to a similar value to that of the able-bodied group.

The initial change could be a result of increased fat and fibrous tissue in the muscle, which are highly reflective and have much larger pixel intensity values compared to the low values of the muscle tissue which appears dark. As the structure of the muscle breaks down over time, the muscle tissue and fat fibrous tissue are evenly distributed throughout the muscle and the pixels become more uniform. It is also possible that the initial change could be a result of total immobilisation following an injury, or medications leading to fluid retention known as odema. This then resolves as patients recover and become more active as a result of physiotherapy. Energy and entropy also appear to decrease initially compared to able-bodied participants, however in this case this may be because there is so much variation within the able-bodied group.

Entropy is the only Haralick feature which suggests that muscles become less homogeneous over time following a SCI. It is a measure of randomness and the degree of disorder. Since entropy increases with time since injury, pixels become more random and less uniform, therefore the overall ROI is actually becoming less homogeneous.

This local increase but global decrease in homogeneity could be the result of the involvement of different motor units. It has previously been shown that myopathies, which are diseases of the muscle itself that affect all muscle fibres equally, show homogeneous changes in muscle echogenicity. On the other hand, neuropathies, which are disorders of the nerves, only cause changes in muscle fibres from an affected motor unit [24, 206]. As participants in this study had incomplete spinal cord injuries, it is possible that muscle fibres were not evenly affected and therefore certain areas of the muscle were affected more than others. This could lead to an overall decrease in homogeneity, while there are still local increases in homogeneity as a result of the breakdown in muscle structure.

Local binary pattern measurements further confirm that homogeneity increases locally. The increase in energy (see Figure 4.13a) suggests that local uniformity increases, which is consistent with a breakdown in structure. Unlike the entropy of the Haralick features (see Figure 4.13b), which suggests a decrease in overall image homogeneity, a decrease in LBP entropy between able-bodied and SCI participants indicates that local homogeneity increases.

Coarseness of the muscle

A decrease in the SRE and increase in the LRE emphasis means there are less short runs and more long runs, therefore the texture of the muscle is becoming more coarse. This is associated with an increase in non-contractile components [207], consistent with an increased proportion of fibrous connective tissue and fat infiltration. The rest of the Galloway features describe the

homogeneity of the coarseness. The GLNU decreases over time within the SCI group, indicating an increased uniformity in terms of grey levels. The RP also decreases, further enforcing the uniformity of runs. Both the GLNU and RP show an initial increase compared to the able-bodied participants, suggesting the disruption to muscle structure is uneven 0-3 months after injury but continues over time until the whole muscle is affected.

In contrast, the RLNU increases, suggesting run lengths become less uniform over time. This means the coarseness is not uniform across the whole muscle, suggesting some areas are more affected by fibrous tissue and fat infiltration than others. Again, this could be caused by selective involvement of different motor units. This may explain why some texture features suggest an increase in homogeneity as muscle structure breaks down, while others suggest that disruption to muscle structure is not uniform across the muscle. The coarseness of the texture is also more consistent with neuropathies [129], where only certain motor units are affected, resulting in larger patches of increased density.

All Haralick and Galloway features are calculated in four different directions (0°, 45°, 90° and 135°). Although a similar trend is seen across all directions for each measurement, there is often a difference in amplitude between the 90° direction and all other directions. In terms of the Haralick features, contrast was much lower, while correlation, energy and homogeneity were higher in the 90° direction. This indicates pixel values are more homogeneous in this direction. The Galloway features GLNU, RLNU and RP were also much lower in the 90° direction, consistent with high uniformity. The organised structure of the muscle does not appear to be detected to the same extent in this direction, perhaps due to the orientation of the muscle fascicles.

4.5.2 Suitability of USI measurements to describe muscle structure

USI measurements of resting muscle thickness show the reduction in muscle size as a result of atrophy between able-bodied and SCI participants. It cannot, however, differentiate between SCI participants at different times post-injury, perhaps due to infiltration of fat to retain muscle bulk. Whatever the mechanism, resting thickness alone is not a useful measurement for monitoring atrophy over the time frame used in this study. It appears that the change in thickness occurred rapidly over the first month following a SCI, before data could be obtained. Further investigation of changes in muscle morphology during this time could therefore be beneficial as resting thickness has shown to be different between able-bodied and SCI groups. Despite the ability of the software to also track the position of muscle fascicles, this was not possible with these ultrasound videos, perhaps due to the increased brightness of the image. As previously discussed, muscle fascicles can normally be seen as bright striations, however, the increased echogenicity and homogeneity of the image limits the ability to differentiate different muscle structures.

First-order statistical descriptors of pixel values describe the increase in muscle echogenicity

associated with the change in muscle composition as a result of atrophy. Variance also indicated the changes in muscle homogeneity as the structure of the muscle breaks down. All first-order features except kurtosis showed differences between SCI participants at different times post-injury, suggesting they could be useful for monitoring the amount of non-contractile components in the muscle composition over time.

While first-order descriptors describe the distribution of pixel intensity values, they do not take into account the spatial arrangement. This means that muscles which have a similar echogenicity could have very different structures. Furthermore first-order descriptors are dependent on the ultrasound device and scanning settings used, limiting their use in clinical settings [7]. The Haralick and Galloway features overcome these limitations and provide more detailed measurements of the echotexture of the muscle.

The Haralick features capture the changes in homogeneity of the muscle as the structure breaks down. All features show differences between SCI participants at different times post-injury, indicating these parameters allow USI to detect changes in muscle structure as a result of atrophy. The LBP features also describe muscle homogeneity, however unlike the Haralick features which describe the overall homogeneity, they quantify the local homogeneity. LBP energy and entropy show significant differences between able-bodied and SCI participants, however they are limited in their ability to differentiate between SCI participants.

Galloway features describe the coarseness of the muscle texture. All features showed differences between SCI groups, however, the SRE and LRE appear to be particularly effective for measuring the increase in coarseness. These parameters are therefore especially useful for measuring the amount of contractile properties and by extension the composition of the muscle.

By combining texture features, SCI participants at different times post-injury can be separated into distinct groups through analysis of the canonical variables. This further supports the idea that measurements of echotexture are suitable for assessing the structural changes which occur in muscles following a SCI.

4.6 Conclusion

USI analysis was successful in describing changes in the muscle structure over time following a SCI. The thickness of the muscle decreases between SCI and able-bodied participants but could not detect changes between SCI participants over the timescale of this study. Thus, USI could be more useful for detecting changes within the first month following an injury.

Greyscale analysis provided much more detail regarding the structural changes within the muscle. Several first-order measurements showed an increase in muscle echogenicity, indicating that the brightness of the muscle increases as a result of increased reflective surfaces. This is most likely the result of changes in muscle composition leading to a higher proportion of fibrous tissue and infiltration of fat. Furthermore, second-order statistical descriptors provided

information on the echotexture of the muscle. Haralick features calculated from the GLCM and LBP measurements provided information on the homogeneity of the muscle, while the Galloway features calculated from the RLM described the coarseness of the muscle texture.

Overall increased homogeneity suggests a breakdown in muscle structure, however, these changes may only be seen at the local level. Decreased homogeneity of the overall ROI and an increase in coarseness suggest that the structural changes do not occur evenly throughout the muscle. This could be a result of incomplete spinal cord injuries affecting different motor units.

Chapter 5

Characterisation of the Functional Status of Muscles

5.1 Summary

In this chapter, the use of ultrasound imaging to provide sensitive diagnostic measurements which describe the functional status of muscles following a SCI is evaluated. Different measurements obtained from the ultrasound videos through tracking software and greyscale analysis are explained. These measurements are then compared between able-bodied participants and SCI participants with different levels of muscle function. The functional status of the muscles was determined through measurements of ankle torque, i.e. the force the muscle was able to generate, and electromyography (EMG), which describes the electrical activity of the muscle. The suitability of the different USI parameters to distinguish between different levels of muscle function are presented and discussed. This chapter includes work that has been submitted to the journal *"Ultrasound in Medicine and Biology"* and is currently under review (see Publications section).

5.2 Introduction

An injury to the spinal cord disrupts the flow of sensory and motor signals between the brain and the rest of the body, resulting in loss of sensation and muscle paralysis. The extent of the injury and the areas of the body which are affected depend on the nature of the injury. Spinal cord injuries (SCI) are defined as either complete or incomplete, depending on whether the cord is fully or partially severed. Complete injuries result in a total loss of function in the affected areas, whereas a certain degree of function can be preserved in incomplete injuries [11].

Accurate assessment of muscle function is therefore an important part of evaluating the severity of a SCI. This is currently done through manual muscle testing (MMT), which is a physical examination performed by a clinician who grades the muscle's ability to generate a

contraction. The results from these tests are combined with the results of sensory tests to give an overall grade on the American Spinal Injuries Association (ASIA) impairment scale (AIS) [3].

Despite the valuable information provided by MMT, there is a need for more objective measurements. Electromyography (EMG) can be useful for making quantitative measurements by recording the electrical activity of the muscle, however, the ability to differentiate between different muscles or assess deeper muscles non-invasively is still limited. It may also be difficult to detect very small contractions which cannot be easily visualised or lie below the noise threshold of EMG [208].

Over recent years, ultrasound imaging (USI) has emerged as an additional tool to assess muscle function. This non-invasive imaging modality is also relatively inexpensive and portable, making it a popular diagnostic tool which is widely used in clinical settings. Not only does it allow internal structures such as muscles to be visualised, and therefore measurements of morphology to be obtained, the dynamic nature of USI allows changes in architecture during a muscle contraction to be measured. USI of skeletal muscles is well-established in the literature, with several studies demonstrating its ability to make accurate measurements of muscle size [209] and establishing relationships between muscle activity and changes in architectural parameters [103, 112]. Furthermore, recent technological advances allow USI to obtain these measurements with excellent resolution, making it possible to detect displacements as small as 5 μm [203]. This accuracy led to the development of mathematical algorithms for extracting features in US images and tracking these features between frames [186, 189, 210].

In this chapter, two analysis methods are used to obtain USI parameters that describe muscle movement. First, tracking software developed by Loram and colleagues at Manchester Metropolitan University [186], which is described in Section 3.8.1 of Chapter 3, is used to describe muscle movement through changes in muscle thickness and small regional movements within the muscle based on feature tracking. Second, another simpler method, which was developed within our research group [8], is used to describe muscle movement based on changes in pixel intensity. These measurements are then compared between a group of healthy able-bodied participants and a group of SCI participants with varying levels of muscle function, determined by measurements of torque and EMG.

The main aim of the investigation presented in this chapter is to evaluate the use of USI to provide sensitive diagnostic measurements which describe muscle movement and determine:

- which USI parameters are most suitable for describing the functional status of the muscle.
- whether the use of these USI parameters can discriminate neurological function by differentiating between different levels of muscle function within the SCI population.

A secondary aim was to compare the measurements obtained from tracking software and pixel difference methods to determine if similar results were obtained from these two analysis methods.

5.3 Methods

5.3.0.1 Overview of data used

This chapter analyses data obtained during attempted voluntary movements. Study 1 provides ultrasound videos of the gastrocnemius medialis (GM) muscle both at rest and during an attempted isometric maximum voluntary contraction (MVC). Full details of the protocol can be found in Sections 3.3.4.2 and 3.3.4.4 of Chapter 3. This data was obtained from 15 SCI participants and 15 age and gender matched able-bodied controls.

5.3.1 USI data pre-processing

Ultrasound videos were recorded during the experiment in the default file extension for Echo Wave II software, known as telemed video data (TVD) files. During offline analysis, these TVD files were converted to a binary file to extract pixel greyscale values as described in Section 4.3 of Chapter 4. These binary files were used for the pixel difference method described in Section 5.3.3.

Tracking software was also used to extract information about muscle movements as explained in Section 5.3.2. In this case the TVD files were converted to AVI file format. The videos were then cropped, showing only the area containing the US image of the gastrocnemius muscle, and individual frames were extracted and saved in the form of a portable grey map (PGM) file.

5.3.2 USI data analysis with tracking software

The use of an active shape model (ASM) to automatically segment the image into anatomically distinct regions and a KLT algorithm to track the movement of features between frames of the ultrasound videos are described in Section 3.8.1 of Chapter 3. In this section, the use of these analysis methods to obtain measurements of muscle deformation and regional displacement is further explained.

5.3.2.1 Automatic segmentation to calculate muscle deformation

As discussed in Section 3.8.1.1 of Chapter 3 and Section 4.3.3 of Chapter 4, the aponeuroses of a muscle can be separated from the muscle tissue itself through the use of the ASM to perform automatic segmentation. As a result, the average distance between the aponeuroses can be used to calculate the thickness of the muscle, providing a single measurement of muscle size.

During a contraction, the thickness of the muscle can change. This change in thickness ($\Delta\Theta$) between the current frame and the resting thickness (Θ_0), can be normalised as percentage of the resting thickness to provide the muscle deformation (δ):

$$\delta = \frac{\Delta\Theta}{\Theta_0} \times 100\% \tag{5.1}$$

This provides an indication of how much the muscle is moving by measuring the change in muscle shape/size. Muscle deformation can be plotted over time during an attempted MVC as shown in Figure 5.1. The maximum value reached during an attempted MVC is used as a single value to describe the amount of muscle movement in terms of deformation, as indicated by the red circle.

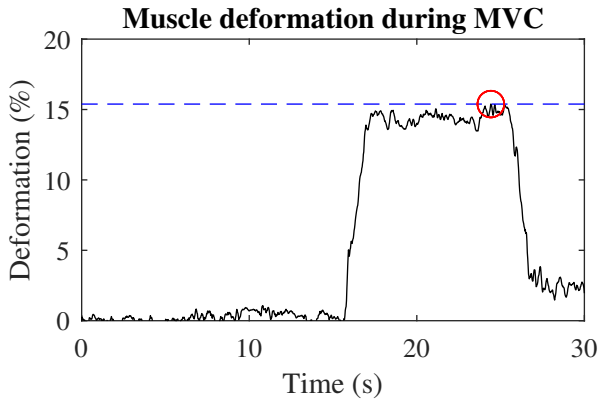

Figure 5.1: Muscle deformation over time during attempted maximum voluntary contraction (MVC) between t=15s and t=25s. The maximum deformation reached is circled in red.

5.3.2.2 Feature tracking for measurements of regional movement

Figure 3.24 on page 60 and Figure 5.2 below show the 80 measurement probes (10 rows, 8 columns) placed across the gastrocnemius muscle based on triangular interpolation of KLT features. Similarly to the segmentation, the output of the tracking software is the x and y components of each probe for every frame of the US video. The sign convention used for tracking the movement of probes between frames is positive in the proximal direction of the horizontal plane (when the probe moves to the left of image towards the knee) and in the deep direction of the vertical plane (when the probe moves down the image to the deeper part of the muscle). When the muscle contracts during ankle plantar flexion, the probes move to the left towards the knee, and when the muscle relaxes the probes move to the right back towards their original position.

This information allows movement of the muscle structures to be measured at various locations, including different depths (comparing rows) and distances from the knee (comparing columns). This regional movement within the muscle is calculated by subtracting the x and y components of each probe position between adjacent frames to find the change in position in the horizontal and vertical directions, respectively. Using Pythagoras theorem, this can be used to calculate the total magnitude of the movement. This change in probe position between frames is termed displacement (Δp):

$$\Delta p_{mn}(f) = \sqrt{(x_{mn}(f) - x_{mn}(f-1))^2 + (y_{mn}(f) - y_{mn}(f-1))^2} \tag{5.2}$$

where Δp_{mn} is the displacement of a measurement probe in row m and column n between frame number f and the previous frame. This is shown in the inset of Figure 5.2.

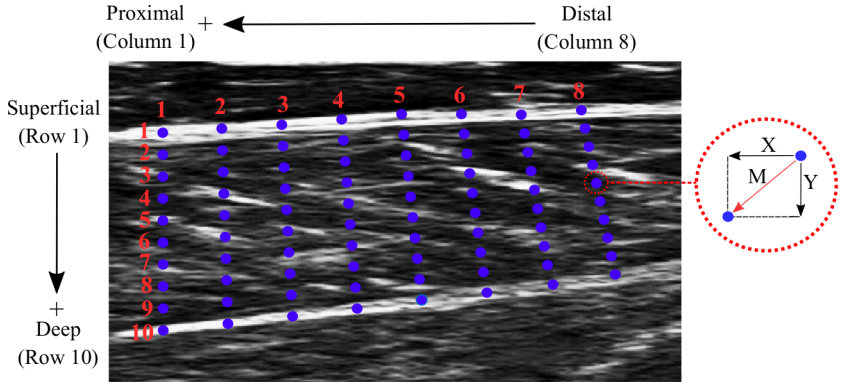

Figure 5.2: Annotation of the probes used to calculate muscle displacement. Adapted from [8].

Similarly to muscle deformation, muscle displacement can be plotted over time to visualise how it changes during an MVC. As shown in Figure 5.3, displacement is much higher during the onset and offset of the contraction, with very little movement when the contraction is sustained at a constant level. The maximum value of displacement (circled in red) and the area under the graph of displacement plotted over time (shaded blue) are both used to describe the displacement as a single value. These two measurements provide different information about muscle displacement as the maximum value describes the biggest change in probe position between two adjacent frames, whereas the area under the graph is the summation of the movements between every frame and therefore describes the total distance a probe has travelled.

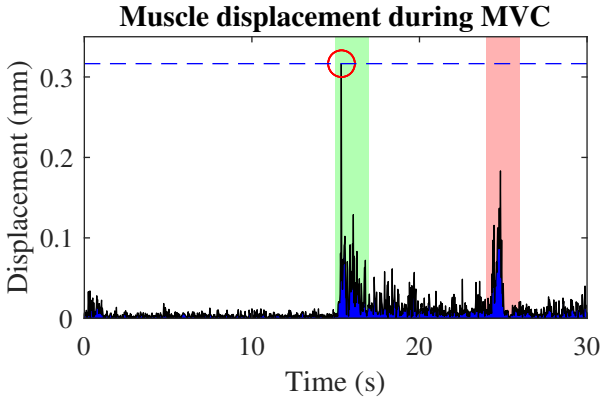

Figure 5.3: Muscle displacement (row 10) over time during attempted maximum voluntary contraction (MVC) between t=15s and t=25s. The onset and offset of the contraction are highlighted in green and red respectively. The maximum displacement is circled in red and the total displacement is represented by the area under the graph shaded blue.

Each value of muscle displacement is the distance the measurement probe has travelled from the previous frame. As the time between each frame is known, this can be used to calculate the speed at which the measurement probe has travelled. The summation of the distance that a measurement probe has travelled over several frames was used to calculate the average speed, v, of a muscle contraction during a particular time period,

$$v_{mn} = \frac{\sum_{f=F_s}^{F_e} \Delta p_{mn}(f)}{t(F_e) - t(F_s)} \tag{5.3}$$

where v_{mn} is the average speed of a measurement probe in row m and column n, and $t(F_s)$ and $t(F_e)$ are the times corresponding to the frame at the start (F_s) and end (F_e) of the time period respectively. In this study, the average speed was calculated for the following phases of the muscle contraction:

- Initial phase: t=15-17.5s
- Constant phase: t=17.5-22.5s

5.3.2.3 Conversion of pixel position to physical movement

The physical length of the ultrasound probe (59mm) and the depth of scanning (50mm) are known, as well as the dimensions of frames from the recorded ultrasound video, as shown in Figure 5.4. This makes it possible to convert the position of markers and probes, which are expressed in pixels when output from the tracking software, to physical movement of features. This is applied to both the measurements of displacement (Δp_{mn}) and average speed (v_{mn}) discussed in the previous section. The following formula was applied to perform the conversion:

$$x = \frac{x_{pixels} \times 59mm}{596px} \qquad y = \frac{y_{pixels} \times 50mm}{498px} \tag{5.4}$$

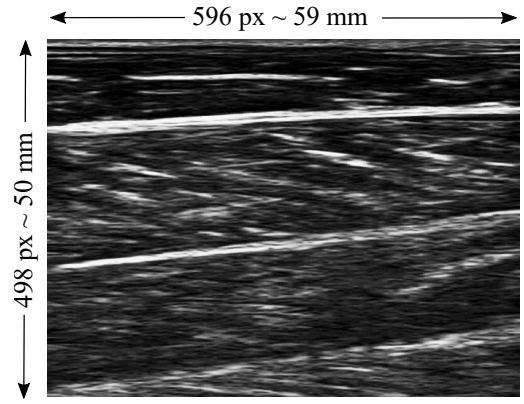

Figure 5.4: Dimensions of ultrasound frame in pixels (px) converted to physical distance in millimetres (mm). Adapted from [8].

5.3.3 Pixel difference method for measurements of regional movement

The pixel difference method measures muscle movement through changes in pixel greyscale values. The method was originally developed within our research group by Anna Sosnowska [8] to analyse ultrasound videos for biofeedback and has been adapted for the purpose of this study.

5.3.3.1 Selection of region of interest

As described in Section 4.3 of Chapter 4, the binary files contain pixel greyscale values (between 0 and 255) for all the pixels in the ultrasound image. A region of interest (ROI) must be selected to only consider the pixels within the area of interest i.e. the gastrocnemius medialis (GM) muscle. In this case the ROI was selected to contain only the GM muscle without including the aponeurosis. This was chosen because the boundaries of the muscle appear very bright in the ultrasound image and therefore even a small movement would result in a relatively large change in pixel values.

5.3.3.2 Comparison of pixel intensity between frames

The pixel values within the selected ROI were subtracted from the corresponding pixel between adjacent frames, as shown in Figure 5.5. The absolute value of this difference was then summed for all the pixels within the ROI for each frame and then divided by the total number of pixels within the ROI to give the Normalised Pixel Difference (NPD),

$$NPD(f) = \frac{\sum_{i=1}^{n} |\rho_i(f) - \rho_i(f-1)|}{n} \tag{5.5}$$

where $\rho_i(f)$ is the greyscale value of the i^{th} pixel on frame f and n is the total number of pixels.

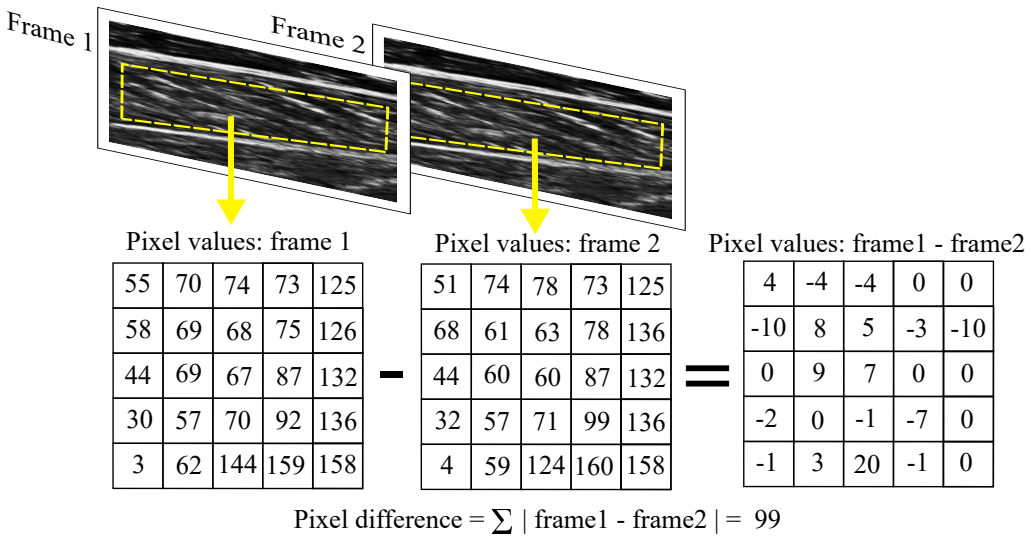

Figure 5.5: Illustration of the calculation of pixel difference between two adjacent frames.

5.3.3.3 Pixel difference method to measure muscle movement

Similarly to the muscle displacement calculated from the feature tracking method, the NPD can be plotted over to time to visualise changes during an attempted MVC. The same measurements of maximum NPD and the area under the graph of NPD plotted over time are used to describe muscle movement with a single value as shown in Figure 5.6. The maximum value describes the biggest changes in pixel intensity between two adjacent frames and the area under the graph is the summation of the changes in pixel intensity between every frame, describing the total change in pixel intensity values.

In a similar way that the average speed of a muscle contraction can be calculated from displacement, it can also be calculated by summing the NPD over several frames.

$$v_{NPD} = \frac{\sum_{f=F_s}^{F_e} NPD(f)}{t(F_e) - t(F_s)} \tag{5.6}$$

where $t(F_s)$ and $t(F_e)$ are the times corresponding to the frame at the start (F_s) and end (F_e) of the time period.

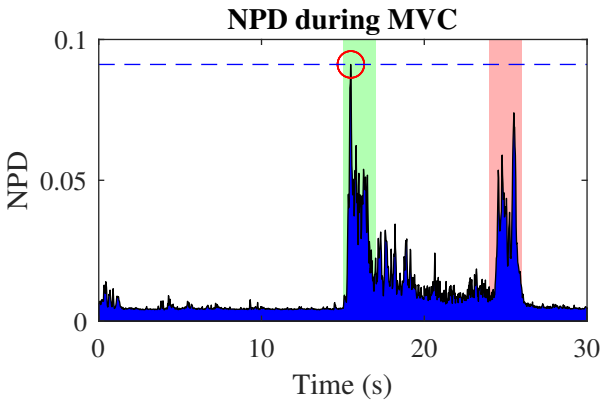

Figure 5.6: Normalised pixel difference (NPD) during attempted MVC between t=15s and t=25s. The onset and offset of the contraction are highlighted in green and red respectively. Maximum NPD is circled in red and total NPD is represented by the area shaded blue.

As can be seen by comparing Figures 5.3 and 5.6, this pixel difference method provides similar information to muscle displacement. The pixel difference method is much more computationally efficient than displacement, which is obtained from the tracking software, therefore this potentially offers a simpler method to obtain similar information on muscle movement.

5.3.4 Comparative measures of muscle function

Ankle torque and EMG were recorded during attempted MVC as discussed in Section 3.4 of Chapter 3. This provides measurements of muscle function from well established techniques which can then be compared with the measurements obtained from the ultrasound videos.

5.3.4.1 Torque

The recorded ankle torque was smoothed using a moving average filter over 0.01s (10 samples for the sampling frequency of 1000Hz). From this, the maximum value of torque was used to describe how much force the muscle is capable of generating. An example of the torque obtained during an attempted MVC is shown in Figure 5.7.

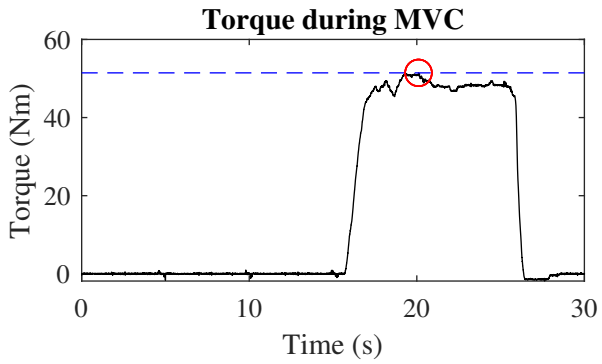

Figure 5.7: Example of torque produced during an attempted maximum voluntary contraction (MVC). The maximum value is circled in red.

5.3.4.2 EMG

Raw EMG data, shown in Figure 5.8a, was bandpass filtered between 10 Hz and 500 Hz using a fifth order Butterworth filter to avoid anti-aliasing effects and notch filtered at 50 Hz to remove electrical interference. Full wave rectification was then performed by taking the absolute values of the signal. Finally, the signal was smoothed using the root mean square (RMS) to produce a linear envelope of the signal, as shown in Figure 5.8b. A window of 100 ms was used as recommended in the literature [211]. The maximum value of the RMS was used to describe the amount of muscle activity in a single value.

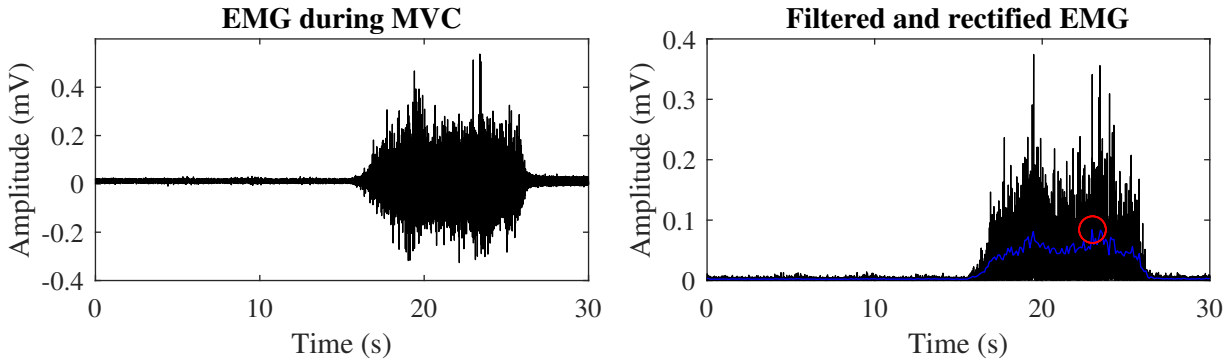

(a) Raw EMG

(b) Processed EMG

Figure 5.8: Examples of the EMG obtained during an attempted MVC, with a) showing the raw EMG and b) showing the EMG after it has been filtered and rectified. The root mean square (RMS) is shown in blue and the maximum value is circled in red.

5.3.4.3 Classification of muscle status

There is large variation in the amount of muscle function between the SCI participants in this study. In order to differentiate between different levels of muscle function within the SCI group, participants were classified as having "low", "medium" or "high" muscle function based on:

1. **Torque:** 0-10 Nm was considered low level torque, 10-20 Nm was considered medium level torque and more than 20 Nm was considered high level torque.
2. **EMG:** Less than 0.001 mV was considered low level EMG, 0.001-0.005 mV was considered medium level EMG and more than 0.005 mV was considered high level EMG.

5.3.5 Statistical analysis

5.3.5.1 Grouping of data

Fifteen able-bodied participants each completed one session, resulting in fifteen data points for each measurement. SCI participants on the other hand, each completed several sessions, resulting in a total of 63 data points for each measurement. These 63 data points are separated into three groups according to the level muscle function: low, medium and high torque or EMG. As the level of muscle function on the first session and recovery seen in further sessions varies between participants, there are participants with several data points in one group and none in at least one group. Data points from the same participant within a group were averaged. The number of data points in each of the independent groups during comparisons is shown in Table 5.1.

Table 5.1: Number of data points in each independent group being compared.

Groups compared	**Number of data points (group 1, group 2)**	
Group 1 and Group 2	*Torque*	*EMG*
AB and SCI Low	8,7	12,3
AB and SCI Med.	10,5	12,3
AB and SCI High	9,6	11,4
SCI Low and SCI Med.	8,5	3,2
SCI Low and SCI High	8,6	3,4
SCI Med. and SCI High	4,4	3,3

5.3.5.2 Calculation of statistically significant difference

When the sample size was ten or more, the Shapiro-Wilk test was used to assess the normality of the data as described in Section 3.9.1. When data was found to be normally distributed, an unpaired t-test was used (see Section 3.9.2.1). When data was not normally distributed or

the sample size was less than ten, the non-parametric Mann-Whitney U test was used as an alternative (see Section 3.9.2.2).

Both tests were performed using a significance level of p=0.05, however as comparisons were carried out in a pairwise manner this was adjusted using the Bonferroni correction for multiple comparisons, as described in Section 3.9.3. One group of able-bodied participants is compared to three SCI groups with different torque or EMG levels. The SCI groups are also compared to each other, resulting in a total of six statistical tests. The adjusted significance value used is therefore p=0.008 (0.05/6).

5.3.5.3 Calculation of Cohen's d effect size

Cohen's d effect size was also calculated in line with an unpaired test using equation 3.5. Further details on Cohen's d effect size and how to interpret it are provided in Section 3.9.4.

5.4 Results

In this section, ultrasound measurements are presented for fifteen able-bodied participants and fifteen SCI participants. SCI participants are divided into subgroups according to their muscle function, which is classified based on a) the amount of torque and b) the amount of muscle activity detected by EMG during an attempted maximum voluntary contraction. First, measurements of muscle structure obtained while the muscle is at rest will be presented, followed by measurements of muscle movement obtained during attempted MVC.

5.4.1 Resting muscle measurements

The results in this section are similar to those presented in Chapter 4, and the details of how these measurements are calculated can be found in Section 4.3. However, Chapter 4 compares these parameters between SCI at different times post-injury, and in this chapter the same measurements are grouped according to muscle function.

5.4.1.1 Thickness

Figure 5.9 shows a decrease in the resting thickness of the muscle (calculated from equation 4.1 in Section 4.3.3 of Chapter 4) for SCI participants compared to able-bodied participants. The p-values and Cohen's d effect size for resting muscle thickness are shown in Table 5.2. There are large to very large effect sizes between the able-bodied group and all SCI groups. There are also very large effect sizes between SCI participants who can produce high levels of torque and other SCI groups (Figure 5.9a) and between SCI participants with low and high levels of EMG (Figure 5.9b). Statistically significant differences can also be seen between SCI with low torque and both able-bodied and SCI with high torque groups.

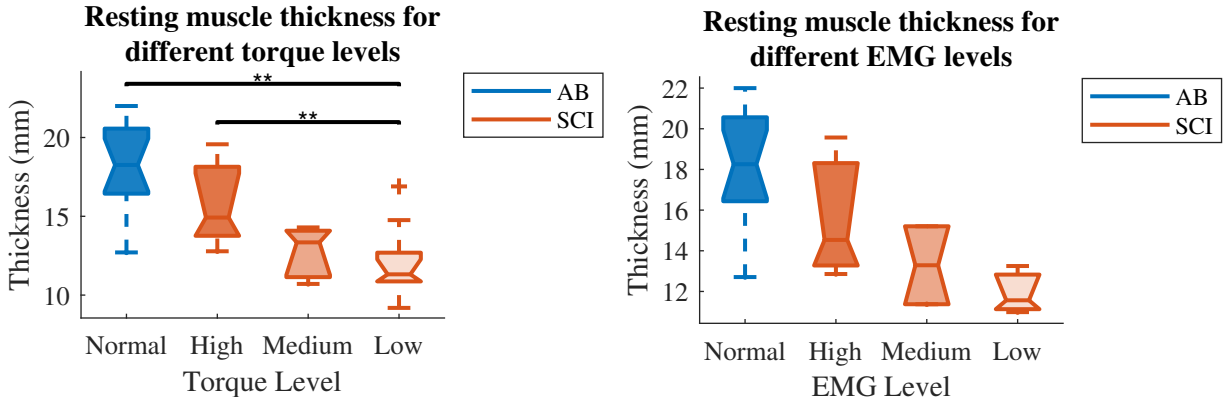

(a) Torque (b) EMG

Figure 5.9: Boxplots of the resting muscle thickness for able-bodied participants and SCI participants with different levels of muscle function ($**-p < 0.01$).

Table 5.2: P-values and effect sizes for resting muscle thickness of able-bodied participants and SCI participants with different levels of muscle function. Values indicating a significant difference or a greater than medium effect size are shown in bold.

	Torque		**EMG**	
	P-value	*Effect Size*	*P-value*	*Effect Size*
AB vs. SCI_{Low}	**0.001**	**1.49**	0.02	**1.68**
AB vs. $SCI_{Med.}$	0.01	**1.46**	0.08	**1.51**
AB vs. SCI_{High}	0.06	**1.04**	0.29	**0.91**
SCI_{Low} *vs.* $SCI_{Med.}$	0.72	0.26	0.80	0.77
SCI_{Low} *vs.* SCI_{High}	**0.005**	**1.43**	0.20	**1.20**
$SCI_{Med.}$ *vs.* SCI_{High}	0.11	**1.26**	0.80	0.76

5.4.1.2 Echogenicity

Echogenicity describes the brightness of the muscle through the greyscale values of pixels within the region of interest selected. Figure 5.10 shows the distribution of these pixel values in the form of histograms for able-bodied participants and groups of SCI participants with different levels of muscle function.

All SCI groups show a clear shift to the right towards higher greyscale values, indicating that muscles in the SCI group appear brighter. There does not, however, appear to be any difference between the SCI groups, with all levels of torque (Figure 5.10a) and muscle activity (Figure 5.10b) showing a similar shift to the right compared to the able-bodied group.

The p-values and effect sizes are shown in Table 5.3. Significant differences are seen between each group, however, as individual pixel values are included (able-bodied: $n = 321,602$; SCI low torque: $n = 441,905$; SCI medium torque: $n = 159,229$; SCI high torque: $n = 349,006$; SCI low EMG: $n = 84,657$; SCI medium EMG: $n = 89,979$; SCI high EMG: $n = 156,561$) this should be interpreted with caution.

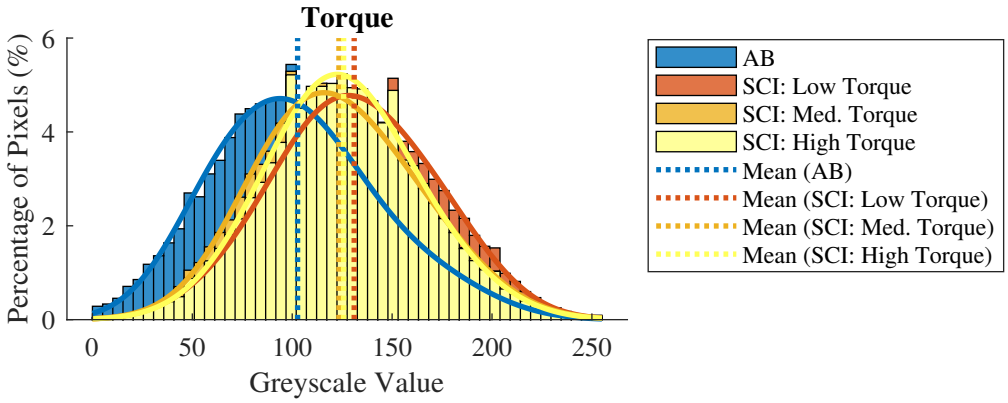

(a) Torque

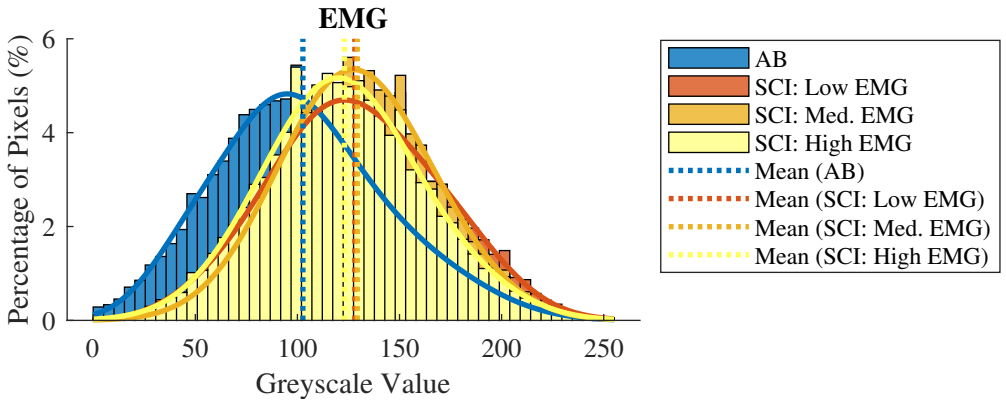

(b) EMG

Figure 5.10: Histograms of pixel greyscale values for able-bodied participants and SCI participants with different levels of muscle function.

Table 5.3: P-values and effect sizes for all pixel intensity values within the selected region of interest for able-bodied participants and SCI participants with different levels of muscle function. Values indicating a significant difference or a greater than medium effect size are shown in bold.

	Torque		**EMG**	
	P-value	*Effect Size*	*P-value*	*Effect Size*
AB vs. SCI_{Low}	**< 0.001**	0.77	**< 0.001**	0.61
AB vs. $SCI_{Med.}$	**< 0.001**	0.55	**< 0.001**	0.78
AB vs. SCI_{High}	**< 0.001**	0.72	**< 0.001**	0.54
SCI_{Low} *vs.* $SCI_{Med.}$	**< 0.001**	0.24	**< 0.001**	0.17
SCI_{Low} *vs.* SCI_{High}	**< 0.001**	0.07	**< 0.001**	0.11
$SCI_{Med.}$ *vs.* SCI_{High}	**< 0.001**	0.18	**< 0.001**	0.30

The effect size is medium when comparing all SCI groups with the able-bodied group, but effect sizes between all SCI groups are small. This is further shown in Figure 5.11 by the increase in the mean greyscale value (calculated from equation 4.3 in Section 4.3.5.1 of Chapter 4) between able-bodied and SCI participants. The p-values and Cohen's d effect sizes for all mean greyscale measurements are shown in Table 5.4.

There are large to very large effect sizes found between the able-bodied group and all SCI groups, although a significant difference is only seen at low torque levels. In contrast, only small differences are seen between SCI groups with low and high levels of torque (Figure 5.11a). High muscle activity, measured with EMG (Figure 5.11b), on the other hand shows large to very large effect sizes with other SCI groups.

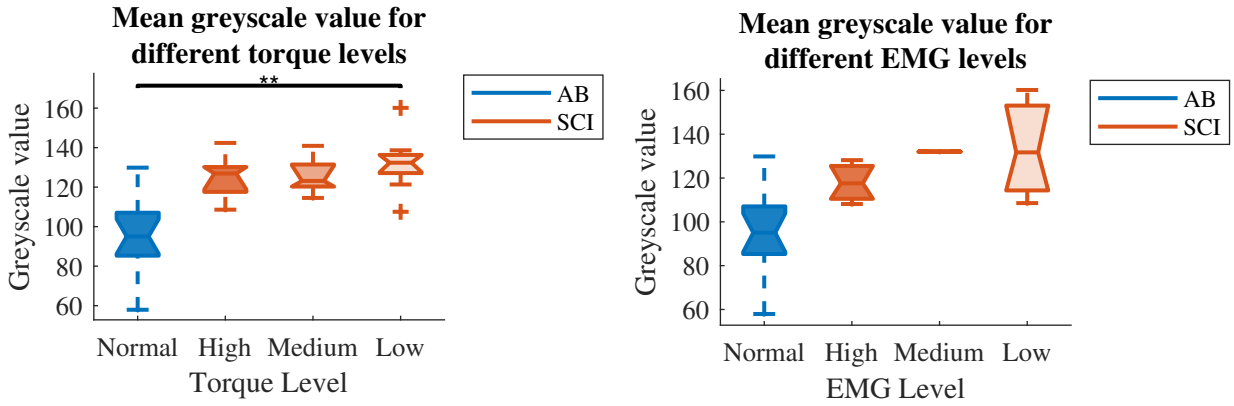

(a) Torque (b) EMG

Figure 5.11: Boxplots of the mean greyscale value for able-bodied participants and SCI participants with different levels of muscle function ($** - p < 0.01$).

Table 5.4: P-values and effect sizes for mean greyscale value for able-bodied participants and SCI participants with different levels of muscle function. Values indicating a significant difference or a greater than medium effect size are shown in bold.

	Torque		**EMG**	
	P-value	*Effect Size*	*P-value*	*Effect Size*
AB vs. SCI_{Low}	**0.001**	**1.49**	0.03	**1.34**
AB vs. $SCI_{Med.}$	0.02	**1.28**	0.02	**1.50**
AB vs. SCI_{High}	0.01	**1.25**	0.18	**0.96**
SCI_{Low} vs. $SCI_{Med.}$	0.44	0.49	0.80	0.08
SCI_{Low} vs. SCI_{High}	0.41	0.48	0.40	**0.80**
$SCI_{Med.}$ vs. SCI_{High}	0.69	0.02	0.20	**1.34**

5.4.2 Measurements of attempted MVC

Measurements of muscle movement obtained during attempted MVC are presented here. Firstly, measurements obtained from tracking software are presented: muscle deformation describes changes in muscle thickness; and muscle displacement describes regional movement within the muscle, including maximum muscle displacement, total muscle displacement, and the speed of muscle displacement during different phases of the muscle contraction. This is followed by the same measurements obtained using the pixel difference method.

5.4.2.1 Deformation

Muscle deformation is calculated from equation 5.1 in Section 5.3.2.1. The p-values and Cohen's d effect sizes for muscle deformation are shown in Table 5.5. Deformation shows a small decrease between able-bodied and SCI participants at all levels of torque as shown in Figure 5.12a, however effect sizes are small and no significant differences are seen. Figure 5.12b shows a decrease in muscle deformation between SCI participants with low level EMG and all other groups, coinciding with large to very large effect sizes, but again no significant differences are seen. SCI with high EMG levels show similar deformation to able-bodied participants with only a small effect size, while medium levels of EMG appear to show higher levels of deformation than all other groups with large effect sizes.

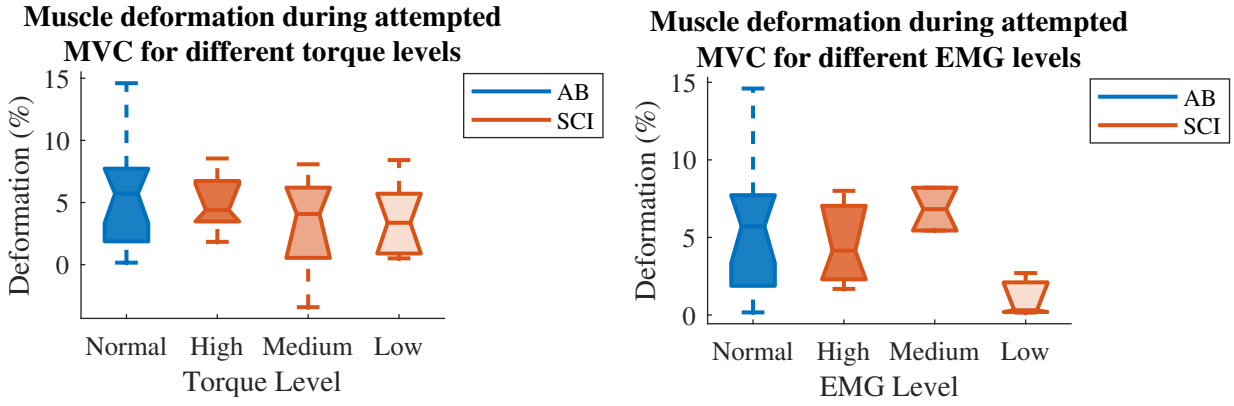

(a) Torque (b) EMG

Figure 5.12: Boxplots of muscle deformation during attempted MVC for able-bodied participants and SCI participants with different levels of muscle function.

Table 5.5: P-value and effect size for muscle deformation during attempted MVC of able-bodied participants and SCI participants with different levels of muscle function. Values indicating a significant difference or a greater than medium effect size are shown in bold.

	Torque		**EMG**	
	P-value	*Effect Size*	*P-value*	*Effect Size*
AB vs. SCI_{Low}	1.00	0.06	0.10	**0.95**
AB vs. $SCI_{Med.}$	0.59	0.44	0.36	**0.80**
AB vs. SCI_{High}	0.51	0.38	0.72	0.35
SCI_{Low} *vs.* $SCI_{Med.}$	0.72	0.03	0.20	**1.67**
SCI_{Low} *vs.* SCI_{High}	0.49	0.35	0.20	**1.21**
$SCI_{Med.}$ *vs.* SCI_{High}	0.89	0.13	0.40	**0.81**

5.4.2.2 Displacement

Muscle displacement is calculated using equation 5.2 and the maximum and total measurements of muscle displacement to describe muscle movement are defined in Section 5.3.2.2. Throughout this section displacement results presented are for rows 1, 5 and 10, and columns 1, 4 and 8. The areas of the muscle which correspond to these locations is illustrated in Figure 5.13.

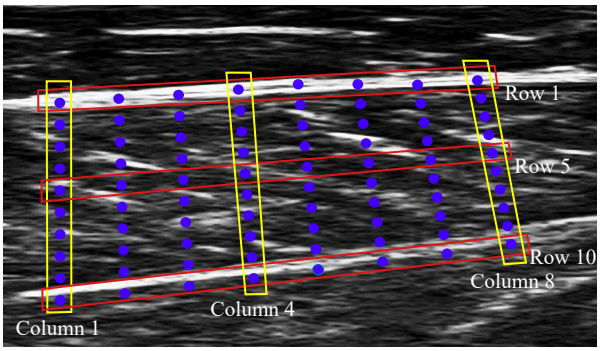

Figure 5.13: Arrangement of probes highlighting the relevant positions which are presented in the results: rows 1, 5 and 10, and columns 1, 4 and 8.

Table 5.6 shows the p-values and Cohen's d effect size for maximum muscle displacement. There is a reduction in maximum muscle displacement with low levels of torque shown in Figure 5.14a. After the Bonferroni correction, the only statistically significant difference seen is between SCI groups with low and high levels of torque at row 10. There are, however, large to very large effect sizes between able-bodied participants and SCI with low levels of torque at all positions of the muscle. As the torque level increases to medium and high, the effect sizes decrease when compared to the able-bodied group. There are large to very large effect sizes between low levels of torque and other SCI groups at row 5, row 10, column 4 and column 8. There are also large to very large effect sizes seen between medium and high levels of torque at row 10 and columns 1 and 4. Some locations on the muscle (row 10, column 4 and column 8) also show that SCI participants with high levels of torque have higher values of maximum displacement than the able-bodied group, however, these results do not reach statistical significance and only small effect sizes are seen.

Figure 5.14b also shows a decrease in the maximum muscle displacement for different levels of EMG, with significant differences seen between able-bodied and SCI with low EMG at all positions except row 1 and column 1. Large to very large effect sizes are seen between able-bodied and the low level EMG group, which contains data from several participants who had such little muscle activity it could not be detected by EMG. When EMG increases to medium level large effect sizes are only seen at row 10 and high level EMG shows only small effect sizes with the able-bodied group. There are large to very large effect sizes seen between all levels of EMG within the SCI groups except for medium and high in the proximal to distal direction

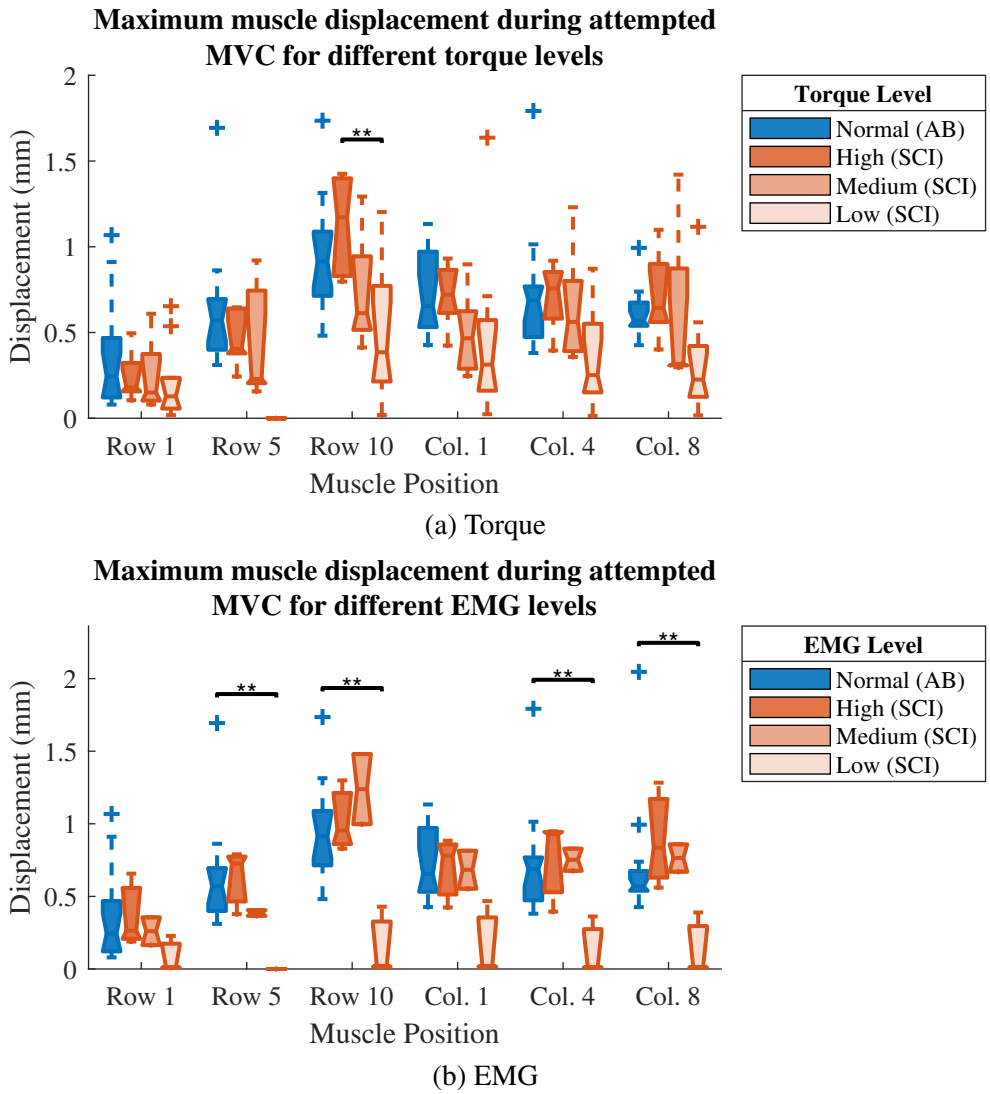

Figure 5.14: Boxplots of maximum muscle displacement during attempted MVC for able-bodied participants and SCI participants with different levels of muscle function ($**-p < 0.01$).

(columns 1, 4 and 8). Higher values of maximum displacement are also seen in SCI participants with high levels of EMG compared to the able-bodied group at all locations across the muscle, however, as with the torque results this did not reach statistical significance and effect sizes are small.

A reduction in the total displacement within the SCI group can also be seen for lower levels of activity. The p-values and Cohen's d effect sizes for total muscle displacement are shown in Table 5.7. Figure 5.15a shows a reduction in total displacement between SCI participants with high and low levels of torque for all locations on the muscle, coinciding with significant differences and very large effect sizes. SCI with low torque also shows significant differences with medium torque levels at row 10, column 4 and column 8, as well as the able-bodied group at columns 1 and 4. SCI participants with high torque levels also show higher muscle movement than the able-bodied group, while SCI with medium torque is more similar to that of the able-

bodied group. This is seen across all positions of the muscle however it is most pronounced at deep areas of the muscle (row 10). There are large to very large effect sizes between all groups except able-bodied and medium torque.

Similar results are seen for different levels of EMG in Figure 5.15b, however significant differences are only seen between able-bodied participants and SCI with low EMG levels. This is seen at all positions except row 1. SCI with high levels of EMG show higher values of displacement compared to the able-bodied group, particularly at row 10. Able-bodied and medium EMG show similar values with small effect sizes at all positions except row 10 where a large increase is seen. There are large to very large effect sizes between all other groups except for medium and high EMG levels at row 10, column 1 and column 4.

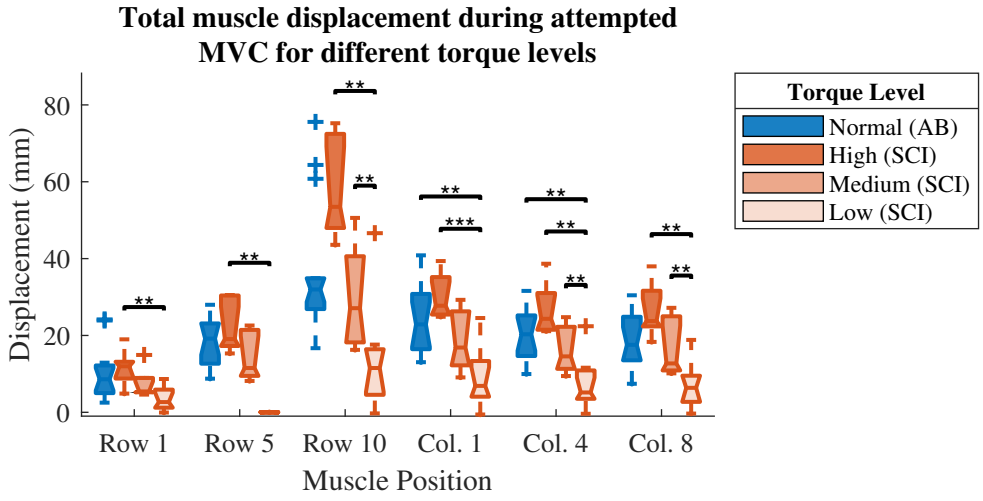

(a) Torque

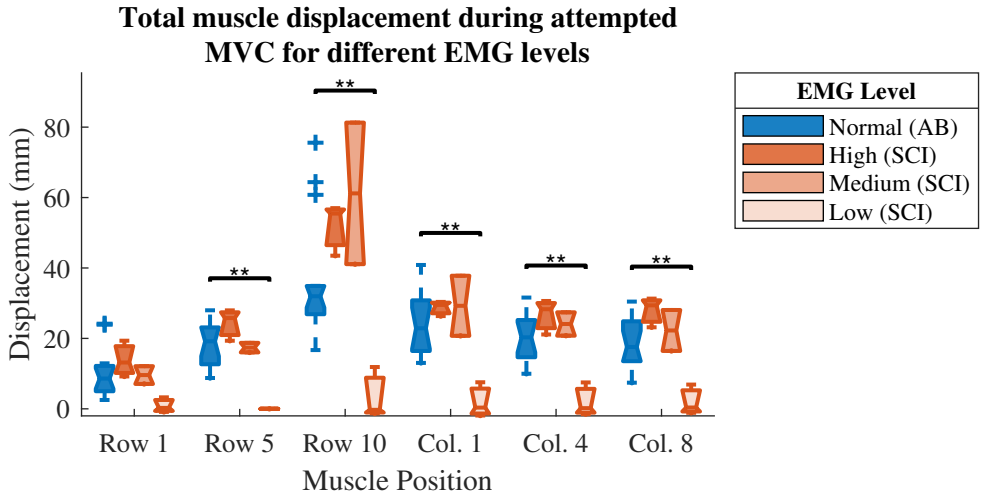

(b) EMG

Figure 5.15: Boxplots of total muscle displacement during attempted MVC for able-bodied participants and SCI participants with different levels of muscle function ($**-p<0.01, ***-p<0.001$).

Table 5.6: Statistical values reported as p-value [effect size] for maximum muscle displacement during attempted MVC of able-bodied participants and SCI participants with different levels of muscle function. Values indicating a significant difference or a greater than medium effect size are shown in bold.

		Torque			**EMG**		
		Low	*Med.*	*High*	*Low*	*Med.*	*High*
AB	*Row 1*	0.05 **[0.82]**	0.59 [0.42]	0.59 [0.42]	0.10 **[0.85]**	0.78 [0.47]	0.72 [0.04]
	Row 5	0.01 **[1.24]**	0.31 [0.53]	0.21 [0.69]	**0.004 [1.73]**	0.17 [0.73]	0.72 [0.01]
	Row 10	0.07 **[1.07]**	0.16 [0.70]	0.44 [0.30]	**0.004 [1.92]**	0.29 **[0.80]**	1.00 [0.01]
	Col. 1	0.01 **[1.35]**	0.10 **[0.88]**	0.93 [0.08]	0.01**[1.71]**	0.69 [0.40]	0.62 [0.22]
	Col. 4	0.04 **[1.03]**	0.51 [0.27]	0.84 [0.32]	**0.004 [1.75]**	0.67 [0.03]	0.52 [0.04]
	Col. 8	0.02 **[0.98]**	0.31 [0.38]	0.75 [0.20]	**0.004 [1.89]**	0.30 [0.08]	0.28 [0.38]
Low	*Row 1*	-	0.28 [0.45]	0.23 [0.17]	-	0.40 **[1.19]**	0.20 **[1.21]**
	Row 5	-	0.17 **[0.80]**	0.14 [0.78]	-	0.20 **[1.46]**	0.10 **[1.56]**
	Row 10	-	0.13 **[0.92]**	**0.005 [1.35]**	-	0.20 **[1.69]**	0.10 **[1.67]**
	Col. 1	-	0.35 [0.14]	0.11 [0.53]	-	0.20 **[1.48]**	0.01 **[1.44]**
	Col. 4	-	0.07 **[1.06]**	0.06 **[1.06]**	-	0.20 **[1.67]**	0.10 **[1.52]**
	Col. 8	-	0.05 **[1.03]**	0.03 **[1.01]**	-	0.20 **[1.64]**	0.10 **[1.53]**
Med.	*Row 1*	-	-	0.69 [0.25]	-	-	0.80 [0.55]
	Row 5	-	-	0.34 [0.69]	-	-	0.40 **[1.19]**
	Row 10	-	-	0.03 **[1.50]**	-	-	0.40 [0.79]
	Col. 1	-	-	0.11 **[1.31]**	-	-	1.00 [0.06]
	Col. 4	-	-	0.34 **[0.80]**	-	-	0.80 [0.02]
	Col. 8	-	-	0.34 [0.37]	-	-	1.00 [0.47]

Table 5.7: Statistical values reported as p-value [effect size] for total muscle displacement during attempted MVC of able-bodied participants and SCI participants with different levels of muscle function. Values indicating a significant difference or a greater than medium effect size are shown in bold.

		Torque			**EMG**		
		Low	*Med.*	*High*	*Low*	*Med.*	*High*
AB	*Row 1*	0.01 **[1.09]**	0.51 [0.40]	0.09 **[0.82]**	0.01 **[1.24]**	0.91 [0.22]	0.14 **[0.84]**
	Row 5	0.01 **[1.23]**	0.37 [0.46]	0.44 [0.52]	**0.004 [1.79]**	0.78 [0.22]	0.18 **[0.96]**
	Row 10	0.01**[1.10]**	0.59 [0.35]	0.05 **[1.03]**	**0.004 [1.55]**	0.11 **[1.19]**	0.23 [0.76]
	Col. 1	**0.003 [1.30]**	0.59 [0.51]	0.26 [0.62]	**0.004 [1.75]**	0.48 [0.50]	0.44 [0.48]
	Col. 4	**0.01 [1.28]**	0.31 [0.52]	0.17 **[0.84]**	**0.004 [1.82]**	0.67 [0.48]	0.18**[0.91]**
	Col. 8	0.01**[1.26]**	0.51 [0.28]	0.09 **[0.86]**	**0.004 [1.73]**	0.67 [0.31]	0.10 **[1.12]**
Low	*Row 1*	-	0.05 **[1.20]**	**0.005 [1.46]**	-	0.20 **[1.64]**	0.10 **[1.64]**
	Row 5	-	0.05**[1.30]**	**0.003 [1.50]**	-	0.20 **[1.71**	0.10 **[1.71]**
	Row 10	-	**0.003 [1.45]**	**0.001 [1.67]**	-	0.20 **[1.65]**	0.10 **[1.77]**
	Col. 1	-	0.02 **[1.35]**	**<0.001 [1.63]**	-	0.20 **[1.65]**	0.10 **[1.78]**
	Col. 4	-	**0.01 [1.45]**	**0.005 [1.59]**	-	0.20 **[1.73]**	0.10 **[1.74]**
	Col. 8	-	**0.003 [1.44]**	**0.001 [1.64]**	-	0.20 **[1.66]**	0.10 **[1.76]**
Med.	*Row 1*	-	-	0.69 [0.66]	-	-	0.40 **[0.92]**
	Row 5	-	-	0.20 **[1.22]**	-	-	0.20 **[1.38]**
	Row 10	-	-	0.03 **[1.66]**	-	-	1.00 [0.58]
	Col. 1	-	-	0.03 **[1.48]**	-	-	1.00 [0.08]
	Col. 4	-	-	0.06 **[1.36]**	-	-	0.40 [0.58]
	Col. 8	-	-	0.20 **[1.23]**	-	-	0.40 **[0.95]**

The speed of the muscle contraction is calculated from displacement using equation 5.3 in Section 5.3.2.2. Tables 5.8 and 5.9 show the p-values and Cohen's d effect sizes for the speed of the muscle contraction during the initial phase and sustained phase respectively. Figure 5.16 shows a decrease in the speed of a muscle contraction with decreased levels of torque within the SCI group. During the initial phase of the contraction (Figure 5.16a), there are significant differences between SCI with low torque and SCI with high torque at row 10, column 4 and column 8. There are also significant differences with the able-bodied group at row 5, column 1 and column 4. There are large to very large effect sizes between all groups except for able-bodied and high torque. At row 10 SCI with high torque shows a higher speed than able-bodied, however only a small effect size is seen. Figure 5.16b shows a similar decrease in speed during the sustained phase of the contraction. Significant differences are seen between high and low levels of torque at all positions except row 5 during the sustained phase of the contrast.

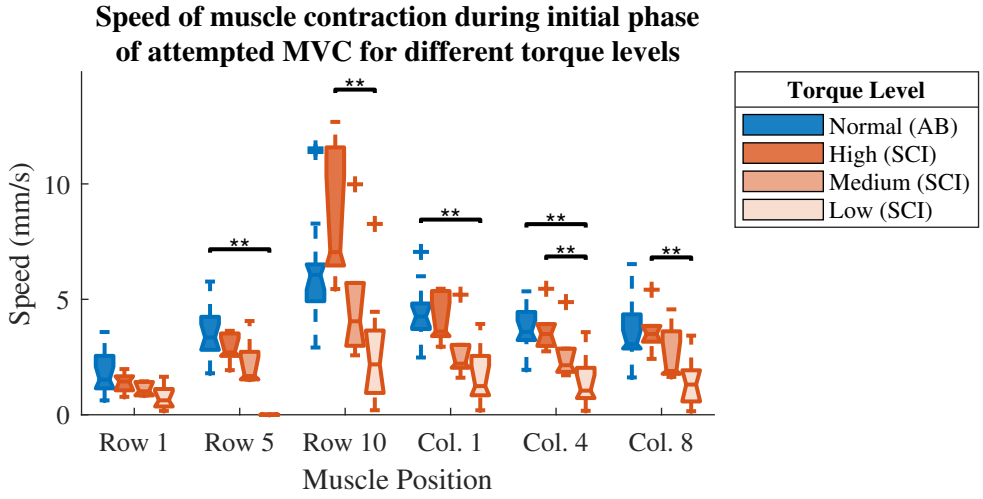

(a) Initial phase

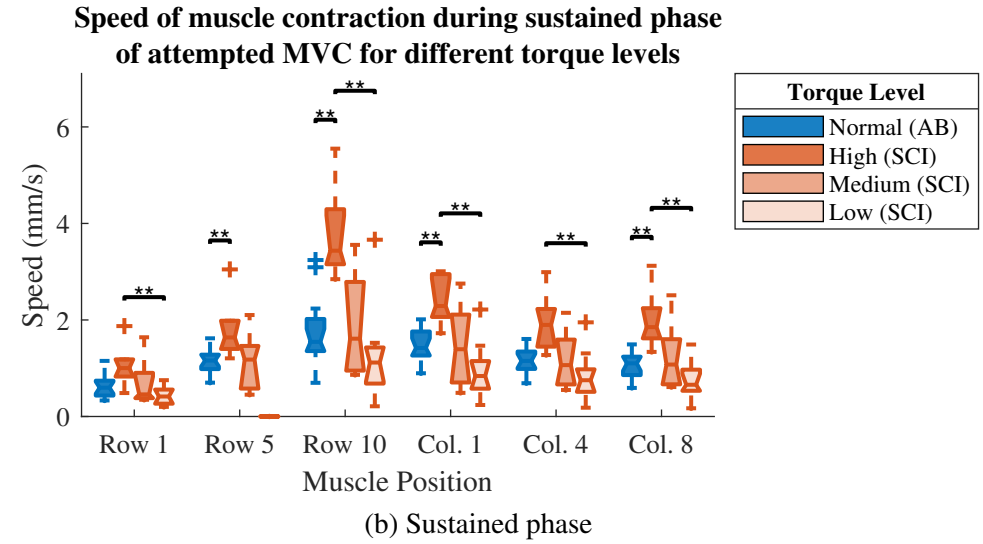

(b) Sustained phase

Figure 5.16: Boxplots of speed of muscle contraction during different phases of attempted MVC for able-bodied participants and SCI participants with different levels of torque ($**-p < 0.01$).

In contrast to the other phases, there is a significant increase between abled-bodied and SCI with high torque at all positions on the muscle except row 1 and column 4. Large to very large effect sizes are seen for all groups except for able-bodied and medium torque.

Figure 5.17 shows a similar decrease in the speed, with decreased levels of EMG for all positions except row 10 during the initial phase of muscle contraction (Figure 5.17a). There are large to very large effect sizes seen between all groups except between able-bodied and SCI with high levels of EMG, however significant differences are only seen between able-bodied and SCI with low EMG at all positions. At row 10, SCI with medium and high levels of EMG show an increase compared to the able-bodied group, with a large effect size for the medium EMG group. During the sustained phase (Figure 5.17b), this is seen at all positions across the muscle. Effect sizes are very large for all groups except between medium and high levels of EMG where small effect sizes are seen for all positions except row 10.

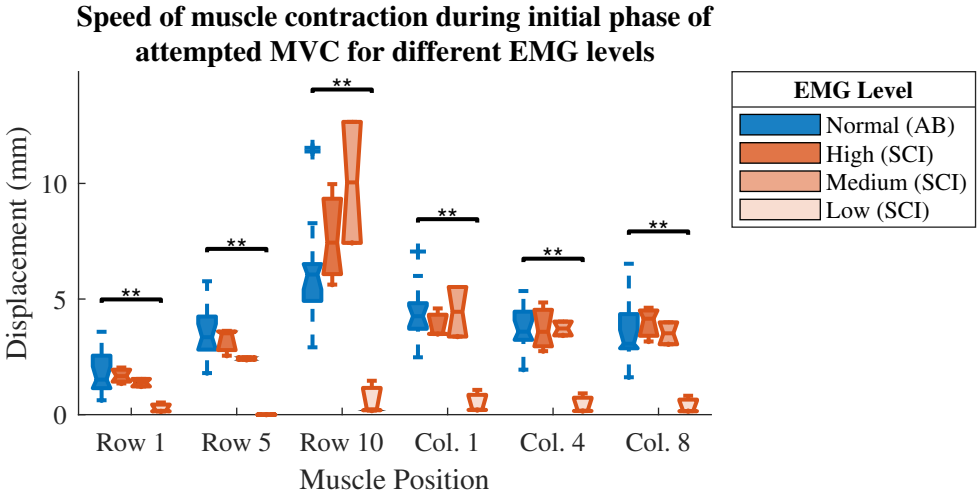

(a) Initial phase

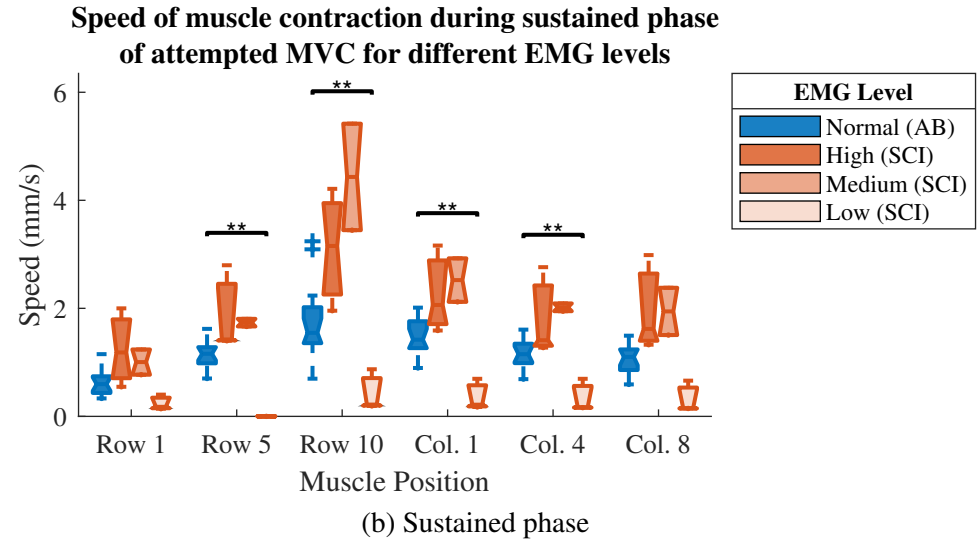

(b) Sustained phase

Figure 5.17: Boxplots of speed of muscle contraction during different phases of attempted MVC for able-bodied participants and SCI participants with different levels of EMG ($**-p < 0.01$).

Table 5.8: Statistical values reported as p-value [effect size] for the speed of muscle contraction during the initial phase of attempted MVC of able-bodied participants and SCI participants with different levels of muscle function. Values indicating a significant difference or a greater than medium effect size are shown in bold.

		Torque			**EMG**		
		Low	*Med.*	*High*	*Low*	*Med.*	*High*
AB	*Row 1*	0.01 **[1.25]**	0.21 **[0.84]**	0.67 [0.36]	**0.004 [1.41]**	0.55 [0.71]	0.72 [0.03]
	Row 5	**0.002 [1.47]**	0.04 **[1.05]**	0.06 **[1.02]**	**0.004 [2.00]**	0.08 **[1.22]**	0.61 [0.41]
	Row 10	0.02 **[1.10]**	0.10 [0.64]	0.17 [0.46]	**0.004 [1.72]**	0.11 **[1.26]**	0.62 [0.37]
	Col. 1	**0.002 [1.50]**	0.03 **[1.11]**	0.25 [0.53]	**0.004 [1.98]**	0.91 [0.10]	0.35 [0.59]
	Col. 4	**0.004 [1.40]**	0.06 **[0.94]**	0.44 [0.44]	**0.004 [2.00]**	0.93 [0.21]	0.71 [0.15]
	Col. 8	0.01 **[1.35]**	0.25 [0.78]	0.93 [0.24]	**0.004 [1.91]**	0.91 [0.25]	0.52 [0.21]
Low	*Row 1*	-	0.07 **[0.96]**	0.06 **[1.07]**	-	0.20 **[1.74]**	0.10 **[1.73]**
	Row 5	-	0.07**[1.06]**	0.02 **[1.34]**	-	0.20 **[1.77]**	0.10 **[1.76]**
	Row 10	-	0.05 **[1.13]**	**0.01 [1.42]**	-	0.20 **[1.71]**	0.10 **[1.71]**
	Col. 1	-	0.09 **[0.94]**	0.02 **[1.35]**	-	0.20 **[1.70]**	0.10 **[1.76]**
	Col. 4	-	0.09 **[1.15]**	**0.005 [1.42]**	-	0.20 **[1.79]**	0.10 **[1.70]**
	Col. 8	-	0.05 **[1.28]**	**0.005 [1.47]**	-	0.20 **[1.77]**	0.10 **[1.76]**
Med.	*Row 1*	-	-	0.34 **[0.88]**	-	-	0.40 **[0.95]**
	Row 5	-	-	0.03 **[1.59]**	-	-	0.20 **[1.32]**
	Row 10	-	-	0.03 **[1.59]**	-	-	0.80 **[0.86]**
	Col. 1	-	-	0.03 **[1.59]**	-	-	1.00 [0.63]
	Col. 4	-	-	0.03 **[1.42]**	-	-	1.00 [0.00]
	Col. 8	-	-	0.06 **[1.38]**	-	-	0.40 [0.69]

Table 5.9: Statistical values reported as p-value [effect size] for the speed of muscle contraction during the sustained phase of attempted MVC of able-bodied participants and SCI participants with different levels of muscle function. Values indicating a significant difference or a greater than medium effect size are shown in bold.

		Torque			**EMG**		
		Low	*Med.*	*High*	*Low*	*Med.*	*High*
AB	*Row 1*	0.07 **[0.95]**	0.77 [0.29]	0.01**[1.15]**	0.01 **[1.39]**	0.11 **[1.20]**	0.10 **[1.52]**
	Row 5	0.34 [0.57]	0.77 [0.07]	**0.01 [1.17]**	**0.004 [1.93]**	0.02 **[1.85]**	0.02 **[1.55]**
	Row 10	0.15 [0.56]	0.86 [0.19]	**0.003 [1.49]**	**0.004 [1.70]**	0.02 **[2.20]**	0.05 **[1.38]**
	Col. 1	0.09 **[0.85]**	0.86 [0.06]	**0.003 [0.99]**	**0.004 [2.00]**	0.02 **[1.97]**	0.05 **[1.47]**
	Col. 4	0.15 [0.61]	0.95 [0.08]	0.01**[1.29]**	**0.004 [1.95]**	0.02 **[2.12]**	0.20 **[1.38]**
	Col. 8	0.40 [0.65]	0.95 [0.43]	**0.002 [1.44]**	0.02 **[1.84**	0.02 **[2.00]**	0.02 **[1.63]**
Low	*Row 1*	-	0.22 **[0.85]**	**0.003 [1.38]**	-	0.20 **[1.66]**	0.10 **[1.39]**
	Row 5	-	0.35 **[0.81]**	0.01 **[1.31]**	-	0.20 **[1.76]**	0.10 **[1.54]**
	Row 10	-	0.17 **[1.05]**	**0.01 [1.53]**	-	0.20 **[1.73]**	0.10 **[1.62]**
	Col. 1	-	0.22 **[0.97]**	**0.005 [1.53]**	-	0.20 **[1.75]**	0.10 **[1.62]**
	Col. 4	-	0.22 **[0.94]**	**0.01 [1.37]**	-	0.20 **[1.77]**	0.10 **[1.50]**
	Col. 8	-	0.22 **[0.97]**	**0.001 [1.51]**	-	0.20 **[1.68]**	0.10 **[1.53]**
Med.	*Row 1*	-	-	0.49 [0.32]	-	-	1.00 [0.43]
	Row 5	-	-	0.34 **[0.93]**	-	-	0.80 [0.24]
	Row 10	-	-	0.20 **[1.26]**	-	-	0.40 **[1.03]**
	Col. 1	-	-	0.20 **[1.04]**	-	-	0.80 [0.39]
	Col. 4	-	-	0.20 **[0.95]**	-	-	0.80 [0.34]
	Col. 8	-	-	0.34 **[0.89]**	-	-	1.00 [0.05]

5.4.2.3 Pixel difference

The pixel difference results provide similar information to the displacement results but measure movement of the whole muscle as opposed to regional areas. The pixel difference is calculated from equation 5.5 in Section 5.3.3.2 and the maximum and total measurements used to describe muscle movement are defined in Section 5.3.3.3. P-values and Cohen's d effect sizes for maximum NPD are shown in Table 5.10. Figure 5.18a shows a decrease in maximum NPD for SCI participants with low torque levels. The maximum NPD of the low torque group has large or very large effect sizes when compared with all other groups, although no significant differences are seen after the Bonferroni correction is applied. There are only small to medium effect sizes between all other groups, indicating that the maximum NPD for SCI with high and medium torque groups is similar to that of the able-bodied group.

A similar result is seen in Figure 5.18b for different levels of EMG with even bigger effect sizes between low EMG and other groups, reaching statistical significance when compared to the able-bodied group. High levels of EMG show increased movement compared to both medium EMG and able-bodied groups, coinciding with medium effect sizes.

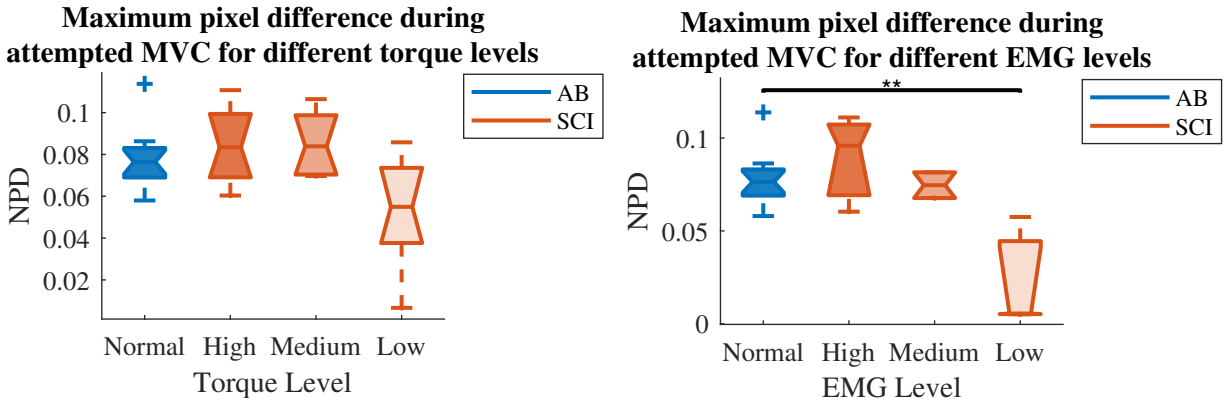

(a) Torque (b) EMG

Figure 5.18: Boxplots of maximum NPD during attempted MVC for able-bodied participants and SCI participants with different levels of muscle function ($**-p < 0.01$).

Table 5.10: P-values and effect sizes for maximum pixel difference during attempted MVC of able-bodied participants and SCI participants with different levels of muscle function. Values indicating a significant difference or a greater than medium effect size are shown in bold.

	Torque		**EMG**	
	P-value	*Effect Size*	*P-value*	*Effect Size*
AB vs. SCI_{Low}	0.03	**1.12**	**0.004**	**2.02**
AB vs. $SCI_{Med.}$	0.31	0.51	0.69	0.29
AB vs. SCI_{High}	0.58	0.36	0.43	0.71
SCI_{Low} vs. $SCI_{Med.}$	0.02	**1.28**	0.20	**1.45**
SCI_{Low} vs. SCI_{High}	0.06	**1.07**	0.10	**1.50**
$SCI_{Med.}$ vs. SCI_{High}	0.49	0.32	0.80	0.70

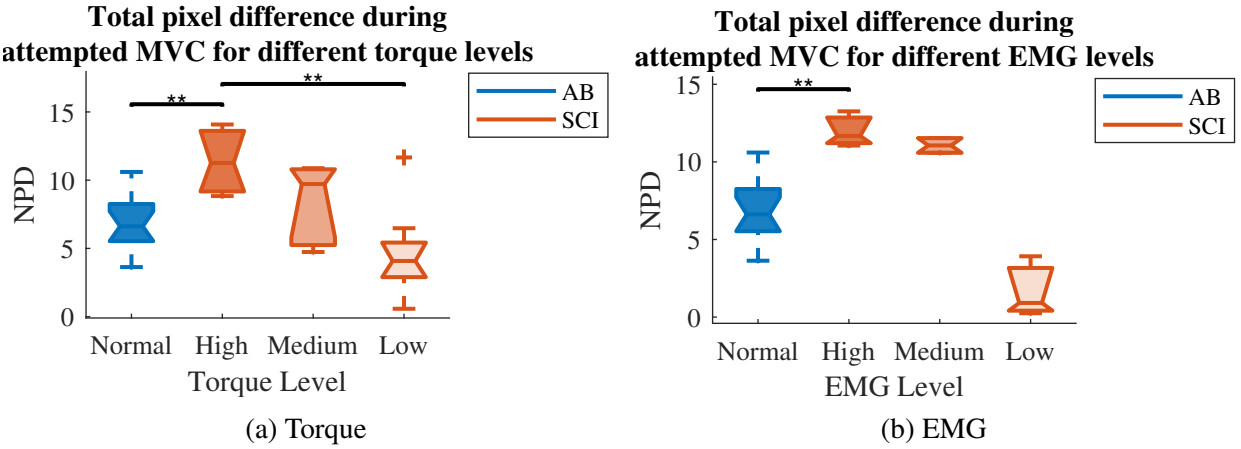

(a) Torque (b) EMG

Figure 5.19: Boxplots of total pixel difference during attempted MVC for able-bodied participants and SCI participants with different levels of muscle function ($** - p < 0.01$).

Figure 5.19 shows the total change in pixel difference, which is a measurement of the total muscle movement during an attempted MVC. The p-values and Cohen's d effect size for total NPD is shown in Table 5.11. Figure 5.19a shows total NPD decreases with torque level within the SCI group, with a statistically significant difference between high and low levels, and large to very large effect sizes between all SCI groups. SCI with low torque levels is less than the able-bodied group and shows a medium effect size, however the SCI with medium and high torque levels increases in comparison to the able-bodied group. SCI with medium torque shows only a medium effect size compared to able-bodied participants, however high torque SCI shows a very large effect size and reaches statistical significance.

A similar result is seen for different EMG levels in Figure 5.19b. In this case the effect sizes between all groups are larger, but the only significant difference seen is between able-bodied and SCI with high EMG levels.

Table 5.11: P-values and effect sizes for total pixel difference during attempted MVC of able-bodied participants and SCI participants with different levels of muscle function. Values indicating a significant difference or a greater than medium effect size are shown in bold.

	Torque		**EMG**	
	P-value	*Effect Size*	*P-value*	*Effect Size*
AB vs. SCI_{Low}	0.09	0.75	0.01	**1.85**
AB vs. SCI_{Medium}	0.37	0.64	0.04	**1.84**
AB vs. SCI_{High}	**0.002**	**1.46**	**0.004**	**1.88**
SCI_{Low} vs. $SCI_{Med.}$	0.02	**1.39**	0.20	**1.76**
SCI_{Low} vs. SCI_{High}	**0.005**	**1.50**	0.10	**1.77**
$SCI_{Med.}$ vs. SCI_{High}	0.20	**1.10**	0.40	**0.92**

The speed of the muscle contraction is calculated from the pixel difference using equation 5.6 in Section 5.3.3.3. The p-values and Cohen's d effect size for the speed of muscle contraction during the initial phase and sustained phase are shown in Table 5.12. Figure 5.20 shows that the

speed of the muscle contraction decreases with reduced torque and EMG level at different phases of muscle contraction. A large to very large effect size is seen between SCI with low torque and all other groups during the initial phase of a muscle contraction (Figure 5.20a), with a significant difference between low and high torque levels within the SCI group. There is also a very large effect size between medium and high torque levels, while SCI participants with medium torque show only a medium effect size when compared to able-bodied participants. SCI participants with high torque levels are also slightly increased compared to the able-bodied group, however, only a medium effect size is seen.

In contrast, during the sustained phase (Figure 5.20c), SCI with high torque is significantly higher than able-bodied participants. There are large to very effect sizes between all SCI groups, however the low and medium levels of torque show only small effect sizes when compared with the able-bodied group.

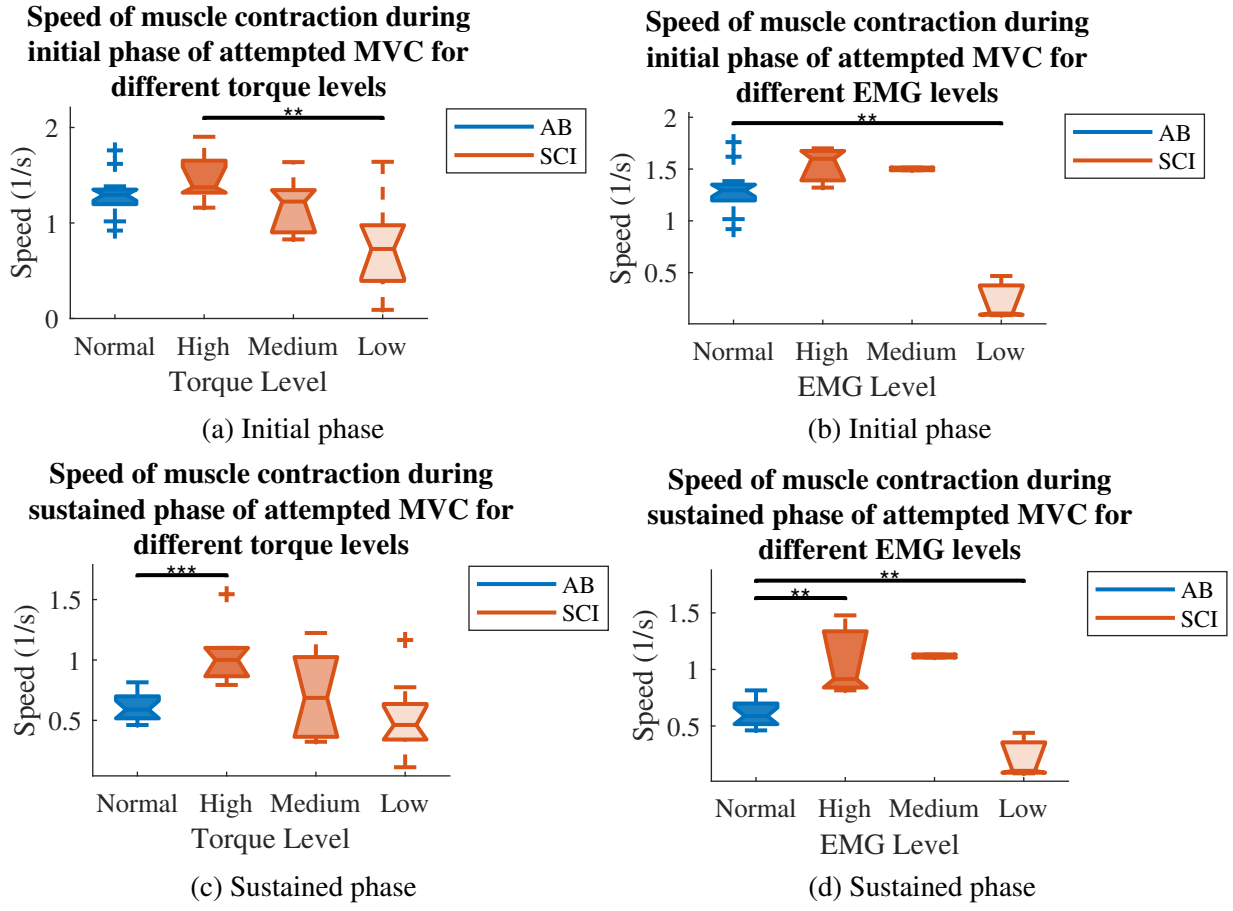

(a) Initial phase

(b) Initial phase

(c) Sustained phase

(d) Sustained phase

Figure 5.20: Boxplots of speed of muscle contraction during different phases of attempted MVC for able-bodied participants and SCI participants with different levels of torque and EMG ($**-p<0.01, ***-p<0.001$).

Similar results are also seen for different levels of EMG. During the initial phase of the contraction (Figure 5.20b), only the able-bodied and low EMG groups show a significant difference, however very large to huge effect sizes are seen between low EMG and all other groups. An

increase between SCI with high EMG level and able-bodied groups is also seen during the initial phase with a large effect size. Furthermore, SCI with medium EMG shows the same increase compared to the able-bodied group with a large effect size. During the constant phase (Figure 5.20d) the difference between able-bodied and low EMG still reaches statistical significance. Medium and high level EMG show much higher values of speed compared to the able-bodied group, with the high EMG group also reaching statistical significance.

Table 5.12: P-value and effect size for speed of muscle contraction during the attempted MVC of able-bodied participants and SCI participants with different levels of muscle function. Values indicating a significant difference or a greater than medium effect size are shown in bold.

Initial phase				
	Torque		**EMG**	
	P-value	*Effect Size*	*P-value*	*Effect Size*
AB vs. SCI_{Low}	0.04	**1.13**	**0.004**	**2.16**
AB vs. $SCI_{Med.}$	0.44	0.50	0.17	**0.98**
AB vs. SCI_{High}	0.37	0.51	0.14	**1.02**
SCI_{Low} *vs.* $SCI_{Med.}$	0.03	**1.26**	0.20	**1.78**
SCI_{Low} *vs.* SCI_{High}	**0.01**	**1.30**	0.10	**1.77**
$SCI_{Med.}$ *vs* SCI_{High}	0.03	**1.34**	0.80	0.27
Sustained phase				
	Torque		**EMG**	
	P-value	*Effect Size*	*P-value*	*Effect Size*
AB vs. SCI_{Low}	0.61	0.23	**0.004**	**1.92**
AB vs. $SCI_{Med.}$	0.86	0.44	0.02	**2.43**
AB vs. SCI_{High}	**< 0.001**	**1.48**	**0.004**	**1.81**
SCI_{Low} *vs.* $SCI_{Med.}$	0.35	**0.92**	0.20	**1.76**
SCI_{Low} *vs.*SCI_{High}	0.01	**1.31**	0.10	**1.60**
$SCI_{Med.}$ *vs.* SCI_{High}	0.69	**0.82**	0.80	0.19

5.5 Discussion

The aim of this work was to evaluate the use of USI to assess the functional status of muscles following a SCI. Ultrasound videos of the gastrocnemius muscle were analysed under two conditions. First, measurements regarding the morphology of the muscle were taken while the muscle was in a relaxed state. This included the use of tracking software to measure the size of the muscle, and greyscale analysis to make measurements describing muscle structure. Secondly, measurements of muscle movement during an attempted MVC were obtained using tracking software and changes in pixel greyscale values. These measurements were compared between 15 able-bodied and 15 SCI participants. Within the SCI group, the measurements were also compared between different levels of muscle function, determined through measurements of ankle torque and EMG. Differences in these measurements between the different groups support the hypothesis that USI measurements of muscle movement are capable of distinguishing

between different levels of muscle movement.

5.5.1 USI measurements of muscle structure in relation to function

5.5.1.1 Muscle echogenicity

The increase in pixel greyscale values between able-bodied and SCI groups indicates that muscles appear brighter following a spinal cord injury and therefore muscle echogenicity increases. As previously discussed in Chapter 4, this is consistent with the structural changes which occur in the muscle as a result of atrophy.

In this chapter, the focus is on the relationship between ultrasound parameters and the functional status of muscles. SCI participants showed a similar increase in echogenicity regardless of torque or EMG level. This suggests that echogenicity is not affected by the functional status of the muscle. These results agree with the findings presented by Gordon et al. [39], suggesting that load bearing of the muscle had a more significant effect on atrophy than muscle activity. Investigations of disuse atrophy of different muscles show that atrophy does not necessarily correlate with muscle activity, with muscles that normally bear weight showing preferential atrophy. This means that even if the GM muscle was able to produce a high level of torque or EMG, if other muscles in the legs were not able to support standing or walking then the muscles would not be loaded. All SCI participants were wheelchair users, therefore this could explain why there is no significant difference between different torque and EMG levels.

Shortening of muscle length is another factor which has been shown to contribute to muscle atrophy [39]. Following a spinal cord injury, muscle contractures are common due to the lack of movement or imbalance of movement around a joint [212, 213]. Therefore, another possible explanation is that a contracture around the ankle joint contributed to the atrophy of the muscle as a result of muscle shortening. Furthermore, other factors such as the type of lesion and spasticity could also affect the amount of atrophy.

Overall there are several factors which could contribute to the amount of atrophy which a muscle undergoes that are not directly related to the amount of muscle activity.

5.5.1.2 Resting muscle thickness

The reduction in resting muscle thickness is also characteristic of atrophy. As previously discussed in Chapter 4 (page 91), atrophy is a reduction in the size and number of muscle fibres, which would result in a decrease in the overall size of the muscle.

Not only is muscle thickness significantly less for the SCI groups compared to the able-bodied group, it also decreases with lower torque and EMG levels within the SCI group. Again, this is consistent with a reduction in muscle fibres as the muscle atrophies, resulting in a decreased net torque produced by the muscle. Several studies have demonstrated the relationship between the size and strength of muscles for able-bodied participants [214] and the reduction

in muscle thickness following a spinal cord injury as a result of atrophy [42], however to our knowledge muscle thickness has not been directly related to muscle function within the SCI population.

The differences between SCI participants does not reach statistical significance between low and medium torque levels. This could be due to fat infiltration replacing muscle bulk and as a result there is a minimum thickness which a muscle will reach [43]. This may make it more difficult to distinguish between different torque levels below a certain threshold and should be taken into consideration when drawing conclusions about muscle function.

5.5.2 USI measurements of muscle movement in relation to function

The movement of muscles during an attempted MVC are described through measures of muscle deformation, displacement and changes in pixel difference. Muscle deformation describes the movement of the aponeuroses, while displacement and pixel difference describe movement within the muscle. The movement within the muscle is described through the maximum value, the total movement and the speed at which the muscle contracts during different phases of an attempted MVC.

5.5.2.1 Muscle deformation

SCI participants who were only able to produce low levels of EMG demonstrated less muscle deformation than both able-bodied participants and SCI with higher levels of muscle activity. This is to be expected as muscles most affected by paralysis will have less movement.

In contrast, SCI participants who were able to produce high levels of muscle activity showed a similar deformation to able-bodied participants. This is most likely due to the fact that there is little change in muscle thickness at high levels of activation [112], therefore muscle deformation cannot be used to differentiate reduced muscle movement due to SCI from normal muscle movement above a certain threshold.

However, the results do not completely conform to the theory that muscles which are able to produce less torque will undergo less muscle deformation. SCI participants showed similar muscle deformation regardless of torque level. Also, SCI participants who were able to produce medium EMG levels were found to have more muscle deformation than any other group. This could be caused by the reduction in muscle fibres as a result of atrophy, leading to a less efficient muscle contraction.

It should also be considered that during these attempted voluntary contractions, several participants showed a reduction in muscle thickness. As discussed in Section 2.3.1.2 of Chapter 2, the thickness of the muscle would be expected to increase as the muscle shortened during a contraction, therefore it is possible that the changes in muscle thickness are a result of other muscles compressing the gastrocnemius muscle and therefore not providing a true measurement

of muscle deformation.

5.5.2.2 Maximum muscle movement

Overall the maximum muscle movement decreases between able-bodied and SCI participants with decreasing levels of muscle function, consistent with a reduction in muscle movement as a result of paralysis.

Maximum muscle displacement decreases with decreasing levels of torque and EMG within the SCI group. It shows large differences between SCI groups with different torque and EMG levels, suggesting that by looking at regional movement, USI is capable of detecting differences in muscle function within the SCI group. In general, effect sizes are largest at row 10, which is the most superficial part of the muscle. Differences between able-bodied and low and medium torque levels have larger effect sizes at column 1, which represents the proximal end of the muscle, while differences between low level torque and other SCI groups are larger at columns 4 and 8, representing the central and distal part of the muscle. Differences between different EMG levels are more uniform across the muscle except for a comparison between medium and high levels which is larger at row 5, the central area of the muscle.

The maximum pixel difference can differentiate between SCI participants with low torque and all other groups, however it may be more representative of the electrical activity of the muscle as it is able to differentiate between varying levels of EMG within the SCI group.

5.5.2.3 Total muscle movement

The total muscle movement also demonstrates the reduced movement in paralysed muscle. Both total muscle displacement and pixel difference can differentiate not only between able-bodied and SCI participants, but also different levels of torque and EMG within the SCI group. Muscle displacement also shows that the differences in muscle movement between different levels of torque are largest at the most superficial position of the muscle (row 10).

5.5.2.4 Speed of muscle movement

A reduction in speed, calculated by both muscle displacement and pixel difference, was seen for SCI participants as the torque levels decreased. This differs from the results of previous studies [61,62], which suggest an increase in muscle contractility following a SCI. It is generally accepted that there is a shift in the composition of muscle fibres following a SCI, resulting in a higher proportion of fast-twitch type IIx fibres. The increased contractility seen in other studies is attributed to this change in fibre composition. With this higher proportion of fast-twitch fibres, it would therefore be expected that the speed of muscle contraction would increase, however the muscles being examined vary considerably and the time when this fibre transformation occurs is still unclear. It is thought that it could be months after the injury before the transformation begins

and muscles may not reach a steady state for years. It is possible that the effects of this change in fibre composition are not seen because the measurements were taken too soon after injury. In addition, the change in fibre composition and its effect on the contractile properties of the muscle reported in these studies [61,62] obtain their results from muscle biopsies, therefore there could be other factors such as muscle stiffness or delayed reaction times contributing to the low speed of contraction. It is also important to note that as the main focus is on the functional status of the muscle, SCI participants are grouped according to torque and EMG levels regardless of time post-injury. This means there is a wide variation in the time post-injury in each group, so if the changes in fibre composition are time dependent then the effects may not be seen in this context.

There are some occasions where an increase in speed is seen. SCI participants with high torque levels have a higher speed compared to able-bodied participants during the sustained phase of the contraction (Figure 5.16b) and SCI participants with high and medium levels of EMG appear to have a higher speed compared to able-bodied participants during the sustained phases of the contraction (Figure 5.17). Similar results are seen when the speed is calculated based on the pixel difference (Figure 5.20). These results could be explained by an increase in contractility, however, it is also possible that this increase is seen due to more muscle displacement as participants attempt to maintain the contraction, particularly during the sustained phase (discussed in further detail below).

5.5.3 Comparison of USI measurements

Muscle deformation, muscle displacement and pixel difference are all USI parameters which describe the movement of a muscle, however, each one provides different information: muscle deformation describes the movement of the aponeuroses and therefore quantifies movement of the whole muscle based on the position of the boundaries; displacement characterises the movement of regional areas within the muscle through movement of different features; pixel difference sums all of the movement at the pixel level within the muscle without the distinction of different regional areas.

5.5.3.1 Muscle deformation vs. regional displacement

Muscle deformation provides some indication of how much movement a muscle is able to produce and is able to differentiate between muscles of able-bodied participants who are able to produce normal movements and those of SCI participants who have low EMG and torque levels. However, very small muscle movements may not produce a change in thickness and conversely, there is little difference in muscle deformation at high values of torque. Muscle deformation therefore may be able to differentiate between large differences in muscle function, but it does not appear to be suitable for detecting subtle differences.

Maximum muscle displacement on the other hand appears to be much more sensitive to these

smaller movements within the muscle, showing differences between different levels of torque and EMG which are not seen with muscle deformation. The regional measurements also provide additional information about the areas of the muscle where movement occurs.

The total muscle displacement during the whole muscle contraction shows even more differences between SCI groups across the different positions of the muscle, suggesting it may be more useful than the maximum difference between two adjacent frames. However, SCI participants with high torque and EMG show a higher displacement than the able-bodied group at several positions on the muscle. This can be explained by the ability of able-bodied participants to sustain a muscle contraction with very little movement. In this case there is a large movement during the initial phase of the contraction, followed by very little movement once the maximum level is reached, and finally another large movement when the muscle relaxes. When this displacement is plotted over time, this results in two large distinct peaks, with a displacement close to zero in between. In contrast, a SCI participant who is capable of producing a relatively large torque is still likely to be affected by muscle fatigue and find it more difficult to maintain the contraction. This may lead to the muscle continuously moving in an attempt to maintain the initial torque level. Graphically, this results in a large displacement during the initial contraction, which continues to fluctuate until the muscle relaxes. As the total displacement is calculated from the sum of the displacement between adjacent frames throughout the whole contraction, this can lead to a larger total displacement, even when the initial peak is not significantly larger.

5.5.3.2 Tracking software vs. pixel difference measurements

The maximum pixel difference provides similar information to maximum muscle displacement, however large differences are only seen between SCI participants with low torque and the other groups. All other groups show similar values, suggesting that pixel difference can differentiate between muscle function at low levels but is not useful for distinguishing different torque levels above a certain threshold. Bigger differences in maximum pixel difference are seen between different EMG levels, therefore the summation of the muscle movements at the pixel level may be more representative of the electrical activity of the muscle than the force being generated.

The total change in pixel difference is also more effective at differentiating between torque levels compared to the maximum value between frames. Similarly to the displacement results, the SCI participants with high and even medium levels of torque and EMG show a greater total change in pixel values than able-bodied participants. Again, this is thought to be due to the continuous movement which occurs in an attempt to maintain the contraction. The total muscle movement during a contraction, for both displacement and pixel difference, shows similar results between different torque and EMG levels.

Differences in speed calculated from both muscle displacement and pixel difference allowed different levels of torque within the SCI group to be differentiated, particularly during the initial phase of the muscle contraction. During the sustained phase SCI with high torque show a higher

speed than able-bodied participants, however this is most likely a result of the increased movement which occurs during repeated attempts to maintain the contraction as discussed previously. Speed was able to differentiate between low levels of EMG and other groups, however medium and high levels of EMG were not so easy to differentiate.

5.5.4 Electrical vs. mechanical events of muscle contraction

Throughout the results, different levels of torque and EMG tend to follow a similar trend, however there are some instances where the results differ. Resting muscle measurements showed similar results, however the differences did not reach statistical significance between different EMG levels. Muscle deformation was similar across all levels of torque, whereas SCI participants with low levels of EMG showed much lower values of deformation than all other groups. This can be explained by the low EMG group including participants with such little muscle movement that the EMG is not detected and therefore no contraction is produced where a change in muscle thickness occurs.

This also explains why both maximum and total displacement are much smaller in the low EMG group compared to other groups, and as a result often show a significant difference with the able-bodied group. Differences can be seen between the different levels of torque within the SCI group, which in the case of total displacement often reach statistical significance. In contrast, both maximum and total displacement show similar values for medium and high levels of EMG. This suggests that these measurements appear to be more representative of the force produced by the muscle rather than the electrical activity.

The maximum pixel difference on the other hand shows larger differences between EMG levels, suggesting changes in pixel difference may be more representative of the electrical activity in the muscle. The total pixel difference was able to differentiate between different levels of torque and EMG, indicating this measurement could represent the electrical activity of the muscle as well as the force it is able to generate. It should be noted, however, that the only significant difference between SCI groups was between high and low levels of torque.

It must be taken into consideration that EMG represents the electrical and not the mechanical events that occur during a muscle contraction, and therefore any interpretation of muscle function based on EMG must be done with caution [215]. It should also be noted that due to problems with signal quality recorded during the experiment, usable EMG data is limited and therefore there are less participants included in the groups of different EMG levels than the groups of different torque levels (see Section 5.3.5.1 for details). Furthermore, processing of the EMG data included notch filtering at 50 Hz, as detailed in Section 5.3.4.2. This was necessary to remove noise from electrical interference, however, it could also have removed physiologically relevant signal from the EMG data. These limitations should be taken into account when interpreting results based on EMG. Having said that, EMG provides a measurement of activity which is more specific to the GM muscle, whereas torque measurements represent the combined force

produced by synergistic muscles in the lower limb. Moreover, it is possible that SCI participants with limited movement in the GM muscle use compensatory movements to produce torque instead of plantar flexion alone. This could also contribute to differences seen between torque and EMG results. Overall, USI measurements are better at differentiating between different levels of torque, however, pixel difference may be more suitable than displacement for differentiating between different levels of EMG.

5.6 Conclusion

Different USI parameters were compared between able-bodied participants and SCI participants with different levels of muscle function. USI was able to detect morphological changes in the muscle between able-bodied and SCI groups as a result of atrophy, however only muscle thickness was able to differentiate between different levels of muscle function. Muscle echogenicity was found to be unaffected by muscle activity.

USI was also able to detect differences in muscle movement through measurements of deformation, displacement and changes in pixel greyscale value. Both displacement and pixel difference were found to be sensitive measurements for differentiating between different levels of muscle activity, demonstrating the ability of USI to assess the amount of muscle function which has been retained following a SCI. Total muscle movement was more useful than the maximum value. The speed of the muscle contraction could also be calculated from both displacement and pixel difference measurements and was found to be a further useful measurement for differentiating between different levels of muscle function and providing an insight into the contractile properties of the muscle.

Measurements of regional displacement obtained from tracking software were also compared to a computationally simpler pixel difference method. Both methods provided similar results, however, displacement appears to be more effective at differentiating between different levels of torque. On the other, pixel difference showed more differences between different levels of EMG. This suggests that displacement may be more representative of the mechanical function of the muscle, while pixel difference appears to represent the electrical activity of the muscle.

Chapter 6

Assessment and Prediction of Recovery

6.1 Summary

In this chapter, the use of ultrasound imaging (USI) measurements to quantify and predict recovery from a spinal cord injury (SCI) is evaluated. Measurements of muscle structure, discussed in Chapter 4, and muscle movement, discussed in Chapter 5, are compared over time for individual participants. The correlation between changes in these USI measurements and the recovery of the muscle is investigated, based on measurements of torque and manual muscle test (MMT) scores. This chapter also investigates whether USI measurements can detect recovery at an earlier stage than other measures, and if USI measurements taken in the early stages provide insight into whether or not the muscle function will recover over time.

6.2 Introduction

As discussed in Chapters 4 and 5, the level and severity of the SCI affects which parts of the body are affected and to what extent. It is therefore essential to accurately evaluate the injury, an important part of which is the assessment of muscle function. This initial assessment of the injury provides valuable information which is used to direct treatment, however, it is equally important to assess changes in muscle function over the course of recovery. This allows clinicians to monitor the progress of patients, assess the success of treatments and rehabilitation interventions, and adjust if necessary.

Furthermore, research on new treatment options for SCI vary widely, including neurological enhancement and regeneration trials, physical training trials and the application of neuromuscular electrical stimulation [83]. In order to accurately assess the success of any clinical intervention, accurate functional outcome measures are necessary [216].

Motor scores based on manual muscle testing as part of the American Spinal Injury Association (ASIA) impairment scale is considered the standard measure of muscle function for recovery as well as initial assessment. This method provides valuable information and is widely

accepted as the gold standard for neurological outcome measures, however it does have its limitations. Manual muscle test scores are performed by a trained clinician, however, the measurements are subjective. As a result, intra- and inter-rater reliability is a concern and reproducibility of results relies on a standardised protocol being strictly followed. There are also statistical limitations when quantifying improvements due to the nonlinear ordinal scale and a so called "ceiling effect" that can make it difficult to distinguish between experimental and control groups in clinical trials [216].

Overall, it is widely agreed that there is a need for more sensitive, quantitative and objective outcome measures. This has led to the development of electrophysiological measurements such as Quantitative Sensory Testing (QST) for measuring somatic sensory function and motor evoked potentials (MEPs) elicited by transcranial magnetic stimulation (TMS) for measuring motor function [217]. Electromyography (EMG) can also be used alone for an objective measurement of muscle activity. Although these techniques may overcome many of the limitations of MMT, their routine use in a clinical setting is limited. Moreover, limitations in the ability to detect very small muscle movements and distinguish between deep muscles still exist.

There are also several measurements which focus on functional recovery such as the Functional Independence Measure (FIM) and Spinal Cord Independence Measure (SCIM) which assess the ability of SCI patients to perform everyday activities. These may be more direct measurements of changes which are clinically meaningful in terms of a participant's functional ability but they are not sensitive enough to show small improvements in muscle movement and are not necessarily a direct result of neurological improvement but could be a result of compensatory strategies [216].

Ultrasound imaging (USI) is a potential additional tool which could provide measurements of muscle structure and function sensitive enough to detect small changes as a result of recovery. Several studies have demonstrated the suitability of USI to make accurate measurements of muscle size. Reeves at al. compared repeated measures of muscle cross-sectional area with measurements made with MRI to show the reliability and validity of USI to measure muscle size, demonstrating its suitability for detecting changes as a result of training or muscle wasting [89]. Mechelli et al. also demonstrated the robustness of USI measurements over time comparing measurements in healthy subjects 2 years apart [218].

USI has been shown to detect increases in muscle size as a result of exercise training programs [219], as well as loss of muscle mass due to disuse, both in healthy participants [220] and patients hospitalised without neuromuscular disorders [138]. It has also been shown to detect changes in muscle thickness and pennation angle as a result of delayed-onset muscle soreness (DOMS) [221].

In addition, USI has been found to detect changes in muscle size as a result of progressive neuromuscular diseases, with several cross-sectional studies demonstrating its ability to distinguish between different levels of severity in disorders such as muscular dystrophy and motor

neuron disease [24, 222]. However, studies which investigated changes in muscle thickness as a result of motor neuron disease through serial measurements had variable success [223, 224].

Previous chapters have investigated the use of USI measurements in the form of a cohort observation study, to distinguish between SCI and able-bodied participants, or cross-sectional studies where groups of SCI participants were compared based on the time since injury had occurred or the functional status of the muscle. This chapter takes the form of a longitudinal study, focusing on how these same USI measurements change over time for individual participants and how this relates to recovery. USI measurements of muscle structure (as discussed in Chapter 4) and muscle movement (as discussed in Chapter 5) are all considered, using data from both Study 1 and Study 2. The changes in these measurements are compared between groups of participants with different levels of recovery, based on other measurements of muscle function.

The aim of this study is to establish if USI is a suitable tool for assessing recovery of muscle following a SCI by investigating:

- whether USI measurements are sensitive enough to detect changes over time for individual participants
- how well these changes in USI measurements correlated with other measures of recovery
- if USI could detect changes in muscle function at an earlier stage than traditional evaluation techniques
- if USI measurements made initially after the injury provided any insight into whether or not the muscle function would recover over time.

6.3 Methods

6.3.1 Overview of data used

This chapter uses data from both Study 1 (see Section 3.3 of Chapter 3) and Study 2 (see Section 3.4 of Chapter 3). Chapters 4 and 5 have previously discussed how data from Study 1 was analysed to provide measurements obtained from USI videos to describe muscle structure and functional movement. In these chapters, the data was used as part of a cohort study to compare groups of able-bodied and SCI participants, or as a cross-sectional study comparing groups of SCI participants at different times post-injury or with different levels of muscle function. This chapter investigates how these same measurements change over time for individual participants as a longitudinal study evaluating recovery. This study provides data from the gastrocnemius medialis (GM) muscle of the right leg of 15 SCI participants attempting an isometric MVC. Participants completed between 2 and 7 sessions at monthly intervals, providing a range of data from 1 to 8 months post-injury.

Study 2 provides data from the gastrocnemius medialis (GM), tibialis anterior (TA) and rectus femoris (RF) muscles of both legs of 6 SCI participants attempting an isotonic contraction. Participants were less than 1 month post-injury on the first session and each completed 5 sessions over a 12 week period.

6.3.2 Overview of measurements

This section summarises the measurements taken with USI during the studies and the parameters that were extracted and investigated. It is followed by the muscle measures obtained using other techniques.

6.3.2.1 USI measurements

Muscle structure: The following measurements were calculated from USI videos recorded in Study 1 to describe the structure of the muscle through measurements of muscle size and greyscale analysis of the pixel greyscale values. Details of analysis and how these measurements were calculated can be found in Section 4.3 Chapter 4 (page 68)

1. Resting muscle thickness: the distance between the boundaries of the muscle
2. First-order descriptors: describe the echogenicity i.e. the brightness of the muscle through statistical measurements of the pixel greyscale values. These are:
    - Integrated optical density (IOD): sum of pixel intensity values within region of interest
    - Mean: average pixel intensity values
    - Energy: brightness of the image
    - Variance: average degree to which each point differs from the central tendency
    - Skewness: asymmetry of probability distribution
    - Kurtosis: combined size of the two histogram tails
3. Haralick features: second-order statistical descriptors which describe the homogeneity of pixel intensity values, including:
    - Contrast: variation between reference and neighbouring pixel
    - Correlation: linear dependency on GLCM
    - Energy: represents local uniformity
    - Entropy: represents degree of disorder
    - Homogeneity: distance of the distribution from the diagonal of the GLCM

4. Galloway features: second-order statistical descriptors which describe the coarseness of pixel intensity values:

    - Short run emphasis (SRE): distribution of short runs
    - Long run emphasis (LRE): distribution of long runs
    - Grey-level non-uniformity (GLNU): distribution of runs over the grey values
    - Run length non-uniformity (RLNU): distribution of runs over the run lengths
    - Run percentage (RP): number of actual runs as a fraction of the maximum potential runs

5. Local binary pattern (LBP) features: second-order statistical descriptors which describe the homogeneity of pixel intensity values. These are:

    - Energy: describes local uniformity
    - Entropy: represents degree of disorder

Isometric MVC: The following measurements of muscle movement during an attempted maximum voluntary contraction (MVC) were calculated from USI videos recorded in Study 1 to describe muscle function. The analysis methods and a description of how these measurements were calculated can be found in Section 5.3 of Chapter 5 (page 100).

1. Deformation: change in muscle thickness as a percentage of the resting thickness
2. Displacement: regional movement of the muscle at different positions

    - Maximum: peak value during contraction
    - Total: summation of displacement during the entire contraction
    - Speed: summation of the displacement per second over i) first 2.5 seconds (initial phase) and ii) 2.5-7.5 seconds (sustained phase) of a muscle contraction

3. Pixel difference: summation of movement at the pixel level over the entire muscle.

    - Maximum: peak value during contraction
    - Total: summation of pixel difference during the entire contraction
    - Speed: summation of the pixel difference per second over i) first 2.5 seconds (initial phase) and ii) 2.5-7.5 seconds (sustained phase) of a muscle contraction

Isotonic attempted movement: The following measures of muscle movement during an attempted isotonic contraction were calculated from USI videos recorded in Study 2 to describe small muscle movements. The analysis methods and a description of how these measurements were calculated can be found in Section 5.3 of Chapter 5 (page 100).

1. Pixel difference: summation of movement at the pixel level over the entire muscle.
    - Maximum: peak value during contraction
    - Total: summation of pixel difference during the entire contraction

6.3.2.2 Muscle function measurements

Isometric MVC: The following measures of muscle function were recorded during an attempted MVC in Study 1.

1. Torque: moment of force generated by muscle while pushing against foot plate of dynamometer.
2. Electromyography (EMG): maximum value of the root mean square (RMS) calculated from the EMG signal after filtering and full wave rectification.

Isotonic attempted movement: The following measures of muscle function were recorded during attempted isotonic movement in Study 2.

1. Manual muscle test (MMT): grade assigned by physiotherapist based on the muscle's ability to perform movement
2. Range of motion (ROM): change in angle between the two segments of a joint
3. Electromyography (EMG): maximum value of the RMS calculated from the EMG signal after filtering and full wave rectification.

6.3.3 Definition of recovery

In order to determine if changes in USI measurements are a result of recovery, other measures of muscle movement are used to define muscle function and how this has changed over time. In Study 1, participants were more than 1 month post-injury and were able to sit on the chair of the dynamometer as described in Section 3.3.2 of Chapter 3, allowing measurements of ankle torque to be obtained as part of the assessment of the GM muscle. In Study 2, participants were less than 1 month post-injury and the protocol was performed bedside to be more in line with clinical applications. Manual muscle testing was performed by a trained physiotherapist on each of the 6 muscles being assessed (gastrocnemius medialis, tibialis anterior and rectus femoris of the right and left legs). Recovery is therefore defined for each study based on these different measurements.

In the case of Study 1, where participants attempted an isometric MVC, torque is used to define muscle function and recovery. Participants in this study all had incomplete spinal cord injuries and were therefore capable of producing some small movement. Those who showed an

increase in torque of at least 5 Nm were classified as recovering, and those who did not were classified as not recovering. In Study 2, the MMT score was used as the main measurement for defining recovery. In this case, the focus was on differentiating between much smaller muscle movements and no muscle movement during an attempted isotonic contraction. Any increase in the MMT score was considered recovery, however we considered recovery in terms of three groups: i) a change in MMT score of 0 (no recovery), ii) a change in MMT score of 1-2 (small recovery) and iii) a change in MMT score of 3 or more (large recovery).

6.3.4 Changes in measurements over time

USI measurements from participants in Study 2 are plotted over time as there are only six participants, with each participant completing 5 sessions (except for P5 who only completed 3 sessions). This allows trends over all sessions to be visualised as well as changes between individual sessions. Due to the small number of participants (n=6), statistical analysis is only performed when each muscle is considered as an independent measurement (see Section 6.3.6 for statistical analysis). As data was recorded from 6 muscles (right and left GM, TA and RF) for each participant, this greatly increases the sample size (n=36). In order to consider changes over time for groups of participants, the change in each measurement (Δa) was calculated as difference between the first (a_1) and last (a_n) session,

$$\Delta a = a_n - a_1 \tag{6.1}$$

where n is the number of sessions completed by the participant. If the measurement is a similar value on the first and last session, i.e. there is no change between sessions, then $\Delta a = 0$. If the measurement increases between sessions, it will result in a positive change, while a decrease will show a negative change. By comparing this change in USI measurements between groups of participants who did and did not recover, as defined in Section 6.3.3, their ability to measure recovery can be investigated.

6.3.5 Prediction of recovery

The definition of recovery in Section 6.3.3 can also be used to investigate whether USI measurements in the early sessions provide an insight into whether or not the muscle will recover. In this case only measurements from the first session are used, and compared between the same groups of participants who recovered some muscle function and those who did not.

For participants from Study 2, plotting measurements of USI against measurements of muscle function can also provide insight into the relationship between the two parameters and how this changes over time. This allows changes in both measurements to be seen over time, and therefore identify if USI measurements increase in line with other measures of function or if improvements can be seen before they are detected by traditional methods.

6.3.6 Statistical analysis

6.3.6.1 Grouping of data

As described in Section 6.3.3, participants were grouped according to their recovery. For Study 1, 6 participants were considered to have shown recovery and 9 participants were not according to the change in torque between the first and last session. For Study 2, each of the 6 muscles were considered individually resulting in a total of 36 data points for 6 participants. These data points were then split into 3 groups according to the change in the MMT score: no change in the MMT score ($n = 17$), a small increase (1-2) in the MMT score ($n = 11$) and a large increase (3+) in the MMT score ($n = 8$).

6.3.6.2 Calculation of statistically significant difference

When the sample size was ten or more, the Shapiro-Wilk test was used to assess the normality of the data as described in Section 3.9.1. When data was found to be normally distributed, an unpaired t-test was used (see Section 3.9.2.1). When data was not normally distributed or the sample size was less than ten, the non-parametric Mann-Whitney U test was used as an alternative (see Section 3.9.2.2). When assessing the changes in a measurement over time, individual groups were also compared to a hypothetical value of zero. This was done using a one sample t-test or the Wilcoxon signed rank test depending on whether data was normally distributed or not.

All tests were performed using a significance level of p=0.05 for comparisons between participants who did and did not recover. When assessing differences between groups who showed varying improvements in MMT scores, three groups were compared in a pairwise manner, therefore the level of significance was adjusted using the Bonferroni correction for multiple comparisons to p=0.016 (0.05/3).

6.3.6.3 Calculation of Cohen's d effect size

Cohen's d effect size was also calculated in line with an unpaired test using equation 3.5. Further details on Cohen's d effect size and how to interpret it are provided in Section 3.9.4.

6.4 Results

The results in this section are based on the changes in USI measurements for individual participants over time. First, the difference in USI measurements obtained during Study 1 are presented, including measurements of muscle structure (discussed in Chapter 4) and function (discussed in Chapter 5). Next, changes in USI measurements based on the pixel difference method which were obtained during Study 2 are presented. In each case, comparisons are made

between different levels of recovery (see Section 6.3.3 for details on how recovery was defined). Finally, results relating to the suitability of USI measurements to predict recovery are presented.

6.4.1 Changes over time for USI measurements obtained during Study 1

In this section, results are presented based on the data obtained during Study 1. USI measurements of muscle structure and function are compared between participants who did and did not recover.

6.4.1.1 Muscle structure

Figure 6.1 shows the change in resting thickness, between the first and last session for participants who were classified as having recovered and those who were not. There is no statistically significant difference between the groups ($p = 0.61$) and only a small effect size is seen ($d = 0.26$). Furthermore, even though the median of the group who recovered is higher, neither group are statistically significantly different from zero, therefore there does not appear to be a significant change in resting muscle thickness between the first and last session.

The only first-order descriptor that shows a change between the first and last session is variance. The no recovery group shows a negative change in Figure 6.2d, indicating a decrease in variance, which reaches statistical significance ($p = 0.02$). Figure 6.3 shows the change in the Haralick features between the first and last session for participants who did and did not show recovery. Only correlation (90°) is significantly less than zero ($p = 0.04$) and energy (90°,135°) is significantly more than zero ($p = 0.04$, $p = 0.02$) in the no recovery group. The only Galloway feature to show a difference between sessions is the RLNU (135°), which appears to increase in the recovery group, as shown in Figure 6.4d, and reaches statistical significance ($p = 0.03$). Figure 6.5 shows the changes in LBP features between the first and last session. Energy increases and entropy decreases in the no recovery group, however, the difference from zero does not reach statistical significance. None of these measurements show a significant difference between the recovery and no recovery groups, as shown in Tables 1 to 4 in Appendix B.1.

6.4.1.2 Isometric MVC

None of the USI measurements of muscle movement during an isometric MVC show a difference between the first and last session, regardless of recovery. There are no differences between the groups of participants who did and did not recover. The changes in muscle deformation, pixel difference measurements and displacement measurements between the first and last session are shown in Figures 45 to 47 in Appendix B.2, along with p-values and Cohen's d effect sizes in Tables 5 and 6. No statistically significant differences are seen, however, some large effect sizes are seen between measurements of displacement in the recovery and no recovery groups.

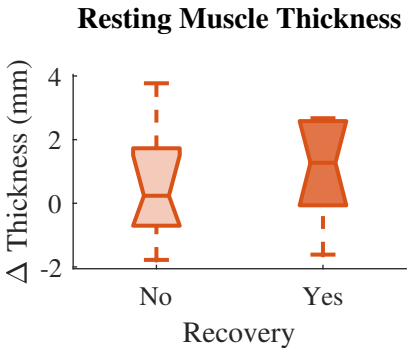

Figure 6.1: Boxplots of the difference between the first and last session for resting muscle thickness.

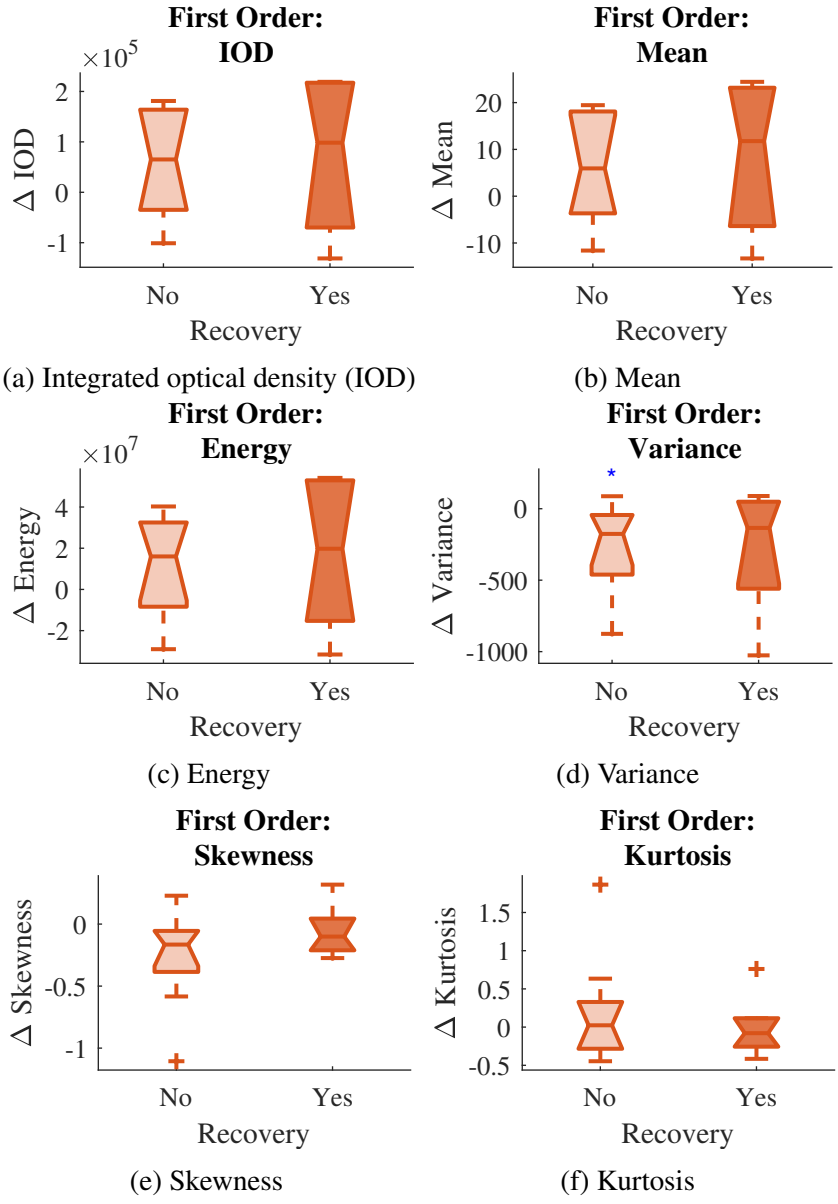

(a) Integrated optical density (IOD)

(b) Mean

(c) Energy

(d) Variance

(e) Skewness

(f) Kurtosis

Figure 6.2: Boxplots of the difference between the first and last session for first-order measurements of muscle echogenicity ($* - p < 0.05$, the blue colour represents a significant difference between a group and 0).

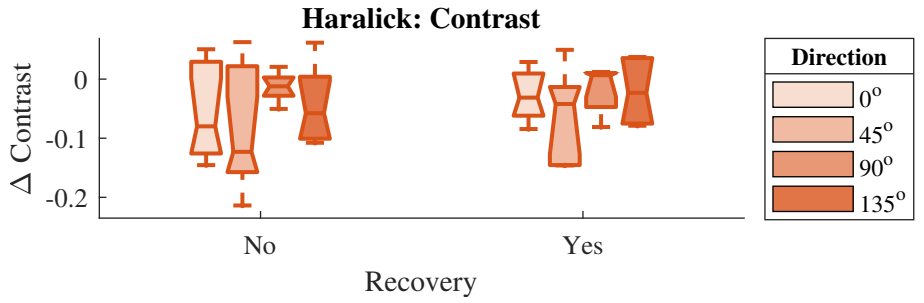

(a) Contrast

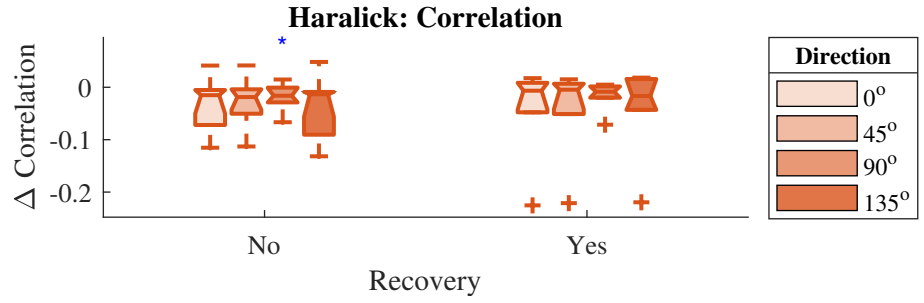

(b) Correlation

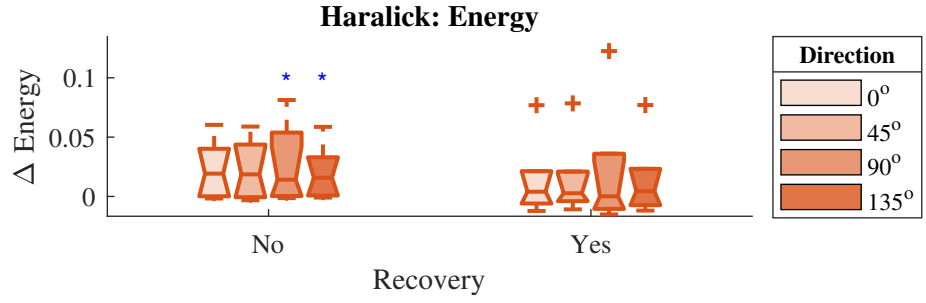

(c) Energy

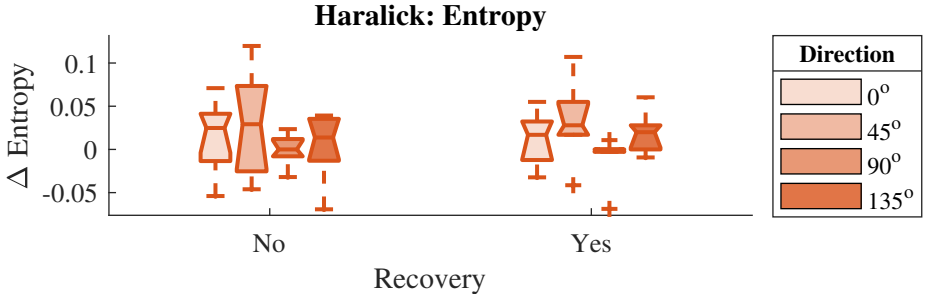

(d) Entropy

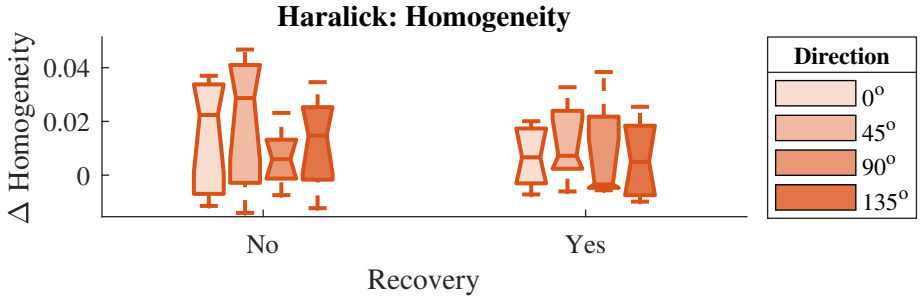

(e) Homogeneity

Figure 6.3: Boxplots of the difference between the first and last session for Haralick features describing muscle echotexture ($* - p < 0.05$, the blue colour represents a significant difference between a group and 0).

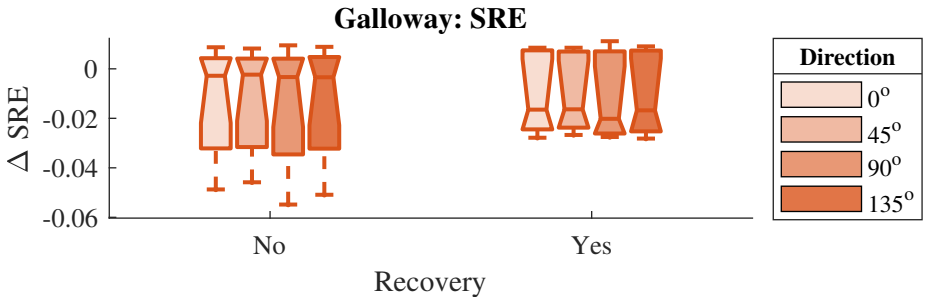

(a) Short run emphasis (SRE)

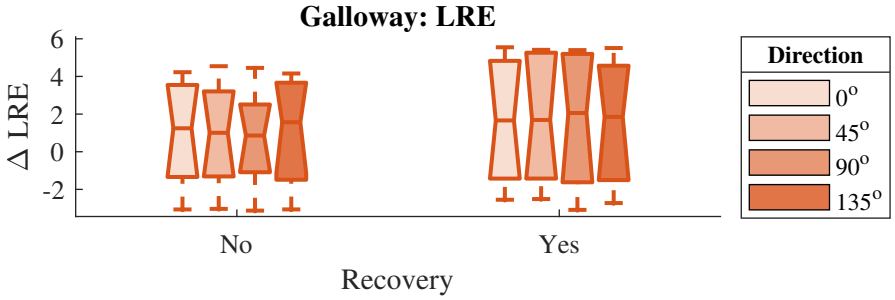

(b) Long run emphasis (LRE)

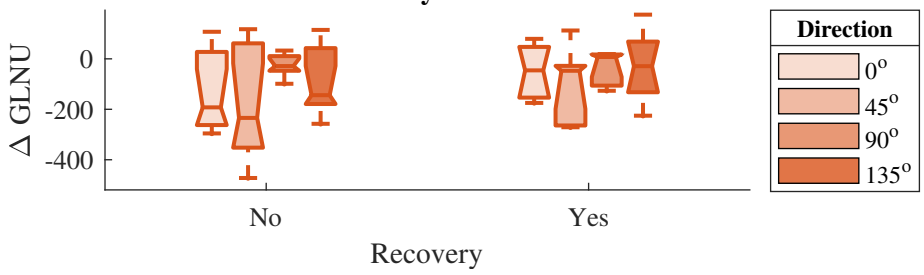

(c) Grey-level non-uniformity (GLNU)

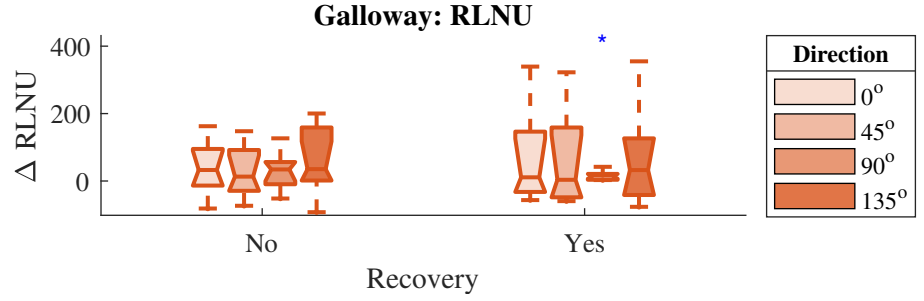

(d) Run length non-uniformity (RLNU)

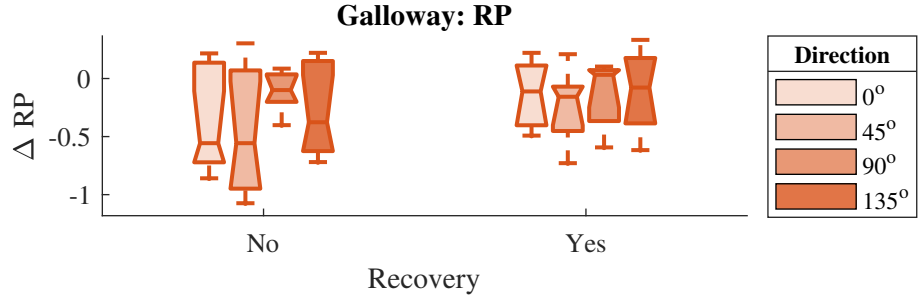

(e) Run Percentage (RP)

Figure 6.4: Boxplots of difference between first and last session for Galloway features describing muscle echotexture ($* - p < 0.05$, the blue colour represents a significant difference between a group and 0).

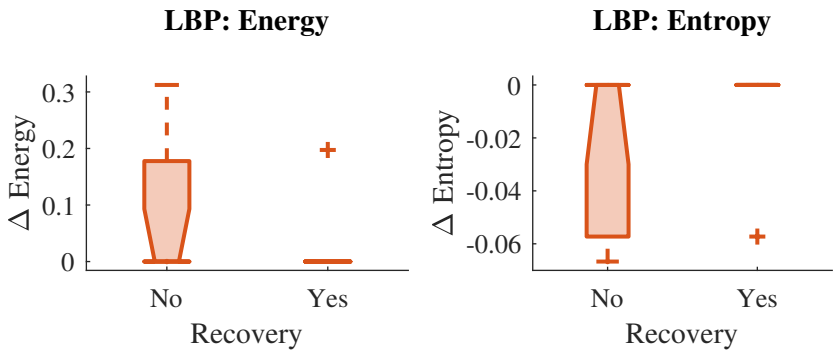

(a) Energy (b) Entropy

Figure 6.5: Boxplots of the difference between the first and last session for LBP features describing muscle echotexture.

6.4.2 Changes over time for USI measurements obtained during Study 2

In this section, results are presented based on the data obtain during Study 2, including USI measurements based on pixel difference and conventional measurements of MMT scores, EMG and range of motion (ROM). First, results are shown for individual participants, plotting each measurement over time. This is followed by group results, comparing the changes in measurements between the first and last session based on the amount of recovery seen.

6.4.2.1 Individual participants who showed no recovery

Figures 6.6, 6.7 and 6.8 show all USI measurements (maximum pixel difference and total pixel difference) and measurements of muscle movement (MMT score, ROM and EMG) at each of the five sessions for participants who showed no signs of recovery in at least five out of the six muscles investigated (P2, P5 and P6). In general, there are no improvements seen across the five sessions for all measurements of muscle function and the USI measurements correspond with this, showing no movement or signs of recovery between sessions. However, there are some exceptions to this. Participant 2 (Figure 6.6) appears to show some movement in the right RF muscle during session 4 (seen in Figure 6.6a), however the participant reported spasms during the recording, most likely explaining the detection of movement by the USI measurements. Participant 5 (Figure 6.7) showed an increase in muscle movement in the GM muscle of both the right and left leg (seen in Figures 6.7a and 6.7b). The right GM muscle did not show any improvement in the MMT score, however, as it was grade 1, there was already some muscle movement during the first session which appears to improve even though the muscle has not reached a higher MMT grade. The left GM muscle also improves from a MMT score of 0 to 1, therefore the USI measurements agree with this small improvement in muscle movement. Finally, participant 6 (Figure 6.8) appears to show an increase in the right RF muscle (seen in Figure 6.8a), however no signs of recovery are seen in the measurements of muscle movement.

The right TA muscle improves from a MMT score of 0 to 1 between sessions 4 and 5 (Figure 6.6c), however no signs of improvement are seen in the USI measurements.

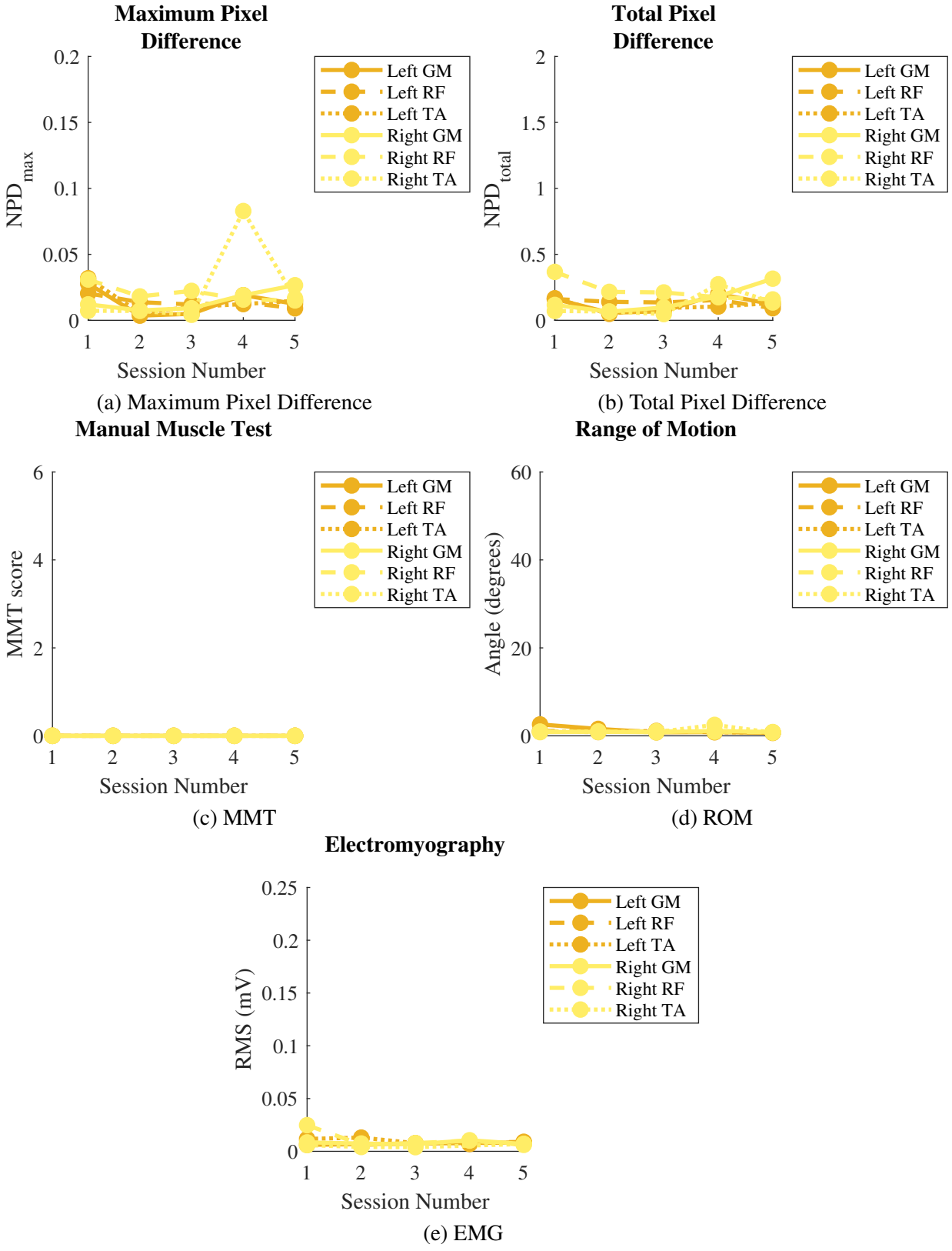

(a) Maximum Pixel Difference

(b) Total Pixel Difference

(c) MMT

(d) ROM

(e) EMG

Figure 6.6: USI measurements and measurements of muscle movement at each session (1-5) for participant 2.

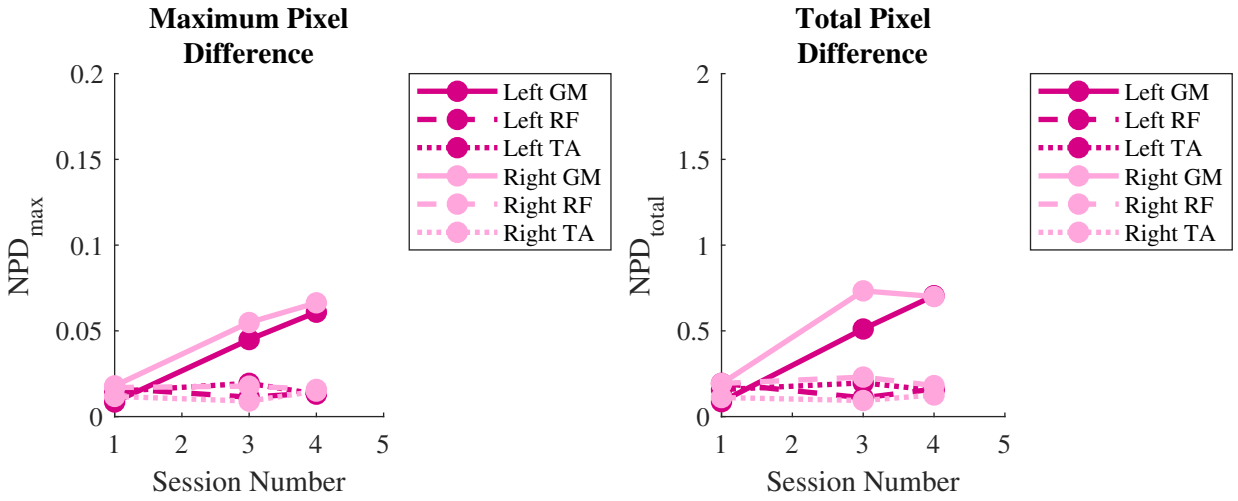

(a) Maximum Pixel Difference

(b) Total Pixel Difference

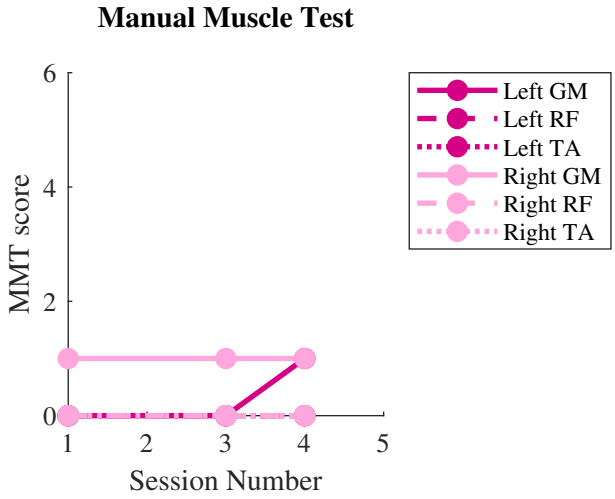

(c) MMT

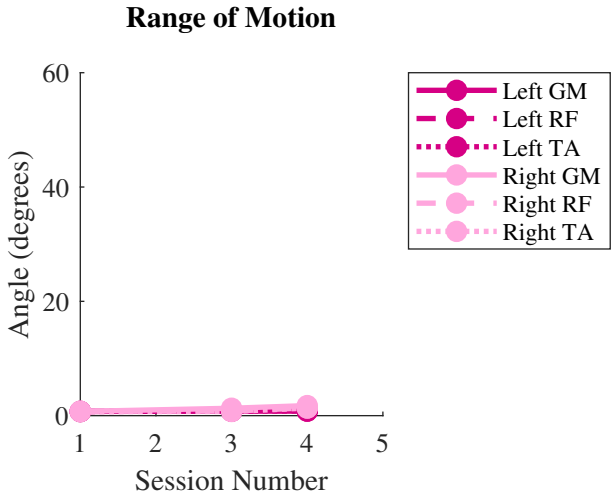

(d) ROM

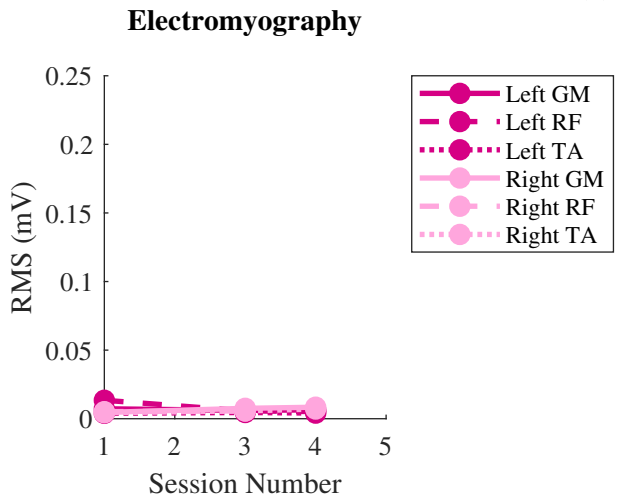

(e) EMG

Figure 6.7: USI measurements and measurements of muscle movement at each session (1, 3 and 4) for participant 5.

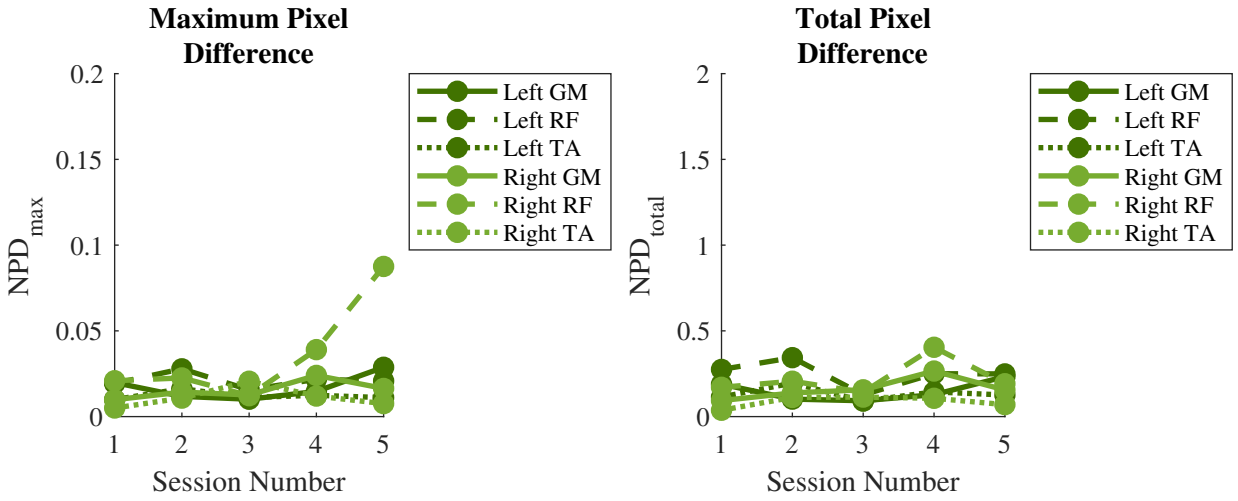

(a) Maximum Pixel Difference

(b) Total Pixel Difference

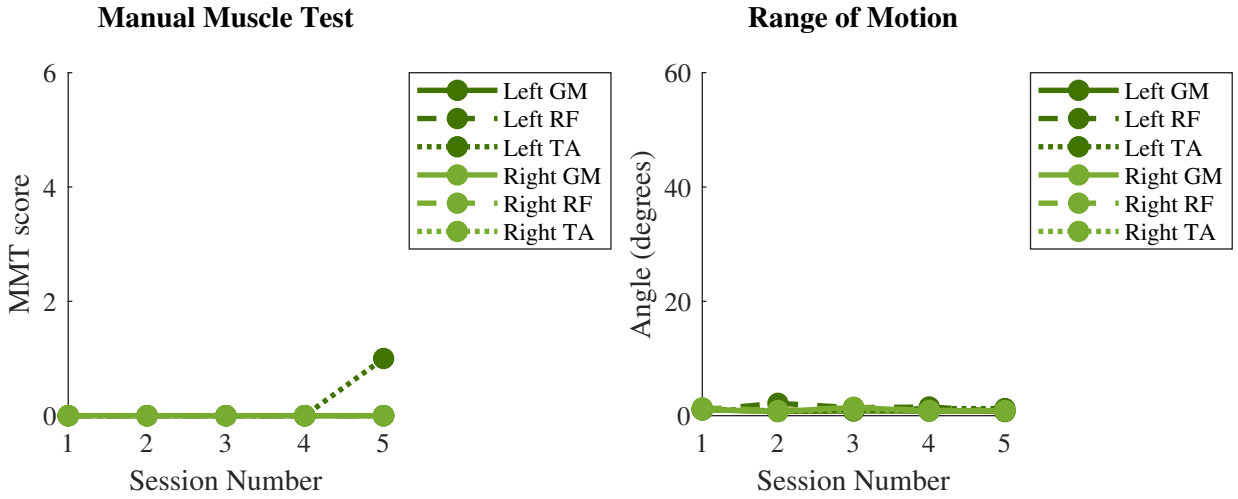

(c) MMT

(d) ROM

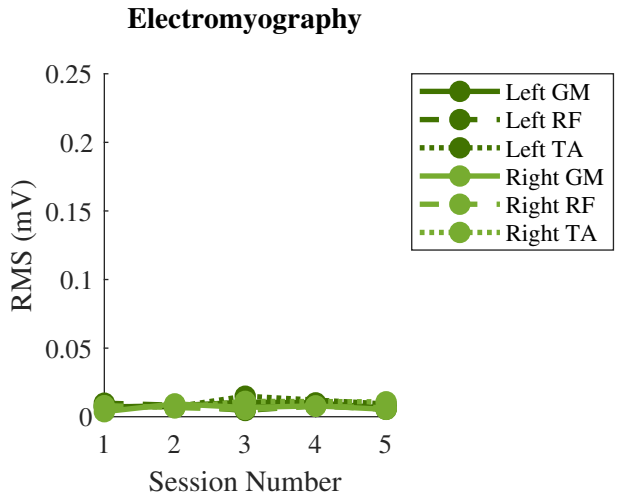

(e) EMG

Figure 6.8: USI measurements and measurements of muscle movement at each session (1-5) for participant 6.

6.4.2.2 Individual participants who showed recovery

Figures 6.9, 6.10 and 6.11 show all USI measurements (maximum pixel difference and total pixel difference) and measurements of muscle movement (MMT score, ROM and EMG) at each of the five sessions for participants who showed signs of recovery (P1, P3 and P4).

Participant 1 had MMT scores of 1 for all muscles at session 1, which then all improved to varying degrees over the five sessions (Figure 6.9c). This is reflected in both the USI measures (Figures 6.9a and 6.9b) and other measures of muscle function (Figures 6.9d and 6.9e). Not only do the USI measures increase with recovery, muscles which showed the biggest recovery in terms of MMT scores also show the largest increase in USI measurements. The maximum pixel difference consistently increases except for the right TA muscle which decreases between sessions 4 and 5, coinciding with a decrease in MMT score as a result of swelling around the joint. In contrast, the total pixel difference shows an overall increase between session 1 and session 5 but also shows a decrease in muscle movement between some of the sessions for several muscles.

Participant 3 shows very little recovery in the muscles in the left leg as MMT scores were already high at session 1. The maximum pixel difference (Figure 6.10a) reflects this, with high values on the first session which show only a small increase between the first two sessions and then fluctuates. The total pixel difference (Figure 6.10b) also shows a small gradual increase across the 5 sessions for left GM and TA muscles and a consistently high value which fluctuates for the left RF muscle. The muscles in the right leg have low MMT scores (1-2) at session 1 and improve their score by 1-2. The maximum pixel difference shows a gradual increase across the five sessions, with the right RF muscle, which increased to a MMT score of 4, showing more muscle movement than the other muscles with lower MMT scores. The total pixel difference shows only a small gradual increase for the right TA muscle which only improved to a MMT score of 2. The right GM also had a MMT score of 2 at sessions 4 and 5, however it had reached a score of 3 at session 3 and shows a much bigger increase in muscle movement. The total pixel difference decreases slightly for the right RF muscle, however, it showed a larger value similar to the muscles in the left leg from the first session.

Participant 4 also has low MMT scores of 0 or 1 at session 1 for all muscles, with some muscles improving more than others by session 5. Both USI measurements and other measures of muscle function show this increase in muscle movement. Again, muscles which improved more show more improvement in the USI measures than those that only improved their MMT score by 1-2, as shown in Figure 6.11.

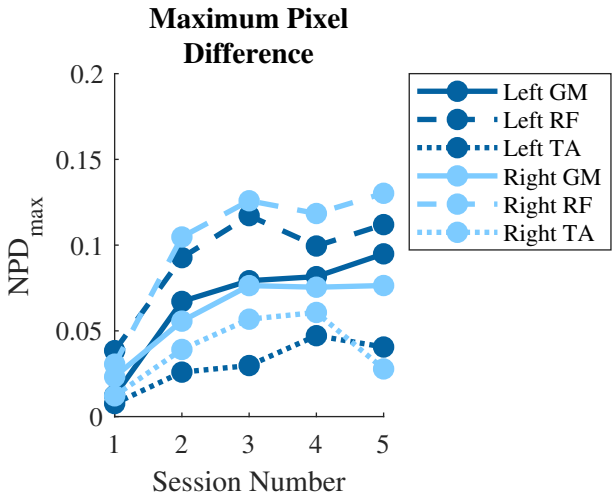

(a) Maximum Pixel Difference

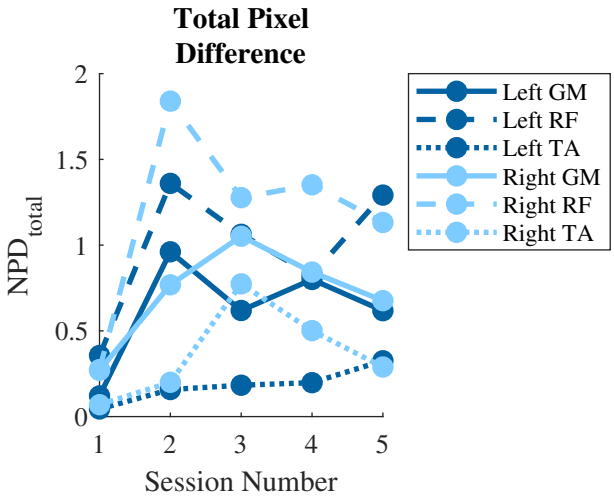

(b) Total Pixel Difference

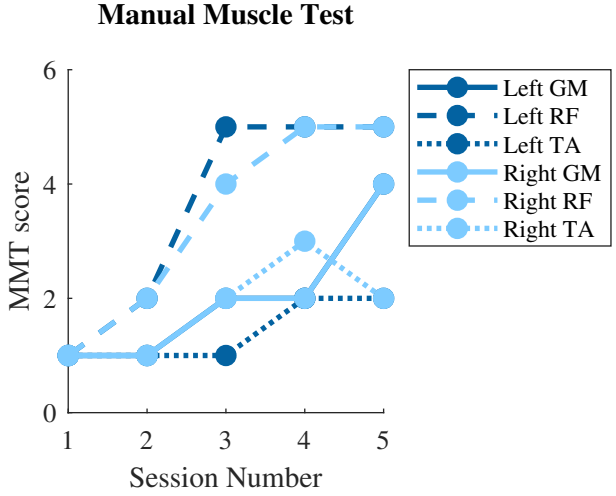

(c) MMT

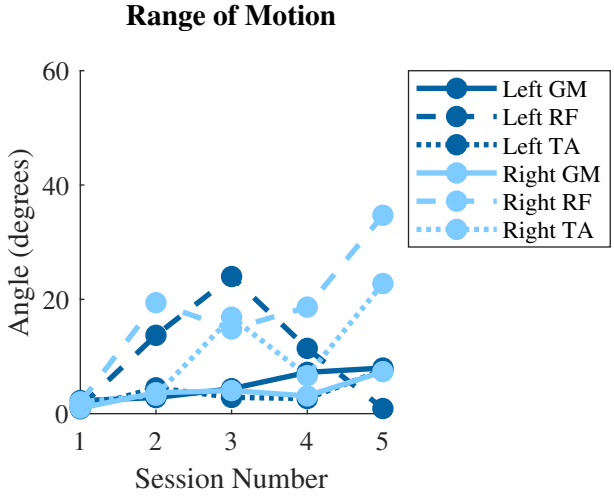

(d) ROM

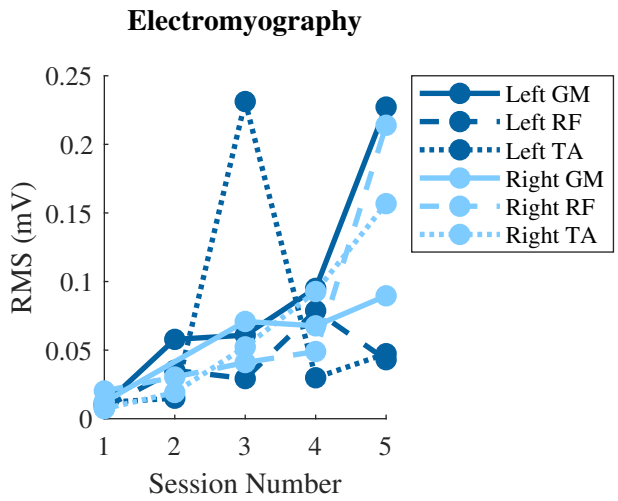

(e) EMG

Figure 6.9: USI measurements and measurements of muscle movement at each session (1-5) for participant 1.

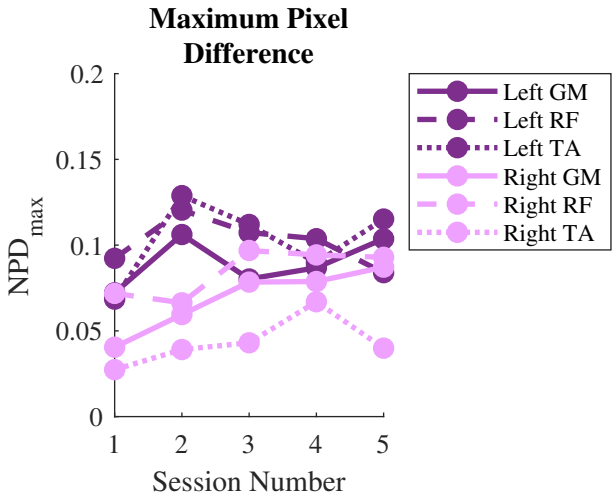

(a) Maximum Pixel Difference

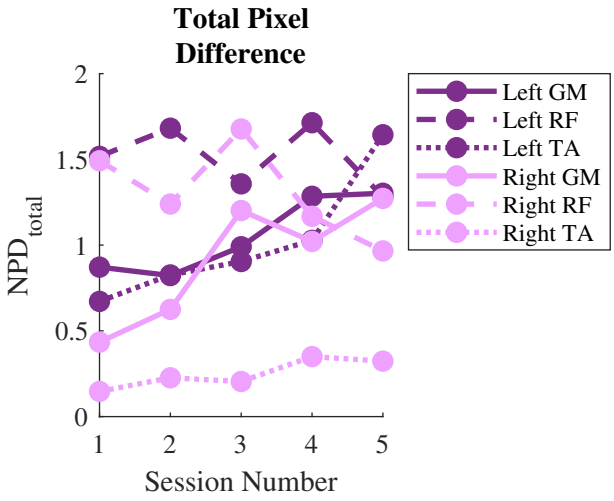

(b) Total Pixel Difference

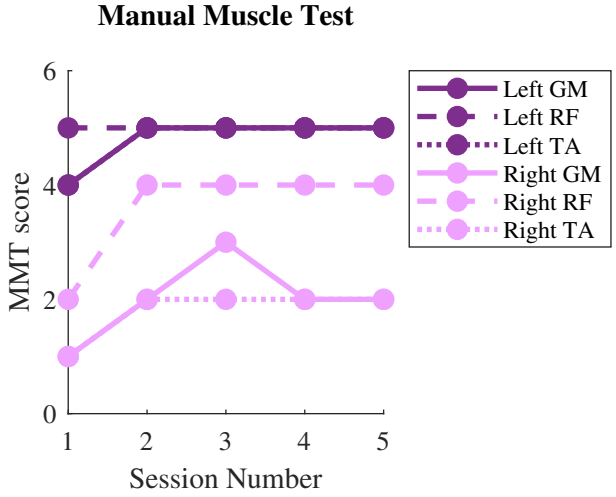

(c) MMT

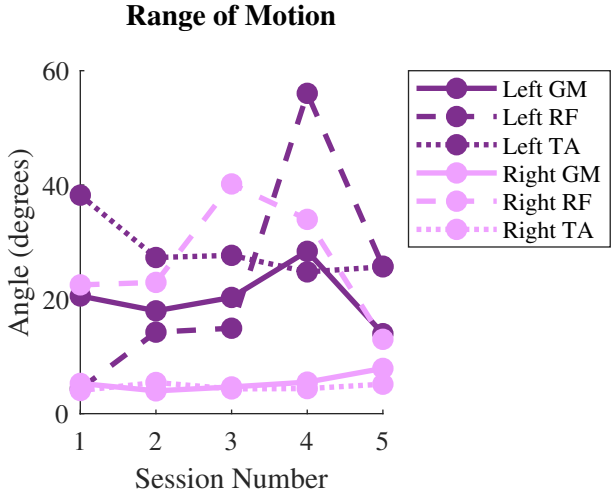

(d) ROM

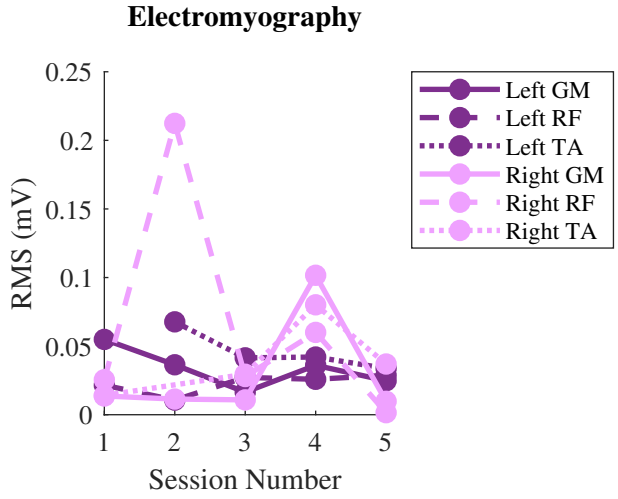

(e) EMG

Figure 6.10: USI measurements and measurements of muscle movement at each session (1-5) for participant 3.

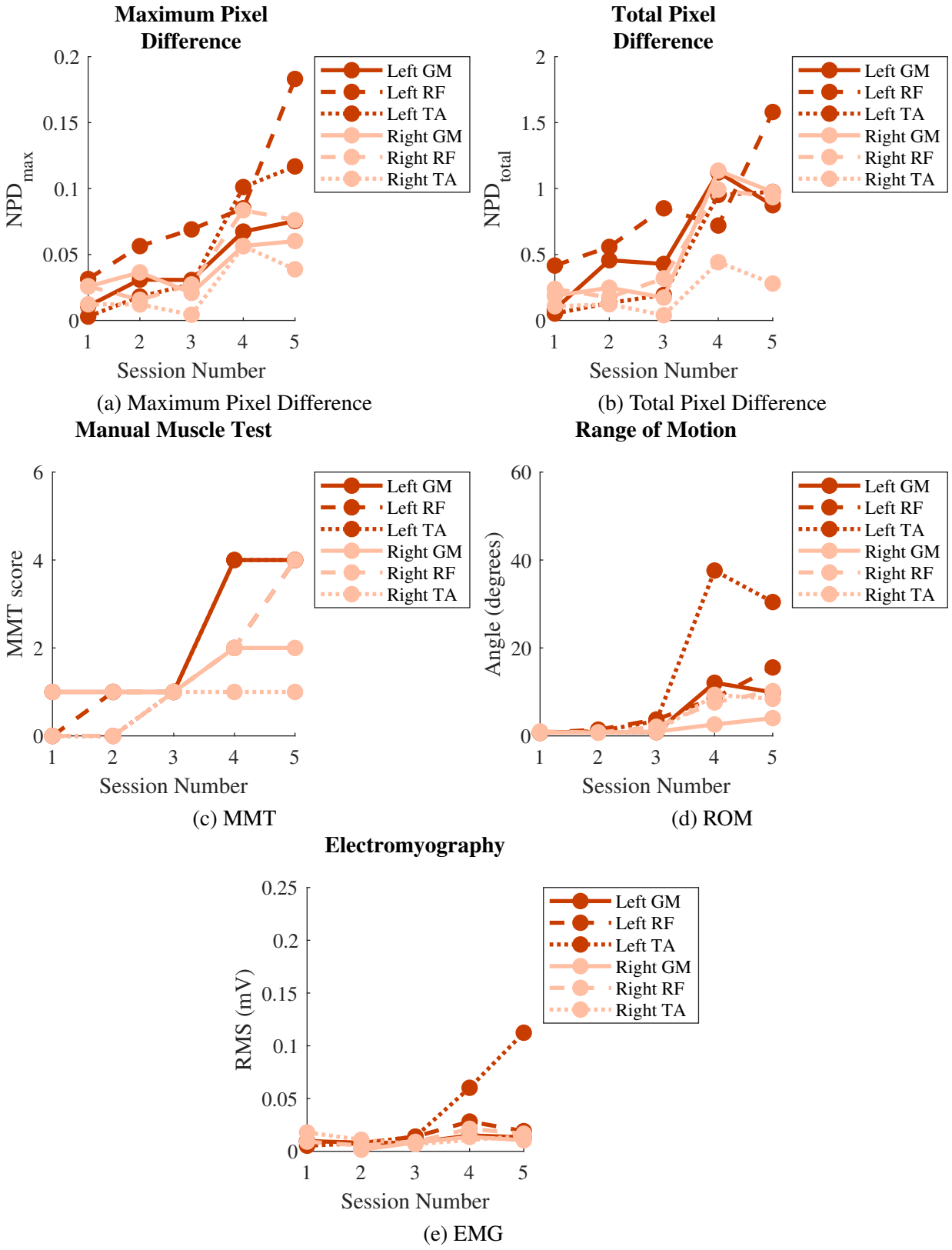

(a) Maximum Pixel Difference

(b) Total Pixel Difference

(c) MMT

(d) ROM

(e) EMG

Figure 6.11: USI measurements and measurements of muscle movement at each session (1-5) for participant 4.

6.4.2.3 Changes in MMT score

Figures 6.12 and 6.13 show the maximum and total pixel difference respectively for each session where each individual muscle is grouped according to the change in MMT score between session 1 and session 5, regardless of participant. It can be clearly seen that muscles which did not improve show very little change in muscle movement based on USI measurements (Figures 6.12a and 6.13a). In contrast muscles which showed an improvement in their MMT score showed an improvement in the USI measurements. Furthermore, the bigger the change in MMT score, the bigger the change in USI measurements of muscle movement.

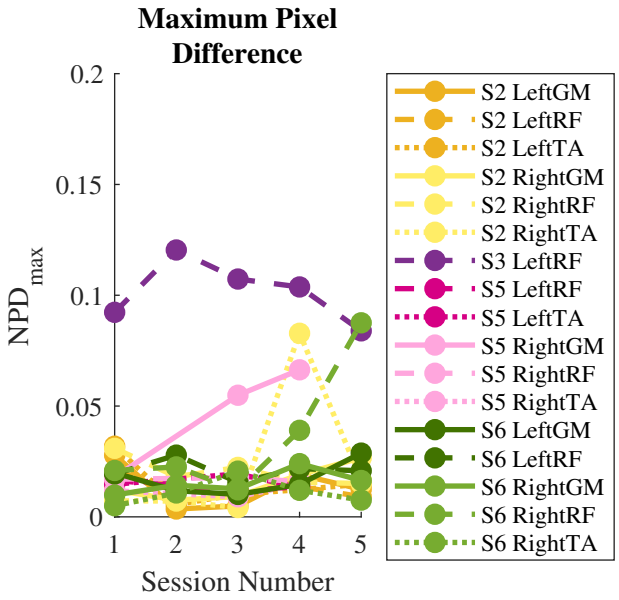

(a) Change in MMT = 0

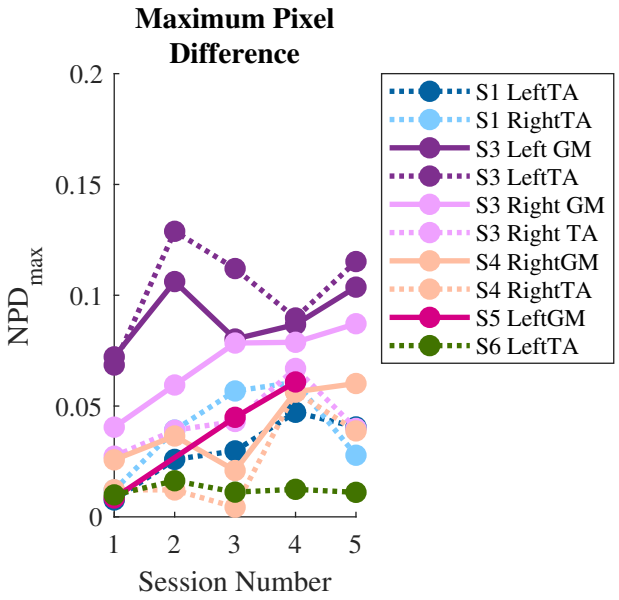

(b) Change in MMT = +1

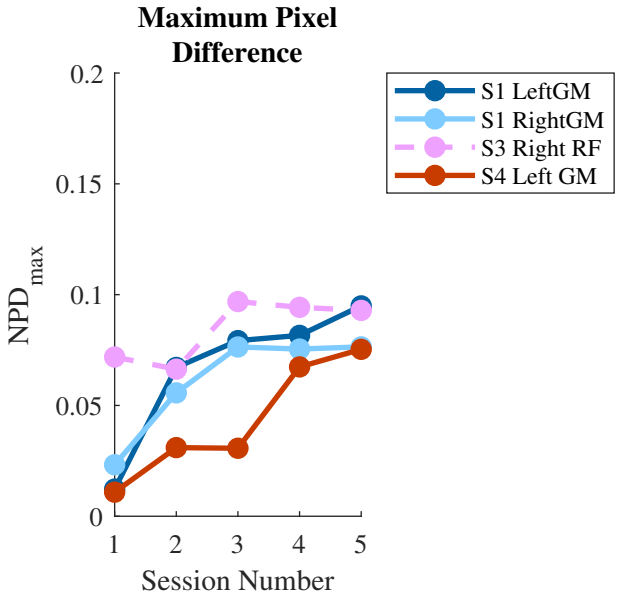

(c) Change in MMT = +2/+3

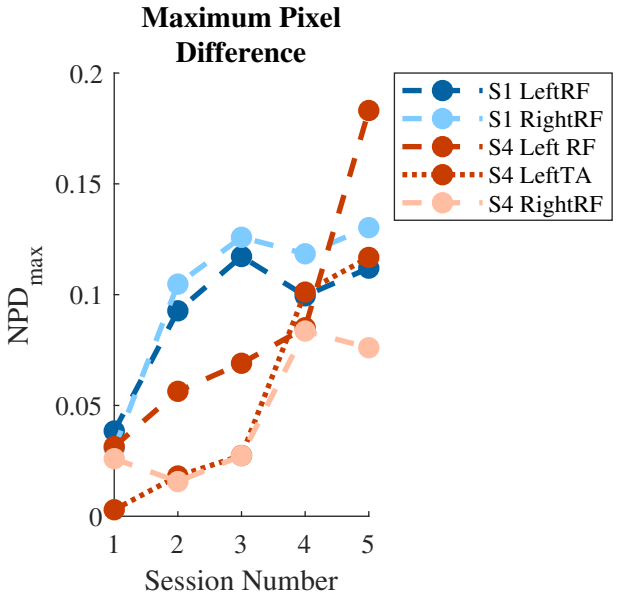

(d) Change in MMT = +4/5

Figure 6.12: Maximum pixel difference at each session (1-5) for different levels of recovery.

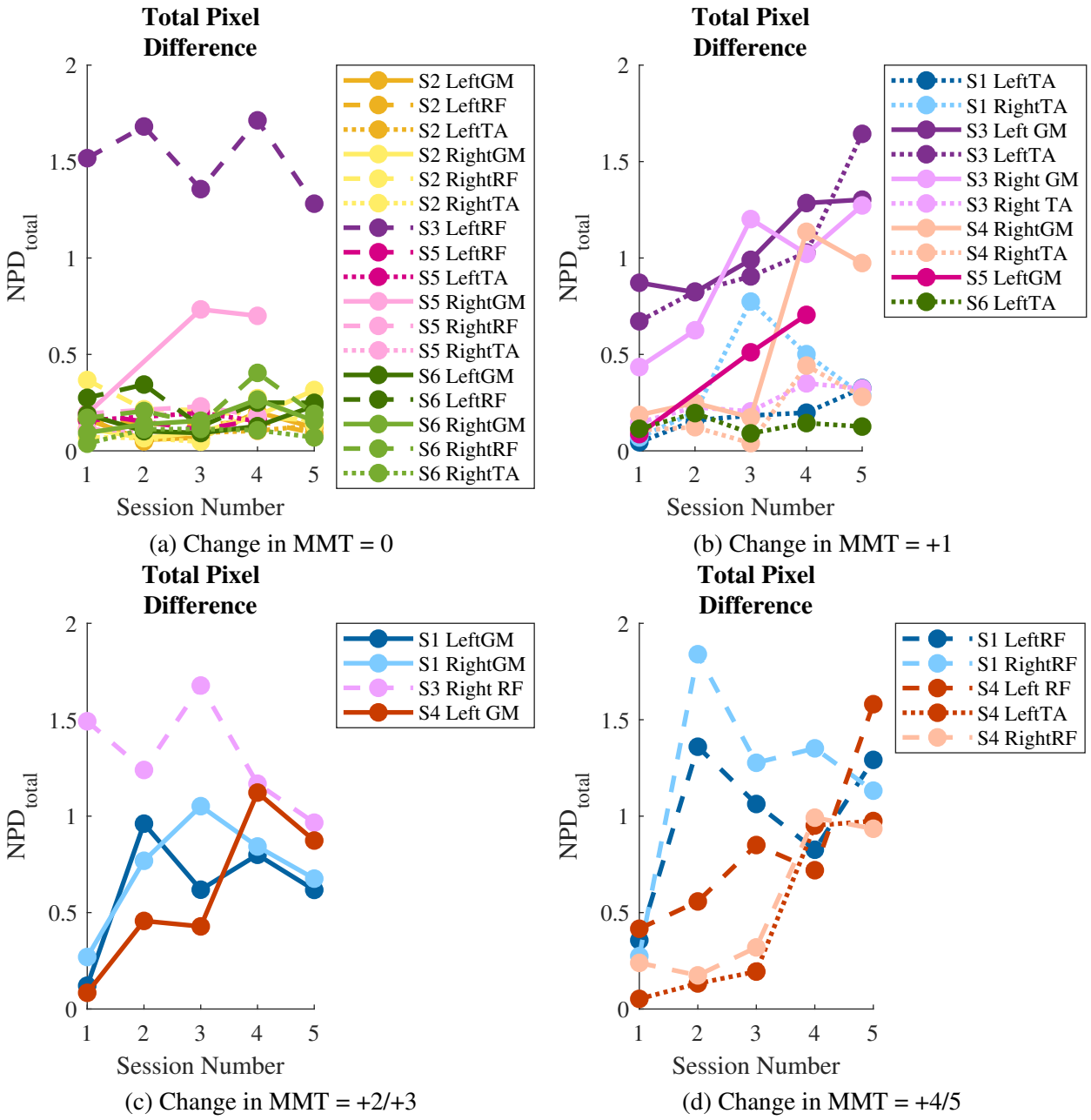

(a) Change in MMT = 0

(b) Change in MMT = +1

(c) Change in MMT = +2/+3

(d) Change in MMT = +4/5

Figure 6.13: Total pixel difference at each session (1-5) for different levels of recovery.

6.4.2.4 Group results for changes over time

Figures 6.14 and 6.15 show the change in USI measurements and other measures of muscle function respectively between session 1 and session 5. P-values and effect sizes for changes in all measures of muscle function are given in Table 6.1. For both the maximum (Figure 6.14a) and total (Figure 6.14b) pixel difference, only the group with no change in MMT scores show no significant difference from a value of zero, suggesting no change in muscle movement. Muscles with a change in MMT score show a positive change, suggesting that these measurements of muscle movement increase between session 1 and session 5.

Moreover, there are large to very large effect sizes between each group of muscles with different changes in MMT scores. These differences also reach statistical significance except between a small (1-2) and large (3+) change for total pixel difference.

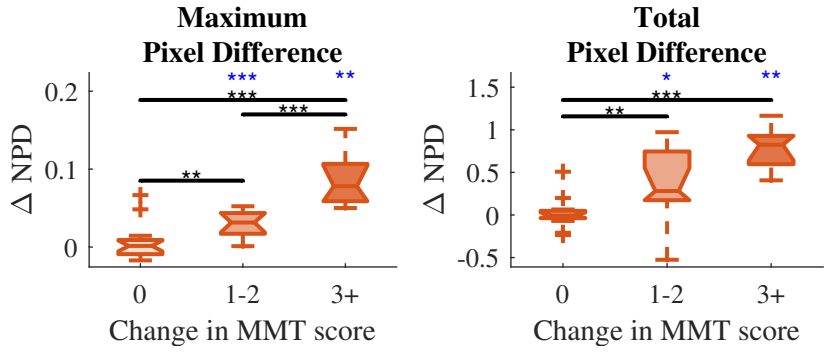

(a) Max Pixel Difference (b) Total Pixel Difference

Figure 6.14: Boxplots of the difference between session 1 and session 5 for USI measurements ($*-p<0.05, **-p<0.01, ***-p<0.001$. The black colour represents a significant difference between two groups and the blue colour represents a significant difference between a group and 0).

Other measures of muscle function also show a significant difference from zero for groups which showed an improvement in MMT score, however they do not appear as effective at differentiating between groups as effect sizes are smaller. ROM (Figure 6.15a) only shows a significant difference between groups with no improvement and an improvement of more than 3.

EMG (Figure 6.15b) also shows a significant difference between those who showed a small (1-2) and large (3+) improvement in MMT score but not between those who did not recover at all and those who recovered only a small amount (1-2).

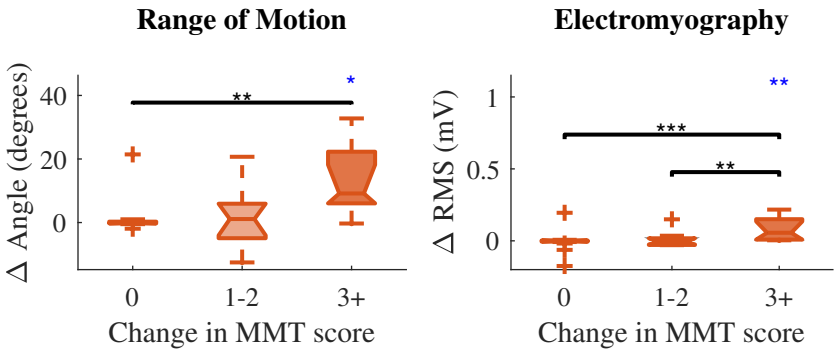

(a) ROM (b) EMG

Figure 6.15: Boxplots of the difference between session 1 and session 5 for measurements of muscle function ($*-p<0.05, **-p<0.01, ***-p<0.001$. The black colour represents a significant difference between two groups and the blue colour represents a significant difference between a group and 0).

Table 6.1: P-values and effect sizes for changes in all measurements of muscle movement between session 1 and session 5. Values indicating a significant difference or a greater than medium effect size are shown in bold.

Maximum pixel difference					
	P-value	*Effect Size*		*P-value*	*Effect Size*
0	0.76	0.24	*0 vs. 1-2*	**0.003**	**1.05**
1-2	**<0.001**	**1.84**	*0 vs. 3+*	**0.002**	**1.74**
3+	**0.01**	**2.51**	*1-2 vs. 3+*	**<0.001**	**1.50**
Total pixel difference					
	P-value	Effect Size		P-value	Effect Size
0	0.98	0.10	0 vs. 1-2	**0.004**	**1.03**
1-2	**0.02**	**0.84**	0 vs. 3+	**<0.001**	**1.87**
3+	**0.01**	**3.18**	1-2 vs. 3+	0.03	**1.01**
ROM					
	P-value	*Effect Size*		*P-value*	*Effect Size*
0	0.69	0.22	*0 vs. 1-2*	0.24	0.01
1-2	0.66	0.14	*0 vs. 3+*	**0.005**	**1.27**
3+	**0.02**	**1.14**	*1-2 vs. 3+*	0.03	**1.04**
EMG					
	P-value	*Effect Size*		*P-value*	*Effect Size*
0	0.55	0.05	*0 vs. 1-2*	0.60	0.66
1-2	0.46	0.43	*0 vs. 3+*	**<0.001**	**1.03**
3+	**0.01**	**0.96**	*1-2 vs. 3+*	**0.01**	0.66

6.4.3 Prediction of recovery

The results presented in this section demonstrate the suitability of USI to show recovery earlier than conventional methods. First, USI measurements obtained during Study 1 are compared between participants who did and did not show recovery. Unlike in the previous section, only USI measurements obtained during the first session are compared, to identify which measurements of structure and function indicate improvements. Second, USI measurements obtained during Study 2 are presented for individual participants. Measurements of pixel difference and the corresponding MMT score are compared for individual participants at each session, demonstrating the timing of when improvements are seen for both methods.

6.4.3.1 USI measurements obtained during Study 1 to predict recovery

The only measurement of muscle structure which shows a significant difference between participants who went on to show recovery and those who did not is the resting thickness, shown in Figure 6.16. Furthermore, the difference between the two groups reaches statistical significance ($p = 0.04$) and shows a large effect size ($d = 1.10$). Measurements of muscle echogenicity and echotexture during the first session for participants who did and did not recover can be found in Figures 48 - 51 in Appendix B.3. The p-values and effect sizes are also shown in Tables 7 - 10.

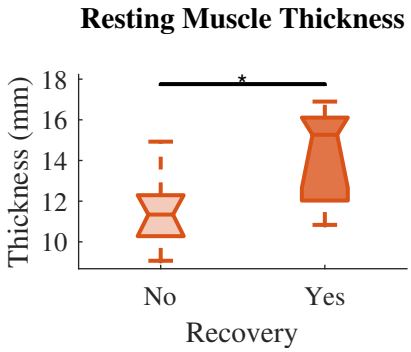

Figure 6.16: Boxplots of muscle thickness on the first session grouped according to whether participants recovered ($* - p < 0.05$).

No measurements of muscle movement show a difference between participants who did and did not recover. Muscle deformation, pixel difference measurements and displacement measurements on the first session are compared between recovery and no recovery groups in Figures 52 - 54 in Appendix B.4, along with p-values and effect sizes in Tables 11 and 12.

6.4.3.2 USI measurements obtained during Study 2 to predict recovery

Figure 6.17 shows the pixel difference during attempted movements of the left TA muscle for two different participants. Participant 2 (Figure 6.17a) shows no increase during attempted movement (highlighted in green) compared to the baseline, indicating no detection of muscle movement. This is to be expected as this muscle had a MMT score of 0. Participant 4 (Figure 6.17b), on the other hand, shows an increase in the pixel difference during attempted movement. These changes cross the threshold (baseline + 3 SDs), indicating the detection of muscle activity, despite also having a MMT score of 0. Participant 2 did not show recovery over the remaining sessions and the MMT score remained 0, however, participant 4 did recover. The MMT score improved to 1 by the third session (2 weeks later), and 4 by session 5.

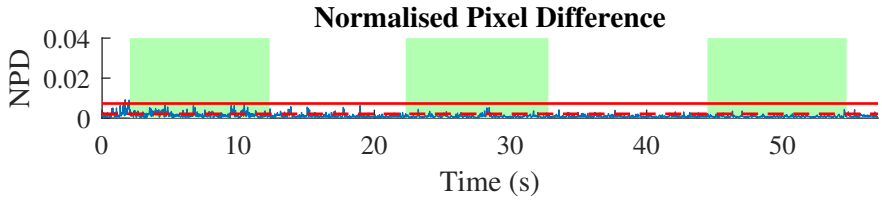

(a) Participant 2

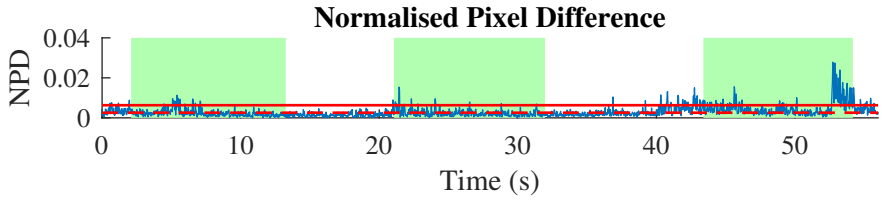

(b) Participant 4

Figure 6.17: Normalised pixel difference plotted over time for the left TA muscle of participants 2 and 4 on session 2.

Figures 6.18 and 6.19 show USI measurements of muscle movement plotted against the MMT score for participants 1 and 4 respectively. The line connecting each point shows the order in which the measurements occurred, demonstrating how the relationship changed over the five sessions. The right and left GM muscles of participant 1 show an increase in USI measurements between sessions 1 and 2. The MMT score is 1 for both these sessions, then improves to 2 on the third session. A similar result is seen for the TA muscles: the right shows an increase in USI measurements between sessions 1 and 2, while the MMT score is 1, and then improves to 2 on the third session; USI measurements of the left TA increase over 3 sessions while the MMT score is 1, which then improves to 2 on the fourth session.

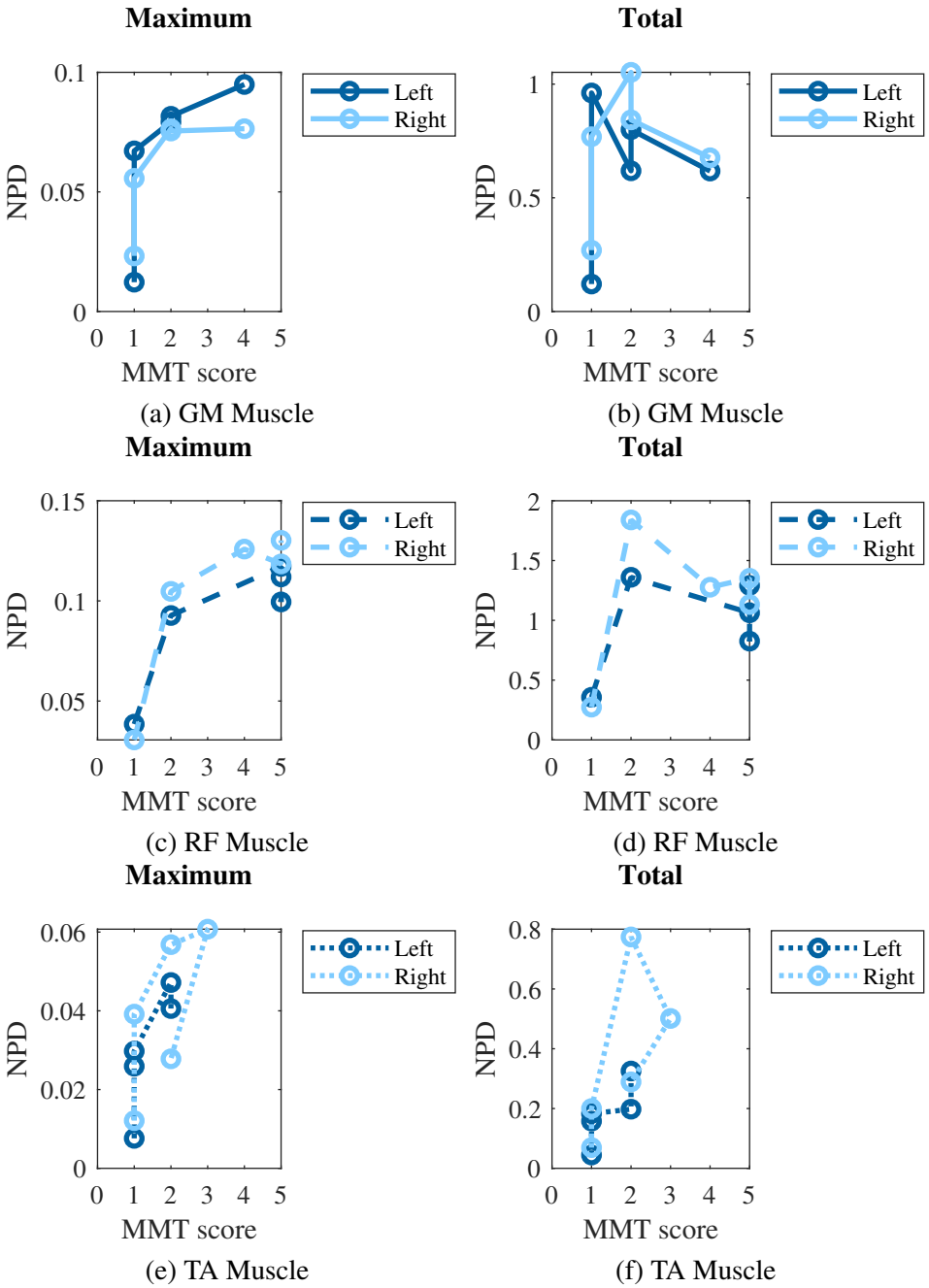

Figure 6.18: Pixel difference measurements vs MMT score for participant 1.

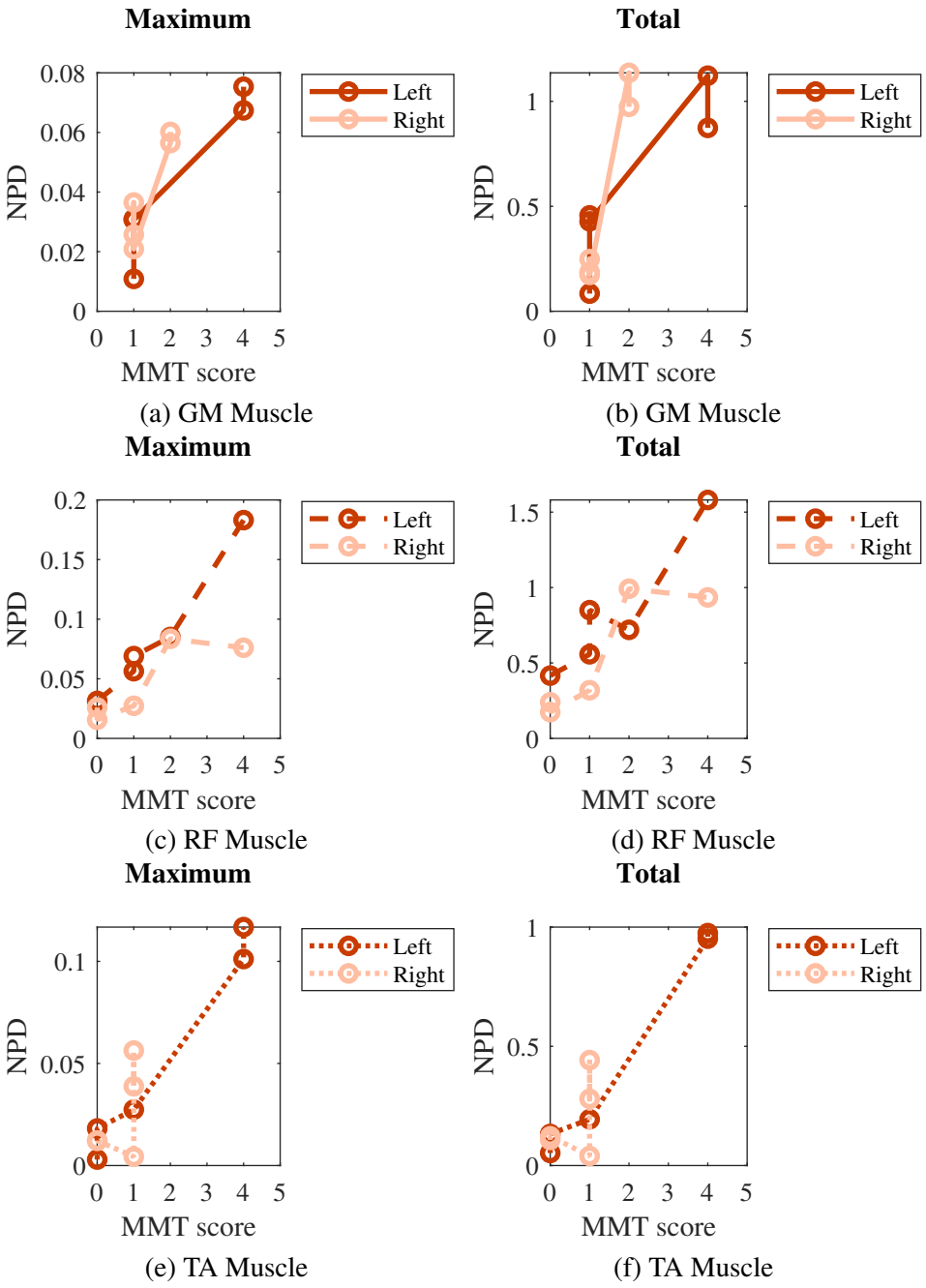

Figure 6.19: Pixel difference measurements vs MMT score for participant 4.

Similar results are also seen for the left GM, RF and TA muscles of participant 4. Out of six participants, participants 1 and 4 were the only ones where a change in USI measurements was seen before an improvement in the MMT score. Participants 2, 5 and 6 did not show any recovery in the USI measurements or MMT scores. Participant 3 recovered relatively quickly, therefore USI measurements of muscle movement were consistent with the MMT scores but did not show improvements any earlier.

6.5 Discussion

Ultrasound videos recorded during two different studies were used to investigate changes in USI measurements over time. Data from Study 1 provided measurements of muscle structure and functional movements during an attempted MVC from the gastrocnemius muscle of 15 SCI participants repeated at monthly intervals between one and eight months post-injury. Data from Study 2 provided measurements of small movements in the gastrocnemius, tibialis anterior and rectus femoris muscles during five sessions over a 12 week period. The changes in these measurements over time along with other measures of muscle function provide an insight into muscle recovery, allowing the suitability of USI as a tool for monitoring recovery to be evaluated.

6.5.1 Ability of USI to detect changes over time to measure recovery

6.5.1.1 Muscle structure

Several measurements of muscle echogenicity and echotexture change between the first and last session, providing an insight into muscle recovery. Although it did not reach statistical significance there is a decrease in skewness seen in participants who did not recover, indicating a histogram which is skewed to the left towards higher greyscale values. As discussed in Chapter 4, this is consistent with an increase proportion of fat and fibrous tissue as a result of muscle atrophy. Variance also decreased in the non-recovery group, consistent with a breakdown in muscle structure causing pixel greyscale values to become more uniform. LBP energy increases and entropy decreases in the group showing no recovery, also suggesting an increase in homogeneity. These changes between sessions are not seen for the group of participants who did recover, suggesting atrophy progresses more in participants who did not recover.

Haralick features show a decrease in contrast and correlation in the no recovery group. Meanwhile, energy and homogeneity are seen to increase, all of which are consistent with the muscle becoming more homogeneous as a result of structural changes in the muscle. In contrast, entropy increases in the recovery group, indicating that pixels are more random and therefore less homogeneous. It should also be considered that homogeneity and contrast (45°) show the same change in both the recovery and non-recovery groups, suggesting that these changes may happen over time following a SCI regardless of recovery.

The Galloway features show that GLNU and RP decrease in the no recovery group, suggesting homogeneity increases in terms of coarseness. However, both measurements also decrease in the recovery group in the 45° direction. RLNU also increases in both recovery and non-recovery groups, again suggesting this change occurs regardless of recovery.

These changes in measurements of echogenicity and echotexture suggest that the effects of atrophy are greater in participants who did not recover, while the effects were lessened in those who did recover. Despite this, there are several measurements which did not show any differences, or showed differences in both groups of participants. As all participants were still

wheelchair users by the last session, there may be changes in greyscale values as a result of atrophy even for those participants who showed an increase in torque.

Changes in resting muscle thickness did not show a difference between the first and last session for either group. As previously discussed in Chapter 4, the decrease in muscle thickness as a result of atrophy appears to happen rapidly within the first month after injury. Therefore the measurement on the first session may be too late to see this change. Furthermore, infiltration of fat will also have an effect on muscle thickness.

6.5.1.2 Muscle movement

USI measurements of small muscle movements during attempted isotonic movements in the acute stage of SCI showed no movement and no change between sessions for muscles which showed no muscle movement or recovery based on MMT scores. In contrast, muscles which showed improved MMT scores over the sessions showed an increase in USI measurements. Furthermore, the bigger the recovery, the bigger the increase in USI measurements, suggesting that not only can USI detect changes indicating recovery, but it can also quantify the amount of recovery. This is clearly seen when individual muscles are grouped according to the amount of recovery (Figures 6.12 and 6.13).

The two exceptions to this pattern are seen for Participant 6. USI measurements show an increase in muscle movement in the right RF muscle, however, the MMT score remains to be 0. As this increase occurred on the final session, it is unclear if this is a real movement which is too small to be detected by manual muscle testing, or if the ultrasound is detecting movement which is not coming from this muscle. In contrast, USI does not detect any muscle movement in the right TA muscle despite the MMT score improving from 0 to 1 between the fourth and fifth session. In this case it appears the USI measurements were not sensitive enough to detect this movement, however it is also possible that the MMT score is a mistake as it can be difficult to differentiate between different muscles when movements are so small and the movement is only palpable and not visible.

Despite this, individual results appear to demonstrate the suitability of USI to detect small muscle movements in line with recovery. When grouping all muscles according to recovery, there is no difference in USI measurements seen between the first and last session when there is no change in MMT score, but an increase when the MMT score improves. The increase in USI measurements also increases further when the change in MMT score is large. There are significant differences between the three groups, further indicating that USI is able to differentiate between different levels of recovery. Moreover the other measurements of muscle function (ROM and EMG) do not appear to be as effective at differentiating between different MMT scores, with MMT scores improving by at least 3 before an increase is seen between the first and last session. There is also no significant difference between a small improvement in MMT score by 1-2 and no improvement at all.

Other USI measurements of muscle movement during attempted isometric MVC also show some differences between participants who did and did not recover. The total pixel difference, the maximum displacement (rows 5 and 10) and the total displacement (row 10) all show an increase in movement in the recovery group. There is also an increase in the speed of the muscle contraction during the ramp phase (displacement row 1, row 10, column 1, column 4) in the recovery group, and a decrease in speed during the constant phase (displacement row 5 and column 8), all of which are consistent with increased movement as a result of recovery. It should be noted however that these differences did not reach statistical significance.

Muscle deformation does not show any difference between the first and last session. As discussed in Chapter 5 measurements may be affected by the GM muscle being compressed by surrounding muscles.

6.5.2 Potential of USI measurements to predict recovery

Figures 6.18 and 6.19 show the USI measures plotted against MMT scores for Participant 1 and Participant 4. This showed improvements in the USI measurements while the MMT score remained unchanged, and then further improvements in the MMT score in subsequent sessions. This supports the idea that USI could show improvements in muscle movement before it is seen in the MMT score. This is particularly significant for the left TA muscle of Participant 4 which shows improvements in USI measurements while the MMT score was 0. This suggests that USI is capable of detecting muscle movements which are too small to be detected by MMT and therefore provide an indication of recovery at an earlier point in time.

The resting muscle thickness on the first session also showed a significant difference between participants who went on to show recovery and those who did not. This indicates that early USI measurements of thickness may be able to show signs of recovery earlier and in effect predict how much muscles will recover.

6.5.3 Limitations and considerations

6.5.3.1 Limitations of USI technique

One of the main limitations of ultrasound imaging in general compared to other techniques such as EMG is that it does not distinguish between active and passive movements. This means that the USI measurements of muscle movement could be a result of other muscles contracting and passively moving the muscle of interest, without the muscle itself contracting. The effects of this are limited by choosing positions and specifying movements which isolate the muscle as much as possible, however it can still make it more difficult to determine exactly where the movement is coming from and should be kept in mind.

Movement of the ultrasound probe itself could also introduce a source of movement. In Study 1 this was minimised by the use of a custom bracket which was secured around the

leg with a Velcro strap. However, in Study 2 this was not possible and the ultrasound probe was held by hand. This is not likely to produce false detections, however, it produces more baseline movement. The pixel difference method calculates movement based on changes in pixel greyscale values between frames, therefore any small flickers in the image or small movements from the pulsation of blood vessels produce baseline noise. If the ultrasound probe is not held perfectly still then this baseline fluctuation will be bigger and make it more difficult to detect very small movements.

Another source of noise to consider when using USI to detect movement in SCI patients is spasms. These involuntary movements cannot be differentiated from intentional attempts to perform the movement. In most cases, participants are aware that they are experiencing a spasm and movements will also be detected when the muscle should be at rest, however it is worth noticing that ultrasound videos recorded during a spasm may not be useful for detecting movements.

6.5.3.2 Different USI measurements

Different USI parameters provide different information about the muscles. The pixel difference method is used for Study 2, providing information on movement at the pixel level for the whole muscle. The maximum pixel difference provides a measurement of the biggest difference between two frames. This method should be sensitive enough to pick up small movements, however, it may also pick up one single spike which is misleading to the size of the overall movement. The total pixel difference is the summation of all changes in pixel difference during the contraction, providing a more complete measurement of the muscle movement. This may explain why an increase was seen in the recovery group between the first and last session for the total pixel difference but not the maximum value.

The limitation of the total pixel difference is that when participants are able to produce a movement easily, this produces a large peak in the pixel difference when the muscle initially contracts, and then another peak when the muscle relaxes, with the time in between showing little movement and low values of pixel difference. In contrast when a participant is struggling to produce a movement, they may produce smaller peaks but they will also move more in between in an attempt to maintain the contraction. Depending on the level of muscle movement they are able to produce, the summation can result in a higher value than someone who easily performs the movement. This may explain why the total pixel difference is seen to decrease between later sessions when the muscle has reached a higher MMT score.

Displacement also measures movement within the muscle however it is based on the tracking of features in the ultrasound image and it provides information on different regions within the muscle. It appears to be more successful than the pixel difference as changes are seen for maximum, total and speed calculations based on displacement. However, these changes are only seen for certain positions.

6.5.3.3 Differences between Study 1 and Study 2

Although the statistical analysis is limited for data from Study 2 due to the small number of participants, it appears to show more differences between participants who recovered and those who did not. Changes between the first and last session showed statistically significant differences between groups with different levels of recovery, however no significant differences were found between groups for measurements obtained from data in Study 1. There are a number of factors which could contribute to this:

1. Type of contraction: Participants in Study 1 were asked to perform isometric MVC whereas participants in Study 2 were asked to perform isotonic contractions. As by definition, the muscle tendon complex does not change in length to bring about joint movement during an isometric contraction, muscle movement may be much smaller than during an isotonic contraction even when the muscle is activated. Isotonic contractions may therefore be more effective when using USI to detect muscle movement.

2. Measurement of muscle function: Study 1 used torque recorded from the dynamometer as the main measurement of muscle function for comparison with USI measurements. Study 2 used MMT scores performed by a trained physiotherapist. MMT score may be a more accurate measurement of muscle movement than torque, or could be more representative of the USI measurements of muscle movement.

3. Time post-injury: There was no restriction on the time post-injury for recruiting participants in Study 1. Once recruited, participants completed sessions on a monthly basis until they were discharged, providing data over a range of 4 to 33 weeks post-injury. Participants in Study 2, on the other hand, were recruited within the first month following an injury and completed five sessions over a 12 week period. This means that for Study 1 the changes between the first and last session were not only happening at different times post-injury for different participants, but the length of time between the first and last session was also variable. Furthermore, participants in Study 1 were usually recruited later than 1 month post-injury, so recovery is often being evaluated in the more chronic phase while Study 2 provides measurements in the acute phase.

6.5.3.4 Different muscles

Another factor which should be considered is the effect of different muscles. Due to the small number of participants in Study 2 and the wide range of recovery seen in the different muscles, it is difficult to understand the effect of different muscle types. The pixel difference values used throughout this thesis are normalised based on the number of pixels in the selected ROI, this should therefore correct for the differences in size between different muscles. There are however other factors to consider, such as the alignment of fibres in different types of muscles.

The three muscles investigated in Study 2 are the gastrocnemius (GM), tibialis anterior (TA) and rectus femoris (RF). All three muscles are pennate muscles, meaning their muscle fibres are arranged at an angle to the long axis of the muscle. All muscles are bipennate, meaning the fibres extend on both sides of the tendon, however the angle of the fibres could be different. Different arrangements of muscle fibres along with varying compositions of tendons and connective tissue in specific muscles will result in differences in the echo intensity of ultrasound images. As the pixel difference is based on changes in pixel greyscale values, different muscle types should be considered when using this USI technique to measure muscle movement.

6.6 Conclusion

Overall, USI shows potential as a tool for measuring recovery of muscle movement following a SCI. Measurements of muscle movement based on pixel difference appear to be capable of detecting different levels of muscle movement during attempted isotonic movements consistent with MMT scores. Furthermore, USI may even show muscle movements which are too small to be detected during manual muscle testing, and show improvements before this is reflected in the MMT score. Although these results show great potential, further research should be performed with a larger sample size. Other measurements of muscle movement through pixel difference and displacement during attempted isometric MVC also show improvements consistent with the muscle's ability to produce torque. Measurements of echogenicity and echotexture also suggest that the results of atrophy were lessened in participants who demonstrated substantial recovery, however, initial measurements may not have been taken early enough to completely understand the effects of recovery on muscle structure. Results from Study 2 provided better results, suggesting that USI analysis is more successful in measuring or predicting recovery when the initial measurements are obtained during the acute phase.

Chapter 7

Evaluation of Neuromuscular Electrical Stimulation

7.1 Summary

This chapter investigates the suitability of ultrasound imaging (USI) to describe muscle behaviour during the application of neuromuscular electrical stimulation (NMES). Tracking software is used to describe the changes in muscle thickness and regional displacement, and the pixel difference method is used to describe movement within the muscle under different conditions. These measurements are compared between different stimulation parameters as well as different patterns of stimulation, including variations in stimulation parameters (variable frequency and variable pulsewidth patterns) and different electrode configurations. Electrical stimulation of healthy muscles and those affected by a SCI are also compared. The suitability of USI to show differences in muscle behaviour under these different conditions is discussed, demonstrating its potential to improve the use of NMES in rehabilitation. This chapter includes work that has been presented at the 21st IFESS Conference (London,UK) and the 22nd IFESS Conference (Nottwil, Switzerland). It has also been published in the *Journal of Rehabilitation and Assistive Technologies Engineering* (see Publications section for full details).

7.2 Introduction

Injury to the spinal cord often results in muscle paralysis, which can be extremely debilitating and prevent people from performing the most basic of everyday tasks. A rehabilitation technique commonly used in these circumstances is NMES, which involves the application of low amplitude current to elicit an artificial muscle contraction by exciting the innervating nerves.

NMES is used in a wide variety of ways to assist in the rehabilitation of paralysed muscles. It can be used in conjunction with cycling and rowing machines to allow exercise, improving muscle strength and overall cardiopulmonary function. It can also be used to produce functional

movements by controlling the timing and order of stimulation of specific muscles, for example in the use of wrist orthroses to produce grasping movements, ankle orthroses to correct foot drop and larger arrays of electrodes to assist in stepping movements and gait correction [31, 32, 36].

Despite the wide range of applications of NMES, its use is limited due to the early onset of muscle fatigue, attributed to differences in muscle fibre recruitment compared to voluntary contractions. During voluntary muscle contractions the size principle dictates smaller more fatigue resistant motor units are recruited first. In contrast, it is widely accepted that NMES-induced contractions do not follow this convention and is thought to be a non-selective process where both large and small motor units are recruited randomly. Premature fatigue could also be attributed to the same muscle fibres being repeatedly recruited, unlike during voluntary contractions where asynchronous activation of varied muscle fibres allows replacement of fatigued fibres. Furthermore, surface electrical stimulation is also limited by the depth of penetration as the current must travel through subcutaneous tissue [13, 31, 32, 36].

Several studies have made efforts to optimise stimulation and reduce the effects of muscle fatigue. This has included modulation of stimulation parameters (current, pulsewidth, frequency), electrode placement, variable frequency pulse patterns and spatial distribution patterns with multi-electrode configurations [36, 180, 225, 226].

Despite these improvements, the exact mechanisms of motor unit recruitment during electrical stimulation are still unclear. Furthermore, previous studies investigating the effect of stimulation parameters and patterns on muscle fatigue [36, 180, 225, 226] focus on the torque produced as the main outcome measurement. Similarly, a study by Han et al. [227] investigated the effect different combinations of stimulation parameters had on the force exerted by the muscle.

Ultrasound imaging (USI) is a potential tool to provide additional information regarding muscle behaviour during the application of electrical stimulation. As discussed in previous chapters of this thesis, USI has been shown to be capable of making accurate measurements of muscle activity through changes in muscle architecture [103, 112]. Information on how stimulation affects muscle architecture and therefore movement could provide further details on the recruitment of muscle fibres and overall muscle behaviour during electrical stimulation. This could in turn facilitate the optimisation of electrical stimulation parameters, reduce the effects of muscle fatigue and improve the overall effectiveness of NMES protocols in rehabilitation.

In this chapter, data from three different studies are used. Study 3A provides US videos of the gastrocnemius muscle during the application of different combinations of stimulation parameters, while Study 3B provides US videos recorded during different multi-electrode patterns of electrical stimulation. Finally, Study 1 provides US videos of NMES-induced contractions for able-bodied participants and SCI participants. Measurements of muscle movement were obtained from tracking software (described in Section 3.8 of Chapter 3), and the pixel difference method developed within our lab group [8] (discussed in Section 5.3.3 of Chapter 5).

The aim of this investigation was to demonstrate the potential of USI to gain greater insight

into the behaviour of muscles during the application of NMES under different conditions. Four aspects of NMES were investigated:

- The effect of different stimulation parameters: current, pulsewidth and inter-pulse interval.
- The effect of stimulation patterns where parameters were varied (variable pulsewidth and variable inter-pulse interval).
- The effect of different multi-electrode patterns of stimulation: conventional synchronous stimulation, asynchronous sequential stimulation and asynchronous random stimulation.
- The differences between the behaviour of muscles of able-bodied participants and those affected by a SCI.

7.3 Methods

7.3.1 Overview of data used

In this chapter, data obtained during three different studies is used to compare USI measurements during the application of NMES under different conditions. The data from Study 3A is used to compare different combinations of stimulation parameters, including measurements of muscle deformation and displacement calculated from the output of the tracking software. Data from Study 3B is used to compare different multi-electrode patterns of stimulation. Deformation is calculated from the tracking software output, however due to the fast nature of the contraction (300ms stimulation duration) and the relatively low frame rate (20 fps), measurements of movement within the muscle are based on changes in pixel greyscale values instead of the output from the tracking software. Finally, data from Study 1 is used to compare the application of electrical stimulation between able-bodied and SCI participants. This includes measurements obtained from tracking software and pixel difference methods. Torque data from Study 3B and Study 1 is also used to measure the effectiveness of the stimulation.

7.3.2 USI measurements

1. Muscle deformation

   Muscle deformation is the change in muscle thickness as a percentage of the resting thickness, calculated using equation 5.1 (see Section 5.3.2.1 of Chapter 5). For further details on how the tracking software is used to perform automatic segmentation to separate the aponeuroses from the muscle tissue, see Section 3.8.1.1 of Chapter 3.

2. Amplitude of movement within the muscle

   There are two methods used for calculating movement within the muscle:

(a) Displacement

Displacement is the distance travelled by a matrix of measurement probes placed across the muscle by tracking software. It is calculated from the x and y components of each probe between adjacent frames using equation 5.2 (see Section 5.3.2.2 of Chapter 5). Further details on how features are identified and tracked between frames, and how the use of measurements probes quantitatively describes regional movement, are provided in Section 3.8.1.2 of Chapter 3.

(b) Pixel difference

The pixel difference method measures muscle movement through changes in the greyscale values of corresponding pixels between adjacent frames. The summation of these changes for all pixels within a given region of interest (ROI), normalised with respect to the number of pixels within the ROI, is known as the normalised pixel difference (NPD), as described in equation 5.5 (see Section 5.3.3.2 of Chapter 5). The extraction of pixel greyscale values from an ultrasound image is described in Section 4.3.4.1 of Chapter 4, and further details on the use of the pixel difference method for measuring muscle movement can be found in Section 5.3.3 of Chapter 5.

For both displacement and pixel difference, the maximum value can be used to find the biggest difference between two adjacent frames, or the summation of these differences can be used to find the total movement within a certain time period. In this study the total muscle movement is calculated for the following phases of the muscle contraction:

- Ramp up phase: stimulation is increasing to its maximum intensity (2.5 s).
- Constant phase: stimulation remains constant at its maximum intensity (5 s).
- Ramp down phase: stimulation is decreasing from its maximum intensity to zero (2.5 s).

3. Timing of movement within the muscle

These calculations describe the timing of the muscle contracting and relaxing, as illustrated in Figure 7.1. In this study they are used to describe very short contractions (<1s) with different patterns of stimulation in Study 3B.

(a) Contraction time

The contraction time (t_{con}) is the time between the onset of the stimulation and the measurement of muscle movement reaching its peak value.

(b) Half-relaxation time

Half-relaxation time ($t_{half-relax}$) is the time taken for the measurement of muscle movement to decay from the peak value to 50% of this value.

(c) Peak-to-peak time

The peak-to-peak time ($t_{peak-to-peak}$) is the time between the peak which occurs when the muscle initially contracts and the second peak which occurs when the stimulation is switched off and the muscle relaxes.

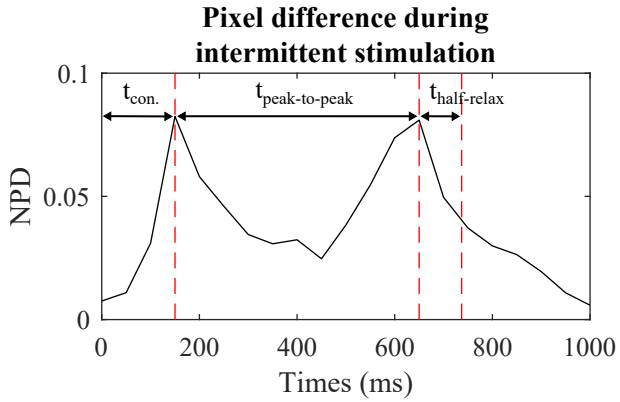

Figure 7.1: An example of the pixel difference for one contraction during intermittent stimulation (stimulation duration of 300 ms), illustrating the contraction time ($t_{con.}$), the half-relaxation time ($t_{half-relax}$), and the peak-to-peak time ($t_{peak-to-peak}$).

4. Speed of muscle contraction

The summation of muscle movement, measured by displacement or pixel difference, is used to calculate the average speed, of a muscle contraction during a particular time period, using equations 5.3 and 5.6 respectively (see Sections 5.3.2.2 and 5.3.3.3 of Chapter 5).

In this study, the average speed was calculated for the following phases of the muscle contraction:

- Ramp up phase: stimulation is increasing to its maximum intensity (2.5 s).
- Constant phase: stimulation remains constant at its maximum intensity (5 s).
- Ramp down phase: stimulation is decreasing from its maximum intensity to zero (2.5 s).

7.3.3 Torque measurements

Ankle torque is recorded as described in Section 3.2.2.3 of Chapter 3. It provides a measurement of the amount of force generated by the muscle.

1. Twitch-tetanus ratio

The twitch-tetanus ratio (TwT) is a ratio of the torque produced during a single pulse of stimulation, eliciting a twitch in the muscle, and a train of stimulation eliciting a fused

tetanic contraction. An illustration of the stimulation applied and the torque produced during the twitch-tetanus ratio is shown in Section 3.3.4.3 of Chapter 3.

$$TwT = \frac{T_{twitch}}{T_{tetanus}}, \tag{7.1}$$

where T_{twitch} and $T_{tetanus}$ are the torque values produced during a twitch and tetanic contraction respectively. This is calculated for the torque data obtained during Study 1 at frequencies of 20Hz (TwT_{20}) and 80Hz (TwT_{80}).

2. Twitch contraction time

   The twitch contraction time (t_{twitch}) is the time between the onset of the stimulation and the torque reaching its peak value.

3. Twitch half-relaxation time

   The half-relaxation time ($t_{0.5twitch}$) is the time taken for the torque to decay from the peak value to 50% of this value.

4. Stimulation efficiency

   The efficiency (E) of the stimulation is calculated as the ratio of torque (T) produced to current (I).

$$E = T/I \tag{7.2}$$

7.3.4 Selection of stimulation current measurements

For all protocols involving NMES, the optimal current was selected for each individual participant based on the amount of torque produced as the current is gradually increased. The response of the muscle during the current selection process provides information on muscle fibre recruitment during NMES. The results presented in this Chapter are based on the current selection process carried out in Study 1 (see Section 3.3.4.3 of Chapter 3 for details).

1. Threshold value to cause muscle movement

   The lowest value of current to cause a detectable muscle movement is the threshold value (I_{thresh}). The baseline is the mean value during a time period of 5 seconds before any stimulation is applied. The threshold is determined as

$$threshold = baseline + 5 \times SD, \tag{7.3}$$

   where SD is the standard deviation during the same 5 second baseline time period. The current threshold value for a particular measurement is the first value of current which

causes the measurement to exceed this threshold value. The current threshold value is calculated for the following measurements:

- Normalised pixel difference (I_{NPD})
- Displacement ($I_{displacement}$)
- Deformation ($I_{deformation}$)
- Torque (I_{torque})

2. Optimal current value for maximum torque

   The lowest value of current that produces the maximum torque possible with electrical stimulation is deemed the optimal current (I_{op}). Increasing the current beyond this value will not produce a higher torque value and therefore this is the optimum value for an efficient NMES-induced contraction. This is the value of current chosen during each current selection process detailed in the protocols for all studies using electrical stimulation (studies 1, 3A and 3B) in Chapter 3.

7.3.5 Statistical analysis

7.3.5.1 Grouping of data

As described in Section 7.3.1, this chapter analyses data obtained from three different studies. Different combinations of stimulation parameters are compared based on data obtained during Study 3A, with 11 participants resulting in 11 matched data points. Data from this study is also used to compare stimulation patterns based on variable stimulation parameters. Each of the 11 participants received 12 trains of stimulation for each pattern, resulting in 132 matched data points. Spatially distributed patterns of stimulation are compared based on data obtained during study 3B, with data from 8 participants resulting in 8 matched data points. Finally, data obtained from Study 1 is used to compare the behaviour of the muscle during NMES between a group of 15 SCI participants and 15 matched able-bodied controls, resulting in 15 matched data points. An overview of this is provided in Table 7.1.

7.3.5.2 Calculation of statistically significant differences

When the sample size was ten or more, the Shapiro-Wilk test was used to assess the normality of the data as described in Section 3.9.1. When data was found to be normally distributed, a paired t-test was used (see Section 3.9.2.1). When data was not normally distributed or the sample size was less than ten, the non-parametric Wilcoxon signed rank test was used as an alternative (see Section 3.9.2.2).

Both tests were performed using a significance level of p=0.05, however as comparisons were carried out in a pairwise manner this was adjusted using the Bonferroni correction for multiple comparisons, as described in Section 3.9.3. The significance level used in each results section is provided in Table 7.1.

7.3.5.3 Calculation of Cohen's d effect size

Cohen's d effect size was also calculated in line with a paired test using equation 3.6. Further details on Cohen's d effect size and how to interpret it are provided in Section 3.9.4.

Table 7.1: Overview of the data used in each section.

Results section	Study	Number of participants	Number of data points	Number of comparisons	Significance level
7.4.1. Stimulation parameters	Study 3A	11	11	24	0.002
7.4.2. Variable parameters	Study 3A	11	132	6	0.008
7.4.3. Spatial patterns	Study 3B	8	8	9	0.005
7.4.4. Able-bodied vs. SCI	Study 1	15 AB, 15 SCI	15	2	0.05

7.4 Results

In this section, USI measurements of muscle movement during the application of NMES are compared between different conditions. First, different combinations of stimulation parameters are compared, followed by different patterns of stimulation where these parameters are varied with time (Study 3A). Next, comparisons are made between spatially distributed patterns of stimulation through multi-electrode configurations (Study 3B). Finally, muscle behaviour during stimulation is compared between healthy muscles and those affected by a SCI (Study 1).

7.4.1 Comparison of different stimulation parameters

In this section, results are presented based on USI measurements of deformation and displacement obtained during different combinations of stimulation parameters. As discussed in Section 3.5.4.3 of Chapter 3, three different pulsewidth values (PW_1 = 300 μs, PW_2 = 350 μs and PW_3 = 400 μs); two different inter-pulse intervals (IPI_1 = 50 ms and IPI_2 = 25 ms); and two values of current based on each participants minimum (I_{min}, mean value of 25 mA) and maximum (I_{max}, mean value of 30 mA) threshold to produce a contraction are used to deliver stimulation of different intensities. This yields a total of 12 different combinations of stimulation intensity, each of which are compared in this section. An example of the deformation, displacement, and torque during these 12 contractions with different stimulation intensities is shown in Figure 7.2.

During each contraction, regardless of the combination of stimulation parameters, the intensity of the stimulation is gradually increased. The pulsewidth gradually increases from zero to

the chosen value (PW_1, PW_2 or PW_3) over 2.5 seconds (ramp up phase), remains at this value for 5 seconds (constant phase), before decreasing back to zero over 2.5 seconds (ramp down phase). This is illustrated in Figure 7.3, with examples of the deformation, displacement and torque produced during a single contraction. Deformation and torque increase during the ramp up phase and reach a steady value during the constant phase. In contrast, displacement shows peaks during the ramp up and ramp down phases as the muscle contracts and relaxes, with little movement during the constant phase.

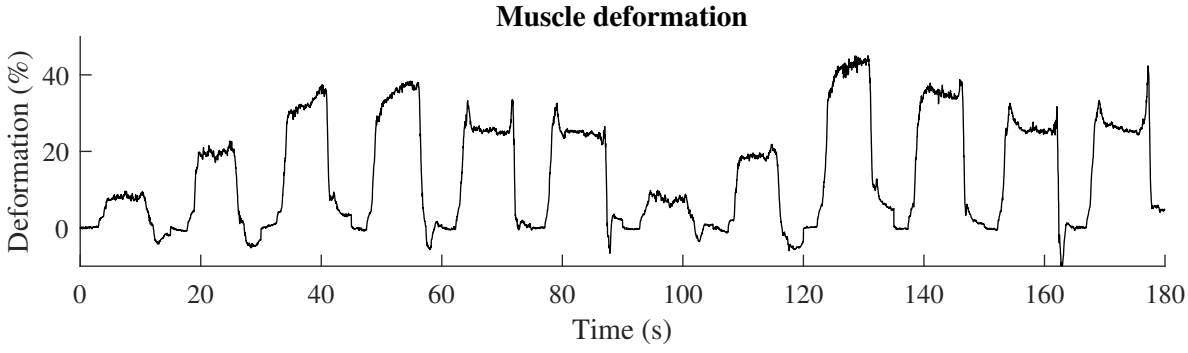

(a) Muscle deformation

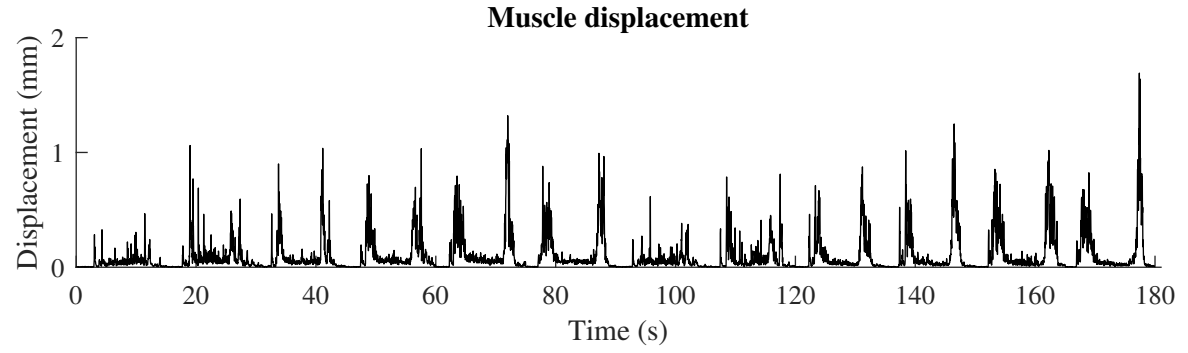

(b) Muscle displacement (row 10)

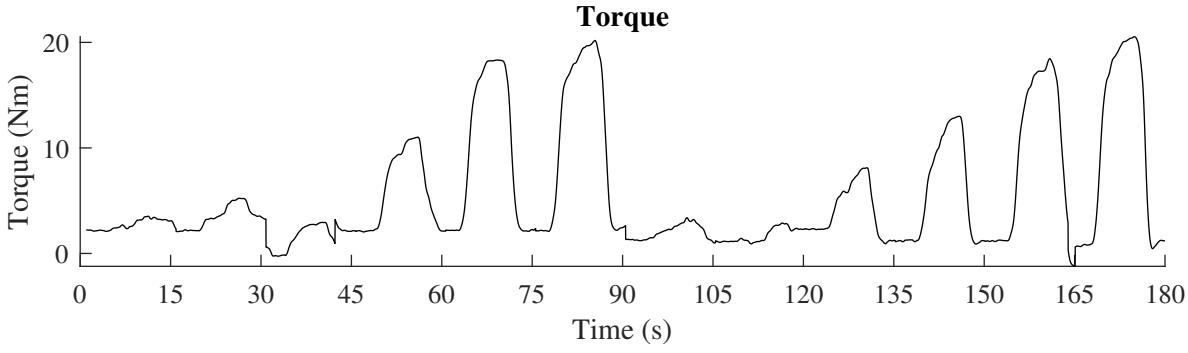

(c) Torque

Figure 7.2: An example of the deformation, displacement (row 10), and torque produced during different combinations of stimulation parameters. IPI = 50 ms for contractions 1-6 and IPI = 25 ms for contraction 7-12. In each case the stimulation intensity is increased with each contraction (I_{min}, PW_1 to PW_3, followed by I_{max}, PW_1 to PW_3).

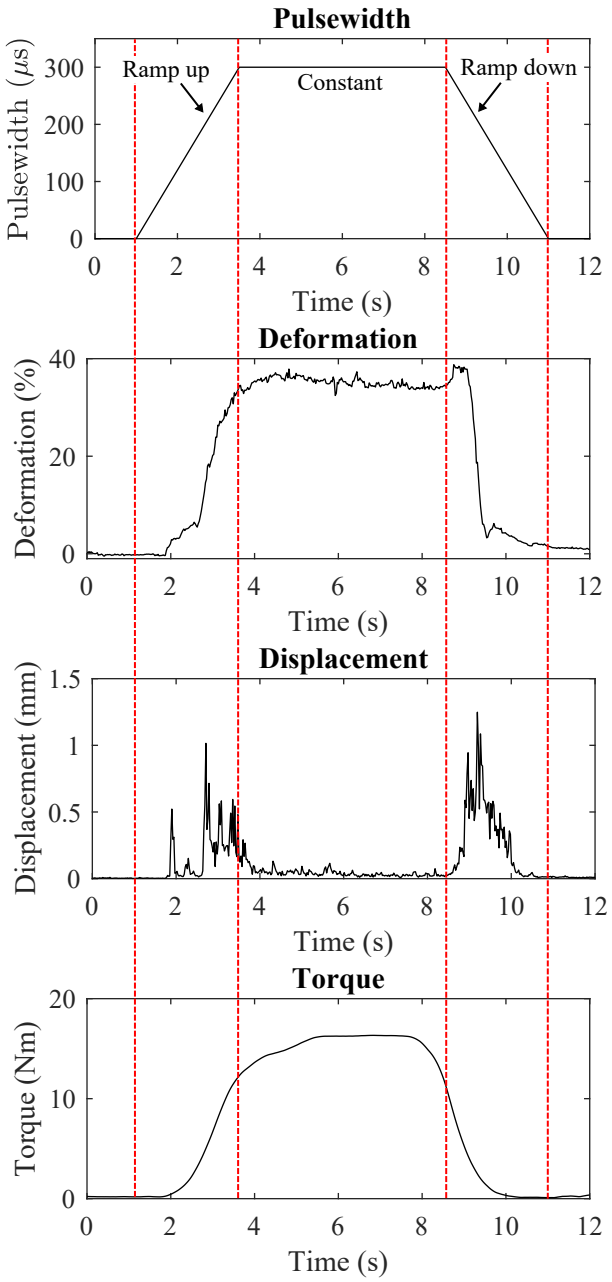

Figure 7.3: An example of the pulsewidth during a single contraction showing the ramp up, constant and ramp down phases of stimulation, and the resulting deformation, displacement (row 10) and torque produced.

Muscle deformation for each of these 12 combinations of stimulation parameters is shown in Figure 7.4a. Deformation appears to increase with an increase in pulsewidth at low levels of current and similarly, it also increases with an increase in current at the minimum pulsewidth value. These differences do not reach statistical significance however medium effect sizes can be seen, as shown in Table 13 in Appendix C.1.

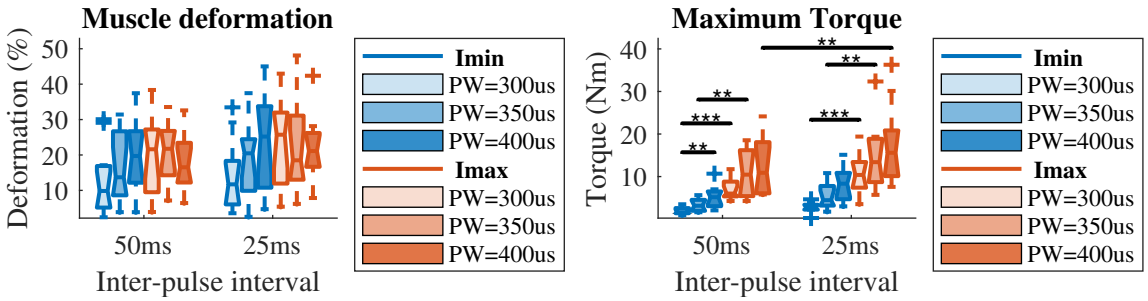

(a) Deformation (b) Torque

Figure 7.4: Boxplots of deformation and torque produced during NMES-induced contractions with different combinations of stimulation parameters ($**-p<0.01, ***-p<0.001$).

Table 7.2: P-values and effect sizes for the torque produced during different combinations of stimulation parameters. Values indicating a significant difference or a greater than medium effect size are shown in bold.

	Torque	
	P-Value	*Effect Size*
I_{min} & I_{max}:		
PW_1, 50ms	**<0.001**	**2.17**
PW_2, 50ms	**0.002**	**1.41**
PW_3, 50ms	0.01	**1.14**
PW_1, 25ms	**< 0.001**	**1.54**
PW_2, 25ms	**0.001**	**1.44**
PW_3, 25ms	0.01	**1.16**
50ms & 25ms:		
I_{min}, PW_1	0.11	0.56
I_{min}, PW_2	0.06	0.67
I_{min}, PW_3	0.04	0.74
I_{max}, PW_1	0.01	**1.03**
I_{max}, PW_2	0.01	**1.06**
I_{max}, PW_3	**0.002**	**1.37**
PW_1 & PW_2:		
I_{min}, 50ms	0.01	**0.97**
I_{max}, 50ms	0.01	**1.13**
I_{min}, 25ms	0.02	**0.87**
I_{max}, 25ms	0.01	**1.12**
PW_1 & PW_3:		
I_{min}, 50ms	**0.002**	**1.35**
I_{max}, 50ms	0.01	**1.15**
I_{min}, 25ms	0.004	**1.23**
I_{max}, 25ms	0.01	**1.11**
PW_2 & PW_3:		
I_{min}, 50ms	0.004	**1.22**
I_{max}, 50ms	0.08	0.61
I_{min}, 25ms	0.11	0.57
I_{max}, 25ms	0.06	0.67

There is no further increase with the increase of current or pulsewidth if either of these parameters is at its maximum value. In contrast, a decrease in deformation can be seen when the pulsewidth is increased at the maximum current value. Deformation also does not appear to be affected by IPI.

The corresponding torque produced is shown in Figure 7.4b and the p-value and effect sizes are provided in Table 7.2. Most significant differences and large to huge effect sizes are seen between the minimum and maximum current, however torque increases in response to an increase in any of the 3 stimulation parameters.

A similar result is seen for the maximum muscle displacement in Figure 7.5. Most significant differences seen are between the maximum and minimum current values at low and medium values of pulsewidth (PW_1 and PW_2), however there is also a difference between the IPI levels at column 8. The p-values and effect sizes are shown in Table 7.3. Again, large to very large effect sizes are mostly seen between minimum and maximum current values, however some large effect sizes are also seen between the different IPI values.

The total muscle displacement for different stimulation parameters during the ramp up, constant and ramp down phases of the contraction are shown in Figures 7.6, 7.7 and 7.8 respectively. P-values and effect sizes for total displacement during the ramp up phase are shown in Table 7.4. During this phase, significant differences and large to very large effect sizes can be seen between minimum and maximum current values at low and medium values of pulsewidth (PW_1 and PW_2) at all locations on the muscle. A similar increase is seen with increased pulsewidth values at low values of current for all positions.

During the constant phase, there is less difference between the different combinations of stimulation parameters. P-values and effect sizes are shown in Table 14 in Appendix C.1. No significant differences are seen, however, there are still some large effect sizes seen, particularly showing a decrease between PW_1 and PW_3 at the maximum current and IPI levels.

P-values and effect sizes for total displacement during the ramp down phase are shown in Table 7.5. This phase shows an increase in muscle displacement with an increase in any of the three stimulation parameters. Most statistically significant differences and effect sizes considered large and above, are seen between minimum and maximum current values, with large effect sizes even being seen at high levels of pulsewidth and IPI. There are also several significant differences and large to very large effect sizes with increasing pulsewidth and although there are large effect sizes seen between different IPI values this only reaches statistical significance at column 1.

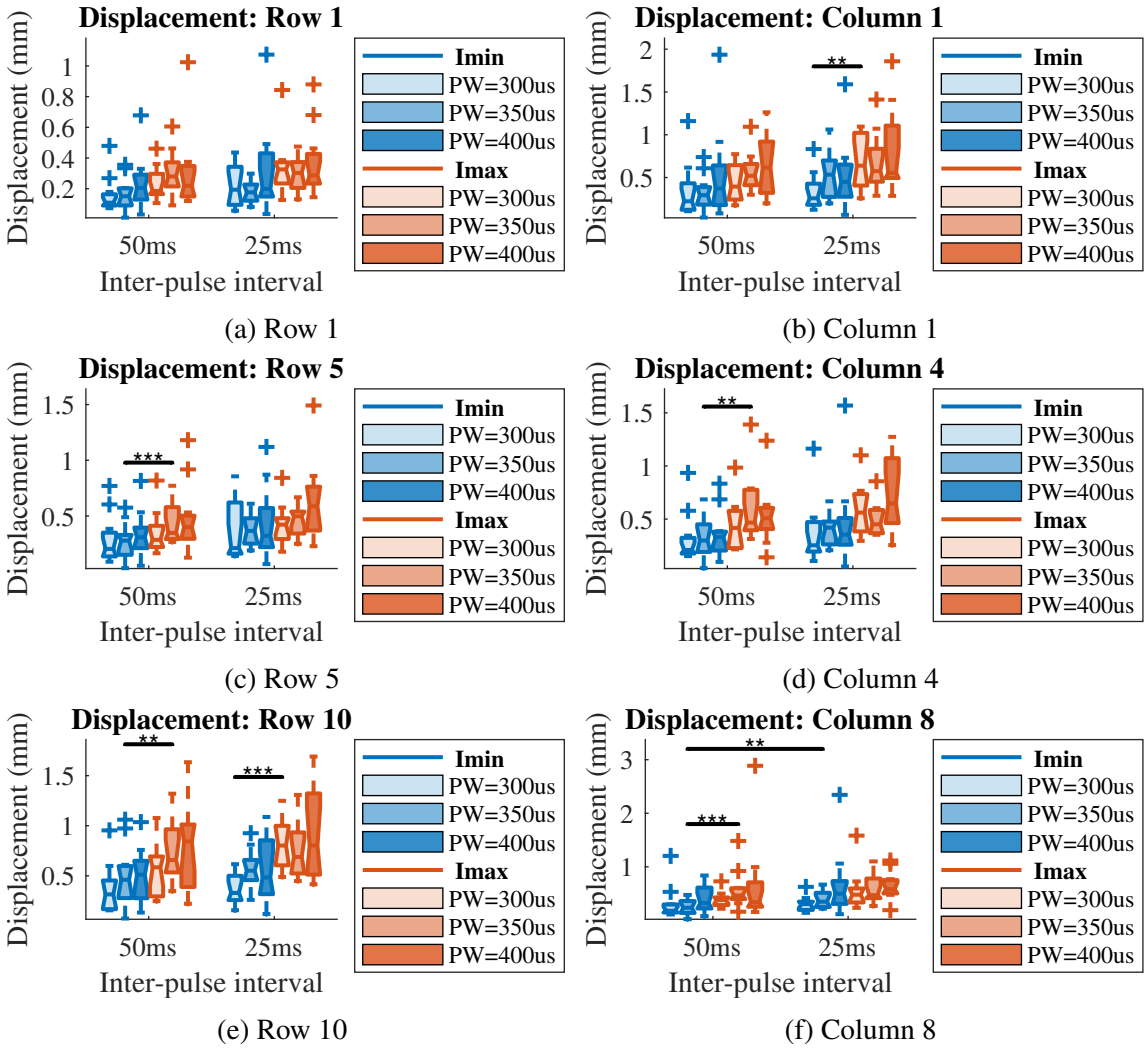

(a) Row 1 (b) Column 1

(c) Row 5 (d) Column 4

(e) Row 10 (f) Column 8

Figure 7.5: Boxplots of maximum muscle displacement during NMES-induced contractions with different combinations of stimulation parameters ($**-p<0.01, ***-p<0.001$).

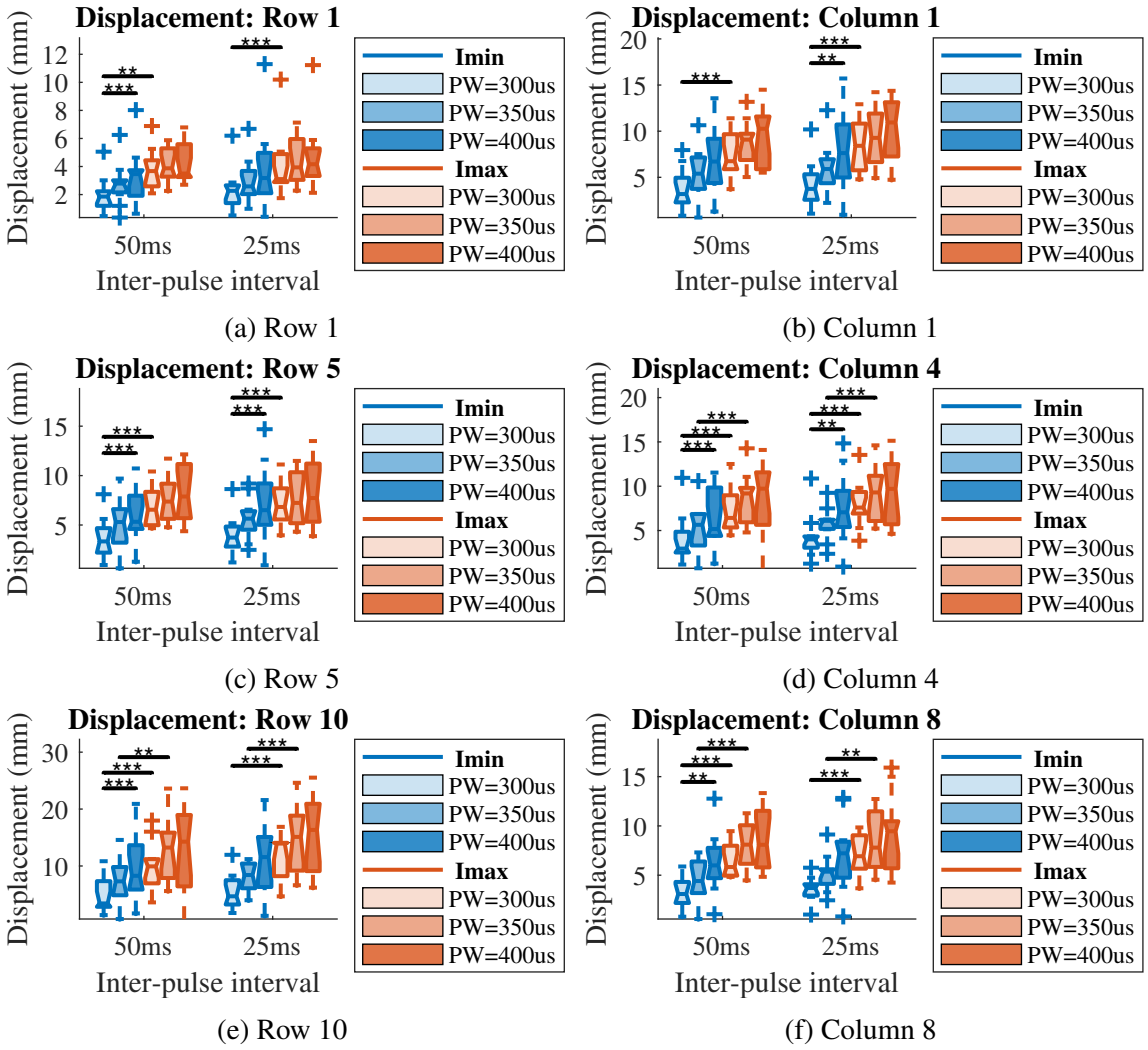

(a) Row 1 (b) Column 1

(c) Row 5 (d) Column 4

(e) Row 10 (f) Column 8

Figure 7.6: Boxplots of total muscle displacement during the ramp up phase of NMES-induced contractions with different combinations of stimulation parameters ($**-p<0.01, ***-p<0.001$).

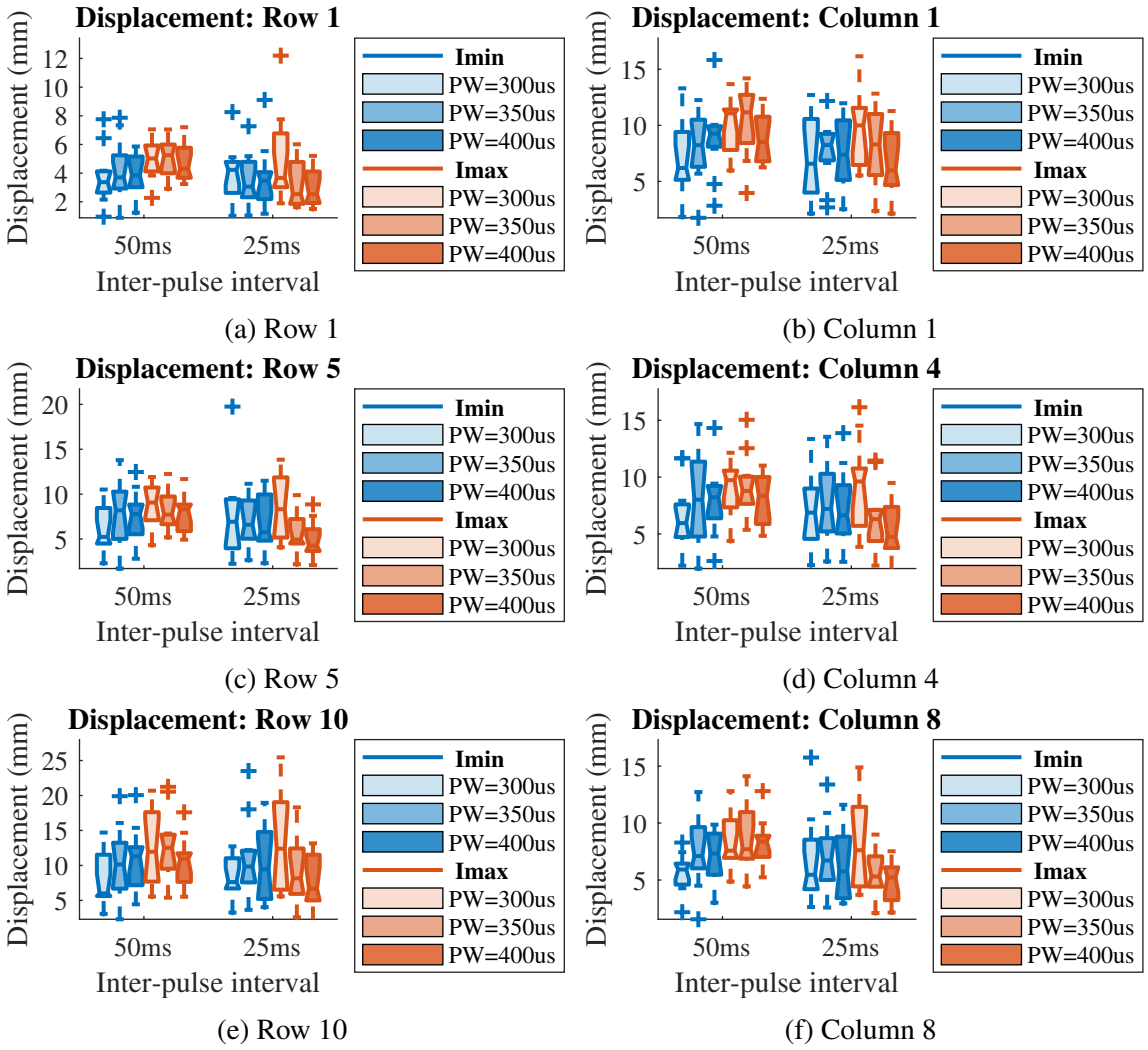

(a) Row 1 (b) Column 1

(c) Row 5 (d) Column 4

(e) Row 10 (f) Column 8

Figure 7.7: Boxplots of total muscle displacement during the constant phase of NMES-induced contractions with different combinations of stimulation parameters.

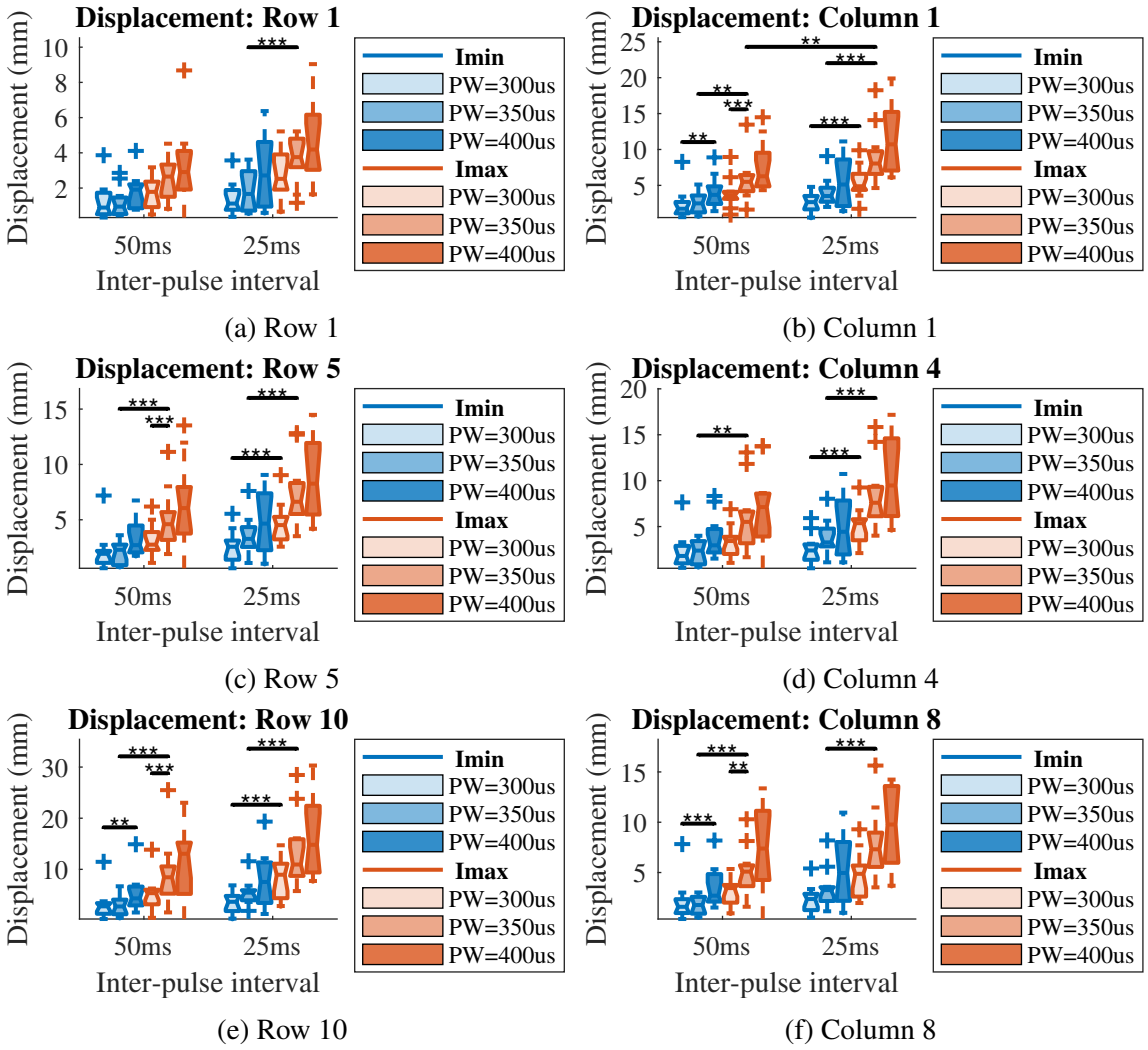

(a) Row 1 (b) Column 1

(c) Row 5 (d) Column 4

(e) Row 10 (f) Column 8

Figure 7.8: Boxplots of total muscle displacement during the ramp down phase of NMES-induced contractions with different combinations of stimulation parameters ($**-p<0.01$, $***-p<0.001$).

Table 7.3: Statistical values reported as p-value [effect size] for maximum muscle displacement during different combinations of stimulation parameters. Values indicating a significant difference or a greater than medium effect size are shown in bold.

	Maximum displacement					
	Row 1	*Row 5*	*Row 10*	*Col. 1*	*Col. 4*	*Col. 8*
I_{min} vs. I_{max}						
PW_1, 50ms	0.15 [0.50]	0.07 [0.37]	0.05 [0.55]	0.07 [0.26]	0.04 [0.65]	0.21 [0.24]
PW_2, 50ms	0.004 **[1.12]**	**<0.001 [1.19]**	**0.001 [1.33]**	0.01 **[0.97]**	**0.002 [1.34]**	**<0.001 [0.99]**
PW_3, 50ms	0.08 [0.61]	0.15 [0.47]	0.04 [0.70]	0.21 [0.22]	0.12 [0.49]	0.32 [0.32]
PW_1, 25ms	0.02 [0.78]	0.46 [0.29]	**<0.001 [2.06]**	**0.002 [1.26]**	0.03 [0.79]	0.01 [0.69]
PW_2, 25ms	0.003 **[1.16]**	0.09 [0.56]	0.01 **[0.97]**	0.08 [0.60]	0.10 [0.54]	0.03 [0.75]
PW_3, 25ms	0.28 [0.36]	0.05 [0.66]	0.01 **[0.94]**	0.21 [0.52]	0.03 [0.78]	0.64 [0.05]
50ms vs. 25ms						
I_{min}, PW_1	0.10 [0.59]	0.24 [0.44]	0.21 [0.02]	0.37 [0.05]	0.24 [0.36]	0.41 [0.02]
I_{min}, PW_2	0.76 [0.09]	0.03 [0.79]	0.41 [0.26]	0.02 **[0.88]**	0.21 [0.40]	**0.001 [1.34]**
I_{min}, PW_3	0.21 [0.48]	0.04 [0.49]	0.31 [0.32]	0.21 [0.00]	0.15 [0.47]	0.05 [0.51]
I_{max}, PW_1	0.04 [0.58]	0.03 **[0.86]**	0.003 **[1.16]**	0.03 [0.75]	0.03 [0.74]	0.12 [0.47]
I_{max}, PW_2	0.97 [0.01]	0.63 [0.20]	0.80 [0.08]	0.23 [0.39]	0.15 [0.50]	0.41 [0.02]
I_{max}, PW_3	0.41 [0.34]	0.17 [0.47]	0.07 [0.62]	0.32 [0.32]	0.15 [0.51]	0.28 [0.03]
PW_1 vs. PW_2						
I_{min}, 50ms	0.76 [0.11]	0.97 [0.08]	0.12 [0.43]	0.32 [0.05]	0.83 [0.08]	0.83 [0.21]
I_{max}, 50ms	0.24 [0.38]	0.21 [0.46]	0.01 **[0.98]**	0.14 [0.49]	0.02 **[0.92]**	0.10 [0.54]
I_{min}, 25ms	0.18 [0.44]	0.83 [0.04]	0.02 **[0.88]**	0.02 **[0.88]**	0.24 [0.13]	0.09 [0.56]
I_{max}, 25ms	0.64 [0.24]	0.47 [0.22]	0.33 [0.31]	0.90 [0.04]	0.17 [0.43]	0.64 [0.06]
PW_1 vs. PW_3						
I_{min}, 50ms	0.02 **[0.83]**	0.32 [0.30]	0.04 [0.52]	0.32 [0.32]	0.70 [0.22]	0.32 [0.28]
I_{max}, 50ms	0.41 [0.30]	0.15 [0.48]	0.11 [0.52]	0.03 [0.77]	0.70 [0.25]	0.37 [0.36]
I_{min}, 25ms	0.37 [0.36]	0.37 [0.24]	0.04 [0.71]	0.01 **[0.80]**	0.17 [0.51]	0.02 [0.60]
I_{max}, 25ms	0.83 [0.23]	0.07 [0.62]	0.48 [0.22]	0.41 [0.22]	0.21 [0.41]	0.37 [0.30]
PW_2 vs. PW_3						
I_{min}, 50ms	0.12 [0.45]	0.14 [0.48]	0.94 [0.02]	0.24 [0.40]	0.51 [0.21]	0.04 [0.70]
I_{max}, 50ms	0.90 [0.01]	0.15 [0.48]	0.73 [0.11]	0.35 [0.30]	0.46 [0.26]	0.52 [0.12]
I_{min}, 25ms	0.10 [0.56]	0.97 [0.21]	0.87 [0.05]	0.97 [0.06]	0.97 [0.17]	0.15 [0.49]
I_{max}, 25ms	0.64 [0.29]	0.12 [0.51]	0.17 [0.45]	0.52 [0.29]	0.01 **[0.87]**	0.20 [0.41]

Table 7.4: Statistical values reported as p-value [effect size] for total muscle displacement during the ramp up phase of different combinations of stimulation parameters. Values indicating a significant difference or a greater than medium effect size are shown in bold.

	Total displacement during ramp up phase					
	Row 1	*Row 5*	*Row 10*	*Col. 1*	*Col. 4*	*Col. 8*
I_{min} vs. I_{max}						
PW_1, 50ms	**0.002 [1.58]**	**<0.001 [1.55]**	**<0.001 [1.27]**	**<0.001 [1.53]**	**<0.001 [1.29]**	**<0.001 [1.72]**
PW_2, 50ms	0.01 **[1.04]**	0.002 **[1.22]**	**0.002 [1.27]**	0.01 **[1.00]**	**<0.001 [1.54]**	**<0.001 [1.76]**
PW_3, 50ms	0.40 [0.26]	0.29 [0.34]	0.23 [0.39]	0.27 [0.35]	0.29 [0.34]	0.20 [0.42]
PW_1, 25ms	**<0.001 [1.33]**	**<0.001 [1.48]**	**<0.001 [1.51]**	**<0.001 [1.62]**	**<0.001 [1.82]**	**<0.001 [1.71]**
PW_2, 25ms	0.02 **[0.85]**	0.003 **[1.15]**	**<0.001 [1.53]**	0.01 **[1.07]**	**<0.001 [1.40]**	**0.001 [1.32]**
PW_3, 25ms	0.10 [0.54]	0.20 [0.44]	0.02 **[0.84]**	0.12 [0.52]	0.05 [0.68]	0.03 [0.75]
50ms vs. 25ms						
I_{min}, PW_1	0.24 [0.40]	0.18 [0.44]	0.10 [0.59]	0.22 [0.39]	0.24 [0.35]	0.23 [0.39]
I_{min}, PW_2	0.54 [0.19]	0.28 [0.35]	0.22 [0.40]	0.24 [0.38]	0.24 [0.38]	0.09 [0.56]
I_{min}, PW_3	0.37 [0.42]	0.06 [0.65]	0.03 [0.75]	0.19 [0.51]	0.09 [0.57]	0.10 [0.54]
I_{max}, PW_1	0.37 [0.26]	0.37 [0.28]	0.07 [0.62]	0.13 [0.50]	0.17 [0.40]	0.24 [0.37]
I_{max}, PW_2	0.41 [0.26]	0.64 [0.15]	0.003 **[1.21]**	0.19 [0.42]	0.01 **[0.89]**	0.14 [0.49]
I_{max}, PW_3	0.90 [0.19]	0.79 [0.08]	0.47 [0.23]	0.44 [0.24]	0.66 [0.14]	0.60 [0.16]
PW_1 vs. PW_2						
I_{min}, 50ms	0.005 **[1.17]**	0.005 **[1.09]**	0.005 **[1.01]**	0.003 **[1.17]**	0.01 **[0.80]**	0.02 **[0.87]**
I_{max}, 50ms	0.19 [0.43]	0.09 [0.56]	0.03 [0.78]	0.05 [0.66]	0.07 [0.67]	0.04 [0.73]
I_{min}, 25ms	0.01 **[0.87]**	0.01 **[0.92]**	0.01 **[1.03]**	0.002 **[1.24]**	0.01 **[0.85]**	0.01 **[0.93]**
I_{max}, 25ms	0.41 [0.18]	0.35 [0.29]	0.02 **[0.80]**	0.19 [0.43]	0.14 [0.48]	0.10 [0.56]
PW_1 vs. PW_3						
I_{min}, 50ms	**<0.001 [1.31]**	**<0.001 [1.56]**	**<0.001 [0.95]**	0.004 **[1.14]**	**<0.001 [1.05]**	**0.001 [1.34]**
I_{max}, 50ms	0.64 [0.14]	0.44 [0.24]	0.21 [0.40]	0.34 [0.30]	0.41 [0.25]	0.16 [0.45]
I_{min}, 25ms	0.005 **[0.98]**	**<0.001 [1.47]**	0.003 **[1.18]**	**0.001 [1.38]**	**0.002 [1.35]**	0.002 **[1.24]**
I_{max}, 25ms	0.24 [0.40]	0.21 [0.40]	0.04 [0.70]	0.10 [0.55]	0.20 [0.42]	0.05 [0.67]
PW_2 vs. PW_3						
I_{min}, 50ms	0.01 **[0.94]**	0.01 **[0.97]**	0.09 [0.57]	0.04 [0.71]	0.01 **[0.89]**	0.03 [0.77]
I_{max}, 50ms	0.80 [0.08]	0.91 [0.03]	0.95 [0.02]	0.90 [0.04]	0.99 [0.00]	0.77 [0.09]
I_{min}, 25ms	0.07 [0.60]	0.05 [0.67]	0.05 [0.67]	0.03 [0.74]	0.06 [0.63]	0.05 [0.68]
I_{max}, 25ms	0.70 [0.14]	0.22 [0.40]	0.25 [0.36]	0.12 [0.51]	0.68 [0.13]	0.11 [0.52]

Table 7.5: Statistical values reported as p-value [effect size] for total muscle displacement during the ramp down phase of different combinations of stimulation parameters. Values indicating a significant difference or a greater than medium effect size are shown in bold.

	Total displacement during ramp down phase					
	Row 1	*Row 5*	*Row 10*	*Col. 1*	*Col. 4*	*Col. 8*
I_{min} vs. I_{max}						
PW_1, 50ms	0.05 [0.36]	0.05 [0.39]	0.05 [0.41]	0.05 [0.45]	0.05 [0.37]	0.05 [0.36]
PW_2, 50ms	0.003 **[1.27]**	**<0.001 [1.38]**	**<0.001 [1.26]**	**0.002 [1.43]**	**0.002 [1.24]**	**<0.001 [1.41]**
PW_3, 50ms	0.08 [0.62]	0.04 [0.72]	0.02 **[0.82]**	0.03 [0.75]	0.03 [0.76]	0.01 **[0.99]**
PW_1, 25ms	0.005 **[1.10]**	**<0.001 [1.64]**	**<0.001 [1.56]**	**<0.001 [1.66]**	**<0.001 [1.46]**	0.01 **[1.07]**
PW_2, 25ms	**<0.001 [2.41]**	**<0.001 [1.51]**	**<0.001 [1.45]**	**<0.001 [1.44]**	**<0.001 [1.47]**	**<0.001 [1.67]**
PW_3, 25ms	0.002 **[1.22]**	0.01 **[1.00]**	0.01 **[0.97]**	0.01 **[1.06]**	0.01 **[0.98]**	0.02 **[0.81]**
50ms vs. 25ms						
I_{min}, PW_1	0.32 [0.11]	0.12 [0.20]	0.08 [0.10]	0.12 [0.09]	0.17 [0.14]	0.08 [0.12]
I_{min}, PW_2	0.02 [0.79]	0.02 **[0.80]**	0.002 **[0.90]**	0.01 [0.76]	0.02 **[0.80]**	0.01 **[0.82]**
I_{min}, PW_3	0.03 **[0.86]**	0.06 [0.64]	0.02 **[0.85]**	0.05 [0.67]	0.04 [0.78]	0.05 [0.72]
I_{max}, PW_1	0.03 [0.77]	0.05 [0.67]	0.02 **[0.83]**	0.05 [0.69]	0.03 [0.75]	0.07 [0.60]
I_{max}, PW_2	0.02 **[0.85]**	0.03 [0.75]	0.03 [0.65]	**0.002 [0.93]**	0.06 [0.65]	0.06 [0.65]
I_{max}, PW_3	0.22 [0.39]	0.19 [0.42]	0.09 [0.58]	0.07 [0.61]	0.13 [0.50]	0.25 [0.36]
PW_1 vs. PW_2						
I_{min}, 50ms	0.28 [0.07]	0.32 [0.09]	0.64 [0.12]	0.21 [0.01]	0.37 [0.06]	0.52 [0.16]
I_{max}, 50ms	0.01 **[1.08]**	**<0.001 [1.42]**	**<0.001 [1.25]**	**<0.001 [1.51]**	0.002 **[1.18]**	**0.002 [1.28]**
I_{min}, 25ms	0.12 [0.51]	0.09 [0.56]	0.02 [0.67]	0.03 [0.64]	0.08 [0.58]	0.07 [0.61]
I_{max}, 25ms	0.03 [0.77]	0.02 **[0.80]**	0.04 [0.71]	0.01**[0.92]**	0.02 **[0.86]**	0.04 [0.73]
PW_1 vs. PW_3						
I_{min}, 50ms	0.07 [0.61]	0.01 **[0.93]**	**0.002 [1.43]**	**0.002 [1.53]**	0.005 **[0.98]**	**<0.001 [1.23]**
I_{max}, 50ms	0.08 [0.58]	0.03 [0.76]	0.02 **[0.85]**	0.04 [0.73]	0.02 **[0.81]**	0.01 **[0.98]**
I_{min}, 25ms	0.02 **[0.84]**	0.2 **[0.81]**	0.2 **[0.82]**	0.02 **[0.83]**	0.03 [0.77]	0.01 **[0.90]**
I_{max}, 25ms	0.01 **[0.90]**	0.01 **[0.95]**	0.01 **[0.97]**	0.004 **[1.12]**	0.01 **[1.07]**	0.01 **[0.90]**
PW_2 vs. PW_3						
I_{min}, 50ms	0.02 **[0.91]**	0.01 **[1.00]**	0.01 [0.64]	0.03 [0.76]	0.02 [0.71]	0.004 **[0.89]**
I_{max}, 50ms	0.39 [0.27]	0.39 [0.27]	0.52 [0.21]	0.58 [0.32]	0.51 [0.20]	0.18 [0.43]
I_{min}, 25ms	0.04 [0.70]	0.10 [0.55]	0.08 [0.66]	0.12 [0.60]	0.06 [0.63]	0.12 [0.64]
I_{max}, 25ms	0.12 [0.51]	0.17 [0.44]	0.14 [0.49]	0.17 [0.56]	0.15 [0.48]	0.19 [0.43]

7.4.2 Variable frequency and variable pulsewidth stimulation patterns

The results in this section are also based on data obtained during Study 3A. Each of the 12 combinations of stimulation described in Section 7.4.1 were applied using three different patterns: constant stimulation, variable pulsewidth and variable IPI (see Section 3.5.4.5 of Chapter 3 for full details). USI measurements of muscle deformation and displacement are compared between each of these patterns of stimulation, as well as voluntary contractions of comparable intensity.

Figure 7.9 shows the muscle deformation during conventional stimulation where parameters remain constant compared to variable IPI and variable pulsewidth patterns of stimulation and voluntary contractions of comparable intensity. P-values and effect sizes for muscle deformation are shown in Table 7.6. Muscle deformation is significantly higher for contractions induced by electrical stimulation with very large effect sizes shown, however there are no significant differences between different patterns of stimulation and effect sizes are small.

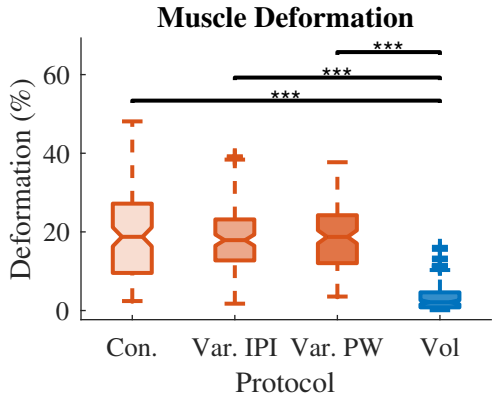

Figure 7.9: Boxplots of muscle deformation during different stimulation protocols: constant stimulation parameters (Con.); variable inter-pulse interval (Var. IPI); variable pulsewidth (Var. PW); and comparable voluntary contractions (Vol.) ($***-p<0.001$).

Table 7.6: P-values and effect sizes for muscle deformation during different patterns of stimulation.

Deformation		
	P-Value	*Effect Size*
FES_c&FES_{IPI}	0.08	0.17
FES_c&FES_{PW}	0.43	0.12
FES_c&$Vol.$	**< 0.001**	**1.35**
FES_{IPI}&FES_{PW}	0.40	0.07
FES_{IPI}&$Vol.$	**< 0.001**	**1.51**
FES_{PW}&$Vol.$	**< 0.001**	**1.60**

Maximum muscle displacement is shown in Figure 7.10 and the total displacement during each phase of the contraction is shown in Figure 7.11. P-values and effect sizes are provided in Table 7.7. Similarly to muscle deformation, there is a large increase in maximum muscle displacement for NMES-induced contractions compared to voluntary but there is no difference seen between variable IPI or variable pulsewidth patterns of stimulation compared to conventional constant stimulation. There is a significant increase in the variable pulsewidth pattern compared to the variable IPI pattern at column 1, however, the effect size is small.

The same result is also seen for the total displacement during the constant phase of the contraction, however, the increase in displacement during the variable pulsewidth pattern compared to the variable IPI is seen at row 5, row 10 and column 8 as well as column 1. During the ramp up phase (Figure 7.11a) there is a statistically significant decrease in the total displacement between constant stimulation and both variable pulsewidth and variable IPI patterns of stimulation. Conversely, during the ramp down phase (Figure 7.11c) there is a statistically significant increase in displacement between constant stimulation and variable pulsewidth and IPI patterns. Again, despite the statistical significance, it should be noted that the effect sizes are still only small to medium.

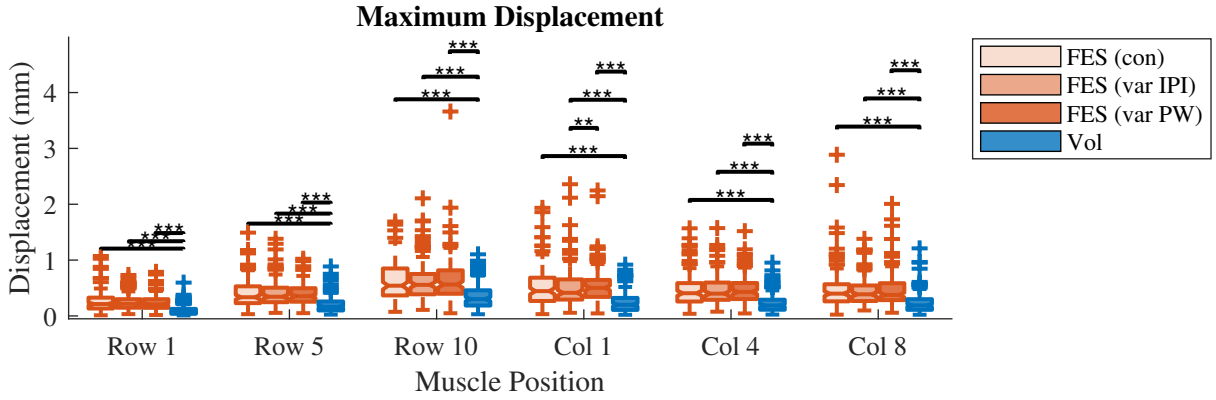

Figure 7.10: Boxplots of maximum muscle displacement during different stimulation protocols: constant stimulation parameters (FES con); variable inter-pulse interval (FES var IPI); variable pulsewidth (FES var PW); and comparable voluntary contractions (Vol.) ($**-p<0.01, ***-p<0.001$).

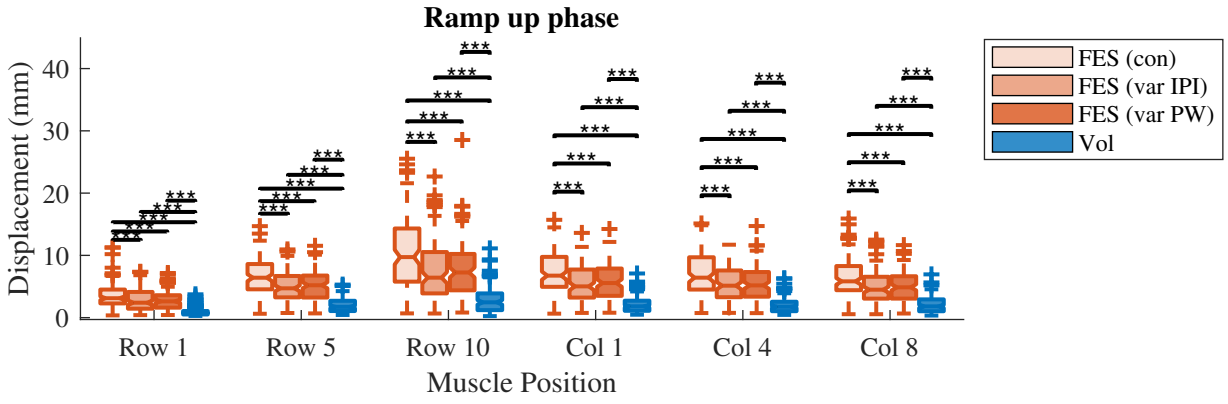

(a) Ramp up phase

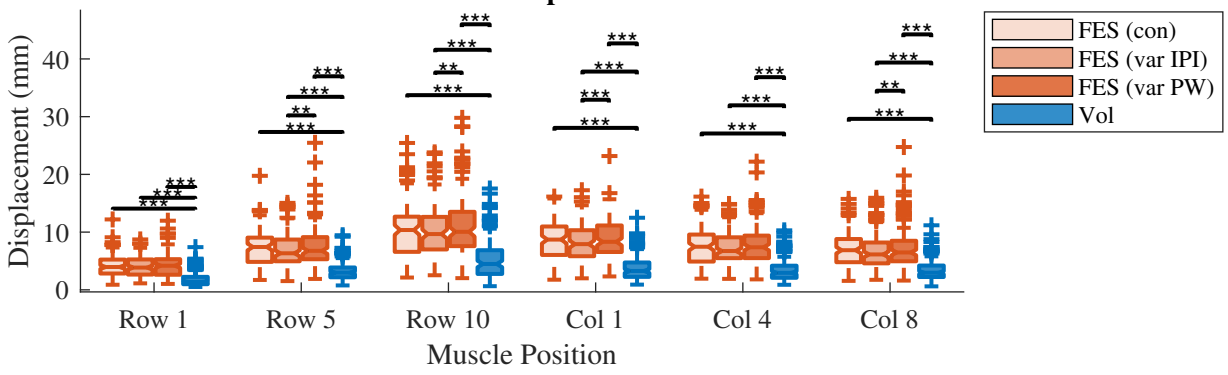

(b) Constant phase

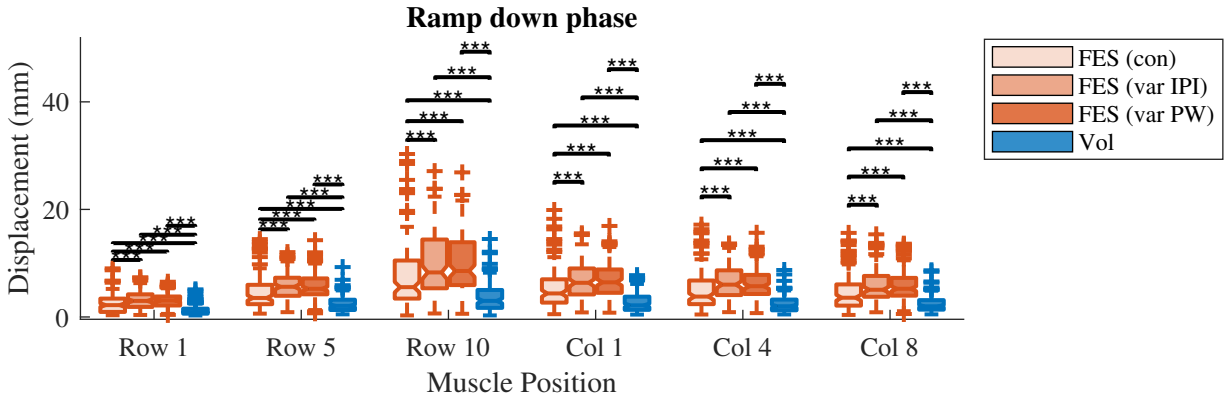

(c) Ramp down phase

Figure 7.11: Boxplots of total muscle displacement during different phases of NMES-induced contractions with different stimulation protocols: constant stimulation parameters (FES con); variable inter-pulse interval (FES var IPI); variable pulsewidth (FES var PW); and comparable voluntary contractions (Vol.) ($**-p<0.01, ***-p<0.001$).

Table 7.7: Statistical values reported as p-value [effect size] for the maximum and total muscle displacement during each phase of different patterns of stimulation. Values indicating a significant difference or a greater than medium effect size are shown in bold.

Maximum displacement						
	Row 1	*Row 5*	*Row 10*	*Col. 1*	*Col. 4*	*Col. 8*
FES_c *vs.* FES_{IPI}	0.80 [0.07]	0.86 [0.002]	0.73 [0.04]	0.47 [0.04]	0.98 [0.003]	0.83 [0.11]
FES_c *vs.* FES_{PW}	0.89 [0.08]	0.88 [0.06]	0.56 [0.09]	0.07 [0.05]	0.44 [0.02]	0.33 [0.02]
FES_c *vs. Vol.*	**<0.001 [0.80]**	**<0.001** [0.74]	**<0.001** [0.71]	**<0.001** [0.72]	**<0.001** [0.73]	**<0.001** [0.57]
FES_{IPI} *vs.*FES_{PW}	0.67 [0.01]	0.80 [0.07]	0.64 [0.06]	**0.01** [0.11]	0.37 [0.03]	0.47 [0.10]
FES_{IPI} *vs. Vol.*	**<0.001 [0.86]**	**<0.001** [0.77]	**<0.001** [0.73]	**<0.001** [0.69]	**<0.001 [0.88]**	**<0.001** [0.68]
FES_{PW} *vs. Vol.*	**<0.001 [0.95]**	**<0.001 [0.86]**	**<0.001** [0.69]	**<0.001 [0.84]**	**<0.001 [0.84]**	**<0.001** [0.70]
Total displacement during ramp up phase						
	Row 1	*Row 5*	*Row 10*	*Col. 1*	*Col. 4*	*Col. 8*
FES_c *vs.* FES_{IPI}	**<0.001** [0.39]	**<0.001** [0.52]	**<0.001** [0.47]	**<0.001** [0.49]	**<0.001** [0.51]	**<0.001** [0.49]
FES_c *vs. FESvp*	**<0.001** [0.41]	**<0.001** [0.47]	**<0.001** [0.46]	**<0.001** [0.46]	**<0.001** [0.49]	**<0.001** [0.47]
FES_c *vs. Vol.*	**<0.001 [1.28]**	**<0.001 [1.47]**	**<0.001 [1.25]**	**<0.001 [1.40]**	**<0.001 [1.41]**	**<0.001 [1.36]**
FES_{IPI} *vs.*FES_{PW}	0.41 [0.03]	0.25 [0.10]	0.07 [0.003]	0.02 [0.09]	0.20 [0.02]	0.14 [0.04]
FES_{IPI} *vs. Vol.*	**<0.001 [1.14]**	**<0.001 [1.34]**	**<0.001 [1.07]**	**<0.001 [1.18]**	**<0.001 [1.30]**	**<0.001 [1.14]**
FES_{PW} *vs. Vol.*	**<0.001 [1.32]**	**<0.001 [1.45]**	**<0.001 [1.17]**	**<0.001 [1.30]**	**<0.001 [1.35]**	**<0.001 [1.37]**
Total displacement during constant phase						
	Row 1	*Row 5*	*Row 10*	*Col. 1*	*Col. 4*	*Col. 8*
FES_c *vs.* FES_{IPI}	0.61 [0.08]	0.32 [0.09]	0.30 [0.06]	0.40 [0.07]	0.13 [0.10]	0.10 [0.09]
FES_c *vs.* FES_{PW}	0.65 [0.03]	0.80 [0.07]	0.21 [0.16]	0.26 [0.13]	0.80 [0.07]	0.98 [0.06]
FES_c *vs. Vol.*	**<0.001 [0.91]**	**<0.001 [1.05]**	**<0.001 [0.81]**	**<0.001 [1.05]**	**<0.001 [1.00]**	**<0.001 [0.95]**
FES_{IPI} *vs.*FES_{PW}	0.08 [0.17]	**0.003** [0.26]	**0.003** [0.30]	**<0.001** [0.31]	0.01 [0.28]	**0.01** [0.24]
FES_{IPI} *vs. Vol.*	**<0.001 [0.91]**	**<0.001 [0.99]**	**<0.001 [0.83]**	**<0.001 [1.01]**	**<0.001 [0.99]**	**<0.001 [0.82]**
FES_{PW} *vs. Vol.*	**<0.001 [0.89]**	**<0.001 [0.95]**	**<0.001 [0.88]**	**<0.001 [1.08]**	**<0.001 [0.99]**	**<0.001 [0.84]**
Total displacement during ramp down phase						
	Row 1	*Row 5*	*Row 10*	*Col. 1*	*Col. 4*	*Col. 8*
FES_c *vs.* FES_{IPI}	**<0.001** [0.50]	**<0.001** [0.41]	**<0.001** [0.39]	**<0.001** [0.42]	**<0.001** [0.40]	**<0.001** [0.37]
FES_c *vs.* FES_{PW}	**<0.001** [0.37]	**<0.001** [0.33]	**<0.001** [0.32]	**<0.001** [0.35]	**<0.001** [0.29]	**<0.001** [0.30]
FES_c *vs. Vol.*	**<0.001** [0.69]	**<0.001** [0.66]	**<0.001** [0.63]	**<0.001** [0.67]	**<0.001** [0.68]	**<0.001** [0.65]
FES_{IPI} *vs.*FES_{PW}	0.06 [0.16]	0.12 [0.09]	0.36 [0.06]	0.49 [0.04]	0.04 [0.14]	0.31 [0.06]
FES_{IPI} *vs. Vol.*	**<0.001 [1.23]**	**<0.001 [1.28]**	**<0.001 [1.15]**	**<0.001 [1.28]**	**<0.001 [1.30]**	**<0.001 [1.14]**
FES_{PW} *vs. Vol.*	**<0.001 [1.23]**	**<0.001 [1.22]**	**<0.001 [1.12]**	**<0.001 [1.21]**	**<0.001 [1.26]**	**<0.001 [1.16]**

7.4.3 Comparison of multi-electrode spatially distributed patterns

The results in this section are based on data obtained during Study 3B, where different spatially distributed patterns of stimulation were applied: conventional synchronous stimulation (CSS), asynchronous stimulation delivered in a sequential order (AsynS) and asynchronous stimulation delivered in a random order (AsynR). Full details on the different stimulation patterns are given in Section 3.6.4 of Chapter 3. For each pattern, intermittent stimulation was delivered for a total of 10 minutes. USI measurements of muscle deformation and pixel difference are compared at the start and end of the 10 minute train of stimulation for each spatially distributed pattern. Each measurement was averaged for 15 contractions at the start and end of the stimulation protocol.

Deformation, maximum pixel difference and total pixel difference describe the amplitude of the contraction. P-values and effect sizes are shown in Table 15 of Appendix C.2. Figure 7.12 shows different measurements of muscle movement at the start and end of different spatially distributed patterns of stimulation. Muscle deformation (Figure 7.12a) appears to be higher during asynchronous patterns of stimulation, both sequential and random, at the start and the end of the stimulation protocol. However, this does not reach statistical significance and effect sizes are small. The maximum pixel difference (Figure 7.12b) appears to decrease more between the start and end of the protocol for the CSS pattern, however, no significant differences are seen despite a large effect size. Total pixel difference (Figure 7.12c) shows a similar result, however, in this case the decrease at the end of the protocol is seen for all patterns with medium effect sizes.

Figure 7.13 shows calculations describing the timing of contractions at the start and end of different spatial patterns of stimulation. P-values and effect sizes can be found in Table 16 of Appendix C.2. The contraction time (Figure 7.13a) appears to increase between the start and end of the protocol for all patterns, however the difference is larger for the CSS pattern, which shows a large effect size, while AsynS shows a medium effect size and AsynR only a small effect size. The half-relaxation time (Figure 7.13b) appears to increase by the end of the CSS protocol, showing a medium effect size. This increase in the CSS protocol is not seen in the asynchronous patterns, resulting in a medium effect size between CSS and AsynS at the end of the protocol. All other effect sizes are small. Finally, the peak-to-peak time (Figure 7.13c) appears to decrease between the start and end of the CSS protocol, with a large effect size seen.

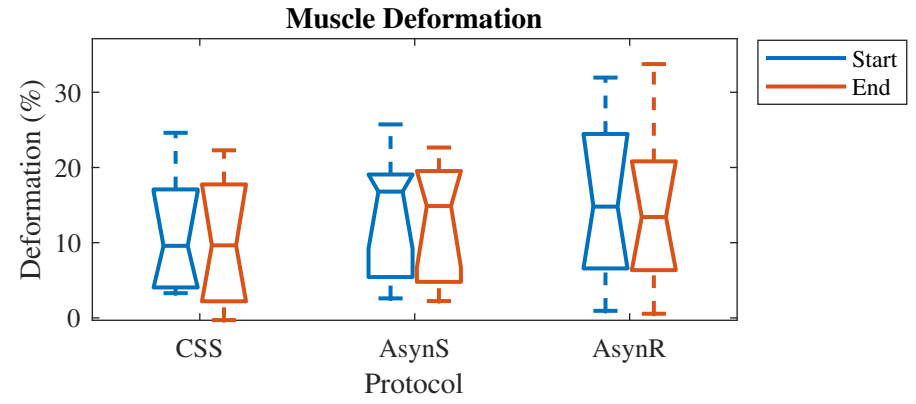

(a) Deformation

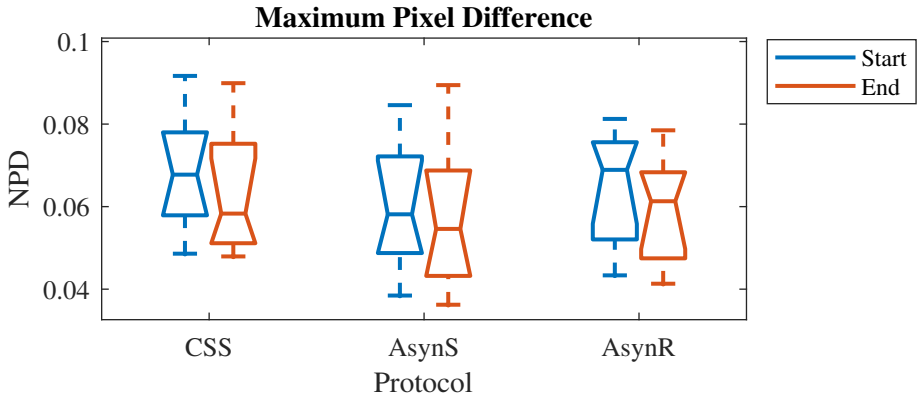

(b) Maximum pixel difference

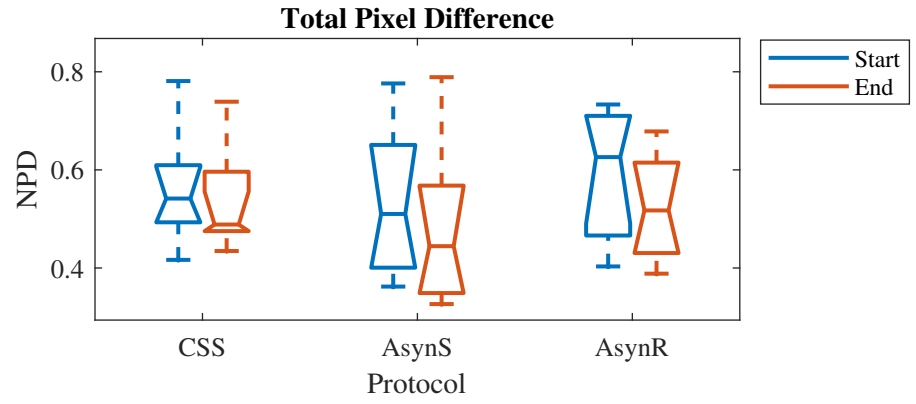

(c) Total pixel difference

Figure 7.12: Boxplots of muscle movement at the start and end of different stimulation patterns.

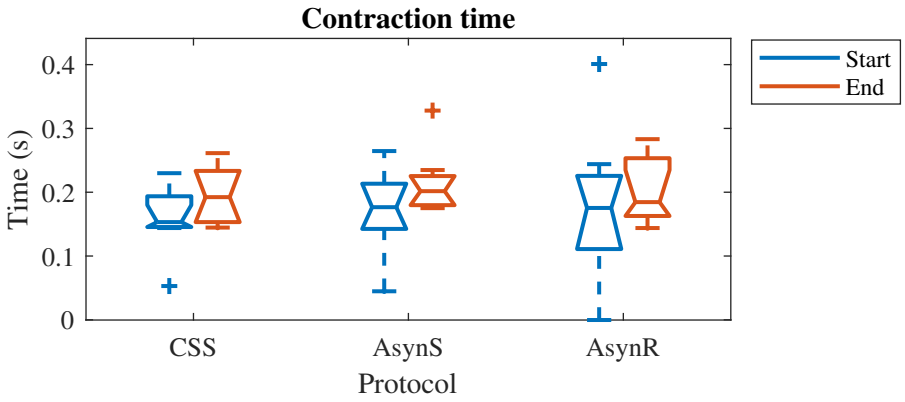

(a) Contraction time

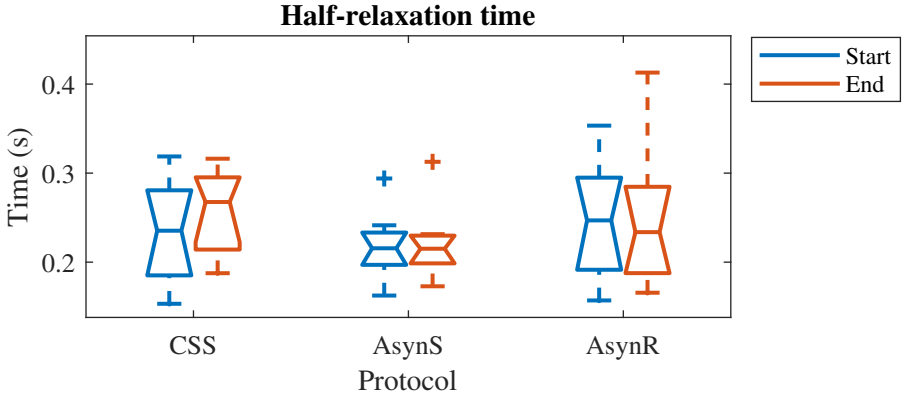

(b) Half-relaxation time

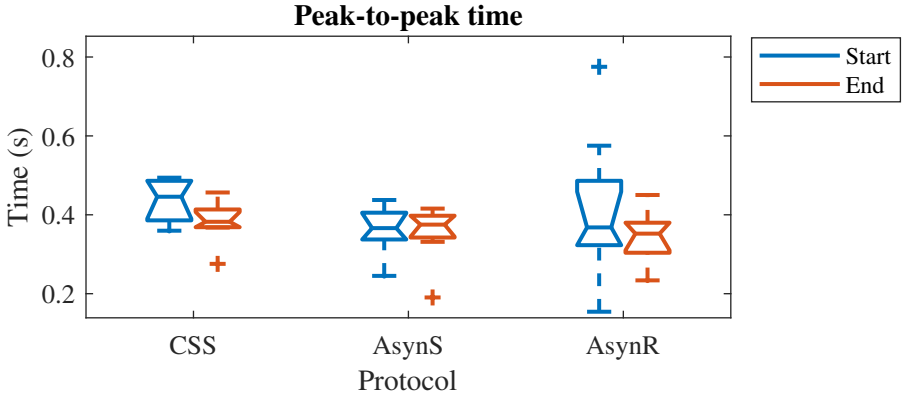

(c) Peak-to-peak time

Figure 7.13: Boxplots of pixel difference measurements describing the timing of the contraction at the start and end of different stimulation patterns.

7.4.4 Stimulation of able-bodied vs. SCI participants

The results in this section are based on data obtained during Study 1. USI measurements of deformation, displacement, and pixel difference, and the torque produced, are compared between SCI participants and able-bodied controls. First, muscle fibre recruitment during the current selection process is compared, followed by muscle behaviour during NMES-induced contractions. Finally, torque measurements are compared (details of protocol in Section 3.3 of Chapter 3).

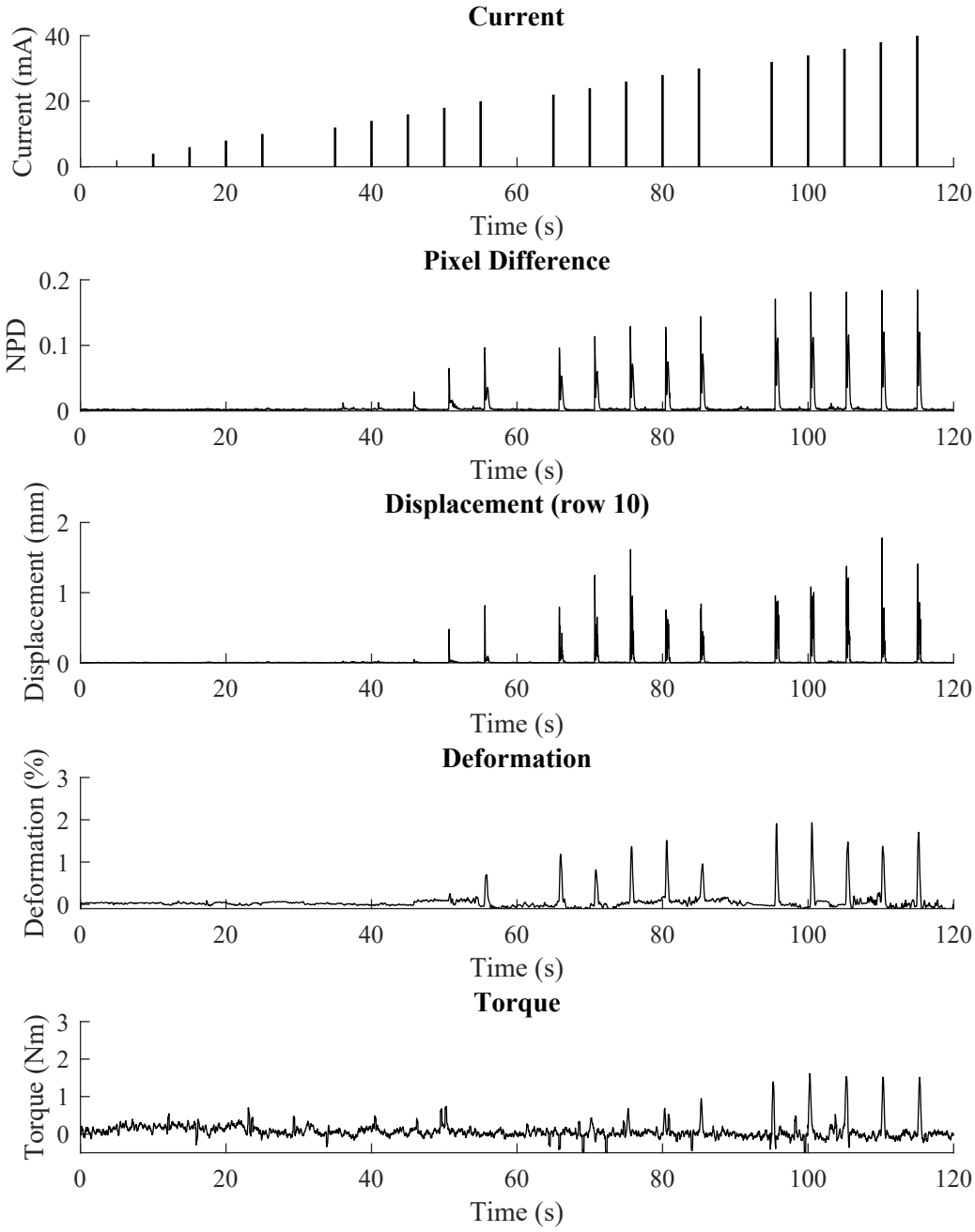

Figure 7.14: An example of the pixel difference, displacement (row 10), deformation and torque during the current selection process in response to increasing current.

7.4.4.1 Current selection

The current selection process involves the delivery of doublet pulse every 5 seconds, with the amplitude of the first pulse equal to 2 mA and each subsequent pulse increasing in increments of 2 mA, as described in Section 3.3.4.3 of Chapter 3. An example of the increasing current and the resulting pixel difference, displacement, deformation and torque are shown in Figure 7.14. Pixel difference is the first measurement to show movement in the muscle, at a current level of 16 mA, closely followed by displacement at 18 mA and then deformation at 20 mA. The current reaches 26 mA before a clear increase in torque is seen. A current value above 34 mA no longer causes an increase in torque, therefore this is the optimal value of current chosen for further NMES contractions (results shown in Section 7.4.4.2).

Figure 7.15 shows the first value of current that caused muscle movement which could be detected by different methods (pixel difference, displacement, deformation and torque) and the optimal current value that was selected for able-bodied and SCI participants. The p-values and effect sizes are shown in Table 7.8. Overall the amount of current required to cause a detectable muscle movement is higher for SCI participants compared to able-bodied participants. Significant differences and large effect sizes are seen for all methods except pixel difference and displacement at row 10. The optimal current value selected was also significantly higher for SCI participants with a very large effect size.

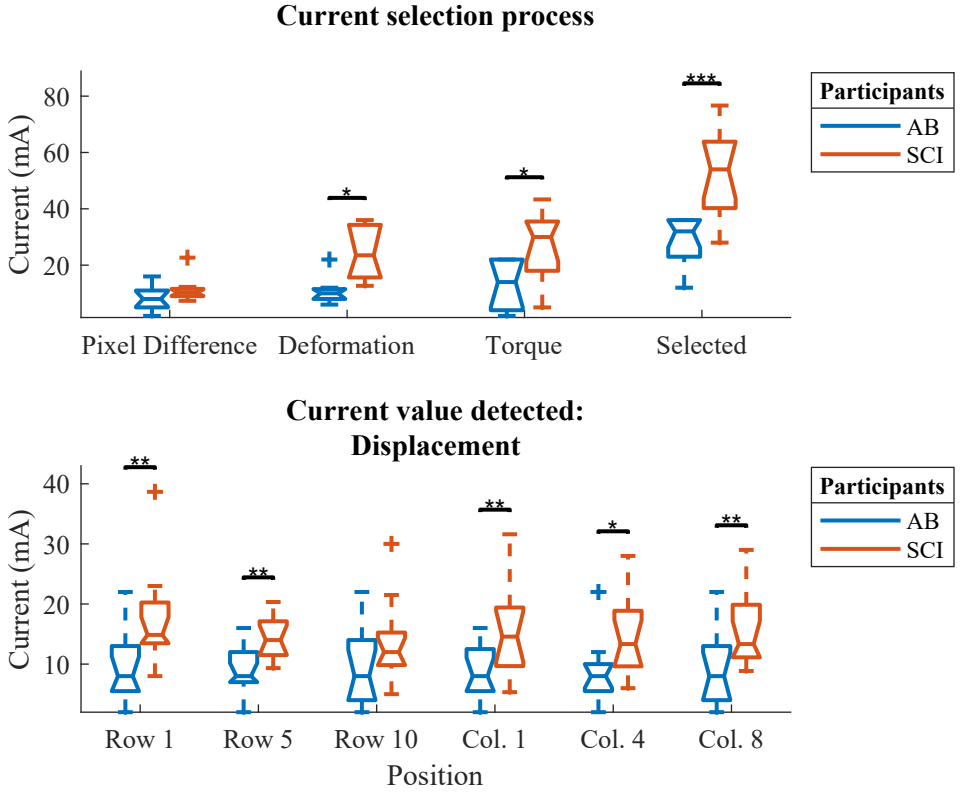

Figure 7.15: Boxplots of current values at which movement was detected and the final current value selected for able-bodied and SCI participants during the current selection process.

Table 7.8: P-values and effect sizes for current values for able-bodied and SCI participants during the current selection process. Values indicating a significant difference or a greater than medium effect size are shown in bold.

Movement detected by pixel difference		
	P-Value	*Effect Size*
	0.19	0.44
Movement detected by displacement		
	P-Value	*Effect Size*
Row 1	**0.01**	**0.84**
Row 5	**0.003**	**1.05**
Row 10	0.07	0.57
Column 1	**0.002**	**1.06**
Column 4	**0.02**	0.79
Column 8	**0.004**	**0.98**
Movement detected by deformation		
	P-Value	*Effect Size*
	0.03	**1.10**
Movement detected by torque		
	P-Value	*Effect Size*
	0.04	**0.85**
Optimal current value selected		
	P-Value	*Effect Size*
	< 0.001	**1.44**

7.4.4.2 NMES-induced ramped contractions

The results presented here describe the muscle behaviour during smooth NMES-induced contractions which last 10 seconds in total and consist of a 2.5s ramp up phase, a 5s constant phase and a 2.5s ramp down phase (similar to that seen in Section 7.4.1). For full details of the stimulation applied see Section 3.3.4.3 in Chapter 3.

Figure 7.16 shows USI measurements of muscle movement for SCI and able-bodied participants. Figure 7.16a shows that muscle deformation is less for SCI participants during NMES-induced contractions, however, this difference does not reach statistical significance ($p = 0.19$) and only a small effect size is seen ($d = 0.35$).

P-values and effect sizes for pixel difference measurements are shown in Table 7.9. The reduction in pixel difference, both maximum (Figure 7.16c) and total (Figure 7.16e), between able-bodied and SCI participants is statistically significant and in the case of total pixel difference is accompanied by a large effect size. The total pixel difference during different phases of the contraction is shown in Figures 7.16b, 7.16d and 7.16f, suggesting that the biggest difference between able-bodied and SCI participants occurs during the ramp down phase. This is the only phase which shows a significant difference or a large effect size.

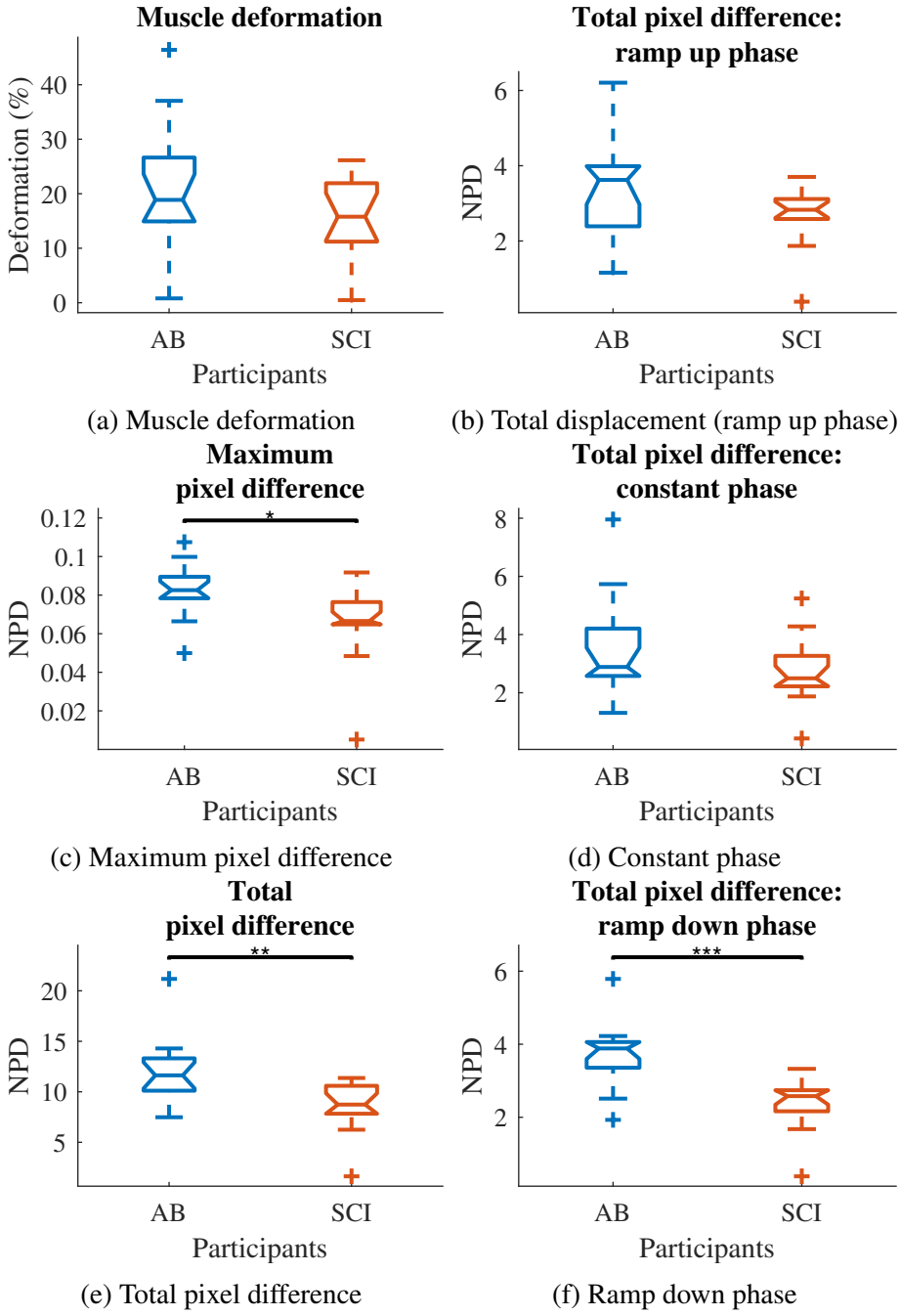

(a) Muscle deformation

(b) Total displacement (ramp up phase)

(c) Maximum pixel difference

(d) Constant phase

(e) Total pixel difference

(f) Ramp down phase

Figure 7.16: Boxplots of USI measurements of muscle movement including deformation, maximum pixel difference and total pixel difference during different phases of NMES-induced contraction for able-bodied and SCI participants.

Table 7.9: P-value and effect size for pixel difference measurements of muscle movement during NMES for able-bodied and SCI participants. Values indicating a significant difference or a greater than medium effect size are shown in bold.

Maximum Pixel Difference		
	P-Value	*Effect Size*
	0.02	0.71
Total Pixel Difference		
	P-Value	*Effect Size*
Full contraction	**0.002**	**0.91**
Ramp up	0.11	0.46
Constant	0.19	0.39
Ramp down	**< 0.001**	**1.19**

P-values and effect sizes of muscle displacement measurements are shown in Table 7.10. Maximum and total muscle displacement, shown in Figure 7.17, is also less in SCI participants compared to able-bodied with significant differences which can be seen at all positions of the muscle. Displacement is higher in superficial regions of the muscle and is uniform in the proximal to distal direction.

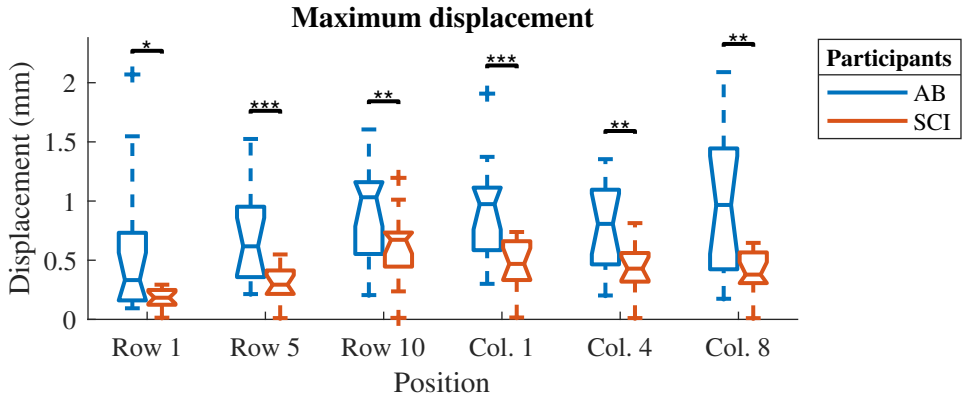

(a) Maximum displacement

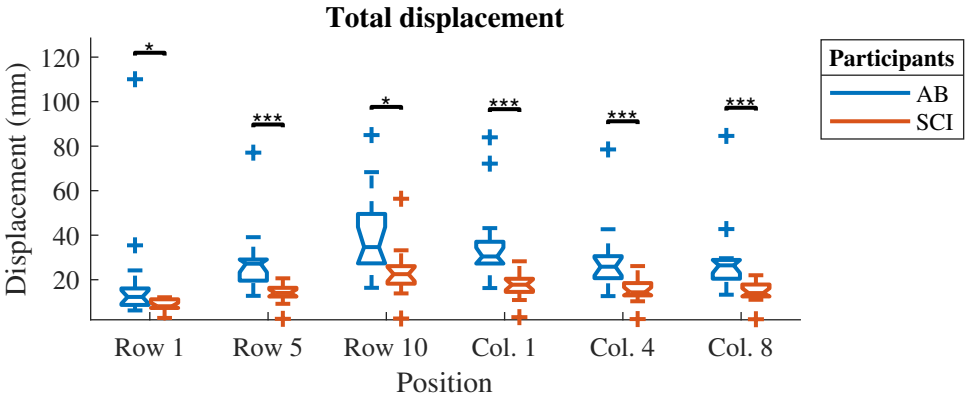

(b) total displacement

Figure 7.17: Boxplots of muscle displacement during NMES-induced contraction for able-bodied and SCI participants.

Figure 7.18 shows the total muscle displacement during each phase of the contraction. In contrast to the pixel difference results, total displacement is statistically significantly less in SCI participants compared to able-bodied for all phases of the contraction at some positions of the muscle. However, the ramp down phase shows larger effect sizes and is the only phase which shows a significant difference at all positions of the muscle.

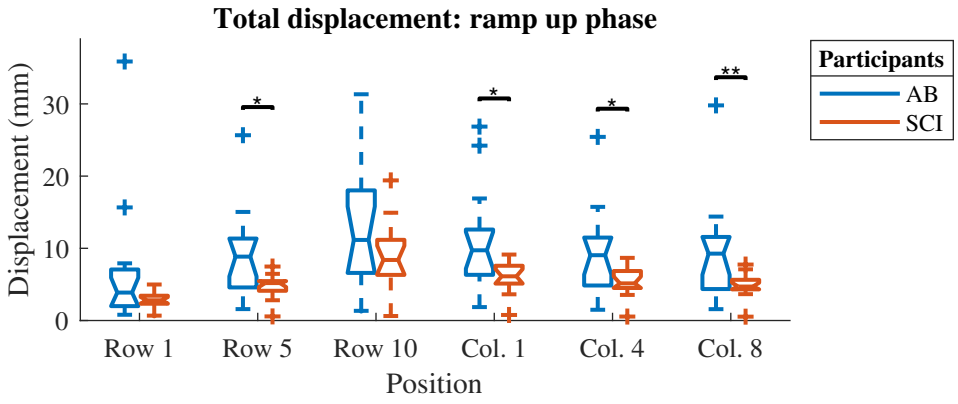

(a) Ramp up phase

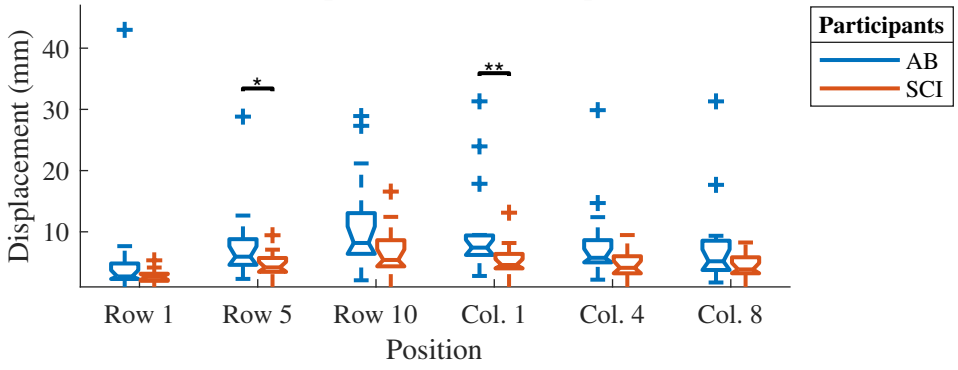

(b) Constant phase

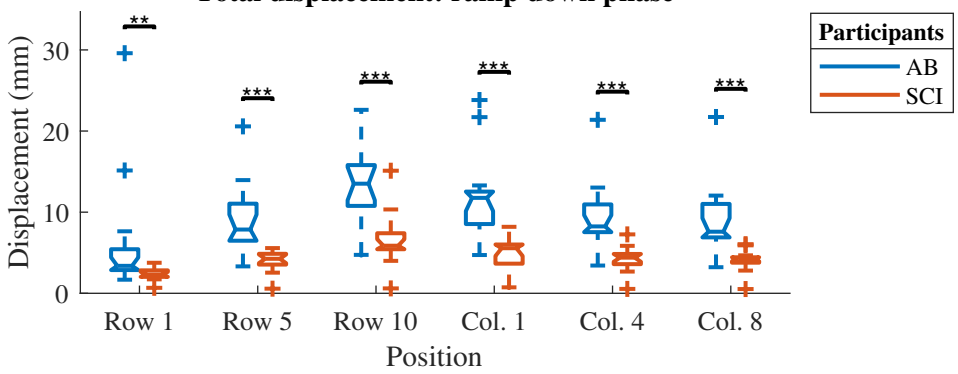

(c) Ramp down phase

Figure 7.18: Boxplots of total muscle displacement during different phases of NMES-induced contraction for able-bodied and SCI participants.

Table 7.10: P-values and effect sizes for displacement measurements of muscle movement during NMES for able-bodied and SCI participants. Values indicating a significant difference or a greater than medium effect size are shown in bold.

Maximum Displacement: Full Contraction		
	P-Value	*Effect Size*
Row 1	**0.03**	0.65
Row 5	**< 0.001**	**1.08**
Row 10	**0.01**	**0.85**
Column 1	**< 0.001**	**1.21**
Column 4	**0.001**	**1.05**
Column 8	**0.002**	**0.99**
Total Displacement: Full Contraction		
	P-Value	*Effect Size*
Row 1	**0.03**	0.42
Row 5	**< 0.001**	**0.96**
Row 10	**0.01**	**0.81**
Column 1	**< 0.001**	**1.03**
Column 4	**< 0.001**	**0.92**
Column 8	**< 0.001**	0.79
Total Displacement: Ramp up		
	P-Value	*Effect Size*
Row 1	0.19	0.40
Row 5	**0.01**	0.73
Row 10	0.09	0.47
Column 1	**0.02**	0.70
Column 4	**0.02**	0.68
Column 8	**0.01**	0.63
Total Displacement: Constant		
	P-Value	*Effect Size*
Row 1	0.30	0.31
Row 5	**0.04**	0.49
Row 10	0.17	0.46
Column 1	**0.01**	0.62
Column 4	0.06	0.50
Column 8	0.14	0.42
Total Displacement: Ramp down		
	P-Value	*Effect Size*
Row 1	**0.002**	0.51
Row 5	**< 0.001**	**1.29**
Row 10	**< 0.001**	**1.33**
Column 1	**< 0.001**	**1.34**
Column 4	**< 0.001**	**1.29**
Column 8	**< 0.001**	**1.08**

7.4.4.3 Torque measurements

The results in this section are based on the torque produced during single pulses to elicit a twitch, and tetanic contractions at a frequency of 20 Hz and 80 Hz (see Section 3.3.4.3 of Chapter 3). During the twitches, the torque value ranged from 0.17 to 1.35 Nm in the able-bodied group and 0.68 to 9.64 Nm in the SCI group; during the tetanic contraction at 20 Hz the torque produced ranged from 0.68 to 9.64 Nm in the able-bodied group, and 0.03 to 17.42 Nm in the SCI group; and during the tetanic contraction at 80 Hz, the torque produced ranged from 1.23 to 13.79 Nm in the able-bodied group and 0.27 to 27.28 Nm in the SCI group. P-values and effect size for all measurements of torque are shown in Table 7.11.

Figure 7.19 compares the twitch-tetanus ratio for able-bodied and SCI participants at both 20 Hz and 80 Hz. In both cases the SCI group showed a significantly higher twitch-tetanus ratio however the effect size is larger for the tetanic contraction at 80 Hz.

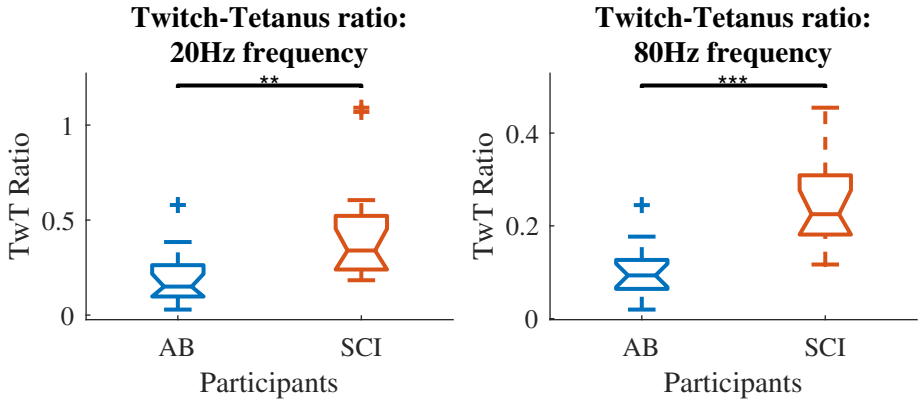

(a) Frequency = 20 Hz (b) Frequency = 80 Hz

Figure 7.19: Boxplots of the twitch-tetanus ratio for able-bodied and SCI participants.

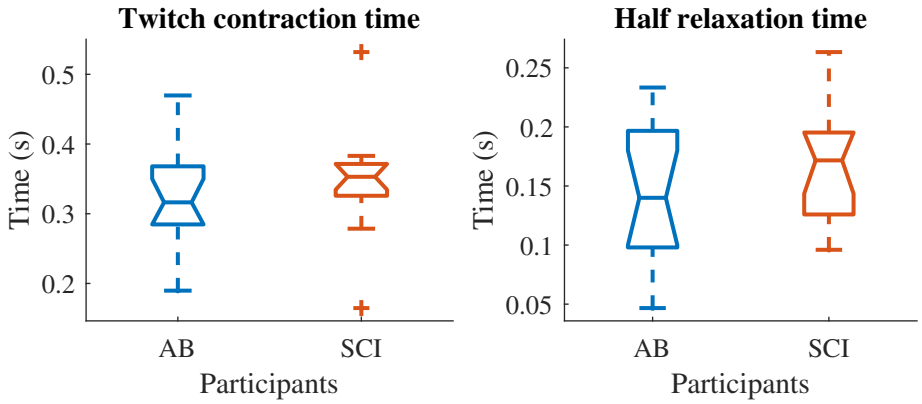

(a) Twitch contraction time (b) Twitch half-relaxation time

Figure 7.20: Boxplots of torque measurements during a muscle twitch elicited by a single pulse for able-bodied and SCI participants.

The twitch contraction time, shown in Figure 7.20a, and the half-relaxation time, shown in Figure 7.20b, show no differences between able-bodied and SCI participants. There are no significant differences and effect sizes are small.

As shown in Figure 7.21, stimulation efficiency is lower for SCI participants compared to able-bodied. Statistical significance and large effect sizes are seen for the tetanic contractions.

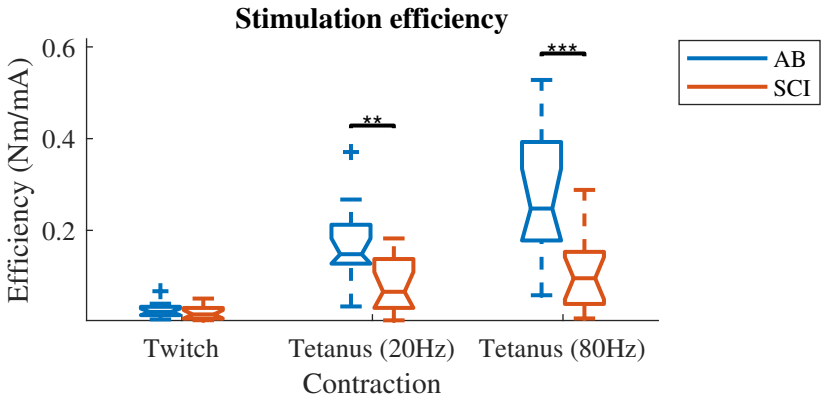

Figure 7.21: Boxplots of stimulation efficiency during muscle twitch and tetanic contractions for able-bodied and SCI participants.

Table 7.11: P-values and effect sizes for torque measurements of able-bodied and SCI participants during the application of NMES. Values indicating a significant difference or a greater than medium effect size are shown in bold.

	Twitch-tetanus ratios	
	P-Value	*Effect Size*
20 Hz	**0.003**	0.71
80 Hz	**< 0.001**	**1.23**
	Twitch measurements	
	P-Value	*Effect Size*
Contraction time	0.46	0.23
Half-relaxation time	0.22	0.33
	Stimulation efficiency	
	P-Value	*Effect Size*
Twitch	0.64	0.18
Tetanus 20Hz	**0.01**	**0.85**
Tetanus 80Hz	**< 0.001**	**1.10**

7.5 Discussion

In this chapter ultrasound videos of the gastrocnemius muscle were recorded during the application of electrical stimulation under different conditions. Different combinations of stimulation parameters were applied to better understand the effect of current, pulsewidth and inter-pulse interval of muscle behaviour; stimulation consisting of variable pulsewidth and variable inter-pulse interval were used to assess the effect of stimulation patterns on recruitment of muscle fibres; similarly different multi-electrode spatially distributed patterns delivered stimulation in sequential and random order to investigate if this more closely mimicked voluntary muscle activation; finally, the application of electrical stimulation was compared between healthy participants and those with a SCI to assess the differences between healthy muscles and those affected by paralysis. In all cases measurements of muscle movement were obtained using tracking software and the pixel difference method.

7.5.1 Effect of stimulation parameters on muscle behaviour

In general, an increase in current or pulsewidth leads to an increase in muscle movement. This is to be expected as increasing these parameters increases the number of motor units being recruited. High amplitude current produces a stronger depolarising effect and an increase in pulsewidth increases the depth of penetration [13, 36]. The overall charge delivered to the muscle is dependent on both of these parameters, therefore an increase in either one increases the amount of motor unit recruitment. The biggest changes occur when one of these parameters is at its minimum level and the other increases.

Muscle deformation only shows differences between high and low pulsewidth values at the minimum current and similarly differences between the maximum and minimum current are only seen at the lowest level of pulsewidth. Once the stimulation reaches a certain intensity, the muscle has already reached its maximum deformation and any further increases in stimulation intensity cannot be seen. These results are consistent with those reported by Hodges et al. [112], which showed that measurements of muscle thickness could describe muscle activity at low levels but was not able to distinguish between higher levels of muscle activity.

Muscle displacement on the other hand, continues to show an increase in regional muscle movement at higher levels of stimulation intensity, with some large effect sizes seen between the maximum and minimum current even at the highest pulsewidth value. A possible explanation for this is that as the thickness of the muscle increases the pennation angle also increases, allowing more muscle fibres to be recruited [17]. The use of the tracking software may therefore allow USI to detect the further recruitment of muscle fibres even after it has reached its maximum change in thickness. These differences are mostly seen during the onset and offset of the stimulation. In contrast, there is little difference in muscle movement during the constant phase of the stimulation. This is because the desired contraction has already been achieved and is only

being sustained at this point. Although there are some differences between the different IPI values, it does not appear to have much of an effect on muscle movement. Current and pulsewidth therefore appear to have more of an effect on the number of motor units which are recruited.

7.5.2 Effect of time-varying stimulation parameters

7.5.2.1 Voluntary vs. NMES-induced contractions

The goal of time-varying patterns of stimulation parameters is to activate different muscle fibres and more closely mimic voluntary muscle contractions. However, the results of this study showed all measurements of muscle movement to be much smaller during voluntary contractions. This could be because voluntary muscle contractions are much more efficient and therefore less muscle fibre activation is required to produce the same level of torque. However, the deformation results show the thickness of the muscle often remains unchanged or could even decrease during voluntary contractions. This does not align with the theory of biomechanics that states muscle thickness increases as they shorten to bring about movement at a joint [17], and is different from the results of other USI studies measuring muscle CSA or thickness [103, 104]. It is possible that as USI views the muscle in two dimensions, thickness is increasing in the third dimension which can't be seen. A more likely explanation however, is that other muscles are also activated and could be producing the force. These other muscles could even be compressing the GM muscle, resulting in the negative deformation.

7.5.2.2 Variable pulsewidth and IPI patterns of stimulation

During the ramp up phase, the constant stimulation pattern resulted in more muscle movement than both variable pulsewidth and variable IPI patterns. This suggests that more motor units are recruited during constant stimulation, which agrees with the idea that this pattern of stimulation would recruit muscle fibres synchronously. As the deformation is the same across all patterns it appears that a similar level of muscle activation is achieved by the constant phase. During the constant phase the variable IPI pattern appears to cause less movement, again suggesting less muscle fibres were activated to achieve this contraction. This result is most noticeable at the central (row 5) and superficial (row 10) parts of the muscle, and at the proximal (column 1) and distal (column 8) ends. Overall variable pulsewidth and variable IPI patterns do appear to vary the muscle fibres being recruited and furthermore, USI analysis can detect differences in muscle behaviour, even if the effect is small.

7.5.3 Effect of multi-electrode spatially distributed patterns

7.5.3.1 Muscle activation

Measurements of muscle movement are generally similar across all patterns of stimulation, with no significant differences seen. In some cases there even appears to be slightly more movement in the asynchronous patterns. This would suggest that even though muscle fibres are not all being activated at the same time, a similar level of muscle activation is achieved through asynchronous stimulation.

Due to the speed of the contractions during the intermittent stimulation of the fatigue protocol, measurements of regional movement could not be obtained. Therefore we cannot comment on the pattern of activation within the muscle. This should be considered in future work, applying stimulation with different patterns continuously instead of intermittently to allow better use of tracking software.

7.5.3.2 Effect on fatigue

There is little difference between the maximum pixel difference at the start and end of the fatigue protocol for asynchronous patterns of stimulation. Synchronous stimulation, on the other hand, shows a large reduction by the end of the protocol, suggesting that there is less muscle movement and therefore less muscle fibres are being successfully recruited as the result of fatigue. This effect is seen in the total pixel difference measurement for all patterns, although to a lesser extent.

There is also an increase in the contraction time at the end of all protocols. This is a reported effect of fatigue, resulting from an increased delay between the application of stimulation and the generation of a contraction [79]. Although this is seen in all protocols the effect is larger for the synchronous pattern. The half-relaxation increases by the end of the synchronous stimulation pattern, possibly due to tendon creep [121].

The reduction in the peak-to-peak time for the CSS pattern suggests contractions are becoming shorter, again indicating the recruitment of less muscle fibres as the muscle fatigues. In contrast, the asynchronous patterns have shorter contractions throughout and do not change.

Overall, these results suggest more fatigue is occurring during conventional synchronous stimulation, compared to the asynchronous stimulation patterns. This supports the hypothesis that asynchronous stimulation patterns do vary the recruitment of muscle fibres, improving the fatigue response. It should, however, be noted that none of the differences seen reach statistical significance.

7.5.4 Electrical stimulation of muscles affected by SCI

The effects of a SCI on skeletal muscle are discussed in detail in Section 2.2.1 of Chapter 2. They include muscle atrophy, increased intramuscular fat and a fibre type transformation, which alter the contractile properties and affect the muscle's ability to generate force. Muscles after a SCI are also much less resistant to fatigue, which is a particularly important limitation as the premature onset of fatigue is seen during the use of NMES in healthy muscles. Despite this, the use of NMES is very important in rehabilitation after a SCI. It allows paralysed muscles to produce functional movements and it enables exercise which not only improves cardiopulmonary function but can also slow down or even reverse some of the structural changes which occur as the result of a SCI. Understanding the differences in muscle behaviour during the application of NMES following a SCI has the potential to improve its use in rehabilitation.

7.5.4.1 Motor unit recruitment

The amount of current required to cause a detectable movement was higher in SCI participants than in able-bodied participants. This is to be expected as animal studies have shown that motor neurons become less excitable after a SCI [66]. Furthermore, as the muscle atrophies there will be a smaller number of muscle fibres and a higher proportion of connective tissue. This combined with the increased intramuscular fat means that more current may be required to activate the remaining motor neurons.

Movement within the muscle is first seen at the lowest levels of current, measured through pixel difference and displacement. At slightly higher levels of current, a change in muscle thickness is seen (deformation) and then a measurable torque is detected. The current value at which movement is detected by displacement and deformation is much higher in the SCI group compared to the able-bodied. Pixel difference on the other hand, detects muscle movement in SCI participants at a level of current which is only slightly higher than in the able-bodied group. This could indicate that some motor neurons are activated in SCI at a similar level to able-bodied, but a higher level of current is required to activate enough motor neurons to produce a visible movement or a strong contraction.

It is therefore not surprising that the optimal current value, which is selected to produce the maximum possible torque, was also significantly higher in the SCI group. Again this could be explained by the reduced excitability of muscle fibres, or muscle atrophy could result in less muscle fibres and therefore a higher number of motor units would be required to produce the required torque. This coincides with a reduction in stimulation efficiency, which was found to be much lower in the SCI group.

7.5.4.2 Muscle movement

The amount of muscle deformation is slightly smaller in the SCI group, despite the application of a higher level of current. The reduction in the number of muscle fibres or the decreased ability to recruit motor units could explain this as less activated muscle fibres would result in less movement of the muscle. This also coincides with reduced force production which is widely reported in the use of NMES on people with a SCI [68, 71–76].

Similarly, movement within the muscle, based on measurements of displacement and pixel difference, was also less in the SCI group. However, the biggest differences are seen in the ramp down phase of the contraction when the stimulation intensity is gradually reduced to zero. Therefore this could be caused by the able-bodied participants voluntarily returning to the original position. In general SCI participants had reduced sensation and would not react to changes in intensity.

7.5.4.3 Contractile properties

The increase in the twitch-tetanus ratio in the SCI group could be the result of motor neuron sprouting. As the number of motor units decreases, motor neurons sprout to reinnervate the denervated muscle fibres, leading to larger motor units which produce a larger force and therefore a larger twitch value [39].

The speed of muscle contraction is widely reported to increase in the chronic stage of a SCI as the result of a fibre transformation from slow-twitch to fast-twitch [68, 72, 76]. The twitch contraction and relaxation times are only slightly increased compared to the able-bodied group and do not show any significant differences. This might be due to the fact that measurements in the SCI group are taken at different times post-injury and the fibre transformation is not thought to occur until several months after injury [42].

7.6 Conclusion

In conclusion, USI has been shown to be a useful tool for gaining further insight into muscle behaviour during the application of NMES. It is able to differentiate between different levels of stimulation intensity, allowing a quantitative measurement of the level of muscle activation produced by the stimulation. It is also capable of providing additional information about muscle behaviour during different patterns of stimulation, both through variations in the stimulation parameters themselves and different spatially distributed patterns. There are some limitations to the results presented in this chapter, mainly that due to the activation of other muscles, stimulation conditions could not be compared to voluntary contractions. There is also limited analysis of muscle behaviour during spatially distributed patterns of stimulation. Nonetheless, USI has potential to be an extremely useful tool during the development of new stimulation protocols

designed to optimise performance and reduce fatigue. It also shows differences between the behaviour of healthy muscles and those affected by a SCI, showing that it could also be useful during the development of rehabilitation interventions. By providing measurements which describe muscle behaviour, the effect of the stimulation can be better understood and the amount of muscle activation can be measured.

Chapter 8

Discussion

This PhD project aimed to investigate the suitability of ultrasound imaging (USI) as a diagnostic tool for the assessment of muscles following a spinal cord injury (SCI). It also aimed to evaluate the use of USI to gain further understanding of muscle behaviour during the rehabilitation technique of neuromuscular electrical stimulation (NMES). The main findings are summarised in this chapter.

8.1 Detection of changes in muscle structure

USI has previously been shown in the literature to be a useful technique to screen for neuromuscular disorders by detecting changes in muscle structure. In the months following a SCI, changes in the muscle structure occur which are similar to those seen in neuromuscular disorders, specifically muscle atrophy and the accumulation of intramuscular fat. In Chapter 4, the ability of USI analysis to detect these changes is discussed, with particular emphasis on whether or not USI parameters can differentiate not only between healthy muscles and those affected by a SCI, but also between SCI participants at different times post-injury. Tracking software was used to obtain measurements of muscle thickness to describe the size of the muscle, and greyscale analysis was used to provide measurements of muscle echogenicity and echotexture.

A reduction in muscle thickness is seen within the SCI group compared to the able-bodied control group. This is in agreement with atrophy of the muscle, which is defined as a reduction in the size and number of muscle fibres, therefore it follows that the size of the muscle would decrease. Thickness does not appear to further decrease with time, suggesting that atrophy occurs rapidly in the first 1-2 months after injury, before data was obtained. It is also possible that the infiltration of intramuscular fat contributes to the preservation of muscle bulk, therefore measurements of muscle thickness may be more useful in the more acute stage after injury.

A SCI also leads to an increase in muscle echogenicity which continues to increase with time after injury. First-order statistical descriptors measure the brightness of the image within the region of interest, which increases due to a higher number of reflective surfaces resulting

from a higher proportion of fibrous tissue and intramuscular fat. These measurements use the pixel intensity values to describe the amount of non-contractile elements within the muscle, however, they do not take into account the spatial arrangement of the pixels. This means that muscles could have a similar echogenicity but the structure could be very different. Moreover, first-order descriptors are dependent on the ultrasound device and scan settings, limiting their application in a clinical environment.

Second-order statistical descriptors, on the other hand, are free from such limitations and describe the spatial arrangement of pixels to provide measurements of echotexture, and therefore provide a greater insight into the composition of the muscle. An increase in muscle homogeneity is shown through the Haralick and local binary pattern features. This means that there is a more equal distribution of light and dark pixels, indicating a breakdown in the normally well-organised structure of the muscle. The Galloway features showed an increase in coarseness, which suggests that this breakdown in muscle structure is not occurring evenly across the muscle. This could be explained by incomplete spinal cord injuries affecting different motor units, which in turn affects different areas of the muscle in a similar way to neuropathies.

In summary, a reduction in muscle thickness consistent with atrophy can be seen for SCI participants, along with increased echogenicity, most likely due to an increase in intramuscular fat and fibrous tissue. Furthermore, measurements of muscle echotexture show an increase in homogeneity that suggests a breakdown in muscle structure, while increased coarseness indicates that these structural changes do not occur evenly throughout the muscle. These USI measurements which describe muscle structure can differentiate between able-bodied and SCI participants, and measurements of echogenicity and echotexture can even differentiate between different times post-injury.

8.2 Characterisation of muscle functional status

The dynamic nature of USI is a great advantage over other imaging modalities. It allows changes in muscle architecture to be measured during movement, which have been shown to be related to the amount of activation and the strength of the contraction. This makes it a potential tool for assessing the functional status of muscles affected by a SCI, and therefore varying degrees of muscle paralysis. Muscle function is currently assessed by a physical exam, however, there is a need for more sensitive and objective measurements. Chapter 5 discusses the suitability of USI to provide additional information on muscle functional status by evaluating the ability of different USI parameters to differentiate between different levels of torque and EMG. Tracking software provided measurements of muscle deformation and regional displacement while the pixel difference method provided a simpler alternative for measuring movement within the muscle based on the pixel intensity values.

Muscle deformation showed some differences between able-bodied and low levels of func-

tion, however, its ability to differentiate between different levels within the SCI group is very limited. This can be explained in part by the fact that very small movements within the muscle will not be enough to result in thickness changes. Conversely, during contractions above a certain torque level there is little further change in muscle thickness, therefore deformation can differentiate between large differences in muscle function, but cannot detect subtle differences.

Muscle displacement, on the other hand, can differentiate between different levels of function within the SCI group, with the biggest differences seen at the superficial part of the muscle. The pixel difference method, which is simpler and computationally more efficient, provides similar information to displacement. The pixel difference method is based on changes in intensity values at the pixel level and displacement is based on the movement of features within the image. As a result, the pixel difference method appears to be slightly more sensitive in detecting small movements but is limited above a certain level of contraction. This suggests that the pixel difference method could provide a simpler alternative but it may be more suited to low level contractions. Perhaps as a result of this, displacement appeared to be better at differentiating between different levels of torque, while the pixel difference method was more in line with different levels of EMG.

As well as quantifying movement, these measurements of displacement and pixel difference are also used to calculate the speed of the muscle contraction. In general, speed was found to decrease with muscle function, which differed from the expected results. The transformation from slow-twitch to fast-twitch muscle fibres which occurs after a SCI is generally accepted to lead to an increase in muscle contractility, however, this may be more related to the time since injury occurred than the level of function.

Measurements of muscle structure discussed in the previous section are also compared between SCI groups with different levels of function. The thickness of the muscle is smaller in SCI participants with low levels of function, compared to those with high levels of function. This is consistent with the idea that muscles with less function undergo more atrophy. Furthermore, muscle size has been shown in the literature to be related to strength. It should be noted that this reduction in muscle thickness could still be underestimated due to the accumulation of intramuscular fat. Muscle structure was otherwise unaffected by the level of muscle function, with echogenicity showing similar results across all groups. This is consistent with the idea that atrophy is affected by other factors such as load bearing and muscle shortening.

In summary, USI is able to provide measurements of muscle movement that can differentiate between different levels of muscle function. This is limited for measurements of deformation, but successful for measurements of displacement. Furthermore, the pixel difference method may offer a simpler and more computationally efficient method to provide similar results. The only measurement describing muscle structure which appeared to be related to functional status is the resting thickness.

8.3 Feasibility of assessing and predicting recovery

Chapters 4 and 5 discuss the use of USI to assess muscle structure and function by evaluating its ability to differentiate between able-bodied and SCI participants, and different groups of SCI participants based on time post-injury and the level of function. It must also be considered, however, that changes resulting from a SCI occur months and even years after the injury. It is therefore also important to assess changes in the muscle throughout the recovery period. This allows progress to be monitored and the success of rehabilitation interventions to be evaluated. USI has previously been used to measure changes in the muscle both as the result of exercise and disuse. Chapter 6 investigates changes in USI measurements for individuals over time.

There are some differences in the measurements of muscle structure which suggest that the effects of atrophy may be greater in participants who did not show recovery, while these effects may be lessened to some degree for participants who did show some recovery. However, there are also several measurements which did not show any differences between the recovery and non-recovery groups. This indicates that atrophy occurs to some degree regardless of recovery. Again, this could be due to other factors besides muscle function, such as load bearing or muscle shortening, particularly as all participants were wheelchair users for the duration of the study.

Pixel difference measurements obtained during attempted isotonic contractions in 6 muscles (gastrocnemius medialis, tibialis anterior and rectus femoris in the right and left legs) of 6 SCI participants, are in agreement with the manual muscle test (MMT) scores obtained from a trained physiotherapist. Muscles which showed no movement or recovery based on the MMT scores showed no movement and no changes between sessions in the USI measurements. In contrast, muscles which showed an improvement in MMT score between sessions showed an increase in USI measurements. Moreover, the bigger the change in MMT scores, the bigger the increase in the USI measurement, suggesting USI can not only detect changes that indicate recovery, but it can actually quantify the amount of recovery. Indeed, USI measurements can differentiate between no change in MMT score, a small change in the MMT score and a large change in the MMT score.

Results of two individual participants also support the idea that these measurements of USI could detect improvements in muscle movement before it is seen in the MMT score. Some muscles showed an increase in USI measures between sessions while the MMT score remained unchanged, and in subsequent sessions a further improvement in the MMT score was seen. These results suggest that USI measurements may even be able to detect a very small muscle movement before it is detected by MMT. It must be noted, however, that these results are seen for a small number of individual participants where no statistical analysis can be performed.

Other measurements of muscle movement obtained over several sessions from 15 SCI participants during attempted isometric maximum voluntary contractions showed some differences consistent with recovery. However, these results did not reach statistical difference and several measurements showed no differences between the first and last session. This may be due to

smaller muscle movements during isometric contractions or it could be because the first measurements were not obtained until several months after injury. Assessment of recovery appears to be more successful when initial measurements are obtained during the acute phase.

Overall, measurements of muscle structure and movement obtained during Study 1 show little correlation with improvements in muscle function. This may be due to several factors including the time post-injury measurements were obtained and the type of contraction being performed. However, measurements of muscle movement obtained during Study 2 show high agreement with recovery based on MMT scores and may even show improvements before they can be seen by traditional methods. These results are promising but are limited by the small sample size.

8.4 Muscle behaviour during the application of neuromuscular electrical stimulation

NMES is a rehabilitation technique which allows the artificial contraction of paralysed muscles, thereby allowing functional movements and exercise to be performed. Despite the wide range of applications, its use is limited due to the early onset of fatigue, which is thought to be due to the differences in muscle fibre recruitment compared to voluntary contractions. Although it is generally accepted that NMES-induced contractions do not follow the conventional size principle, the exact mechanisms of fibre recruitment are still unclear. USI provides a potential additional tool to gain further insight into the behaviour of the muscle during the application of NMES. Chapter 7 discusses the differences in USI parameters, which describe muscle movement, under different conditions of NMES.

The most common way to control the stimulation applied is to modulate the stimulation parameters. An increase in current or pulsewidth resulted in increased muscle movement. This is expected as high amplitude current has a strong depolarising effect and the depth of penetration increases with pulsewidth, therefore an increase in either of these parameters increases the number of motor units being recruited. Changes in muscle deformation are only seen when one of these parameters is low and the other is increased. Once stimulation is above a certain intensity, a further increase does not cause any more muscle deformation, which is consistent with findings in the literature that changes in thickness cannot differentiate between higher levels of activity. Displacement, on the other hand, shows more differences between different levels of stimulation intensity even at higher levels. This suggests that the tracking of regional movement within the muscle allows the recruitment of further muscle fibres to be detected, even when the maximum deformation has been reached.

A limitation of NMES-induced contractions compared to voluntary contractions is the repetitive activation of the same motor units. Attempts to reduce fatigue during NMES have therefore often focused on varying the motor units which are being recruited. One way to do this

is to vary the stimulation parameters with time. Patterns of stimulation which varied the inter-pulse interval (IPI) and the pulsewidth were compared to conventional stimulation and voluntary contractions. The goal was to mimic voluntary contractions, however, all stimulation patterns resulted in much higher levels of muscle movement than voluntary contractions. Comparisons between voluntary and NMES-induced contractions are limited due to co-activation of muscles during voluntary contractions. The variable pulsewidth and IPI patterns do, however, show less displacement than conventional stimulation patterns. This suggests that less muscle fibres are recruited during these variable patterns, and as the deformation is constant across all patterns it appears the same level of activation is achieved.

Another method for activating different muscle fibres is the use of multi-electrode spatially distributed patterns. Asynchronous stimulation delivered in sequential and random patterns showed similar muscle movement to conventional stimulation, suggesting that even though all muscle fibres were not being recruited at the same time, a similar level of muscle activation is achieved. Furthermore, changes in measurements of muscle movement, as well as contraction and relaxation times, between the start and end of the fatigue protocol all suggest that more muscle fatigue has occurred during the conventional synchronous stimulation pattern. Further research is required however, USI analysis has shown to be capable of differentiating between these different patterns of stimulation, therefore it could be useful in providing information about muscle behaviour during the optimisation of NMES protocols.

Much of the research on improving the use of NMES is carried out on healthy muscles, however, the final applications are for people with paralysed muscles such as those who have suffered a SCI. As previously discussed, there are many changes which occur in the muscle following a SCI, altering their contractile properties and ability to generate force. They are also less resistant to fatigue. It is therefore important to understand the differences in muscle behaviour during the application of NMES following a SCI. More current was required to cause a detectable movement in SCI participants, possibly due to neurons becoming less excitable, or the increase in intramuscular fat and fibrous tissue which the current has to penetrate to reach the neurons. However, the pixel difference method appears to detect movement in SCI participants at a level only slightly higher than in able-bodied participants. This could indicate that some motor neurons are activated in SCI at a similar level to able-bodied, but a higher level of current is required to activate enough motor neurons to produce a visible movement or strong contraction. The amount of muscle movement is slightly smaller in the SCI group, despite the application of a higher level of current. The reduction in the number of muscle fibres or the decreased ability to recruit motor units could explain this as less activated muscle fibres would result in less movement of the muscle. This also coincides with reduced force production which is widely reported in the use of NMES on people with a SCI.

In summary, USI measurements of muscle movement could differentiate between different stimulation intensities during the application of different combinations of stimulation parame-

ters; they could detect differences between different patterns of stimulation created by varying stimulation parameters with time or through a multi-electrode configuration to vary the spatial distribution; and finally, USI measurements were able to show differences between muscles of able-bodied and SCI participants. Overall, this demonstrates the use of USI to provide further insight into muscle behaviour during the application of NMES.

8.5 Summary

Overall, USI has shown great potential as a diagnostic tool for assessing muscles following a SCI. Measurements of muscle size, obtained from tracking software, and measurements of muscle echogenicity and echotexture, obtained through greyscale analysis, describe structural changes in the muscle. These measurements can differentiate between able-bodied and SCI groups, as well as different times post-injury. Measurements of muscle movement, obtained from tracking software and the pixel difference method, can differentiate between different levels of muscle function. Furthermore, changes in USI measurements of muscle movement in acute SCI patients agree with improvements in muscle function based on MMT scores. This demonstrates the potential of USI to monitor recovery, and may even show improvements earlier than traditional assessment methods.

USI has also been shown to provide insight into muscle behaviour during the application of NMES. Measurements of muscle movement can show differences between different levels of stimulation intensity and different patterns of stimulation, both through varying parameters with time and varying the spatial distribution of stimulation. It can also show differences between the application of NMES in healthy muscles and those affected by a SCI. USI could therefore be used to provide further information on muscle behaviour when developing NMES protocols for rehabilitation.

Chapter 9

Conclusions and Future Work

9.1 Conclusions

The main aim of the PhD project was to investigate the suitability of ultrasound imaging (USI) as a diagnostic tool for the assessment of muscles following a spinal cord injury (SCI). Measurements of muscle thickness were obtained from the tracking software, and greyscale analysis was performed on the pixel intensity values to obtain measurements of echogenicity and echotexture. These measurements were compared between an able-bodied group and a SCI group at different times post-injury, resulting in the following findings:

- Muscle thickness decreases following a SCI. This change appears to occur rapidly within the first month after injury.
- Echogenicity increases with time after a SCI, representing an increase in the amount of non-contractile components.
- Homogeneity increase with time after a SCI, describing the breakdown in muscle structure.
- Coarseness increases with time after a SCI, indicating changes in muscle structure are uneven and dependent on the motor units affected.
- These USI measurements can differentiate between SCI participants at different times post-injury.

Measurements of muscle movement were obtained, including muscle deformation and regional displacement from the tracking software, and the pixel difference based on pixel intensity values. These measurements were compared between an able-bodied group and SCI participants with different levels of muscle function, leading to the following findings:

- Resting thickness is related to the amount of torque the muscle can produce.

- Echogenicity is not related to function.
- Deformation can only differentiate between large differences in function as it is limited by co-activation of muscles.
- Displacement provides sensitive measurements of regional movement within the muscle which can differentiate between levels of function.
- Pixel difference is similar to displacement and can provide comparable results but may be limited to low levels of movement.

Measurements of muscle structure and movement were also compared over time for individual participants. This lead to the following findings:

- The pixel difference method appears to be successful in showing changes in muscle movement consistent with assessment by conventional manual muscle testing, however, further research is required.
- The pixel difference method may even be able to detect subtle changes or very small movements that are not detected by traditional methods.
- Assessing recovery is more successful when initial measurements are obtained during the acute phase.

Measurements of muscle movement were also obtained during the application of NMES under different conditions, to investigate the use of USI to gain further insight into muscle behaviour. The following findings were obtained:

- USI measurements of muscle movement can differentiate between different levels of stimulation intensity.
- These USI measurements can also detect differences in different stimulation patterns including variations in the parameters themselves and variations in the spatial distribution using multi-electrode configurations.
- Differences in muscle behaviour between healthy muscles and those affected by a SCI can also be detected by USI measurements.

9.2 Future work

The work carried out in this PhD project provides the basis for the use of USI in a clinical setting for the assessment of muscles following a SCI. It also demonstrates the potential for USI to provide insight into muscle behaviour during the application of NMES. Future work should therefore mainly focus on refining the protocol for clinical assessment of muscles, however, there is potential for further research to optimise NMES in rehabilitation applications.

9.2.1 Clinical assessment of muscles

This thesis provides analysis techniques for the assessment of muscle structure and function. These techniques should be further analysed in a larger group, with a more comprehensive range of muscle function for SCI of varying severity and at different times post-injury. It would be beneficial to include measurements obtained as soon as possible after injury, to provide more data from the acute phase of the injury. Furthermore, much of the analysis in this thesis focused on the gastrocnemius muscle. Further work should also include a range of different muscles, particularly as the pixel difference method can provide similar measurements to displacement without the restrictions of the tracking software.

Measurements of muscle structure, such as resting thickness and echogenicity, could be used to provide a database of normal values. This has been done for other neuromuscular disorders, however, it must also be noted that there are several factors which affect these measurements such as age, gender and general fitness before injury. The individual nature of SCI may also make this challenging and for this reason, measurements of muscle movement may be more useful for determining whether or not movement is present, or for monitoring the progress of recovery. The detection of small changes which precede measurable improvements in function could provide useful information for physiotherapists when determining the most appropriate rehabilitation strategy. These changes in individual muscles can be considered general indicators of whole limb recovery and therefore allow an insight into the effectiveness of an intervention at an earlier point in time. Furthermore, signs of improvement can be motivational for the patients themselves, encouraging them to engage fully in rehabilitation activities.

Part of the work in this thesis did take steps towards a protocol which was more closely aligned with clinical assessment. During Study 2 (see Section 3.4 of Chapter 3), measurements were obtained at the bedside and included different muscles in the lower legs. However, this was only done for 6 participants and should be verified with a larger sample size. Furthermore, some limitations to this protocol were identified, the main one being that the ultrasound probe was handheld throughout, potentially introducing a source of variability.

The protocol could therefore be further refined to ensure the best results are achieved. It is also worth noting that the protocol was developed for research purpose, with electromyography and changes in joint angle recorded for comparison, and complicated offline analysis. A major component of any further research should be the implementation of this technique in a clinical environment. This should involve making the process as user friendly as possible and automating the analysis of the US videos.

9.2.2 Optimisation of NMES in rehabilitation interventions

The work in this thesis demonstrates the ability of USI to differentiate between different conditions during the application of NMES. Further work should employ the analysis techniques

in this thesis to optimise the use of NMES in a rehabilitation intervention. For example, by using USI to ensure the maximum possible muscle activation is achieved. The success of USI techniques to improve performance should be validated against measurements such as the time taken for fatigue to occur or the maximum force output.

Bibliography

[1] J. T. Bushberg and J. M. Boone, *The essential physics of medical imaging*. USA: Lippincott Williams & Wilkins, 3rd ed., 2012.

[2] R. Seeley, C. VanPutte, J. Regan, and A. Russo, *Seeley's anatomy & physiology*. New York, USA: McGraw-Hill, 9th ed., 2011.

[3] S. C. Kirshblum, S. P. Burns, F. Biering-Sórensen, W. Donovan, D. E. Graves, A. Jha, M. Johansen, L. Jones, A. Krasssioukov, M. J. Mulcahey, M. Schmidt-Read, and W. Waring, "International standards for neurological classification of spinal cord injury (revised 2011)," *The Journal of Spinal Cord Medicine*, vol. 34, no. 6, pp. 535–546, 2011.

[4] R. T. Abresch, J. J. Han, and G. T. Carter, "International standards for the classification of spinal cord injury, motor exam guide," 2008.

[5] R. Ruslee, J. Miller, and H. Gollee, "Investigation of different stimulation patterns with doublet pulses to reduce muscle fatigue," *Journal of Rehabilitation and Assistive Technologies Engineering*, vol. 6, 2019.

[6] M. Armentano, *In vivo investigation of muscle behaviour during voluntary and electrically induced muscle contraction using B-Mode ultrasound imaging.* PhD thesis, University of Glasgow, United Kingdom, 2016.

[7] F. Molinari, C. Caresio, U. R. Acharya, M. R. K. Mookiah, and M. A. Minetto, "Advances in quantitative muscular ultrasonography using texture analysis of ultrasound images.," *Ultrasound in Medicine and Biology*, vol. 41, no. 9, pp. 2520–2532, 2015.

[8] A. J. Sosnowska, *Diagnostics and biofeedback training of motor activity based on electroencephalography (EEG) and ultrasound imaging (USI).* PhD thesis, University of Glasgow, United Kingdom, 2018.

[9] M. F. Bear, B. W. Connors, and M. A. Paradiso, *Neuroscience exploring the brain*. USA: Lippincott Williams & Wilkins, 3rd ed., 2007.

[10] W. D. McArdle, F. I. Katch, and V. L. Katch, *Exercise physiology: Nutrition, energy and human performance*. USA: Lippincott Williams & Wilkins, 7th ed., 2010.

[11] N. A. Silva, N. Sousa, R. L. Reis, and A. J. Salgado, "From basics to clinical: a comprehensive review on spinal cord injury," *Progress in Neurobiology*, vol. 114, no. 1, pp. 25–27, 2014.

[12] C. S. Sherrington, "Remarks on some aspects of reflex inhibition," *Proc. R. Soc. Lond.*, vol. 97, pp. 519–545, 1925.

[13] C. S. Bickel, C. M. Gregory, and J. C. Dean, "Motor unit recruitment during neuromuscular electrical stimulation: a critical appeaisal," *European Journal of Applied Physiology*, vol. 111, pp. 2399–2407, 2011.

[14] H. P. Clamman, "Motor unit recruitment and the gradiation of muscle force," *Physical Therapy*, vol. 73, no. 12, pp. 830–843, 1993.

[15] H. Huxley and J. Hanson, "Changes in the cross-striations of muscle during contraction and stretch and their structural interpretation," *Nature*, vol. 173, no. 4412, pp. 973–976, 1954.

[16] R. L. Lieber and S. C. Bodine-Fowler, "Skeletal muscle mechanics: implications for rehabilitation," *Physical Therapy*, vol. 73, no. 12, pp. 844–856, 1993.

[17] V. M. Zatsiorsky and B. I. Prilutsky, *Biomechanics of skeletal muscle*. Human Kinetics, 2012.

[18] R. L. Lieber and J. Fridén, "Clinical significance of skeletal muscle architecture," *Clinical Orthopaedics and Related Research*, no. 383, pp. 140–151, 2001.

[19] D. McDaid, A. Park, A. Gall, M. Purcell, and M. Bacon, "Understanding and modelling the economic impact of spinal cord injuries in the united kingdom," *Spinal Cord*, vol. 57, pp. 778–788, 2019.

[20] K. Nas, L. Yazmalar, V. Şah, A. Aydin, and K. Öneş, "Rehabilitation of spinal cord injuries," *World Journal of Orthopedics*, vol. 6, no. 1, pp. 8–16, 2015.

[21] L. D. Hachem, C. S. Ahuja, and M. G. Fehlings, "Assessment and management of acute spinal cord injury: From point of injury to rehabilitation," *The Journal of Spinal Cord Injury Medicine*, vol. 40, no. 6, pp. 665–675, 2017.

[22] R. J. Marino, T. Barros, F. Biering-Sorensen, S. P. Burns, W. H. Donovan, D. E. Graves, M. Haak, L. M. Hudson, and M. Priebe, "International standards for neurological classification of spinal cord injury," *The Journal of Spinal Cord Medicine*, vol. 26, no. 2, pp. 50–56, 2003.

[23] J. F. Ditunno, W. Young, W. H. Donovan, and G. Creasey, "The international standards booklet for neurological and functional classification of spinal cord injury.," *Paraplegia*, vol. 32, pp. 70–80, 1994.

[24] S. Pillen, I. M. P. Arts, and M. J. Zwarts, "Muscle ultrasound in neuromuscular disorders," *Muscle & Nerve*, vol. 37, pp. 679–693, 2008.

[25] J. L. Whittaker, D. S. Teyhen, J. M. Elliott, K. Cook, H. M. Langevin, H. H. Dahl, and M. Stokes, "Rehabilitative ultrasound imaging: understanding the technology and its applications," *The Journal of Oethopaedics and Sports Physical Therapy*, vol. 37, no. 8, pp. 434–449, 2007.

[26] S. Pillen and N. van Alfen, "Skeletal muscle ultrasound," *Neurological Research*, vol. 33, no. 10, pp. 1016–1024, 2011.

[27] H. Al-Nashash and N. Qaddoumi, *Assessment of Bone Healing Using Ultrasound*, pp. 283–297. 10 2012.

[28] B. Ihnatsenka and A. P. Boezaart, "Ultrasound: Basic understanding and learning the language.," *International Journal of Shoulder Surgery*, vol. 4, no. 3, pp. 55–62, 2010.

[29] J. M. Daniels and W. W. Dexter, *Basics of musculoskeletal ultrasound*. New York: Springer, 2013.

[30] E. Silvestri, A. Muda, and L. M. Sconfienza, *Normal ultrasound anatomy of the musculoskeletal system*. Italy: Springer, 2012.

[31] N. A. Maffiuletti, "Physiological and methodological considerations for the use of neuromuscular electrical stimulation," *Clinical Neurophysiology*, vol. 110, pp. 223–234, 2010.

[32] L. R. Sheffler and J. Chae, "Neuromuscular electrical stimulation in neurorehabilitation," *Muscle & Nerve*, vol. 35, no. 5, pp. 562–590, 2007.

[33] R. Martin, C. Sadowsky, K. Obst, B. Meyer, and J. McDonald, "Functional electrical stimulation in spinal cord injury: from theory to practice," *Topics in Spinal Cord Injury Rehabilitation*, vol. 18, no. 1, pp. 28–33, 2012.

[34] B. Reed, "The physiology of neuromuscular electrical stimulation," *Pediatric Physical Therapy*, vol. 9, pp. 96–102, 1997.

[35] T. P. Martin, R. B. Stein, P. T. Hoepner, and D. R. Reid, "Influence of electrical stimulation on the morphological and metabolic properties of paralyzed muscle," *Journal of Applied Physiology*, vol. 72, pp. 1401–1406, 1992.

[36] B. M. Doucet, A. Lam, and L. Griffin, "Neuromuscular electrical stimulation for skeletal muscle function," *Yale Journal of Biology and Medicine*, vol. 85, no. 1, pp. 201–215, 2012.

[37] A. R. ALLEN, "SURGERY OF EXPERIMENTAL LESION OF SPINAL CORD EQUIVALENT TO CRUSH INJURY OF FRACTURE DISLOCATION OF SPINAL COLUMN: A PRELIMINARY REPORT," *Journal of the American Medical Association*, vol. LVII, no. 11, pp. 878–880, 1911.

[38] B. A. Kakulas, "Neuropathology: the foundation for new treatments in spinal cord injury," *Spinal Cord*, vol. 42, pp. 549–563, 2004.

[39] T. Gordon and J. Mao, "Muscle atrophy and procedures for training after spinal cord injury," *Physical Therapy*, vol. 74, no. 1, pp. 50–60, 1994.

[40] T. Gordon and M. C. Pattullo, "Plasticity of muscle fibre and motor unit types," *Exercise and Sport Sciences Reviews*, vol. 21, pp. 331–362, 1993.

[41] R. R. Roy, K. M. Baldwin, and V. R. Edgerton, "The plasticity of skeletal muscle: effects of neuromuscular activity," *Exercise and Sport Sciences Reviews*, vol. 19, pp. 269–312, 1991.

[42] M. J. Castro, D. F. A. Jr, E. A. Hillegass, and G. A. Dudley, "Influence of complete spinal cord injury on skeletal muscle cross-sectional area within the first 6 months of injury," *Journal of Applied Physiology*, vol. 86, no. 1, pp. 350–358, 1999.

[43] A. S. Gorgey and G. A. Dudley, "Skeletal muscle atrophy and increased intramuscular fat after incomplete spinal cord injury," *Spinal Cord*, vol. 45, no. 4, pp. 304–309, 2007.

[44] C. D. Moore, B. C. Craven, L. Thabane, A. C. Laing, A. W. Frank-Wilson, S. A. K. A. P. J. D. Adachi, and L. M. Giangregorio, "Lower-extremity muscle atrophy and fat infiltration after chronic spinal cord injury," *Journal of Musculoskeletal & Neuronal Interactions*, vol. 15, no. 1, pp. 32–41, 2015.

[45] L. Giangregorio and N. McCartney, "Bone loss and muscle atrophy in spinal cord injury: epidemiology, fracture prediction, rehabilitation strategies," *The Journal of Spinal Cord Medicine*, vol. 29, no. 5, pp. 489–500, 2006.

[46] D. Y. Solandt and J. W. Magladery, "A comparison of effects of upper and lower motor neurone lesions on skeletal muscle," *Journal of Neurophysiology*, vol. 5, pp. 373–380, 1942.

[47] P. H. Peckham, J. T. Mortimer, and E. B. Marsolais, "Upper and lower motor neuron lesions in the upper extremity muscles of tetraplegics," *Paraplegia*, vol. 14, pp. 115–121, 1976.

[48] J. F. Yang, R. B. Stein, J. Jhamandas, and T. Gordon, "Motor unit numbers and contractile properties after spinal cord injury," *Annals of Neurology*, vol. 67, pp. 496–502, 1990.

[49] P. H. Peckham, J. T. Mortimer, and E. B. Marsolais, "Alteration in the force and fatigability of skeletal muscle in quadriplegic humans following exercise induced by chronic electrical stimulation," *Clinical Orthopaedics and Related Research*, vol. 114, pp. 326–333, 1976.

[50] D. J. Pierotti, R. R. Roy, S. C. Bodine-Fowler, J. A. Hodgson, and V. R. Edgerton, "Mechanical and morphological properties of chronically inactive cat tibialis anterior motor units," *The Journal of Physiology*, vol. 444, pp. 175–192, 1991.

[51] R. R. Roy and R. A. Jr., "Fiber type and fiber size changes in selected thigh muscles six months after low thoracic spinal cord transection in adult cats: exercise effects," *Experimental Neurology*, vol. 92, pp. 675–685, 1986.

[52] B. R. Pachter and A. Eberstein, "Neuromuscular plasticity following limb immobilzation," *Journal of Neurocytology*, vol. 13, pp. 1013–1025, 1984.

[53] J. H. Baker and D. E. Matsumoto, "Adaptation of skeletal muscle to immobilization in a shortened position," *Muscle & Nerve*, vol. 11, pp. 231–244, 1988.

[54] J. H. Baker, "Segmental necrosis in tenotomized muscle fibres," *Muscle & Nerve*, vol. 6, pp. 29–39, 1983.

[55] E. K. Alford, R. R. Roy, and J. A. H. V. R. Edgerton, "Electromyography of rat soleus, medial gastrocnemius, and tibialis anterior during hind-limb suspension," *Experimental Neurology*, vol. 96, pp. 635–649, 1989.

[56] R. Scelsi, C. Marchetti, P. Poggi, s Lotta, and G. Lommi, "Muscle fiber type morphology and distribution in paraplegic patients with traumatic cord lesion: histochemical and ultrastruetural aspects of rectus femoris muscle.," *Acta Neuropathologica*, vol. 57, pp. 243–248, 1982.

[57] R. L. Lieber, C. B. Johansson, H. L. Vahlsing, A. R. Hargens, and E. R. Feringa, "Long-term effects of spinal cord transection on fast and slow rat skeletal muscle, i contractile properties," *Experimental Neurology*, vol. 91, pp. 423–434, 1986.

[58] S. Cha, J. Yun, Y. Myong, and H. Shin, "Spasticity and preservation of skeletal muscle mass in people with spinal cord injury," *Spinal Cord*, vol. 57, pp. 317–323, 2019.

[59] C. A. Pelletier and A. L. Hicks, "Muscle fatigue characteristics in paralyszed muscle after spinal cord injury," *Spinal Cord*, vol. 49, pp. 125–130, 2011.

[60] S. Dudley-Javaroski and R. K. Shields, "Muscle and bone plasticity after spinal cord injury: review of adaptations to disuse and to electrical muscle stimulation," *Journal of Rehabilitation Research and Development*, vol. 45, no. 2, pp. 283–296, 2008.

[61] B. Biering-Sørensen, I. B. Kristensen, M. Kjaer, and F. Biering-Sørensen, "Muscle after spinal cord injury," *Muscle & Nerve*, vol. 40, no. 4, pp. 499–519, 2009.

[62] R. Burnham, T. Martin, R. Stein, I. MacLean, and R. Steadward, "Skeletal muscle fibre type transformation following spinal cord injury," *Spinal Cord*, vol. 35, no. 2, pp. 86–91, 1997.

[63] G. M. Graham, J. A. Siedlik, L. Harlow, K. Sahbani, W. A. Bauman, H. A. Tawfeek, and C. P. Cardozo, "Key glycolytic metabolites in paralyzed skeletal muscle are altered seven days after spinal cord injury in mice," *Journal of Neurotrauma*, vol. 36, pp. 2722–2731, 2019.

[64] H. Rahemi, N. Nigam, and J. M. Wakeling, "The effect of intramuscular fat on skeletal muscle mechanics: implications for the elderly and obese," *Journal of the Royal Society Interface*, vol. 12, no. 109, 2015.

[65] P. K. Shah, C. M. Gregory, J. E. Stevens, N. C. Pathare, A. Jayaraman, A. L. Behrman, and G. A. Walter, "Non-invasive assessment of lower extremity muscle composition after incomplete spinal cord injury," *Spinal Cord*, vol. 46, pp. 565–570, 2008.

[66] T. C. Cope, S. C. Bodine, M. Fournier, and V. R. Edgerton, "Soleus motor units in chronic spinal transected cats: physiological and morphological alterations," *Journal of Neurophysiology*, vol. 55, pp. 1202–1220, 1986.

[67] M. Gaviria and F. Ohanna, "Variability of the fatigue response of paralyzed skeletal muscle in relation to the time after spinal cord injury: mechanical and electrophysiological characteristics," *European Journal of Applied Physiology and Occupational Physiology*, vol. 80, no. 2, pp. 145–153, 1999.

[68] W. B. Scott, S. C. K. Lee, T. E. Johnston, J. Binkley, and S. A. Binder-Macleod, "Contractile properties and the force-frequency relationship of the paralyzed human quadriceps femoris muscle.," *Physical Therapy*, vol. 86, no. 6, pp. 788–799, 2006.

[69] H. L. Gerrits, A. de Haan, A. J. Sargeant, A. Dallmeijer, and M. T. E. Hopman, "Altered contractile properties of the quadriceps muscle in people with spinal cord injury following functional electrical stimulated cycle training," *Spinal Cord*, vol. 38, no. 4, pp. 214–223, 2000.

[70] C. S. Klein, C. K. Häger-Ross, and C. K. Thomas, "Fatigue properties of human thenar motor units paralyzed by chronic spinal cord injury," *The Journal of Physiology*, vol. 573, pp. 161–171, 2006.

[71] R. K. Shields, L. F. Law, B. Reiling, K. Sass, and J. Wilwert, "Effects of electrically induced fatigue on the twitch and tetanus of paralyzed soleus muscle in humans," *Journal of Applied Physiology*, vol. 82, no. 5, pp. 1499–1507, 1997.

[72] L. Rochester, M. J. Barron, C. S. Chandlet, R. A. Sutton, S. Miller, and M. A. Johnson, "Influence of electrical stimulation of the tibialis anterior muscle in paraplegic subjects. 2. morphological and histochemical properties," *Spinal Cord*, vol. 33, pp. 514–522, 1995.

[73] C. K. Thomas, E. Y. Zaidner, B. Calancie, J. G. Broton, and B. R. Bigland-Ritchie, "Muscle weakness, paralysis, and atrophy after human cervical spinal cord injury.," *Experimental Neurology*, vol. 148, no. 2, pp. 414–423, 1997.

[74] C. K. Thomas, "Contractile properties of human thenar muscles paralyzed by spinal cord injury.," *Muscle & Nerve*, vol. 20, no. 7, pp. 788–799, 1997.

[75] H. L. Gerrits, C. N. Maganaris, , N. D. Reeves, A. J. Sargeant, D. A. Jones, and A. de Haant, "Influence of knee joint angle on muscle properties of paralyzed and non-paralyzed human knee extensors," *Muscle & Nerve*, vol. 32, no. 1, pp. 73–80, 2005.

[76] H. L. Gerrits, M. T. E. Hopman, A. J. Sargeant, and A. de Haan, "Reproducibility of contractile properties of the human paralysed and non-paralysed quadriceps muscle," *Clinical Physiology*, vol. 21, no. 1, pp. 105–113, 2001.

[77] C. K. Häger-Ross, C. S. Klein, and C. K. Thomas, "Twitch and tetanic properties of human thenar motor units paralyzed by chronic spinal cord injury," *Journal of Neurophysiology*, vol. 96, no. 1, pp. 165–174, 2006.

[78] H. L. Gerrits, A. D. Haan, M. T. E. Hopman, L. H. V. van Der Woude, D. A. Jones, and A. J. Sargeant, "Variability of the fatigue response of paralyzed skeletal muscle in relation to the time after spinal cord injury: mechanical and electrophysiological characteristics," *Muscle & Nerve*, vol. 22, no. 9, pp. 1249–1256, 1999.

[79] C. D. P. Rinaldin, L. P. A. Cabral, E. Krueger, G. N. Nogueira-Neto, P. Nohama, and E. M. Scheeren, "Fatigue in complete spinal cord injury and implications on total delay," *Artificial Organs*, vol. 44, no. 3, pp. 305–313, 2020.

[80] L. S. Lundell, M. Savikj, E. Kostovski, P. O. Iversen, J. R. Zierath, A. Krook, A. V. Chibalin, and U. Widegren, "Protein translation, proteolysis and autophagy in human skeletal muscle atrophy after spinal cord injury," *Acta Physiol (Oxf)*, vol. 223, no. 3, pp. 1–14, 2017.

[81] M. Savikj, E. Kostovski, L. S. Lundell, P. O. Iversen, J. Massart, and U. Widegren, "Altered oxidative stress and antioxidant defence in skeletal muscle during the first year following spinal cord injury," *Physiological Reports*, vol. 7, no. 6, 2019.

[82] H. Hyatt, R. Deminice, T. Yoshihara, and S. K. Powers, "Mitochondrial dysfunction induces muscle atrophy during prolonged inactivity: a review of the causes and effects," *Archives of Biochemistry and Biophysics*, vol. 662, pp. 49–60, 2019.

[83] J. F. Ditunno, A. S. Burns, and R. J. Marino, "Neurological and functional capacity outcome measures: essential to spinal cord injury clinical trials," *Journal of Rehabilitation Research & Development*, vol. 42, no. 3, pp. 35–42, 2005.

[84] P. H. Ellaway, M. Catley, N. J. Davey, A. Kuppuswamy, P. Strutton, H. L. Frankel, A. Jamous, and G. Savic, "Review of physiological motor outcome measures in spinal cord injury using transcranial magnetic stimulation and spinal reflexes," *Journal of Rehabilitation Research & Development*, vol. 44, no. 1, pp. 69–76, 2007.

[85] M. P. Ghatas, M. E. Holman, and A. S. Gorgey, "Methodological considerations for near-infrared spectroscopy to assess mitochondrial capacity after spinal cord injury," *The Journal of Spinal Cord Injury Medicine*, 2019.

[86] A. Bjerkefors, J. W. Squair, R. Malik, T. Lam, Z. Chen, and M. G. Carpenter, "Diagnostic accuracy of common clinical tests for assessing abdominal muscle function after motor-complete spinal cord injury above t6," *Spinal Cord*, vol. 53, no. 2, pp. 114–119, 2015.

[87] K. T. Dussik, D. J. Firtch, M. Kyriazidou, and R. S. Sear, "Measurement of articular tissues with ultrasound," *American Journal of Physical Medicine*, vol. 37, no. 3, pp. 160–165, 1958.

[88] A. Young, I. Hughes, P. Russel, M. J. Parkers, and P. J. Nichols, "Measurement of quadriceps muscle wasting by ultrasonography," *Rheumatology and Rehabilitation*, vol. 19, no. 3, pp. 141–148, 1980.

[89] N. D. Reeves, C. N. Maganaris, and M. V. Narici, "Ultrasonographic assessment of human skeletal muscle size," *European Journal of Applied Physiology*, vol. 91, no. 1, pp. 116–118, 2004.

[90] C. O'Sullivan, J. Meaney, G. Boyle, J. Gormley, and M. Stokes, "The validity of rehabilitative ultrasound imaging for measurement of trapezius muscle thickness," *Manual therapy*, vol. 14, no. 5, pp. 572–578, 2009.

[91] M. D. Mendis, S. J. Wilson, W. Stanton, and J. A. Hides, "Validity of real-time ultrasound imaging to measure anterior hip muscle size: a comparison with magnetic resonance imaging," *The Journal of Orthopaedics and Sports Physical Therapy*, vol. 40, no. 9, pp. 577–581, 2010.

[92] A. Kositsky, B. A. M. Gonçalves, L. Stenroth, R. S. Barret, and L. E. Diamond, "Reliability and validity of ultrasonography for measurement of hamstring muscle and tendon cross-sectional area," *Ultrasound in Medicine and Biology*, vol. 46, pp. 55–63, 2020.

[93] J. M. Scott, D. S. Martin, R. Ploutz-Snyder, T. Caine, T. Matz, N. M. Arzeno, R. Buxton, and L. Ploutz-Snyder, "Reliability and validity of panoramic ultrasound for muscle quantification.," *Ultrasound in Medicine and Biology*, vol. 38, no. 9, pp. 1656–1661, 2012.

[94] T. J. MacGillivray, E. Ross, H. A. H. R. W. Simpson, and C. A. Greig, "3d freehand ultrasound for in vivo determination of human skeletal muscle volume," *Ultrasound in Medicine and Biology*, vol. 35, no. 6, pp. 928–935, 2009.

[95] J. Berger, D. Bunout, G. Barrera, M. O. de la Maza, S. H. L. Leiva, and S. Hirsch, "Rectus femoris (rf) ultrasound for the assessment of muscle mass in older people," *Archives of Gerontology and Geriatrics*, vol. 61, no. 1, pp. 33–38, 2015.

[96] J. G. Rosenberg, E. D. Ryan, E. J. Sobolewski, M. J. Scharville, B. J. Thompson, and G. E. King, "Reliability of panoramic ultrasound imaging to simultaneously examine muscle size and quality of the medial gastrocnemius," *Muscle & Nerve*, vol. 49, no. 5, pp. 736–740, 2014.

[97] N. D. M. Jenkins, H. C. Bergstrom, K. C. Cochrane, E. C. Hill, C. Smith, J. M. Miller, T. J. Housh, J. Cramer, and S. Buckner, "Test-retest reliability of single transverse versus panoramic ultrasound imaging for muscle size and echo intensity of the biceps brachii," *Ultrasound in Medicine & Biology*, vol. 41, no. 6, pp. 1584–1591, 2015.

[98] N. I. Tanaka, M. Ogawa, A. Yoshiko, R. Ando, and H. Akima, "Reliability of size and echo intensity of abdominal skeletal muscles using extended field-of-view ultrasound imaging," *European Journal of Applied Physiology*, vol. 117, no. 11, pp. 2263–2270, 2017.

[99] A. Schneebeli, M. Elgoff, A. Giampietro, R. Clijsen, and M. Barbero, "Rehabilitative ultrasound imaging of the supraspinatus muscle: Intra- and interrater reliability of thickness and cross-sectional area.," *Journal of Bodywork and Movement Therapies*, vol. 18, no. 2, pp. 266–272, 2014.

[100] M. Ogawa, N. Mitsukawa, M. G. Bemben, and T. Abe, "Ultrasound assessment of adductor muscle size using muscle thickness of the thigh," *Journal of Sport Rehabilitation*, vol. 21, no. 3, pp. 244–248, 2012.

[101] K. H. Cho, H. J. Lee, and W. H. Lee, "Reliability of rehabilitative ultrasound imaging for the medial gastrocnemius muscle in poststroke patients," *Clinical Physiology and Functional Imaging*, vol. 34, no. 1, pp. 26–31, 2014.

[102] T. G. O'brien, M. L. C. Gonzalez, P. S. Gosh, J. Mandrekar, and A. J. Bon, "Reliability of a novel ultrasound system for gray-scale analysis of muscle," *Muscle & Nerve*, vol. 56, no. 3, pp. 408–412, 2017.

[103] M. V. Narici, T. Binzoni, E. Hiltbrand, J. Fasel, F. Terrier, and P. Cerretelli, "In vivo human gastrocnemius architecture with changing joint angle at rest and during graded isometric contraction," *Journal of Physiology*, vol. 496, no. 1, pp. 287–297, 1996.

[104] C. N. Maganaris, V. Baltzopoulos, and A. J. Sargeant, "In vivo measurements of the triceps surae complex architecture in man: implications for muscle function," *The Journal of Physiology*, vol. 512, no. 2, pp. 603–614, 1998.

[105] N. D. Reeves and M. V. Narici, "Behavior of human muscle fascicles during shortening and lengthening contractions in vivo," *Journal of Applied Physiology*, vol. 95, no. 3, pp. 1090–1096, 2003.

[106] T. Fukunaga, Y. Kawakami, S. Kuno, K. Funato, and S. Fukashiro, "Muscle architecture and function in humans," *Journal of Biomechanics*, vol. 30, no. 5, pp. 457–463, 1997.

[107] T. Fukunaga, Y. Ichinose, M. Ito, Y. Kawakami, and S. Fukashiro, "Determination of fascicle length and pennation in a contracting human muscle in vivo.," *Journal of Applied Physiology*, vol. 82, no. 1, 1997.

[108] C. N. Maganaris, V. Baltzopoulos, and A. J. Sargeant, "Human calf muscle responses during repeated isometric plantarflexions," *Journal of Biomechanics*, vol. 39, no. 7, pp. 1249–1255, 2006.

[109] T. Fukunaga, K. Kubo, Y. Kawakami, S. Fukashiro, H. Kanehisa, and C. N. Maganaris, "In vivo behaviour of human muscle tendon during walking.," *Proceedings of the Royal Society B: Biological Sciences*, vol. 268, no. 1464, pp. 229–233, 2001.

[110] G. A. Lichtwark, K. Bougoulias, and A. M. Wilson, "Muscle fascicle and series elastic element length changes along the length of the human gastrocnemius during walking and running," *Journal of Biomechanics*, vol. 40, no. 1, pp. 157–164, 2007.

[111] Y. Kawakami, T. Abe, and T. Fukunaga, "Muscle-fiber pennation angles are greater in hypertrophied than in normal muscles," *Journal of Applied Physiology*, vol. 74, no. 6, pp. 2740–2744, 1993.

[112] P. W. Hodges, L. H. M. Pengel, R. D. Herbert, and S. C. Gandevia, "Measurement of muscle contraction with ultrasound imaging," *Muscle & Nerve*, vol. 27, no. 1, pp. 682–692, 2003.

[113] A. V. Dieterich, C. M. Pickard, L. E. Deshon, G. R. Straussa, W. Gibson, P. Davey, and J. McKay, "M-mode ultrasound used to detect the onset of deep muscle activity," *Journal of Electromyography and Kinesiology*, vol. 25, no. 2, pp. 224–231, 2015.

[114] O. Vasseljen, H. H. Dahl, P. J. Mork, and H. G. Torp, "Muscle activity onset in the lumbar multifidus muscle recorded simultaneously by ultrasound imaging and intramuscular electromyography.," *Clinical Biomechanics (Bristol,Avon)*, vol. 21, no. 9, pp. 905–913, 2006.

[115] A. V. Dieterich, A. Botter, T. M. Vieira, A. Peolsson, F. Petzke, P. Davey, and D. Falla, "Spatial variation and inconsistency between estimates of onset of muscle activation from emg and ultrasound," *Scientific Reports*, vol. 7, 2017.

[116] A. J. Tweedell, M. S. Tenan, and C. A. Haynes, "Differences in muscle contraction onset as determined by ultrasound and electromyography.," *Muscle & Nerve*, vol. 59, no. 4, pp. 494–500, 2019.

[117] F. Lindberg, F. Öhberg, L. Å. Brodin, and C. Grönlund, "Long-term effects of spinal cord transection on fast and slow rat skeletal muscle, i contractile properties," *Experimental Neurology*, vol. 91, pp. 423–434, 1986.

[118] X. Chen, Y.-P. Zheng, J.-Y. Guo, Z. Zhu, S.-C. Chan, and Z. Zhang, "Sonomyographic responses during voluntary isometric ramp contraction of the human rectus femoris muscle," *European Journal of Applied Physiology*, vol. 112, no. 7, pp. 2603–2614, 2012.

[119] J. Shi, Y.-P. Zheng, Q.-H. Huang, and X. Chen, "Continuous monitoring of sonomyography, electromyography and torque generated by normal upper arm muscles during isometric contraction: sonomyography assessment for arm muscles," *IEEE Transactions on Biomedical Engineering*, vol. 55, no. 3, pp. 1191–1198, 2008.

[120] J. Shi, Y. P. Zheng, X. Chen, and Q. H. Huang, "Assessment of muscle fatigue using sonomyography: muscle thickness change detected from ultrasound images," *Medical Engineering & Physics*, vol. 29, no. 4, pp. 472–479, 2007.

[121] L. Mademli and A. Arampatzis, "Behaviour of the human gastrocnemius muscle architecture during submaximal isometric fatigue," *European Journal of Applied Physiology*, vol. 94, no. 5-6, pp. 611–617, 2005.

[122] L. Mademli, A. Arampatzis, and M. Walsh, "Effect of muscle fatigue on the compliance of the gastrocnemius medialis tendon and aponeurosis," *Journal of Biomechanics*, vol. 39, no. 3, pp. 426–434, 2006.

[123] J. Bojsen-Møller, S. Schwartz, K. K. Kalliokoski, T. Finni, and S. P. Magnusson, "Intermuscular force transmission between human plantarflexor muscles in vivo," *Journal of Applied Physiology*, vol. 109, no. 6, pp. 1608–1618, 2010.

[124] A. I. L. Namburete and J. M. Wakeling, "Regional variations in fascicle curvatures within a muscle belly change during contraction," *Journal of Biomechanics*, vol. 45, no. 16, pp. 2835–2840, 2012.

[125] A. Sarvazyan, S. Tsyuryupa, and O. Rudenko, "Ability of skeletal muscle to protect bones and joints from external impacts: Acoustical assessment," *Proceedings of Meetings on Acoustics*, vol. 23, 2015.

[126] J. Z. Heckmatt, V. Dubowitz, and S. Leeman, "Detection of pathological change in dystrophic muscle with B-scan ultrasound imaging," *The Lancet*, vol. 315, no. 8183, pp. 1389–1390, 1980.

[127] J. Z. Heckmatt, S. Leeman, and V. Dubowitz, "Ultrasound imaging in the diagnosis of muscle disease," *The Journal of Paediatrics*, vol. 101, no. 5, pp. 656–660, 1982.

[128] K. Brockmann, P. Becker, G. Schreiber, K. Neubert, E. Brunner, and C. Bönneman, "Sensitivity and specificity of qualitative muscle ultrasound in assessment of suspected neuromuscular disease in childhood," *Neuromuscular Disorders*, vol. 17, no. 7, pp. 517–523, 2007.

[129] N. M. Maurits, E. A. Beenakker, D. E. van Schaik, J. M. Fock, and J. H. V. D. Hoeven, "Muscle ultrasound in children: normal values and application to neuromuscular disorders," *Ultrasound in Medicine and Biology*, vol. 30, no. 8, pp. 1017–1027, 2004.

[130] S. Pillen, A. Verrips, N. van Alfen, I. M. P. Arts, L. T. L. Sie, and M. J. Zwarts, "Quantitative skeletal muscle ultrasound: Diagnostic value in childhood neuromuscular disease," *Neuromuscular Disorders*, vol. 17, no. 7, pp. 509–516, 2007.

[131] S. Pillen, M. van Keimpema, R. A. J. Nievelstein, A. Verrips, W. van Kruijsbergen-Raijmann, and M. J. Zwarts, "Skeletal muscle ultrasonography: Visual versus quantitative evaluation," *Ultrasound in Medicine & Biology*, vol. 32, no. 9, pp. 1315–1321, 2006.

[132] G. J. R. Dubois, D. Bachasson, L. Lacourpaille, O. Benveniste, and J.-Y. Hogrel, "Local texture anisotropy as an estimate of muscle quality in ultrasound imaging," *Ultrasound in Medicine & Biology*, vol. 44, no. 5, pp. 1133–1140, 2018.

[133] S. Pillen, R. O. Tak, M. J. Zwarts, M. M. Y. Lammens, K. N. Verrijp, I. M. P. Arts, J. A. van der Laak, P. M. Hoogerbrugge, B. G. M. van Engelen, and A. Verrips, "Skeletal muscle ultrasound: correlation between fibrous tissue and echo intensity," *Ultrasound in Medicine & Biology*, vol. 35, no. 3, pp. 443–446, 2009.

[134] N. Shahrizaila, Y. Noto, N. G. Simon, W. Huynh, K. Shibuya, J. M. Matamala, T. Dharmadasa, E. Devenney, M. L. Kennerson, G. A. Nicholson, and M. C. Kiernan, "Quantitative muscle ultrasound as a biomarker in charcot-marie-tooth neuropathy," *Clinical Neurophysiology*, vol. 128, no. 1, pp. 227–232, 2017.

[135] A. Grimm, T. Prell, B. F. Décard, U. Schumacher, O. W. Witte, and H. Axer, "Muscle ultrasonography as an additional diagnostic tool for the diagnosis of amyotrophic lateral sclerosis," *Clinical Neurophysiology*, vol. 126, no. 4, pp. 820–827, 2015.

[136] S. Pillen, M. Nienhuis, J. P. van Dijk, I. M. P. Arts, N. van Alfen, and M. J. Zwarts, "Muscles alive: Ultrasound detects fibrillations," *Clinical Neurophysiology*, vol. 120, no. 5, pp. 932–936, 2009.

[137] A. Botter, M. Carbonaro, T. M. Vieira, and E. Hodson-Tole, "Identification of muscle fasciculations from surface emg: comparison with ultrasound-based detection," *Conference Proceedings: Annual International Conference of the IEEE Engineering in Medicine and Biology Society*, pp. 5117–5120, 2019.

[138] M. S. Cartwright, G. Kwayisi, L. P. Griffin, A. Sarwal, F. O. Walker, J. M. Haris, M. J. Berry, P. S. Chahal, and P. E. Morris, "Quantitative neuromuscular ultrasound in the intensive care unit," *Muscle & Nerve*, vol. 47, no. 2, pp. 255–259, 2013.

[139] A. Grimm, U. Teschner, C. Porzelius, K. Ludewig, J. Zielske, O. W. Witte, F. M. Brunkhorst, and H. Axer, "Muscle ultrasound for early assessment of critical illness neuromyopathy in severe sepsis," *Critical Care*, vol. 17, no. 5, pp. 1–11, 2013.

[140] M. J. Berry, D. C. Files, C. L. Campos, R. N. Bakhru, B. M. Skaggs, and P. E. Morris, "Echogenicity is related to skeletal muscle strength in patients with acute respiratory failure," *Journal of cardiopulmonary rehabilitation and prevention*, vol. 39, no. 3, pp. 17–20, 2019.

[141] J. M. Scott, D. S. Martin, R. Ploutz-Snyder, T. Matz, T. Caine, M. Downs, K. Hackney, R. Buxton, J. W. Ryder, and L. Ploutz-Snyder, "Panoramic ultrasound: a novel and

valid tool for monitoring change in muscle mass .," *Journal of Cachexia, Sarcopenia and Muscle*, vol. 8, no. 3, pp. 475–481, 2017.

[142] M. Aubertin-Leheudre, D. Martel, M. Narici, and M. Bonnefoy, "The usefulness of muscle architecture assessed with ultrasound to identify hospitalized older adults with physical decline," *Experimental Gerontology*, vol. 125, 2019.

[143] A. Young, M. Stokes, and M. Crowe, "Size and strength of the quadriceps muscles of old and young women," *European Journal of Clinical Investigation*, vol. 14, no. 4, pp. 282–287, 1984.

[144] G. Sergi, C. Trevisan, N. Veronese, P. Lucato, and E. Manzato, "Imaging of sarcopenia.," *European Journal of Radiology*, vol. 85, no. 8, pp. 1519–1524, 2016.

[145] M. E. Kuyumcu, M. Halil, Ö. Kara, B. Çuni, G. Çağlayan, S. Güven, Y. Yeşil, G. Arık, B. B. Yavuz, M. Cankurtaran, and L. Özçakar, "Ultrasonographic evaluation of the calf muscle mass and architecture in elderly patients with and without sarcopenia," *Archives of Gerontology and Geriatrics*, vol. 65, pp. 218–224, 2016.

[146] S. Zhu, W. Lin, S. Chen, H. Qi, S. Wang, A. Zhang, J. Cai, B. Lai, Y. Sheng, and G. Ding, "The correlation of muscle thickness and pennation angle assessed by ultrasound with sarcopenia in elderly chinese community dwellers," *Clinical Interventions in Aging*, vol. 14, pp. 987–996, 2019.

[147] Y. Watanabe, Y. Yamada, Y. Fukumoto, T. Ishihara, K. Yokoyama, T. Yoshida, M. Miyake, E. Yamagata, and M. Kimura, "Echo intensity obtained from ultrasonography images reflecting muscle strength in elderly men," *Clinical Intervention in Aging*, vol. 8, pp. 993–998, 2013.

[148] I. S. Raj, S. R. Bird, and A. J. Shield, "Ultrasound measurements of skeletal muscle architecture are associated with strength and functional capacity in older adults," *Ultrasound in Medicine & Biology*, vol. 43, no. 3, pp. 586–594, 2017.

[149] M. Hioki, N. Kanehira, T. Koike, A. Saito, K. Shimaoka, H. Sakakibara, and Y. O. H. Akima, "Age-related changes in muscle volume and intramuscular fat content in quadriceps femoris and hamstrings," *Experimental Gerontology*, vol. 132, 2020.

[150] J. A. Mota and M. S. Stock, "Rectus femoris echo intensity correlates with muscle strength, but not endurance, in younger and older men," *Ultrasound in Medicine & Biology*, vol. 43, no. 8, pp. 1651–1657, 2017.

[151] W. A. Cuellar, L. Blizzard, M. L. Callisaya, J. A. Hides, G. Jones, C. Ding, and T. M. Winzenberg, "Test-retest reliability of measurements of abdominal and multifidus muscles using ultrasound imaging in adults aged 50-79 years," *Musculoskeletal Science & Practice*, vol. 28, pp. 79–84, 2017.

[152] M. S. Stock, M. Whitson, A. M. Burton, N. T. Dawson, E. J. Sobolewski, and B. J. Thompson, "Echo intensity versus muscle function correlations in older adults are influenced by subcutaneous fat thickness," *Ultrasound in Medicine & Biology*, vol. 44, no. 8, pp. 1597–1605, 2018.

[153] A. Young, M. Stokes, J. M. Round, and R. H. Edwards, "The effect of high-resistance training on the strength and cross-sectional area of the human quadriceps," *European Journal of Clinical Investigation*, vol. 13, no. 5, pp. 411–417, 1983.

[154] Y. Kawakami, T. Abe, S. Y. Kuno, and T. Fukunaga, "Training-induced changes in muscle architecture and specific tension," *European Journal of Applied Physiology and Occupational Physiology*, vol. 72, no. 1-2, pp. 37–43, 1995.

[155] S. Sipilä and H. Suominen, "Quantitative ultrasonography of muscle: detection of adaptations to training in elderly women," *Archives of Physical Medicine and Rehabilitation*, vol. 77, no. 11, pp. 1173–1178, 1996.

[156] P. Liu, Y. Wang, H. Hu, Y.-R. Mao, D. Huang, and L. Li, "Change of muscle architecture following body weight support treadmill training for persons after subacute stroke: Evidence from ultrasonography," *BioMed Research International*, vol. 2014, no. 1, 2014.

[157] A. S. Gorgey, M. K. Timmons, D. R. Dolbow, J. Bengel, K. C. Fugate-Laus, L. A. Michener, and D. R. Gater, "Electrical stimulation and blood flow restriction increase wrist extensor cross-sectional area and flow mediated dilation following spinal cord injury," *European Journal of Applied Physiology*, vol. 116, no. 6, pp. 1231–1244, 2016.

[158] A. M. D. Acqua, A. Sachetti, L. J. Santos, F. A. Lemos, T. Bianchi, W. S. Naue, A. S. Dias, G. Sbruzzi, and S. R. R. Vieira, "Use of neuromuscular electrical stimulation to preserve the thickness of abdominal and chest muscles of critically ill patients: a randomized clinical trial," *Journal of Rehabilitation Medicine*, vol. 49, no. 1, pp. 40–48, 2017.

[159] J. M. Day, H. Bush, A. J. Nitz, and T. L. Uhl, "Scapular muscle performance in individuals with lateral epicondylalgia," *Journal of Orthopaedic and Sports Physical Therapy*, vol. 45, no. 5, pp. 414–424, 2015.

[160] Y. Nakai, M. Kawada, T. Miyazaki, and R. Kiyama, "Trunk muscle activity during trunk stabilizing exercise with isometric hip rotation using electromyography and ultrasound," *Journal of Electromyography and Kinesiology*, vol. 49, 2019.

[161] N. B. M. Voet, E. L. van der Kooi, I. I. Riphagen, E. Lindeman, B. G. M. van Engelen, and A. C. H. Geurts, "Strength training and aerobic exercise training for muscle disease," *Cochrane Database of Systematic Reviews*, no. 7, 2013.

[162] R. T. Abresch, J. J. Han, and G. T. Carter, "Rehabilitation management of neuromuscular disease: the role of exercise training," *Journal of Clinical Neuromuscular Disease*, vol. 11, no. 1, pp. 7–21, 2009.

[163] P. L. Jacobs and M. S. Nash, "Exercise recommendations for individuals with spinal cord injury," *Sports Medicine*, vol. 34, no. 11, pp. 727–751, 2004.

[164] D. E. R. Warburton, J. J. Eng, A. Krassioukov, and S. Sproule, "Cardiovascular health and exercise in rehabilitation in spinal cord injury," *Topics in Spinal Cord Injury Rehabilitation*, vol. 13, no. 1, pp. 98–122, 2007.

[165] C. S. Bickel, C. Yarar-Fisher, E. T. Mahoney, and K. K. McCully, "Neuromuscular electrical stimulation – induced resistance training after sci: A review of the dudley protocol," *Topics in Spinal Cord Injury Rehabilitation*, vol. 21, no. 4, pp. 294–302, 2015.

[166] A. Carty, K. McCormack, G. F. Coughlan, L. Crowe, and B. Caulfield, "Increased aerobic fitness after neuromuscular electrical stimulation training in adults with spinal cord injury," *Archives of Physical Medicine and Rehabilitation*, vol. 93, no. 5, pp. 790–795, 2012.

[167] J. S. Petrofsky and R. Stacy, "The effect of training on endurance and the cardiovascular responses of individuals with paraplegia during dynamic exercise induced by functional electrical stimulation," *European Journal of Applied Physiology and Occupational Physiology*, vol. 64, no. 6, pp. 487–492, 1992.

[168] L. Griffin, M. J. Decker, J. Y. Hwang, B. Wang, K. Kitchen, Z. Ding, and J. L. Ivy, "Functional electrical stimulation cycling improves body composition, metabolic and neural factors in persons with spinal cord injury," *Journal of Electromyography and Kinesiology*, vol. 19, no. 4, pp. 614–622, 2009.

[169] E. Henneman, G. Somjen, and D. O. Carpenter, "Functional significance of cell size in spinal motoneurons," *Journal of Neurophysiology*, vol. 28, pp. 560–580, 1965.

[170] C. M. Gregory and C. S. Bickel, "Recruitment patterns in human skeletal muscle during electrical stimulation," *Physical Therapy*, vol. 85, no. 4, pp. 358–364, 2005.

[171] T. Kesar and S. A. Binder-Macleod, "Effect of frequency and pulse duration on human muscle fatigue during repetitive electrical stimulation," *Experimental Physiology*, vol. 91, no. 6, pp. 967–976, 2006.

[172] M. B. Kebaetse, A. E. Turner, and S. A. Binder-Macleod, "Effects of stimulation frequencies and patterns on performance of repetitive, nonisometric tasks," *Journal of Applied Physiology*, vol. 92, pp. 109–116, 2002.

[173] W. B. Scott, S. C. K. Lee, T. E. Johnston, J. Binkley, and S. A. Binder-Macleod, "Switching stimulation patterns improves performance of paralyzed human quadriceps muscle.," *Muscle & Nerve*, vol. 31, no. 5, pp. 581–588, 2005.

[174] G. Deley, J. Denuziller, N. Babault, and J. A. Taylor, "Effects of electrical stimulation pattern on quadriceps isometric force and fatigue in individuals with spinal cord injury.," *Muscle & Nerve*, vol. 52, no. 2, pp. 260–264, 2015.

[175] G. M. Graham, T. A. Thrasher, and M. R. Popovic, "The effect of random modulation of functional electrical stimulation parameters on muscle fatigue," *IEEE Transactions on Neural Systems and Rehabilitation Engineering*, vol. 14, no. 1, pp. 38–45, 2006.

[176] T. Kesar, L.-W. Chou, and S. A. Binder-Macleod, "Effects of stimulation frequency versus pulse duration modulation on muscle fatigue," *Journal of Electromyography and Kinesiology*, vol. 18, no. 4, pp. 662–671, 2008.

[177] S. A. Binder-Macleod and W. A. McLaughlin, "Effects of asynchronous stimulation on the human quadriceps femoris.," *Archives of Physical Medicine and Rehabilitation*, vol. 78, no. 3, pp. 294–297, 1997.

[178] M. J. Decker, L. Griffin, L. D. Abraham, and L. Brandt, "Alternating stimulation of synergistic muscles during functional electrical stimulation cycling improves endurance in persons with spinal cord injury.," *Journal of Electromyography and Kinesiology*, vol. 20, no. 6, pp. 1163–1169, 2010.

[179] L. Z. Popovic and N. M. Malesevic, "Muscle fatigue of quadriceps in paraplegics: comparison between single vs. multi-pad electrode surface stimulation.," *Conference proceedings: IEEE Engineering in Medicine and Biology Society*, pp. 6785–6788, 2009.

[180] D. G. Sayenko, R. Nguyen, T. Hirabayashi, M. R. Popovic, and K. Masani, "Method to reduce muscle fatigue during transcutaneous neuromuscular electrical stimulation in major knee and ankle muscle groups," *Neurorehabilitation and Neural Repair*, vol. 29, no. 8, pp. 722–733, 2015.

[181] G. R. Adams, R. T. Harris, D. Woodard, and G. A. Dudley, "Mapping of electrical muscle stimulation using mri," *Journal of Applied Physiology*, vol. 74, no. 2, pp. 532–537, 1993.

[182] E. A. Hillegass and G. A. Dudley, "Surface electrical stimulation of skeletal muscle after spinal cord injury," *Spinal Cord*, vol. 37, no. 4, 1999.

[183] Delsys, *Bagnoli^{TM} EMG system user's guide*.

[184] Biodex Medical Systems, Inc., *Biodex multi-joint system - MVP setup\operating manual*.

[185] Biometrics Ltd., *Goniometer and torsiometer operating manual*.

[186] J. Darby, E. F. Hodson-Tole, N. Costen, and I. D. Loram, "Automated regional analysis of b-mode ultrasound images of skeletal muscle movement," *Journal of Applied Physiology*, vol. 112, no. 2, pp. 313–327, 2012.

[187] T. Cootes, C. Taylor, D. Cooper, and J. Graham, "Active shape models - their training and application," *Computer Vision and Image Understanding*, vol. 61, no. 1, pp. 38–59, 1995.

[188] B. Lucas and T. Kanade, "An iterative image registration technique with an application to stereo vision," *In Proceedings of the 7th International Joint Conference on Artificial Intelligence*, vol. 2, pp. 674–679, 1981.

[189] I. D. Loram, C. N. Maganaris, and M. Lakie, "Use of ultrasound to make noninvasive in vivo measurements of continuous changes in human muscle contractile length," *The Journal of Applied Physiology*, vol. 100, no. 1, pp. 1311–1323, 2006.

[190] S. S. Shapiro and M. B. Wilk, "An analysis of variance test for normality (complete samples)," *Biometrika*, vol. 52, no. 3, pp. 591–611, 1965.

[191] M. H. Katz, *Study design and statistical analysis*. Cambridge: Cambridge University Press, 2006.

[192] T. K. Kim, "T test as a parametric statistic," *Korean Journal of Anesthesiology*, vol. 68, no. 6, pp. 540–546, 2015.

[193] D. Rey and M. Neuhäuser, *Wilcoxon-Signed-Rank Test*, pp. 1658–1659. Berlin, Heidelberg: Springer Berlin Heidelberg, 2011.

[194] H. B. Mann and D. R. Whitney, "On a test of whether one of two random variables is stochastically larger than the other," *Ann. Math. Statist.*, vol. 18, pp. 50–60, 03 1947.

[195] J. M. Bland and D. G. Altman, "Multiple significance tests: the bonferroni method," *British Medical Journal*, vol. 310, no. 6973, p. 170, 1995.

[196] T. V. Perneger, "What's wrong with the bonferroni adjustments," *British Medical Journal*, vol. 316, no. 7139, pp. 1236–1238, 1998.

[197] S. Sawilowsky, J. Sawilowsky, and R. J. Grissom, *Effect Size*, pp. 426–429. Berlin, Heidelberg: Springer Berlin Heidelberg, 2011.

[198] D. Lakens, "Calculating and reporting effect sizes to facilitate cumulative science: a practical primer for t-tests and anovas," *Frontiers in Psychology*, vol. 4, no. 863, pp. 1–12, 2013.

[199] W. J. Krzanowski, *Principles of Multivariate Analysis: A User's Perspective*. New York: Oxford University Press, 1988.

[200] MathWorks, "Manova." online: https://uk.mathworks.com/help/stats/manova.

[201] C. A. Pelletier and A. L. Hicks, "Muscle characteristics and fatigue properties after spinal cord injury," *Critical reviews in biomedical engineering*, vol. 37, no. 1-2, pp. 139–164, 2009.

[202] L. K. Kwah, R. Z. Pinto, J. Diong, and R. D. Herbert, "Reliability and validity of ultrasound measurements of muscle fascicle length and pennation in humans: a systematic review," *Journal of Applied Physiology*, vol. 114, no. 1, pp. 761–769, 2013.

[203] P. J. Harding, I. D. Loram, N. Combes, and E. F. Hodson-Tole, "Ultrasound-based detection of fasculations in healthy and diseased muscles," *IEEE Transactions on Biomedical Engineering*, vol. 63, no. 3, pp. 512–518, 2016.

[204] B. S. V, A. Unnikrishnan, and K. Balakrishnan, "Grey level co-occurrence matrices: Generalisation and some new features.," *International Journal of Computer Science, Engineering, Information and Technology*, vol. 2, no. 2, pp. 152–157, 2012.

[205] "Image processing toolbox user's guide: Using a gray-level co-occurrence matrix (glcm)."

[206] N. M. Maurits, A. E. Bollen, A. Windhausen, A. E. D. Jager, and J. H. V. D. Hoeven, "Muscle ultrasound analysis: normal values and differentiation between myopathies and neuropathies," *Ultrasound in Medicine and Biology*, vol. 29, no. 2, pp. 215–225, 2003.

[207] P. K. Nielsen, B. R. Jensen, T. Darvann, K. Jørgensen, and M. Bakke, "Quantitative iltrasound tissue characterization in should and thigh muscle - a new approach," *BMC Musculoskeletal Disorders*, vol. 7, no. 2, 2006.

[208] T. T. Roberts, G. R. Leonard, and D. J. Cepela, "Classifications in brief: American spinal injury association (asia) impairment scale," *Clinical Orthopaedics and Related Research*, vol. 475, no. 1, pp. 1499–1504, 2017.

[209] D. Mayans, M. S. Cartwright, and F. O. Walker, "Neuromuscular ultrasonography: quantifying muscle and nerve measurements," *Physical Medicine and Rehabilitation Clinincs of North America*, vol. 23, no. 1, pp. 133–148, 2012.

[210] N. J. Cronin, C. P. Carty, R. S. Barret, and G. Lichtwark, "Automatic tracking of medial gastrocnemius fascicle length during human locomotion," *Journal of Applied Physiology*, vol. 111, no. 5, pp. 1491–1496, 2011.

[211] P. Konrad, "The abc of emg," *A practical introduction to kinesiological electromyography*, vol. 1.4, March 2006.

[212] J. Diong, L. A. Harvey, L. K. Kwah, J. Eyles, M. J. Ling, M. Ben, and R. D. Herbert, "Incidence and predictors of contracture after spinal cord injury—a prospective cohort study," *Spinal Cord*, vol. 50, pp. 579–584, 2012.

[213] J. Diong, L. A. Harvey, L. K. Kwah, J. L. Clarke, L. E. Bilston, S. C. Gandevia, and R. D. Herbert, "Gastrocnemius muscle contracture after spinal cord injury: a longitudinal study," *American Journal of Physical Medicine and Rehabiltation*, vol. 92, no. 7, pp. 565–574, 2013.

[214] T. Fukunaga, M. Miyatani, M. Tachi, M. Kouzaki, Y. Kawakami, and H. Kanehisa, "Muscle volume is a major determinant of joint torque in humans," *Acta Physiol Scand*, vol. 172, no. 4, pp. 249–255, 2001.

[215] T. J. Roberts and A. M. Gabaldón, "Interpreting muscle function from emg: lessons learned from direct measurements of muscle force," *Integr Comp Biol.*, vol. 48, no. 2, pp. 312–320, 2008.

[216] J. D. Steeves, D. Lammertse, A. Curt, J. W. Fawcett, M. H. Tuszynski, J. F. Ditunno, P. H. Ellaway, M. G. Fehlings, J. D. Guest, N. Kleitman, P. F. Bartlett, A. R. Blight, V. Dietz, B. H. Dobkin, R. Grossman, D. Short, M. Nakamura, W. P. Coleman, M. Gaviria, and A. Privat, "Guidelines for the conduct of clinical trials for spinal cord injury (sci) as developed by the iccp panel: clinical trial outcome measures," *Spinal Cord*, vol. 45, no. 1, pp. 206–221, 2007.

[217] P. H. Ellaway, A. Kuppuswamy, A. V. Balasubramaniam, R. Maksimovis, A. Gall, M. D. Craggs, C. J. Mathias, M. Bacon, A. Prochazka, J. Kowalczewski, B. A. Conway, S. Galen, C. J. Catton, D. B. Allan, A. Curt, B. Wirth, and H. J. A. van Hedel, "Development of quantitative and sensitive assessments of physiological and functional outcome during recovery from spinal cord injury: a clinical initiative," *Brain Research Bulletin*, vol. 84, pp. 343–357, 2011.

[218] F. Mechelli, L. Arendt-Nielsen, M. Stokes, and S. Agyapong-Badu, "Ultrasound imaging for measuring muscle and subcutaneous fat tissue thickness of the anterior thigh: a 2 year longitudinal study in middle age," *JCSM Clinical Reports*, vol. 5, no. 1, pp. 3–7, 2020.

[219] J. R. Krentz and J. P. Farthing, "Neural and morphological changes in response to a 20-day intense eccentric training protocol," *European Journal of Applied Physiology*, vol. 110, no. 1, pp. 333–340, 2010.

[220] Y. Kawakami, H. Akima, and K. Kubo, "Changes in muscle size, architecture and neural activation after 20 days of bed rest with and without resistance exercise," *European Journal of Applied Physiology*, vol. 84, pp. 7–12, 2001.

[221] J.-Y. Yu, J.-G. Jeong, and B.-H. Lee, "Evaluation of muscle damage using ultrasound imaging," *Journal of Physical Therapy Science*, vol. 27, no. 2, pp. 531–534, 2015.

[222] W.-C. Weng, P.-H. Tsui, C.-W. Lin, C.-H. Lu, C.-Y. Lin, J.-Y. Shieh, F. L. Lu, T.-W. Ee, K.-W. Wu, and W.-T. Lee, "Evaluation of muscular changes by ultrasound nakagami imaging in duchenne muscular dystrophy," *Scientific Reports*, vol. 7, no. 4429, pp. –153, 2008.

[223] C. D. Lee, Y. Song, and A. C. Peltier, "Muscle ultrasound quantifies the rate of reduction of muscle thickness in amyotrophic lateral sclerosis," *Muscle & Nerve*, vol. 42, no. 5, pp. 814–819, 2010.

[224] I. M. A. andS Overeem and S. Pillen, "Muscle changes in amyotrophic lateral sclerosis: a longitudinal ultrasonography study," *Clinical Neurophysiology*, vol. 122, pp. 623–628, 2011.

[225] M. O. Ibitoye, N. A. Hamzaid, N. Hasnan, A. K. A. Wahab, and G. M. Davis, "Strategies for rapid muscle fatigue redcution during fes exercise in individuals with spinal cord injury: a systematic review," *PLoS One*, vol. 11, no. 2, p. e0149024, 2016.

[226] M. Behringer, S. Grüzer, J. Montag, M. McCourt, M. Ring, and J. Mester, "Effects of stimulation frequency, amplitude, and impulse width on muscle fatigue," *Muscle & Nerve*, vol. 53, no. 4, pp. 608–616, 2016.

[227] T. R. Han, D. Kim, S. J. Lim, and K. J. Lee, "The control of parameters within the therapeutic range in neuromuscular electrical stimulation," *International Journal of Neuroscience*, vol. 117, no. 1, pp. 107–119, 2009.

Appendices

A MATLAB code and Simulink models

A.1 Study 1

```
%% Setup Path for Saving
[pathname1,pathname2,sub_no] = set_dir;

%% Muscle at Rest
Wf = Calibration;
[Muscle_Rest] = Run_Muscle_Rest;
SaveUS(pathname2,'Rest');
save([pathname1 'back-up1']);

%%
trial=0;

%% Setting Current
Wf = Calibration;
a = str2double(inputdlg('Enter the First value of Current'));
[Setting_Current] = Run_Setting_Current;
trial = trial+1;
save([pathname1 'Curr_Select_' num2str(trial)]);
SaveUS(pathname2,['Current_Select_' num2str(trial)]);
save([pathname1 'back-up2']);

%% FES Contractions
Wf = Calibration;
I = str2double(inputdlg('Enter the value of Current'));
[FES_Contractions] = Run_FES_Contractions;
SaveUS(pathname2,'FES_Contractions');
save([pathname1 'back-up3']);

%% Twitch-Tetanus
Wf = Calibration;
I = str2double(inputdlg('Enter the value of Current'));
[TwitchTetanus1,TwitchTetanus2] = Run_TwitchTetanus;
SaveUS(pathname2,'TwT');
save([pathname1 'back-up4']);
```

Continued on the next page.

```
%% Voluntary Activation 1a (No FES)
Wf = Calibration;
PW=0;
[Voluntary_Activation1a] = Run_VoluntaryActivation;
SaveUS(pathname2,'Vol1a');
save([pathname1 'back-up5']);


%% Voluntary Activation 1b (No FES)
Wf = Calibration;
[Voluntary_Activation1b] = Run_VoluntaryActivation;
SaveUS(pathname2,'Vol1b');
save([pathname1 'back-up6']);

%% Voluntary Activation 1c (No FES)
Wf = Calibration;
[Voluntary_Activation1c] = Run_VoluntaryActivation;
SaveUS(pathname2,'Vol1c');
save([pathname1 'back-up7']);

%% Voluntary Activation 2a (FES)
Wf = Calibration;
PW=300;
[Voluntary_Activation2a] = Run_VoluntaryActivation;
SaveUS(pathname2,'Vol2a');
save([pathname1 'back-up8']);

%% Voluntary Activation 2b (FES)
Wf = Calibration;
[Voluntary_Activation2b] = Run_VoluntaryActivation;
SaveUS(pathname2,'Vol2b');
save([pathname1 'back-up9']);

%% Voluntary Activation 2c (FES)
Wf = Calibration;
[Voluntary_Activation2c] = Run_VoluntaryActivation;
SaveUS(pathname2,'Vol2c');
save([pathname1 'back-up10']);

%% Save
save([pathname1 sub_no]);
```

Figure 1: MATLAB code: "Full_Protocol.mat". This is the main script where each section (denoted by "%%" symbols and a green title) runs a part of the experiment. The MATLAB functions and Simulink models called within this script are detailed in subsequent figures in this section.

```
function [pathname1, pathname2, sub_no] = set_dir

sub_no = char(inputdlg('Enter the Subject ID Code','s'));
makepath1 =
mkdir(['D:\Users\scisci\Documents\MATLAB\Jennifer\Data\'
sub_no]);
makepath2 = mkdir(['D:\Echo Images\' sub_no]);

pathname1 = ['D:\Users\scisci\Documents\MATLAB\Jennifer\Data\'
sub_no '\'];
pathname2 = ['D:\Echo Images\' sub_no '\'];
```

Figure 2: MATLAB code: "set_dir.mat". This function generates a text box where the user is asked to enter a subject ID code. A folder is created with the appropriate name where data is saved.

```
function [Wf] = Calibration
sim('Dynamometer');
Wf = mean(squeeze(simout_Dynamometer));
```

Figure 3: MATLAB code: "Calibration.mat". This function runs the "Dynamometer.mdl" Simulink model to obtain the value of torque from the weight of the foot resting on the foot plate. This value is then subtracted from torque readings

```
function [cmd] = ControlUS()
% set path to Echo Wave II automation interface client .Net
assembly (dll)
asm_path = 'D:\Program Files\TELEMED\Echo Wave
II\Config\Plugins\autoint1client.dll';

% load assembly
asm = NET.addAssembly(asm_path);

% create commands interface object
cmd = AutoInt1Client.CmdInt1();

% connect to started Echo Wave II software
ret = cmd.ConnectToRunningProgram();
if (ret ~= 0)
msgbox('Error. Cannot connect to Echo Wave II software. Please
make sure that software is running.', 'Error')
end
cmd.FreezeRun(); %Start recording
```

Figure 4: MATLAB code: "ControlUS.mat". This function is adapted from open source code (Telemed, Lithuania) to start and stop the ultrasound device recording.

```
function [cmd] = SaveUS(path, filename)

% set path to Echo Wave II automation interface client .Net
assembly (dll)
asm_path = 'D:\Program Files\TELEMED\Echo Wave
II\Config\Plugins\autoint1client.dll';

% load assembly
asm = NET.addAssembly(asm_path);

% create commands interface object
cmd = AutoInt1Client.CmdInt1();

% connect to started Echo Wave II software
ret = cmd.ConnectToRunningProgram();
if (ret ~= 0)
msgbox('Error. Cannot connect to Echo Wave II software. Please
make sure that software is running.', 'Error')
end

cmd.WmCopyDataCmd(['-save^#^' path filename '.tvd^#^'])
```

Figure 5: MATLAB code: "SaveUS.mat". This function is adapted from open source code (Telemed, Lithuania) to save ultrasound videos.

```
function [Muscle_Rest] = Run_Muscle_Rest

open_system('Muscle_Rest/Force Scope');
ControlUS;
sim('Muscle_Rest');
ControlUS;

Torque = squeeze(simout_Torque_Rest);
RawTorque = squeeze(simout_RawTorque_Rest);
EMG = squeeze(simout_EMG_Rest);
Time = squeeze(simout_Time_Rest);

Muscle_Rest =
struct('Torque',Torque,'RawTorque',RawTorque,'EMG',EMG,'Time',T
ime);
```

Figure 6: MATLAB code: "Run_Muscle_Rest.mat". This function controls the ultrasound recording, runs the Simulink model "Muscle_Rest.mdl", and stores the output variables torque, EMG and time.

```
function [Setting_Current] = Run_Setting_Current

open_system('Setting_Current/Force Scope');
ControlUS;
sim('Setting_Current');
ControlUS;

Torque = squeeze(simout_Torque_SettingCurrent);
RawTorque = squeeze(simout_RawTorque_SettingCurrent);
Time = squeeze(simout_Time_SettingCurrent);
I = squeeze(simout_I_SettingCurrent);

Setting_Current =
struct('Torque',Torque,'RawTorque',RawTorque,'Time',Time,'I',I)
```

Figure 7: MATLAB code: "Run_Setting_Current.mat". This function controls the ultrasound recording, runs the Simulink model "Setting_Current", and stores the output variables torque, time and current (I).

```
function [FES_Contractions] = Run_FES_Contractions

open_system('FES_Contractions/Force Scope');
ControlUS;
sim('FES_Contractions');
ControlUS;

Torque = squeeze(simout_Torque_FEScon);
RawTorque = squeeze(simout_RawTorque_FEScon);
Time = squeeze(simout_Time_FEScon);
I = squeeze(simout_I_FEScon);
PW = squeeze(simout_FES_PW);

FES_Contractions =
struct('Torque',Torque,'RawTorque',RawTorque,'Time',Time,'I',I,
'PW',PW);
```

Figure 8: MATLAB code: "Run_FES.mat". This function controls the ultrasound recording, runs the Simulink model "FES_Contractions", and stores the output variables torque, time, current (I) and pulsewidth (PW).

```
function [TwitchTetanus1,TwitchTetanus2] = Run_TwitchTetanus

ControlUS;

open_system('TwitchTetanus1/Force Scope');
sim('TwitchTetanus1');
Torque = squeeze(simout_Torque_TwT);
RawTorque = squeeze(simout_RawTorque_TwT);
Time = squeeze(simout_Time_TwT);
TwitchTetanus1 =
struct('Torque',Torque,'RawTorque',RawTorque,'Time',Time);

open_system('TwitchTetanus2/Force Scope');
sim('TwitchTetanus2');
Torque = squeeze(simout_Torque_TwT);
RawTorque = squeeze(simout_RawTorque_TwT);
Time = squeeze(simout_Time_TwT);
TwitchTetanus2 =
struct('Torque',Torque,'RawTorque',RawTorque,'Time',Time);

ControlUS;
```

Figure 9: MATLAB code: "Run_TwitchTetanus.mat". This function controls the ultrasound recording, runs the Simulink models "TwitchTetanus1" and "TwitchTetanus2". In each case the output variables torque and time are stored.

```
function [Vol_activation] = Run_VoluntaryActivation

open_system('VoluntaryActivation/Force Scope');
ControlUS;
sim('VoluntaryActivation');
ControlUS;

Torque = squeeze(simout_Torque_VolActivation);
RawTorque = squeeze(simout_RawTorque_VolActivation);
EMG = squeeze(simout_EMG_VolActivation);
Time = squeeze(simout_Time_VolActivation);
PW = squeeze(simout_PW_VolActivation);

Vol_activation =
struct('Torque',Torque,'RawTorque',RawTorque,'EMG',EMG,'Time',T
ime,'PW',PW);
```

Figure 10: MATLAB code: "Run_VoluntaryActivation.mat". This function controls the ultrasound recording, runs the Simulink model "VoluntaryActivation", and stores the output variables torque, EMG, time and pulsewidth (PW).

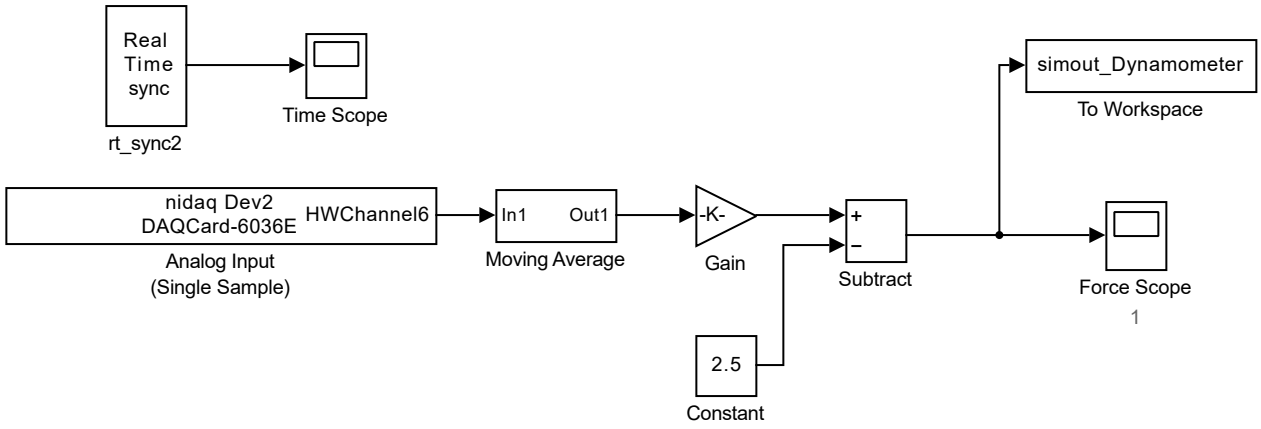

Figure 11: Simulink model "Dynamometer.mdl". This model reads the input from the dynamometer, applies a moving average filter, applies a conversion factor to convert the voltage signal to torque (K) and zeros the baseline. The output is sent to the MATLAB workspace and displayed on a scope.

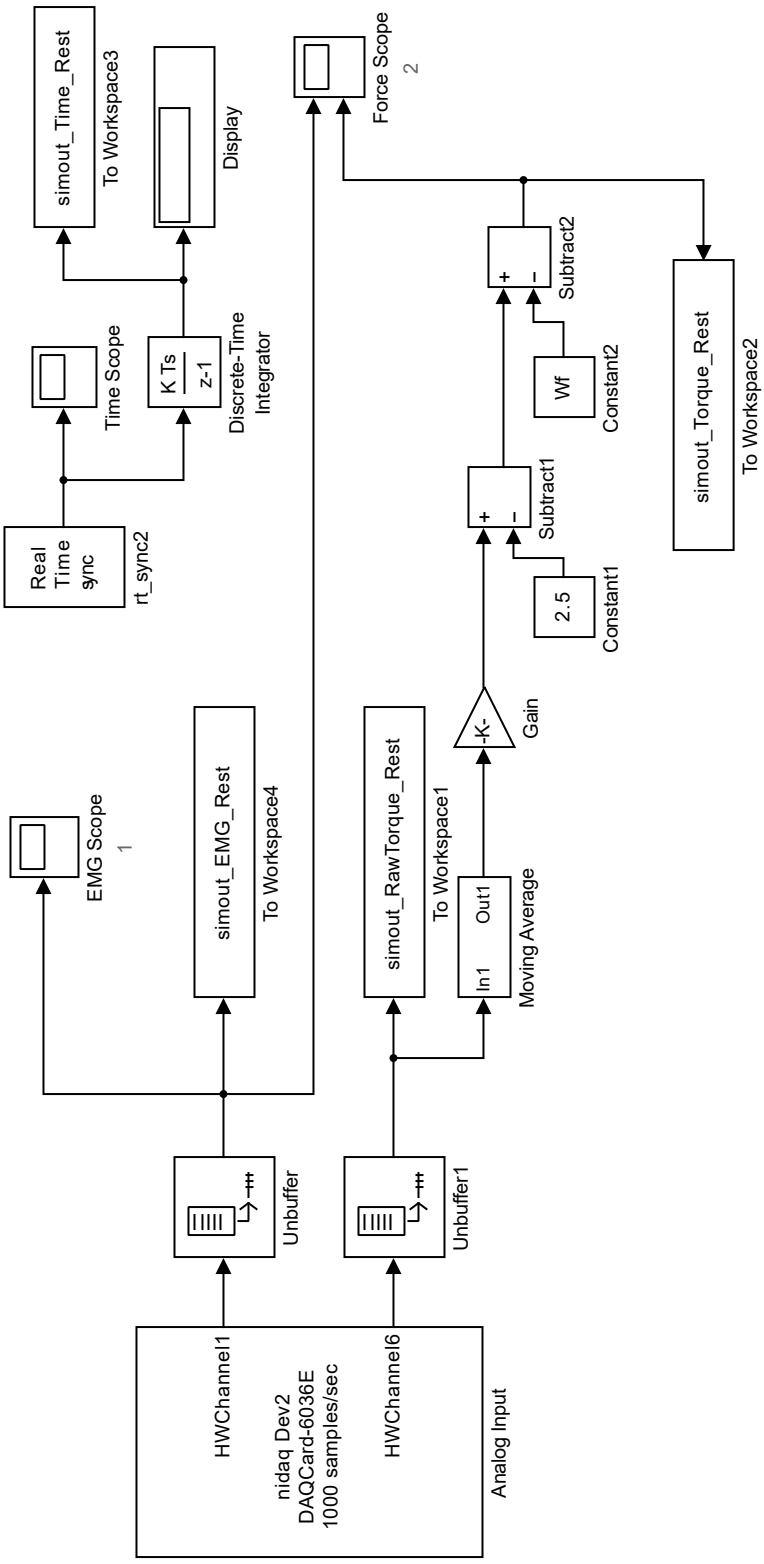

Figure 12: Simulink model "Muscle_Rest.mdl". This model reads the input from the dynamometer and EMG device. The output is sent to the MATLAB workspace and displayed on a scope.

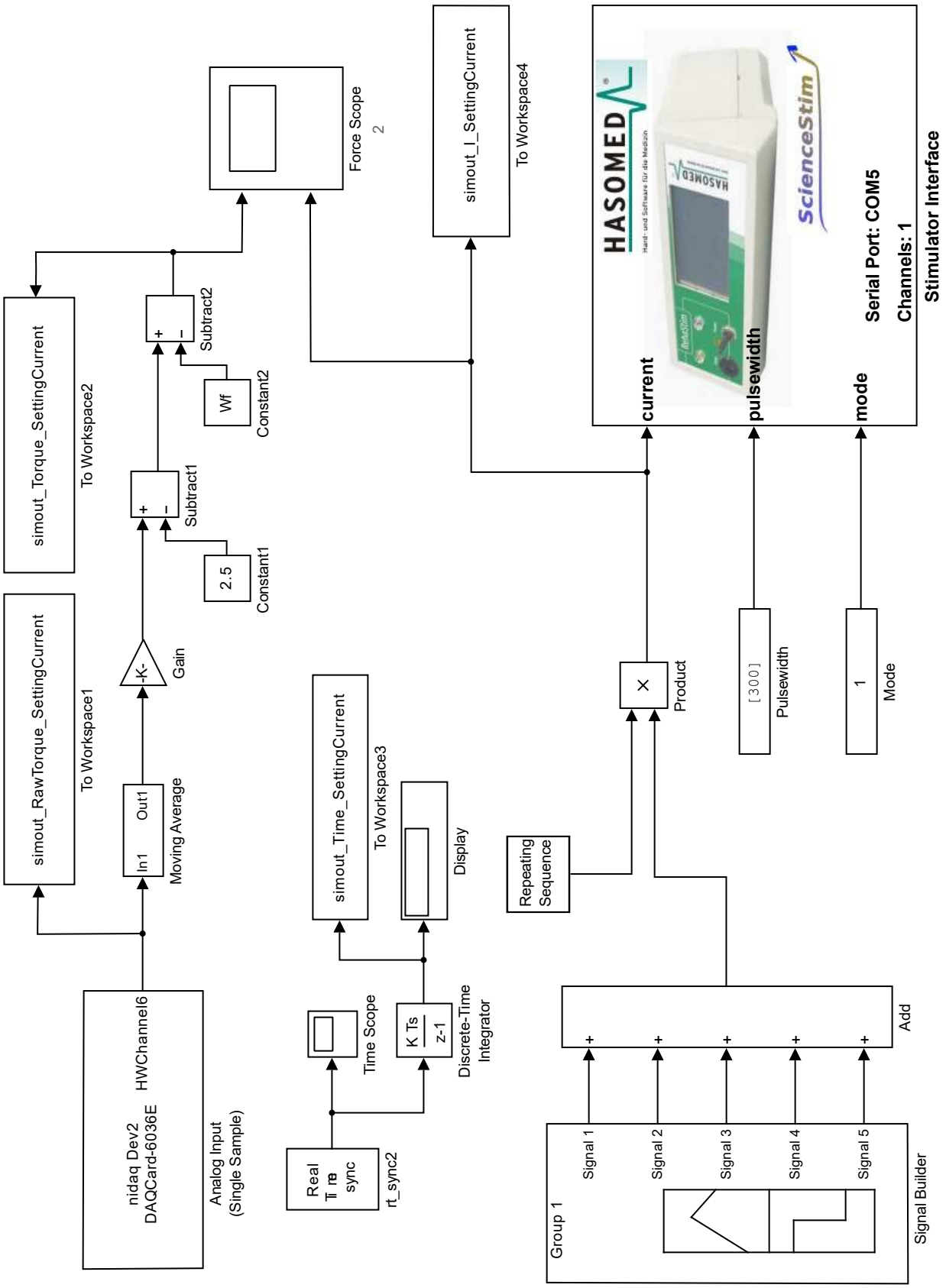

Figure 13: Simulink model "Setting_Current.mdl". This model reads the input from the dynamometer while stimulation is applied. The current, pulsewidth and frequency are controlled to deliver doublet pulses every 5 seconds. The output is sent to the MATLAB workspace and displayed on a scope.

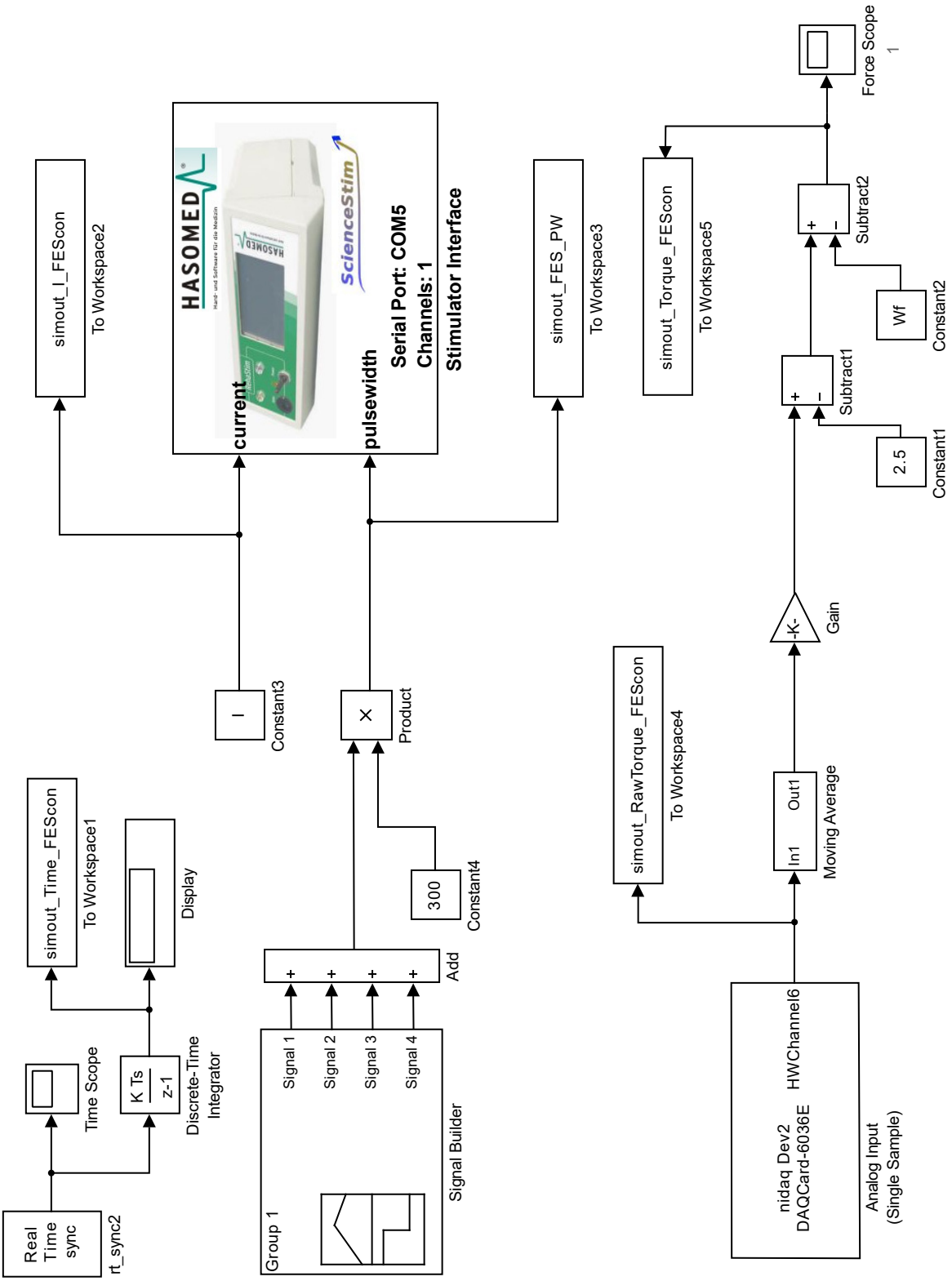

Figure 14: Simulink model "FES_Contraction.mdl". This model reads the input from the dynamometer while stimulation is applied. The current, pulsewidth and frequency are controlled to deliver 4 ramped contractions lasting 10 seconds each with a 5 second rest period. The output is sent to the MATLAB workspace and displayed on a scope.

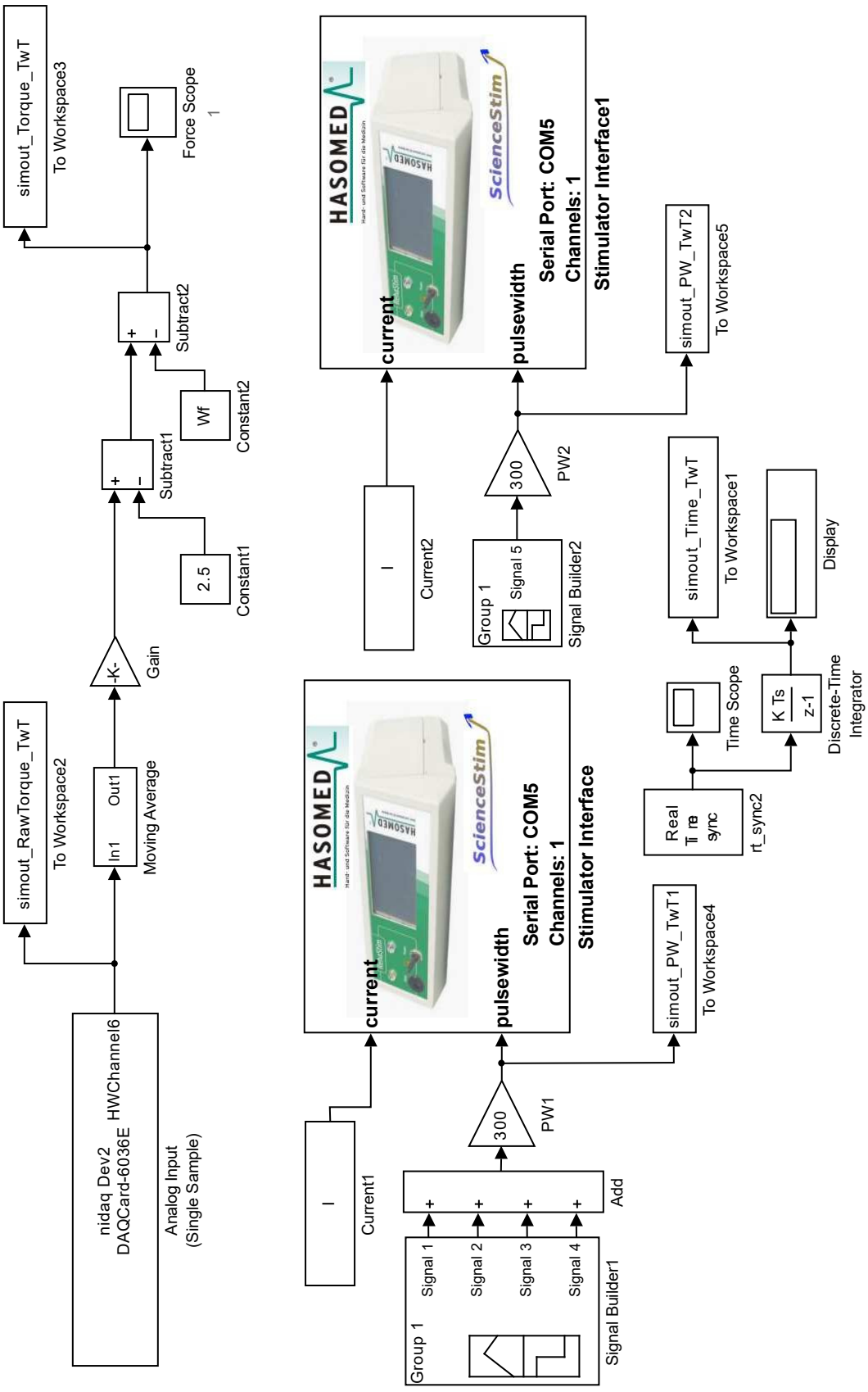

Figure 15: Simulink model "TwitchTetanus1.mdl". This model reads the input from the dynamometer while stimulation is applied. The current, pulsewidth and frequency are controlled to deliver 3 single pulses followed by 1 second train at 20 Hz and then a 1 second train at 80 Hz. The output is sent to the MATLAB workspace and displayed on a scope.

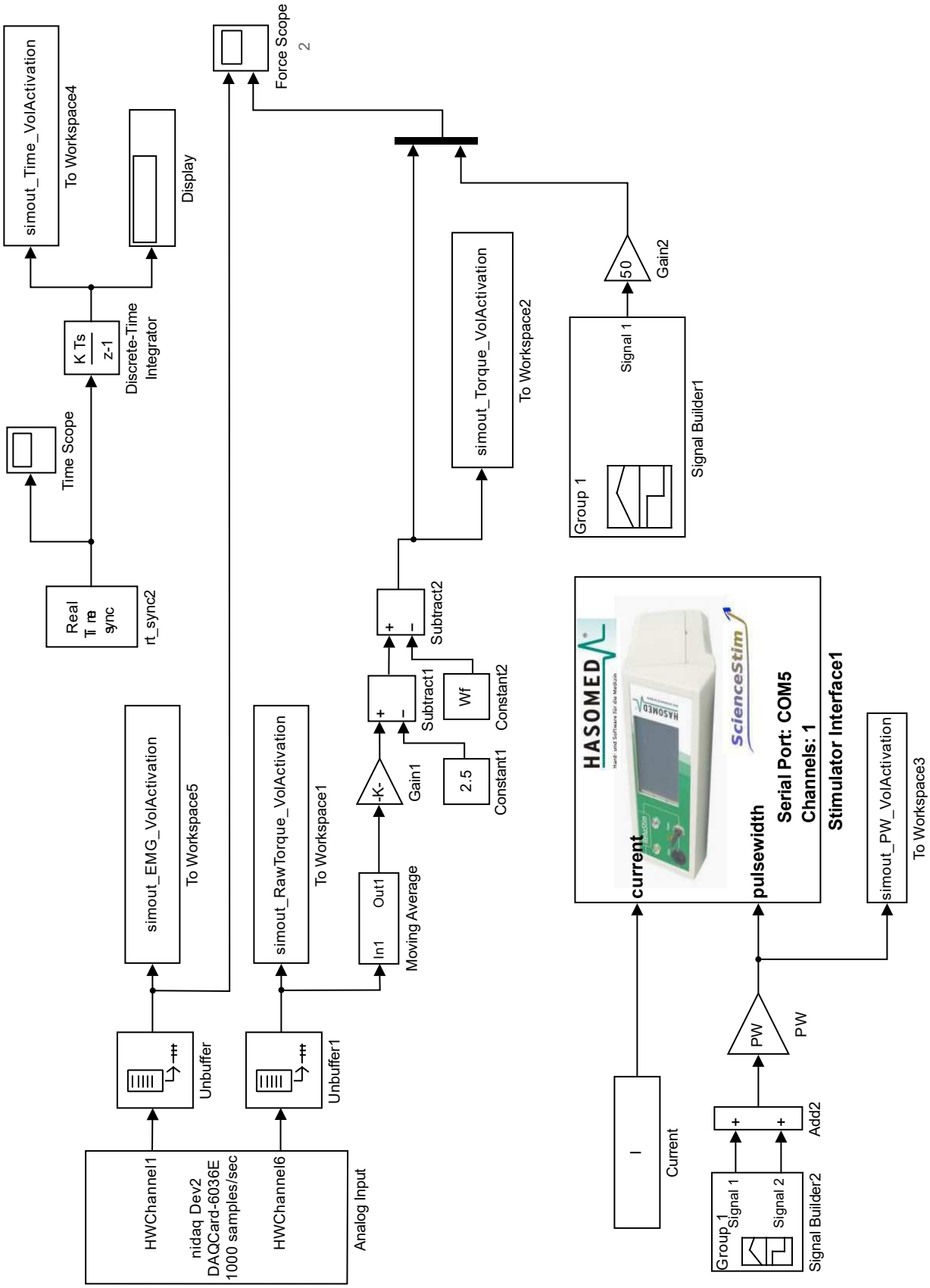

Figure 16: Simulink model "VoluntaryActivation.mdl". This model reads the input from the dynamometer and EMG device while participants attempt a voluntary contraction. During 3 of these attempts a single pulse of stimulation is applied before and during the contraction. The output is sent to the MATLAB workspace and displayed on a scope.

A.2 Study 2

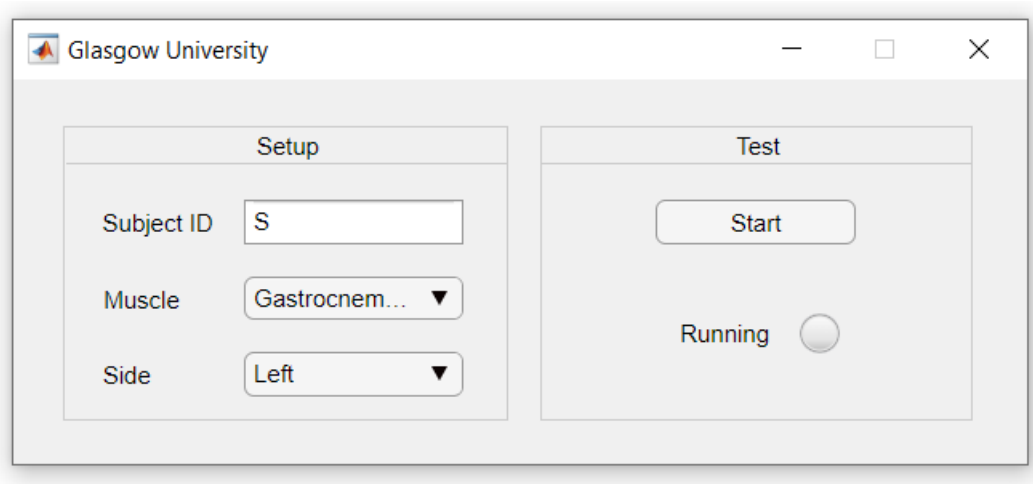

Figure 17: Interface of application created in MATLAB. The subject identification number can be entered, the muscle can be selected from the drop-down menu (gastrocnemius medialis, tibialis anterior or rectus femoris) and the side which is being examined can also be selected from a drop-down menu (left or right). When the start button is pressed, the "running" light turns amber. Once the ADC has started recording the EMG and goniometer signals, and the ultrasound has started recording the light turns green.

```
classdef app_us < matlab.apps.AppBase


    % Properties that correspond to app components
    properties (Access = public)
        uiUltrasound      matlab.ui.Figure
        pnlSetup          matlab.ui.container.Panel
        SubjectIDLabel    matlab.ui.control.Label
        editID            matlab.ui.control.EditField
        MuscleLabel       matlab.ui.control.Label
        comboMuscle       matlab.ui.control.DropDown
        SideLabel         matlab.ui.control.Label
        comboSide         matlab.ui.control.DropDown
        pnlTest           matlab.ui.container.Panel
        StartButton       matlab.ui.control.StateButton
        RunningLampLabel  matlab.ui.control.Label
        RunningLamp       matlab.ui.control.Lamp
    end

properties (Access = private)
        oADC = ClsEMGAndUS();
        oUS = ClsUSAction();
        TimeStart = [];
        TimeStop = [];
    end

    methods (Access = private)

        function fn_protocol_ended(app)
            try
                sID = app.editID.Value; % get the patient ID
                sSide = app.comboSide.Value; % get the side
                switch app.comboMuscle.Value % get the muscle
                    case 'Gastrocnemius'
                        sMuscle = 'GM';
                    case 'Tibialis Anterior'
                        sMuscle = 'TA';
                    case 'Quadriceps'
                        sMuscle = 'RF';
                    otherwise
                        sMuscle = 'NA';
                end
                fprintf(' ID: %s\n Muslce: %s\n Side: %s\n',
sID, sMuscle, sSide);

Time = app.oADC.Ts;
                EMG_Ch1 = app.oADC.Data(:,1);
                EMG_Ch2 = app.oADC.Data(:,2);
                EMG_Ch3 = app.oADC.Data(:,3);
```

Continued on the next page.

```
            US = app.oADC.Data(:,4);
             Goniometer_Ch1 = (app.oADC.Data(:,5)-2)/0.0111111;
             Goniometer_Ch2 = (app.oADC.Data(:,6)-2)/0.0111111;
                Trigger = app.oADC.Data(:,7);
                Time_Start = app.TimeStart;
                Time_Stop = app.TimeStop;

                path_SaveData =
'C:\Users\1105121m\Documents\Experimental Setup\Evaluation of
USI in Acute SCI\Data\';
                path_SaveUS = 'C:\Echo Images\';
                filename = [sID '_' sSide sMuscle '_'
datestr(now,'mmddyy_HHMMSS')];

                save([path_SaveData
filename],'Time','Time_Start','Time_Stop','EMG_Ch1','EMG_Ch2','
EMG_Ch3','US','Goniometer_Ch1','Goniometer_Ch2','Trigger');
                app.oUS.Ultrasound('save_tvd', [path_SaveUS
filename '.tvd']);

            catch ex
                fprintf('%s unexpected error in
fn_protocol_ended(), %s\n', datestr(now), ex.message);
            end
        end
    end

    % Callbacks that handle component events
    methods (Access = private)

        % Code that executes after component creation
        function cb_start_app(app)

            try
% initialise: creating the objects for the ADC and US
                app.oUS.EchoWaveIIStartupDelay = 40;
                app.oUS.Ultrasound('stop_record');

            catch ex
                fprintf('%s unexpected error in cb_start_app(),
%s\n', datestr(now), ex.message);
            end
        end

% Close request function: uiUltrasound
        function cb_stop_app(app, event)
            try
                delete(app)
            catch ex
```

Continued on the next page

```
fprintf('%s unexpected error in cb_stop_app(), %s\n',
datestr(now), ex.message);
            end
        end

        % Value changed function: StartButton
        function cb_start_stop_proc4(app, event)

            try
                if app.StartButton.Value % start the protocol
                   app.StartButton.Text = 'Stop';
                   app.StartButton.BackgroundColor = [0.96 0.96
0.96];
                    app.RunningLamp.Color = [0.93,0.69,0.13];

         % code here for starting the protocol
                    app.oADC.start_adc()     % Start ADC
                    app.TimeStart = now();   % Time ADC started
                    pause(2)                 % pause for 2
seconds (let ADC see US start through trigger signal)
                    app.oUS.Ultrasound('start_run'); % Start US
                    app.RunningLamp.Color = [0.00,1.00,0.00];

                else % stop the protocol
                    app.StartButton.Text = 'Start';
                    app.StartButton.BackgroundColor = [0.96
0.96 0.96];
                    app.RunningLamp.Color = [0.93,0.69,0.13];

                    % code here for stopping the protocol
                    app.oUS.Ultrasound('stop_run'); % Stop US
                    pause(2)                        % pause for
2 seconds (let ADC see US stop through trigger signal)
                    app.oADC.stop_adc();     % Stop ADC
                    app.TimeStop = now();    % Time ADC stopped
                    app.RunningLamp.Color = [0.90,0.90,0.90];

                    app.fn_protocol_ended(); % call the
function for dealing with the files

                end
            catch ex
                fprintf('%s unexpected error in
cb_start_stop_proc(), %s\n', datestr(now), ex.message);
            end
        end
    end
end
```

Figure 18: MATLAB code: "app_us.mlapp". This is the code view of the application created in the MATLAB app designer.

```
classdef ClsEMGAndUS < handle

    properties (SetAccess = public)
        Ts = [];
        Data = [];
        Events = [];
        s = [];
        oListener = [];
    end

    methods (Access = public)

        function obj = ClsEMGAndUS() % initialiser
        end

        function stop_adc(obj)
            try
            fprintf('%s %s\n', datestr(now()), 'stopping ADC');
                obj.s.stop();
                delete(obj.oListener);
                obj.s.release;
                daqreset();
            catch ex
                fprintf('%s Error: %s\n', datestr(now()),
ex.message);
            end
        end

        function start_adc(obj)

            daq.reset;
            obj.Ts = [];
            obj.Data = [];
            obj.Events = [];
            obj.s = daq.createSession('ni'); % nidaq object

            try
                % configure s
                obj.s.IsContinuous = true; % continuous op.
                obj.s.Rate = 2000; % 2000Hz
                obj.s.NotifyWhenDataAvailableExceeds = 4000;

                oAI1 = obj.s.addAnalogInputChannel('Dev1',
'ai1', 'Voltage'); % EMG ch1
                oAI1.TerminalConfig = 'SingleEnded';
                oAI1.Range = [-5 5];

                oAI2 = obj.s.addAnalogInputChannel('Dev1',
'ai2', 'Voltage'); % EMG ch2
                oAI2.TerminalConfig = 'SingleEnded';
                oAI2.Range = [-5 5];
```

Continued on the next page.

```
oAI3 = obj.s.addAnalogInputChannel('Dev1', 'ai3', 'Voltage'); %
EMG ch3
                oAI3.TerminalConfig = 'SingleEnded';
                oAI3.Range = [-5 5];

                oAI4 = obj.s.addAnalogInputChannel('Dev1',
'ai4', 'Voltage'); % US trigger
                oAI4.TerminalConfig = 'SingleEnded';
                oAI4.Range = [-10 10];

                oAI5 = obj.s.addAnalogInputChannel('Dev1',
'ai5', 'Voltage'); % Goniometer ch1
                oAI5.TerminalConfig = 'SingleEnded';
                oAI5.Range = [-5 5];

                oAI6 = obj.s.addAnalogInputChannel('Dev1',
'ai6', 'Voltage'); % Goniometer ch2
                oAI6.TerminalConfig = 'SingleEnded';
                oAI6.Range = [-5 5];

                oAI0 = obj.s.addAnalogInputChannel('Dev1',
'ai0', 'Voltage'); % Switch
                oAI0.TerminalConfig = 'SingleEnded';
                oAI0.Range = [-10 10];

                obj.oListener =
obj.s.addlistener('DataAvailable', @(src, event)
obj.addData(event));
                obj.s.prepare();
                fprintf('%s %s\n', datestr(now()), 'starting
ADC as background task');
                obj.s.startBackground(); % start background
task
            catch ex
                fprintf('%s Error: %s\n', datestr(now()),
ex.message);
            end
        end

function addData(obj, event)
            if isempty(obj.Ts)
                obj.Ts = event.TimeStamps;
                obj.Data = event.Data;
                obj.Events = event;
            else
                obj.Ts = [obj.Ts; event.TimeStamps];
                obj.Data = [obj.Data; event.Data];
                obj.Events = [obj.Events; event];
            end
```

Continued on the next page

```
            obj.plotData(20000, 1, 1, [-0.25,0.25],{'-0.2','-
      0.1','0','0.1','0.2'},'Amplitude (mV)','EMG: Rectus
      Femoris');
            obj.plotData(20000, 2, 3, [-0.25,0.25],{'-0.2','-
0.1','0','0.1','0.2'},'Amplitude (mV)','EMG: Tibialis
Anterior');
            obj.plotData(20000, 3, 5, [-0.25,0.25],{'-0.2','-
0.1','0','0.1','0.2'},'Amplitude (mV)','EMG: Gastrocnemius');
            obj.plotData(20000, 4, 2, [-
1,6],{'0','2','4','6'},'Amplitude (V)','US Trigger');
            obj.plotData(20000, 5, 4, [1,3],{'-90','-
45','0','45','90'},'Angle (degrees)','Joint Angle 1');
            obj.plotData(20000, 6, 6, [1,3],{'-90','-
45','0','45','90'},'Angle (degrees)','Joint Angle 2');
        end

        function plotData(obj, numSamples, chan, fig_no,
ylimits,ticklabels, axes_label, figure_title)
            if ~isempty(obj.Ts)
                dTs = obj.Ts;
                dData = obj.Data(:, chan);
                trigger_signal = obj.Data(:, 7);
                x = [0 0 0 0];
                y = [0 0 0 0];
                if length(dTs) > numSamples
                    dTs = dTs(end-numSamples+1:end);
                    dData = dData(end-numSamples+1:end);
                    trigger_signal = trigger_signal(end-
numSamples+1:end);

                    x1 = find(trigger_signal>5,1);
                    x2 = find(trigger_signal(x1:end)<5,1)+x1;

                    if isempty(x1) == 1 && isempty(x2) == 1
                            x = [dTs(end-numSamples+1)
dTs(end) dTs(end) dTs(end-numSamples+1)];
                        y = [0 0 0 0];
                    elseif isempty(x1) == 0 && isempty(x2) == 1
                        x = [dTs(x1) dTs(end) dTs(end)
dTs(x1)];
                        y = [ylimits(1) ylimits(1) ylimits(2)
ylimits(2)];
                    elseif isempty(x1) == 0 && isempty(x2) == 0
                        x = [dTs(x1) dTs(x2) dTs(x2) dTs(x1)];
                        y = [ylimits(1) ylimits(1) ylimits(2)
ylimits(2)];
                    end
                end
```

Continued on the next page

```
figure(1)
                set(gcf, 'Units', 'Normalized',
'OuterPosition', [0, 0, 1, 1]);
                subplot(3,2,fig_no)
                plot(dTs,dData)
                patch(x,y,'green','LineStyle','none') % add
patch for trigger signal
                set(gca,'children',flipud(get(gca,'children')))
                alpha(0.3) % make transparent
                ylim(ylimits)
                yticklabels(ticklabels);
                xlim([-inf inf]);
                xlabel('Time (seconds)');
                ylabel(axes_label);
                title(figure_title);
            end
        end
    end
end
```

Figure 19: MATLAB code: "ClsEMGandUS.mat". This is a MATLAB class that reads the input from each channel of the ADC, plots the output on a figure and saves the data with an appropriate filename based on the subject identification number, the muscle and the side being examined. This class is called from within the code of the application.

A.3 Study 3A

```
%% Setup Path for Saving
[pathname1,pathname2,sub_no] = set_dir;

%% MVC
Wf = Calibration;
[MVC_F,MVC_raw, MVC_T,MVC_PW] = MVC_run;
SaveUS(pathname2,'MVC');

%% Setting Pulsewidth
PW1 = 200; PW2 = 300; PW3 = 400;
trial=0;

%% Finding Minimum Current
a= 2;
Wf = Calibration;
[Imin, minI_F,minI_F_raw, minI_I,minI_T,minI_PW] = Min_I;
trial = trial+1;
save([pathname1 'Min_Curr_' num2str(trial)],'Imin',
'minI_F','minI_F_Raw','minI_I','minI_PW','minI_T');
SaveUS(pathname2,['Min_Current_' num2str(trial)]);

%%
trial = 0;

%% Current Activation Curve
Wf = Calibration;
Imax = str2double(inputdlg('Enter the value of Current'));
[Imax_F,Imax_F_Raw,Imax_PW,Imax_T] = Set_Imax;
trial = trial+1;
save([pathname1 'Curr_Select_' num2str(trial)],'Imax_F',
'Imax_F_Raw','Imax_PW','Imax_T','Imax');
SaveUS(pathname2,['Current_Activation_Curve_' num2str(trial)]);


%% Pre-FES Twitch-Tetanus

Wf = Calibration;
[TwT_PreFESc,TwT_F_Raw_PreFESc, TwT_PW_PreFESc,TwT_T_PreFESc] =
TwT;
SaveUS(pathname2,'TwT_PreFESc');
```

Continued on the next page.

```
% Constant FES (1)
Freq1 = First_Frequency; Freq = Freq1;
[a1,b1,c1,d1,e1,f1,g1,h1,i1,j1,k1,l1] = Random_Combination(PW1,
PW2, PW3, Imin, Imax);
a=a1;b=b1;c=c1;d=d1;e=e1;f=f1;g=g1;h=h1;i=i1;j=j1;k=k1;l=l1;
[FESc1,FESc1_raw,FESc1_t, FESc1_PW,FESc1_I] = FES_Con;
SaveUS(pathname2,'FES_Con1');

% Constant FES (2)
Freq2 = Second_Frequency(Freq1); Freq = Freq2;
[a2,b2,c2,d2,e2,f2,g2,h2,i2,j2,k2,l2] = Random_Combination(PW1,
PW2, PW3, Imin, Imax);
a=a2;b=b2;c=c2;d=d2;e=e2;f=f2;g=g2;h=h2;i=i2;j=j2;k=k2;l=l2;
[FESc2,FESc2_raw,FESc2_t, FESc2_PW,FESc2_I] = FES_Con;
SaveUS(pathname2,'FES_Con2');

% Post-FES2 Twitch-Tetanus
[TwT_PostFESc,TwT_F_Raw_PostFESc,
TwT_PW_PostFESc,TwT_T_PostFESc]= TwT;
SaveUS(pathname2,'TwT_PostFESc');

%% Pre-FES (Variable Frequency) Twitch-Tetanus
Wf = Calibration;
[TwT_PreFESvf,TwT_F_Raw_PreFESvf,
TwT_PW_PreFESvf,TwT_T_PreFESvf] = TwT;
SaveUS(pathname2,'TwT_PreFESvf');

%% Variable Freq FES (1)
PWv1 = 0; IPIv1 = 5;
IPI = Freq1; PW_V=PWv1; IPI_V=IPIv1;
a=a1;b=b1;c=c1;d=d1;e=e1;f=f1;g=g1;h=h1;i=i1;j=j1;k=k1;l=l1;
[FESvf1,FESvf1_raw,FESvf1_t, FESvf1_PW,FESvf1_I] = FES_Var;
SaveUS(pathname2,'FES_VarF1');


% Variable Freq FES (2)
IPI = Freq2;
a=a2;b=b2;c=c2;d=d2;e=e2;f=f2;g=g2;h=h2;i=i2;j=j2;k=k2;l=l2;
[FESvf2,FESvf2_raw,FESvf2_t, FESvf2_PW,FESvf2_I] = FES_Var;
SaveUS(pathname2,'FES_VarF2');


%% Post-FES2 (Variable Frequency) Twitch-Tetanus
[TwT_PostFESvf,TwT_F_Raw_PostFESvf,
TwT_PW_PostFESvf,TwT_T_PostFESvf]= TwT;
SaveUS(pathname2,'TwT_PostFESvf');
```

Continued on the next page

```
%% Pre-FES (Variable Pulsewidth) Twitch-Tetanus
Wf = Calibration;
[TwT_PreFESvp,TwT_F_Raw_PreFESvp,
TwT_PW_PreFESvp,TwT_T_PreFESvp] = TwT;
SaveUS(pathname2,'TwT_PreFESvp');

%% Variable PW FES (1)
PWv2 = 20; IPIv2 = 0;
IPI = Freq1; PW_V=PWv2; IPI_V=IPIv2;
a=a1;b=b1;c=c1;d=d1;e=e1;f=f1;g=g1;h=h1;i=i1;j=j1;k=k1;l=l1;
[FESvp1,FESvp1_raw,FESvp1_t, FESvp1_PW,FESvp1_I] = FES_Var;
SaveUS(pathname2,'FES_VarPW1');

% Variable PW FES (2)
IPI = Freq2;
a=a2;b=b2;c=c2;d=d2;e=e2;f=f2;g=g2;h=h2;i=i2;j=j2;k=k2;l=l2;
[FESvp2,FESvp2_raw,FESvp2_t, FESvp2_PW,FESvp2_I] = FES_Var;
SaveUS(pathname2,'FES_VarPW2');

%% Post-FES2 (Variable Pulsewidth) Twitch-Tetanus
[TwT_PostFESvp,TwT_F_Raw_PostFESvp,
TwT_PW_PostFESvp,TwT_T_PostFESvp]= TwT;
SaveUS(pathname2,'TwT_PostFESvp');

%% Pre-Vol Twitch-Tetanus
Wf = Calibration;
[TwT_PreVol,TwT_F_Raw_PreVol, TwT_PW_PreVol,TwT_T_PreVol] =
TwT;
SaveUS(pathname2,'TwT_PreVol');

%% Voluntary Protocol (1)
[u1,v1,w1,x1,y1,z1] = Target(FESc1,FESvf1,FESvp1);
u=u1;v=v1;w=w1;x=x1;y=y1;z=z1;
[Vol1,Vol_Raw1, Vol_T1, Vol_Target_Warning1,Vol_Target_Actual1]
= Vol_Run;
SaveUS(pathname2,'Vol1');

%% Voluntary Protocol (2)
[u2,v2,w2,x2,y2,z2] = Target(FESc2,FESvf2,FESvp2);
u=u2;v=v2;w=w2;x=x2;y=y2;z=z2;
[Vol2,Vol_Raw2, Vol_T2, Vol_Target_Warning2,
Vol_Target_Actual2] = Vol_Run;
SaveUS(pathname2,'Vol2');

%% Post-Vol2 Twitch-Tetanus
[TwT_PostVol,TwT_F_Raw_PostVol, TwT_PW_PostVol,TwT_T_PostVol] =
TwT;
SaveUS(pathname2,'TwT_PostVol');

%% Saving Required Data
save([pathname1 'Subject' num2str(sub_no)]);
```

Figure 20: MATLAB code: "Full_Protocol.mat". This is the main script where each section (denoted by "%%" symbols and a green title) runs a part of the experiment. The MATLAB functions and Simulink models called within this script are detailed in subsequent figures in this section.

```
function [pathname1, pathname2, sub_no] = set_dir

sub_no = char(inputdlg('Enter the Subject ID Code','s'));
makepath1 =
mkdir(['D:\Users\scisci\Documents\MATLAB\Jennifer\Data\'
sub_no]);
makepath2 = mkdir(['D:\Echo Images\' sub_no]);

pathname1 = ['D:\Users\scisci\Documents\MATLAB\Jennifer\Data\'
sub_no '\'];
pathname2 = ['D:\Echo Images\' sub_no '\'];
```

Figure 21: MATLAB code: "set_dir.mat". This function generates a text box where the user is asked to enter a subject ID code. A folder is created with the appropriate name where data is saved.

```
function [Wf] = Calibration
sim('Dynamometer');
Wf = mean(squeeze(simout_Dynamometer));
```

Figure 22: MATLAB code: "Calibration.mat". This function runs the "Dynamometer.mdl" Simulink model to obtain the value of torque from the weight of the foot resting on the foot plate. This value is then subtracted from torque readings

```
function [cmd] = ControlUS()
% set path to Echo Wave II automation interface client .Net
assembly (dll)
asm_path = 'D:\Program Files\TELEMED\Echo Wave
II\Config\Plugins\autoint1client.dll';

% load assembly
asm = NET.addAssembly(asm_path);

% create commands interface object
cmd = AutoInt1Client.CmdInt1();

% connect to started Echo Wave II software
ret = cmd.ConnectToRunningProgram();
if (ret ~= 0)
msgbox('Error. Cannot connect to Echo Wave II software. Please
make sure that software is running.', 'Error')
end
cmd.FreezeRun(); %Start recording
```

Figure 23: MATLAB code: "ControlUS.mat". This function is adapted from open source code (Telemed, Lithuania) to start and stop the ultrasound device recording.

```
function [cmd] = SaveUS(path, filename)

% set path to Echo Wave II automation interface client .Net
assembly (dll)
asm_path = 'D:\Program Files\TELEMED\Echo Wave
II\Config\Plugins\autoint1client.dll';

% load assembly
asm = NET.addAssembly(asm_path);

% create commands interface object
cmd = AutoInt1Client.CmdInt1();

% connect to started Echo Wave II software
ret = cmd.ConnectToRunningProgram();
if (ret ~= 0)
msgbox('Error. Cannot connect to Echo Wave II software. Please
make sure that software is running.', 'Error')
end

cmd.WmCopyDataCmd(['-save^#^' path filename '.tvd^#^'])
```

Figure 24: MATLAB code: "SaveUS.mat". This function is adapted from open source code (Telemed, Lithuania) to save ultrasound videos.

```
function [MVC,MVC_raw, Time,PW] = MVC_run

open_system('MVC/Force Scope');
ControlUS;
sim('MVC');
ControlUS;
True_MVC(squeeze(simout_MVC));

MVC = squeeze(simout_MVC);
MVC_raw = squeeze(simout_MVC_raw);
Time = squeeze(simout_MVC_Time);
PW = squeeze(simout_MVC_PW);
```

Figure 25: MATLAB code: "MVC.mat". This function controls the ultrasound recording, runs the Simulink model "MVC", and stores the output variables torque (MVC), time and pulsewidth (PW).

```
function True_MVC(MVC)

Fs=50;

MVC_before = max(MVC(9.5*Fs:9.9*Fs));
MVC_after = max(MVC(10.1*Fs:10.8*Fs));
Limit = MVC_before + (MVC_before*0.1);

if MVC_after>Limit
    msgbox('True MVC has not been achieved')
else
    msgbox('True MVC has been achieved')
end
```

Figure 26: MATLAB code: "MVC_True.mat". This function calculates the increase in torque when stimulation is delivered during attempted MVC. Depending on whether or not the increase is less than 10%, a message notifies the user if a true MVC has been achieved or not.

```
function[Imin, minI_F,minI_F_raw, minI_I,minI_T,minI_PW] =
Min_I

open_system('Min_Current/I_Force Scope')
ControlUS;
sim('Min_Current')
ControlUS;
Imin = str2double(inputdlg('Enter the Minimum Value of
Current'));

minI_F = squeeze(simout_Force_minI);
minI_F_raw = squeeze(simout_Force_minI_raw);
minI_I = squeeze(simout_minI_I);
minI_PW = squeeze(simout_minI1_PW);
minI_T = squeeze(simout_Min_I_Time);
```

Figure 27: MATLAB code: "Min_I.mat". This function controls the ultrasound recording, runs the Simulink model "Min_Current", and stores the output variables torque (minI_F), time (minI_T), current (minI_I) and pulsewidth (minI_PW).

```
function[Imax_F,Imax_F_Raw,Imax_PW,Imax_T]= Set_Imax

open_system('Setting_Current/Force Scope')
ControlUS;
sim('Setting_Current')
ControlUS;

Imax_F = squeeze(simout_Force_I);
Imax_F_Raw = squeeze(simout_Force_I_Raw);
Imax_PW = squeeze(simout_Set_I_PW);
Imax_T = squeeze(simout_Set_I_Time);
```

Figure 28: MATLAB code: "Set_Imax.mat". This function controls the ultrasound recording, runs the Simulink model "Setting_Current", and stores the output variables torque (Imax_F), time (Imax_T), and pulsewidth (Imax_PW).

```
function Freq = First_Frequency

choice = questdlg('Which Frequency Value Should Be Used First?
', ...
    'Frequency Value', ...
    '20 Hz','40 Hz','40 Hz');

switch choice
    case '20 Hz'
        Freq = 50;
    case '40 Hz'
        Freq = 25;
end
FES_I = squeeze(simout_FES_I);
```

Figure 29: MATLAB code: "First_Frequency.mat". This function opens a dialogue box, giving the user the option to select the frequency at which the first trains of stimulation will be delivered.

```
function Freq2 = Second_Frequency(Freq1)

if Freq1 == 50
Freq2 = 25;
end
```

Figure 30: MATLAB code: "Second_Frequency.mat". This function determines which frequency will be designated "Freq2" based on the value of "Freq1" that was chosen.

```
function [a,b,c,d,e,f,g,h,i,j,k,l] = Random_Combination(PW1,
PW2, PW3, Imin, Imax)

Combinations = [PW1 Imin; PW1 Imax; PW2 Imin; PW2 Imax; PW3
Imin; PW3 Imax];

ordering = randperm(6);
Shuffled = Combinations(ordering, :);

a = Shuffled(1,1);
b = Shuffled(2,1);
c = Shuffled(3,1);
d = Shuffled(4,1);
e = Shuffled(5,1);
f = Shuffled(6,1);

g = Shuffled(1,2);
h = Shuffled(2,2);
i = Shuffled(3,2);
j = Shuffled(4,2);
k = Shuffled(5,2);
l = Shuffled(6,2);
```

Figure 31: MATLAB code: "Random_Combination.mat". This function takes each pair of current and pulsewidth values and generates a random order

```
function [TwT_F,TwT_F_Raw, TwT_PW,TwT_T] = TwT

open_system('Twitch_Tetanus/Force Scope')
ControlUS;
sim('Twitch_Tetanus');
ControlUS;

TwT_F = squeeze(simout_TwTF);
TwT_F_Raw = squeeze(simout_TwTF_Raw);
TwT_PW = squeeze(simout_TwT_PW);
TwT_T = squeeze(simout_TwT_Time);
Plot_TwT(TwT_F);
```

Figure 32: MATLAB code: "TwT.mat". This function controls the ultrasound recording, runs the Simulink model "Twitch_Tetanus", and stores the output variables torque (TwT_F), time (TwT_T) and pulsewidth (TwT_PW). The torque is also plotted in a figure.

```
function [FES,FES_Raw,FES_t, FES_PW,FES_I] = FES_Con

open_system('FES_Constant/Force Scope')
open_system('FES_Constant/Participant Scope')
ControlUS;
sim('FES_Constant');
ControlUS;

FES = squeeze(simout_FES);
FES_Raw = squeeze(simout_FES_Raw);
FES_t = squeeze(simout_FES_Time);
FES_PW = squeeze(simout_FES_PW);
FES_I = squeeze(simout_FES_I);
```

Figure 33: MATLAB code: "FES_Constant.mat". This function controls the ultrasound recording, runs the Simulink model "FES_Constant", and stores the output variables torque (FES), time (FES_t), current (FES_I) and pulsewidth (FES_PW).

```
function [FES,FES_Raw,FES_t,FES_PW,FES_I] = FES_Var

open_system('FES_Variable/Force Scope')
open_system('FES_Variable/Participant Scope')
ControlUS;
sim('FES_Variable');
ControlUS;

FES = squeeze(simout_FES);
FES_Raw = squeeze(simout_FES_Raw);
FES_t = squeeze(simout_FES_Time);
FES_PW = squeeze(simout_FES_PW);
FES_I = squeeze(simout_FES_I);
```

Figure 34: MATLAB code: "FES_Var.mat". This function controls the ultrasound recording, runs the Simulink model "FES_Variable", and stores the output variables torque (FES), time (FES_t), current (FES_I) and pulsewidth (FES_PW).

```
function [Vol,Vol_Raw, Vol_T,
Vol_Target_Warning,Vol_Target_Actual] = Vol_Run

open_system('Voluntary/Scope')
sim('Voluntary');
Vol = squeeze(simout_Vol);
Vol_Raw = squeeze(simout_Vol_Raw);
Vol_T = squeeze(simout_Vol_Time);
Vol_Target_Warning = squeeze(simout_Vol_Target_Warning);
Vol_Target_Actual = squeeze(simout_Vol_Target_Actual);
```

Figure 35: MATLAB code: "Run_Voluntary.mat". This function controls the ultrasound recording, runs the Simulink model "Voluntary", and stores the output variables torque (Vol), time (Vol_T) the warning (Vol_Target_Warning), and the target (Vol_Target_Actual) signal the participant is following.

```
function[u,v,w,x,y,z]=Target(FES_Constant, FES_VariableF,
FES_VariablePW)

Fs = 50;

t1 = 7.5*Fs;
t2 = t1 + (5*Fs);
t3 = t2 + (10*Fs);
t4 = t3 + (5*Fs);
t5 = t4 + (10*Fs);
t6 = t5 + (5*Fs);
t7 = t6 + (10*Fs);
t8 = t7 + (5*Fs);
t9 = t8 + (10*Fs);
t10 = t9 + (5*Fs);
t11 = t10 + (10*Fs);
t12 = t11 + (5*Fs);

u1 = mean(FES_Constant(t1:t2));
v1 = mean(FES_Constant(t3:t4));
w1 = mean(FES_Constant(t5:t6));
x1 = mean(FES_Constant(t7:t8));
y1 = mean(FES_Constant(t9:t10));
z1 = mean(FES_Constant(t11:t12));

u2 = mean(FES_VariableF(t1:t2));
v2 = mean(FES_VariableF(t3:t4));
w2 = mean(FES_VariableF(t5:t6));
x2 = mean(FES_VariableF(t7:t8));
y2 = mean(FES_VariableF(t9:t10));
z2 = mean(FES_VariableF(t11:t12));

u3 = mean(FES_VariablePW(t1:t2));
v3 = mean(FES_VariablePW(t3:t4));
w3 = mean(FES_VariablePW(t5:t6));
x3 = mean(FES_VariablePW(t7:t8));
y3 = mean(FES_VariablePW(t9:t10));
z3 = mean(FES_VariablePW(t11:t12));

u = (u1+u2+u3)/3;
v = (v1+v2+v3)/3;
w = (w1+w2+w3)/3;
x = (x1+x2+x3)/3;
y = (y1+y2+y3)/3;
z = (z1+z2+z3)/3;
```

Figure 36: MATLAB code: "Target.mat". This script generates the target value of torque participants must attempt to reach based on the average torque produced during constant, variable frequency and variable pulsewidth stimulation for each combination of stimulation parameters.

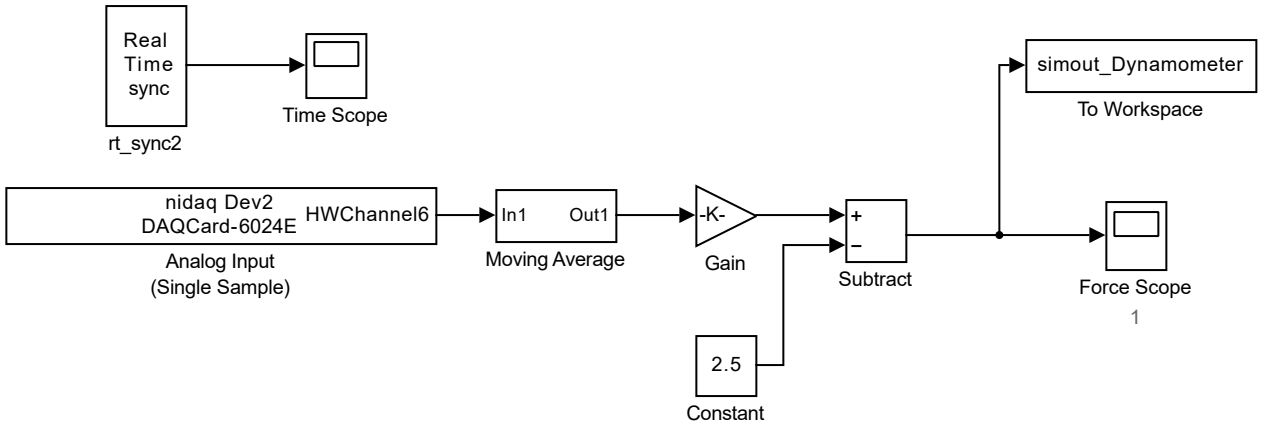

Figure 37: Simulink model "Dynamometer.mdl". This model reads the input from the dynamometer, applies a moving average filter, applies a conversion factor to convert the voltage signal to torque (K) and zeros the baseline. The output is sent to the MATLAB workspace and displayed on a scope.

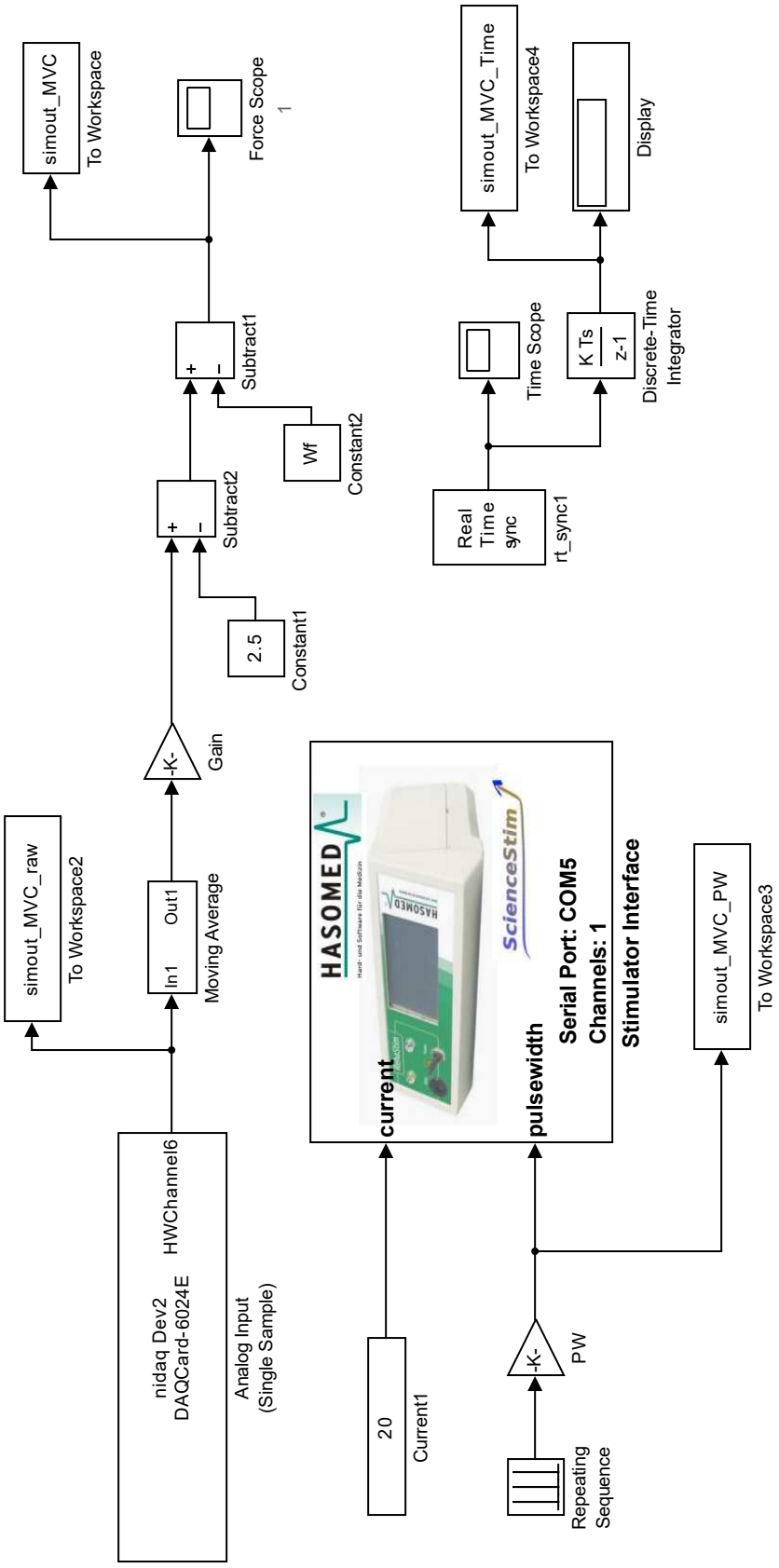

Figure 38: Simulink model "MVC.mdl". This model reads in the torque from the dynamometer during an attempted MVC. Current, pulsewidth and frequency are controlled to deliver a pulse of stimulation during the contraction. The output is sent to the MATLAB workspace and displayed on a scope.

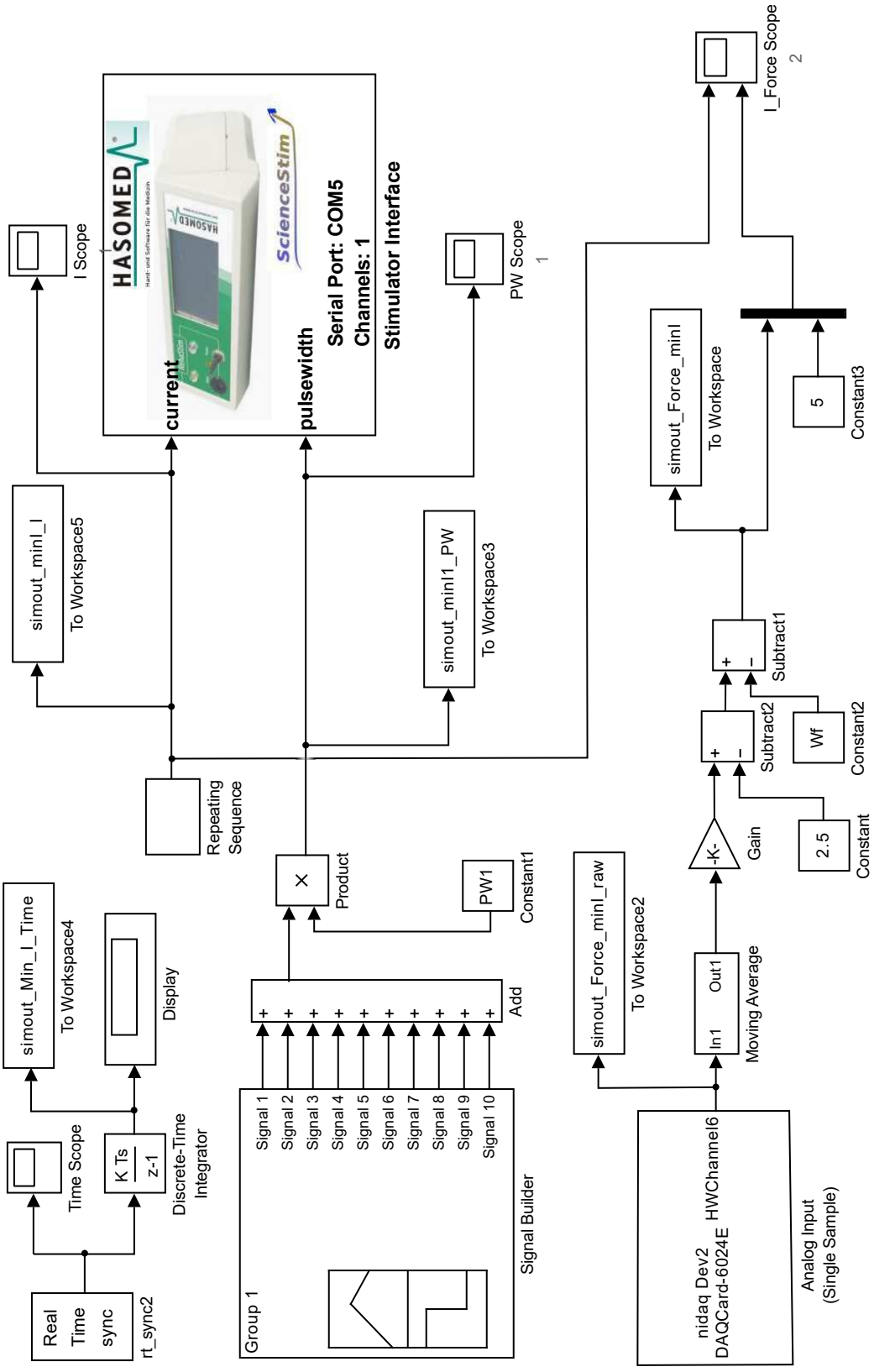

Figure 39: Simulink model "Min_Current.mdl". This model reads the input from the dynamometer while stimulation is applied. The current, pulsewidth and frequency are controlled to deliver ramped contractions lasting 10 seconds. The output is sent to the MATLAB workspace and displayed on a scope.

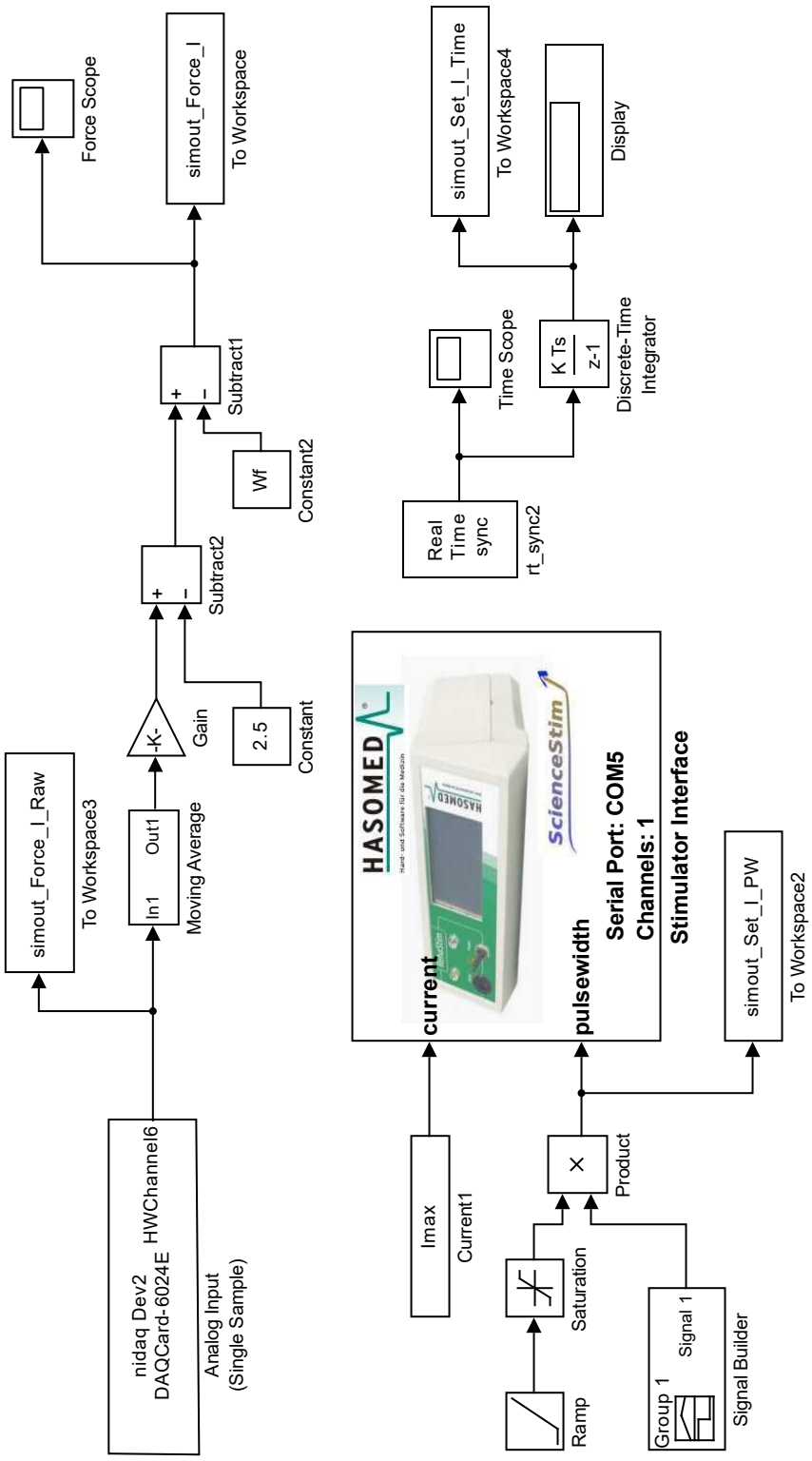

Figure 40: Simulink model "Setting_Current.mdl". This model reads the input from the dynamometer while stimulation is applied. The current, pulsewidth and frequency are controlled to gradually increase the stimulation over 10 seconds and remain constant for 5 seconds. The output is sent to the MATLAB workspace and displayed on a scope.

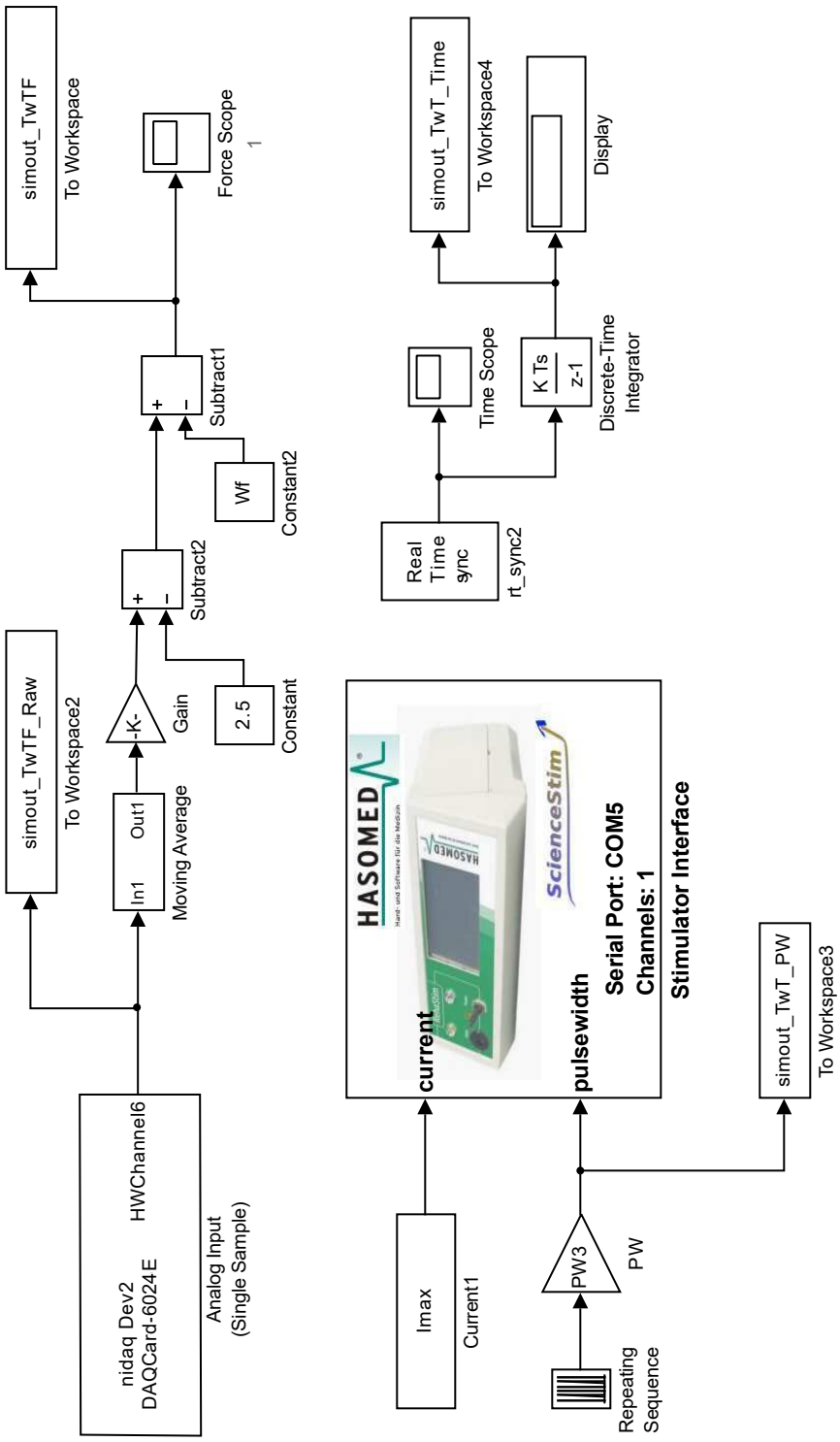

Figure 41: Simulink model "TwitchTetanus.mdl". This model reads the input from the dynamometer while stimulation is applied. The current, pulsewidth and frequency are controlled to deliver a single pulse, followed by a 1 second train of stimulation. The output is sent to the MATLAB workspace and displayed on a scope.

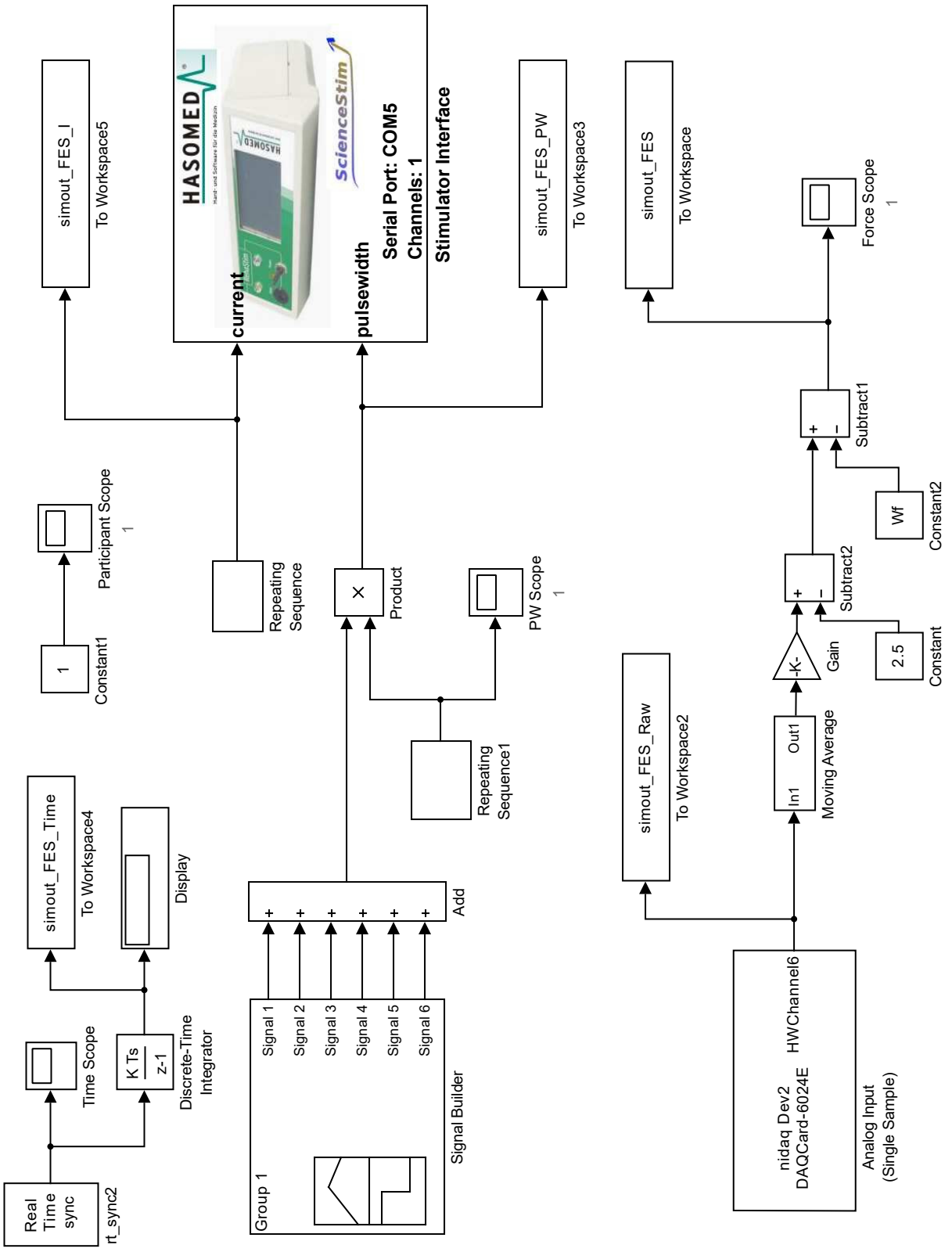

Figure 42: Simulink model "FES_Constant.mdl". This model reads the input from the dynamometer while stimulation is applied. The current, pulsewidth and frequency are controlled to deliver ramped contractions lasting 10 seconds each with 5 second rest periods. Each train of stimulation delivers a different combination of current, pulsewidth and frequency. The output is sent to the MATLAB workspace and displayed on a scope.

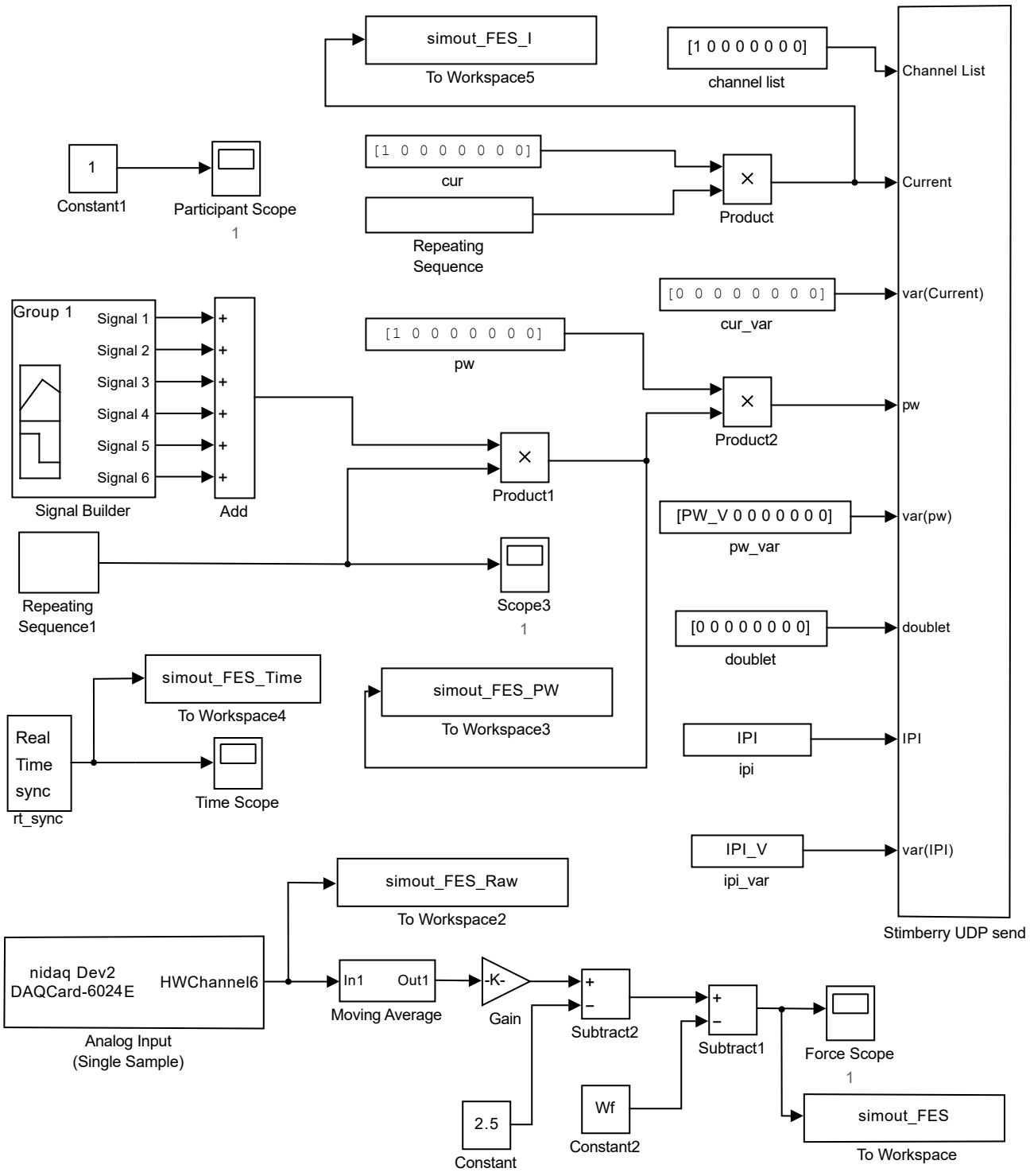

Figure 43: Simulink model "FES_Variable.mdl". Similar to "FES_Constant model" (see Figure 42) but instead of communicating directly with the stimulator, the interface is with a raspberry pi single board-computer to allow the inter-pulse interval and pulsewidth to be varied. The output is sent to the MATLAB workspace and displayed on a scope.

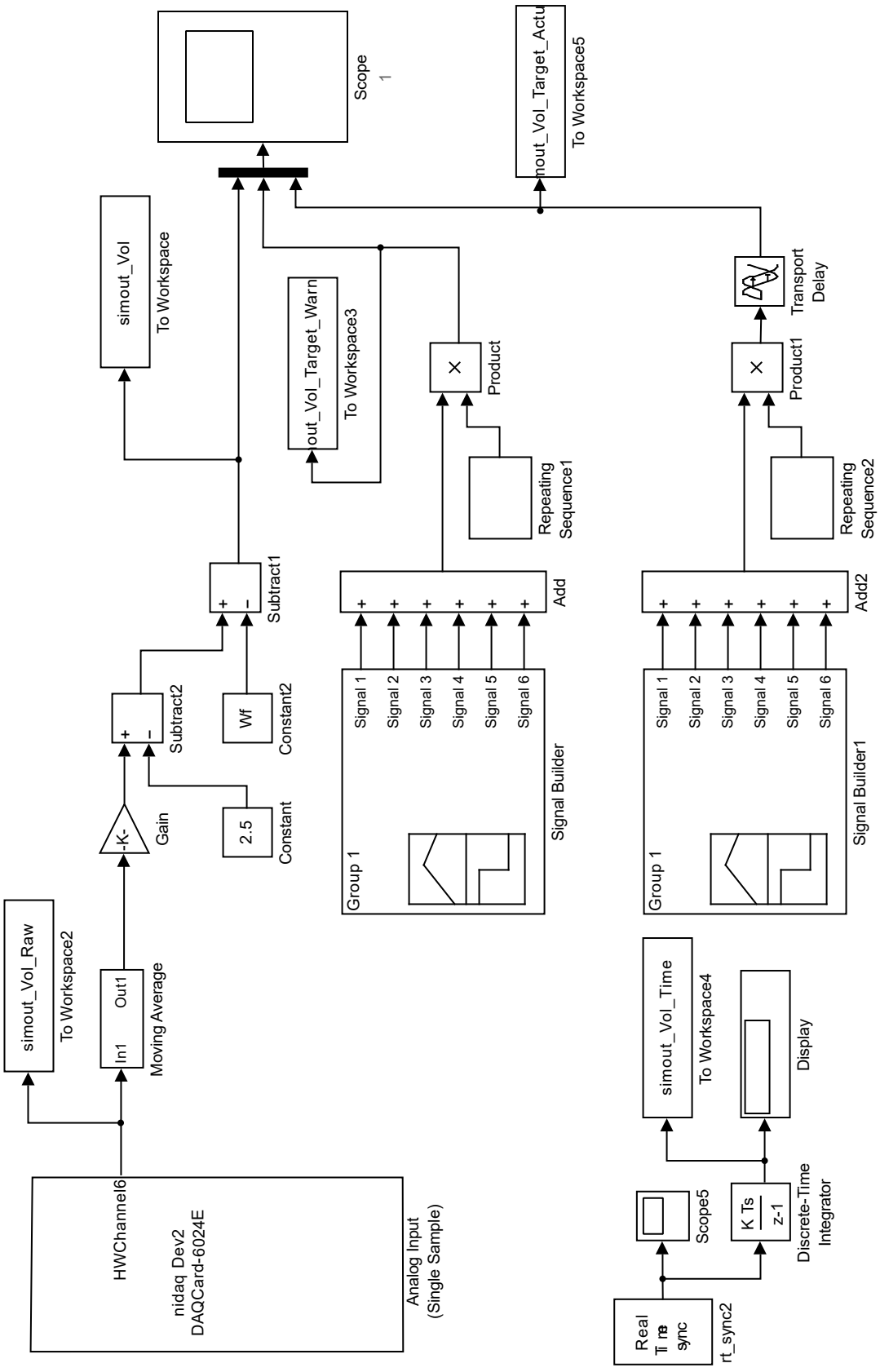

Figure 44: Simulink model "Voluntary.mdl". This model reads the input from the dynamometer while the participant performs voluntary contractions. The torque is shown to the participant on a scope in real time along with a target torque signal to follow. The output is sent to the MATLAB workspace.

B USI measurements for assessing and predicting recovery

B.1 Changes in measurements of muscle structure

Table 1: P-values and effect sizes for the changes in first-order descriptors of muscle echogenicity between the first and last session.

First-order descriptors		
	P-Value	*Effect Size*
Mean	0.78	0.18
Variance	0.86	0.02
Skewness	0.39	0.61
Kurtosis	0.95	0.30
Energy	0.78	0.22
IOD	0.78	0.11

Table 2: P-values and effect sizes for changes in Haralick features between sessions.

Contrast		
	P-Value	*Effect Size*
0 °	0.53	0.43
45 °	0.86	0.30
90 °	0.53	0.07
135 °	0.39	0.37
Correlation		
	P-Value	*Effect Size*
0 °	0.78	0.18
45 °	0.69	0.23
90 °	0.61	0.08
135 °	0.78	0.09
Energy		
	P-Value	*Effect Size*
0 °	0.46	0.23
45 °	0.61	0.22
90 °	0.46	0.09
135 °	0.46	0.18
Entropy		
	P-Value	*Effect Size*
0 °	0.86	0.08
45 °	0.93	0.08
90 °	0.62	0.40
135 °	0.75	0.42
Homogeneity		
	P-Value	*Effect Size*
0 °	0.33	0.54
45 °	0.53	0.45
90 °	0.53	0.03
135 °	0.61	0.37

Table 3: P-values and effect sizes for changes in Galloway features between the sessions.

SRE		
	P-Value	*Effect Size*
0 °	0.86	0.05
45 °	0.86	0.05
90 °	0.86	0.05
135 °	0.86	0.06
LRE		
	P-Value	*Effect Size*
0 °	0.69	0.26
45 °	0.61	0.28
90 °	0.53	0.29
135 °	0.78	0.24
GLNU		
	P-Value	*Effect Size*
0 °	0.27	0.53
45 °	0.46	0.47
90 °	0.86	0.11
135 °	0.46	0.42
RLNU		
	P-Value	*Effect Size*
0 °	0.95	0.24
45 °	0.86	0.30
90 °	0.95	0.17
135 °	0.86	0.10
RP		
	P-Value	*Effect Size*
0 °	0.33	0.59
45 °	0.33	0.54
90 °	0.69	0.06
135 °	0.46	0.44

Table 4: P-values and effect sizes for changes in LBP features describing muscle echogenicity between the first and last session.

LBP features		
	P-Value	*Effect Size*
Energy	0.55	0.42
Entropy	0.74	0.39

B.2 Changes in measurements of muscle function

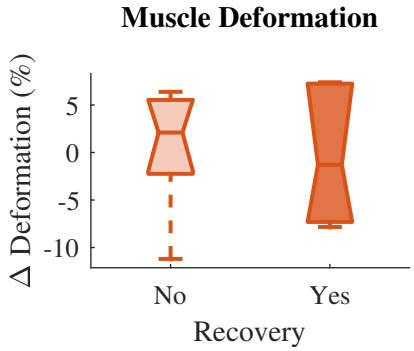

Figure 45: Boxplots of the difference between the first and last session for muscle deformation during attempted MVC.

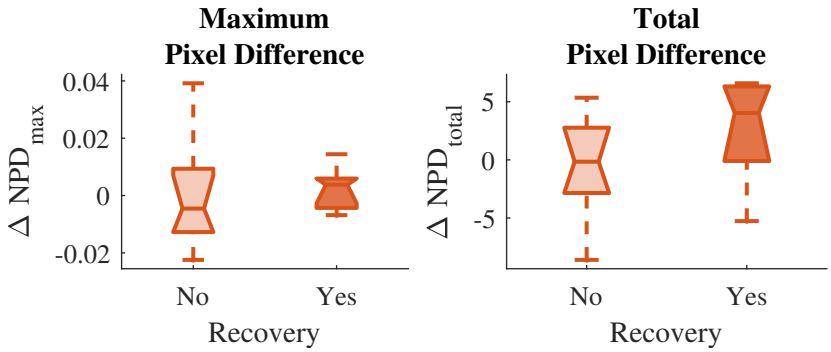

(a) Maximum (b) Total

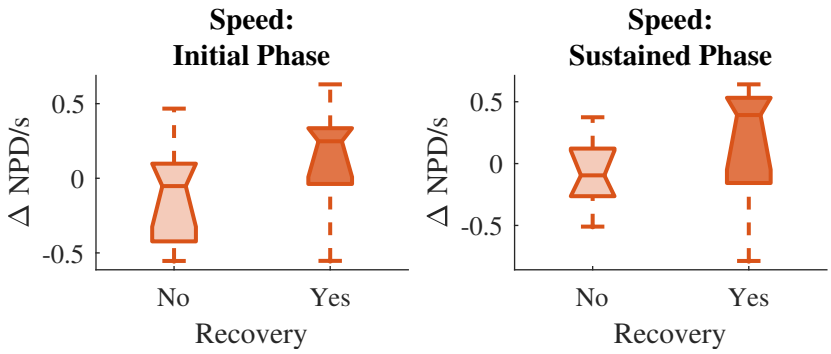

(c) Speed: Initial Phase (d) Speed: Sustained Phase

Figure 46: Boxplots of the difference between the first and last session for measurements of pixel difference during attempted MVC.

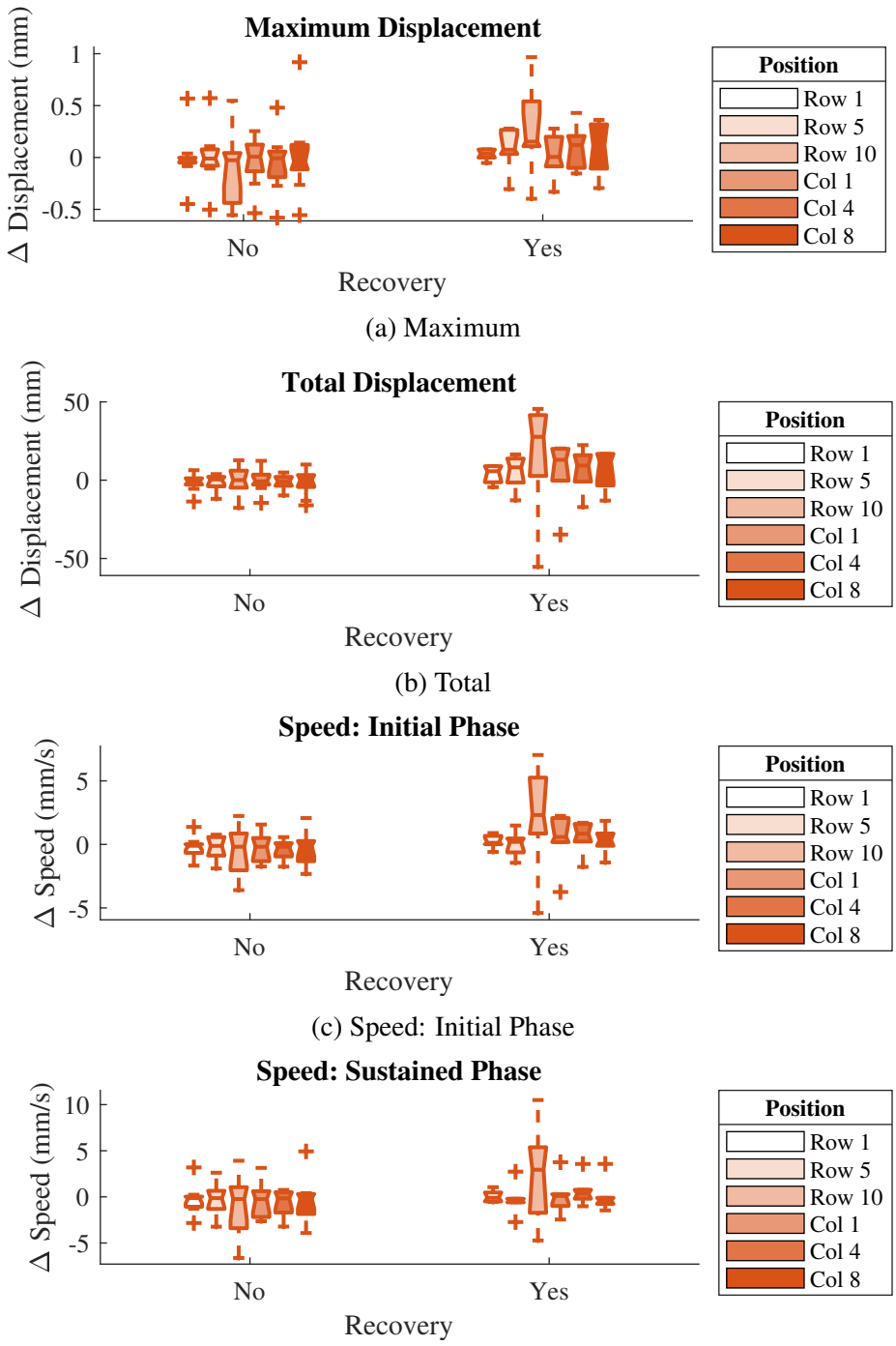

(a) Maximum

(b) Total

(c) Speed: Initial Phase

(d) Speed: Sustained Phase

Figure 47: Boxplots of the difference between the first and last session for measurements of muscle displacement during attempted MVC.

Table 5: P-values and effect sizes for changes in measurements of muscle movement calculated from the pixel difference between the first and last session.

Pixel difference measurements		
	P-Value	*Effect Size*
Maximum	0.45	0.24
Total	0.14	0.69
Speed (initial)	0.18	0.63
Speed (sustained)	0.22	0.58

Table 6: P-values and effect sizes for changes in measurements of muscle movement calculated from displacement between the first and last session.

Maximum displacement		
	P-Value	*Effect Size*
row 1	0.14	0.17
row 5	0.27	0.28
row 10	0.09	**0.85**
column 1	0.86	0.19
column 4	0.27	0.58
column 8	0.53	0.19
Total displacement		
	P-Value	*Effect Size*
row 1	0.14	**0.90**
row 5	0.18	**0.82**
row 10	0.11	0.60
column 1	0.14	0.37
column 4	0.11	0.78
column 8	0.18	0**.80**
Speed: initial (displacement)		
	P-Value	*Effect Size*
row 1	0.14	0.62
row 5	0.61	0.39
row 10	0.09	0.79
column 1	0.22	0.41
column 4	0.07	**0.92**
column 8	0.33	0.54
Speed: sustained (displacement)		
	P-Value	*Effect Size*
row 1	0.39	0.27
row 5	0.95	0.08
row 10	0.22	0.78
column 1	0.53	0.32
column 4	0.14	**0.87**
column 8	0.95	0.18

B.3 Measurements of muscle structure to predict recovery

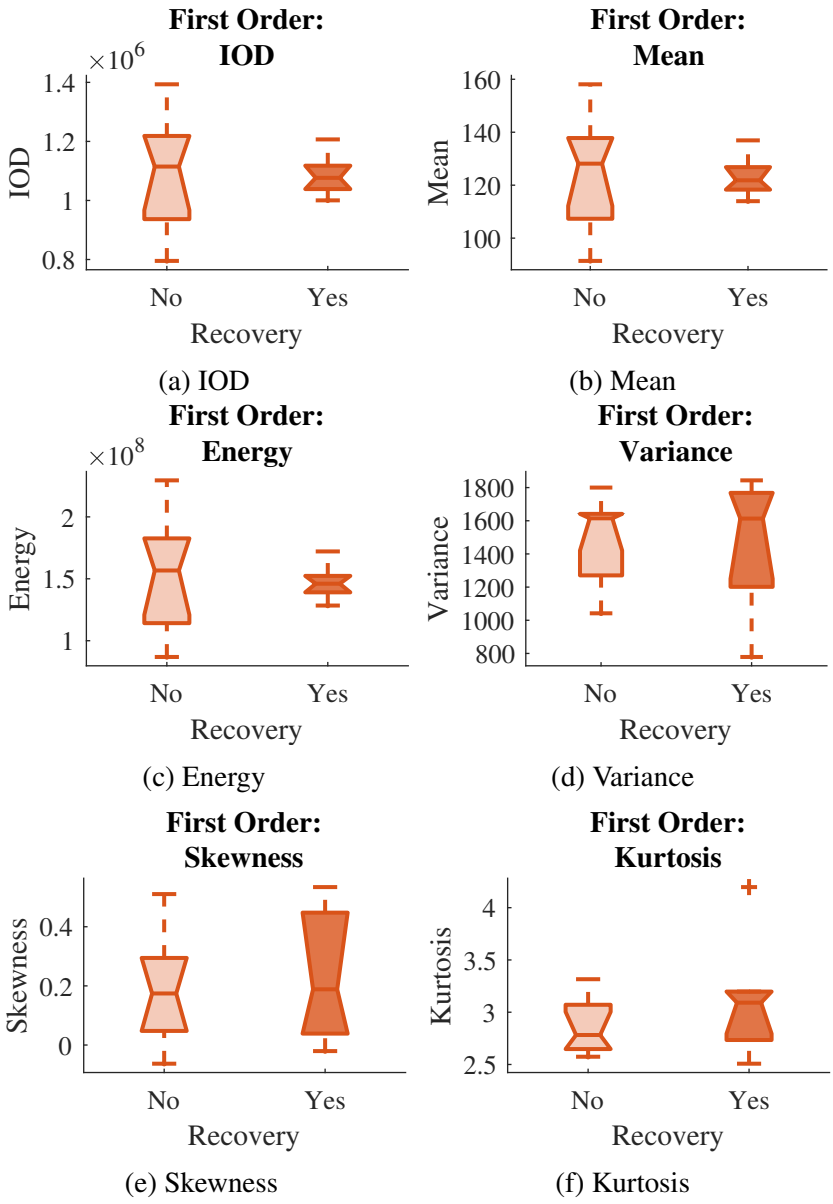

(a) IOD (b) Mean

(c) Energy (d) Variance

(e) Skewness (f) Kurtosis

Figure 48: Boxplots of first-order measurements of muscle echogenicity on the first session grouped according to whether participants showed significant recovery.

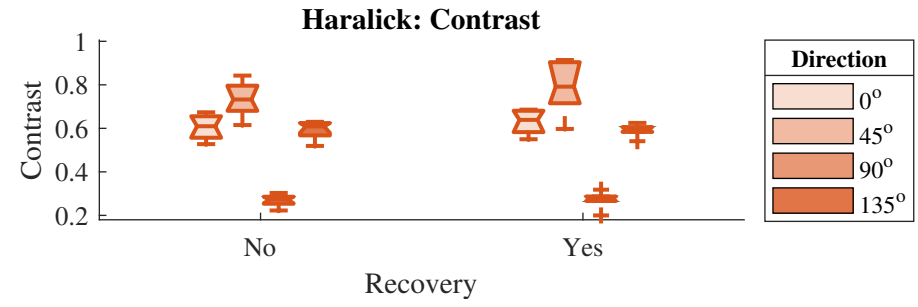

(a) Contrast

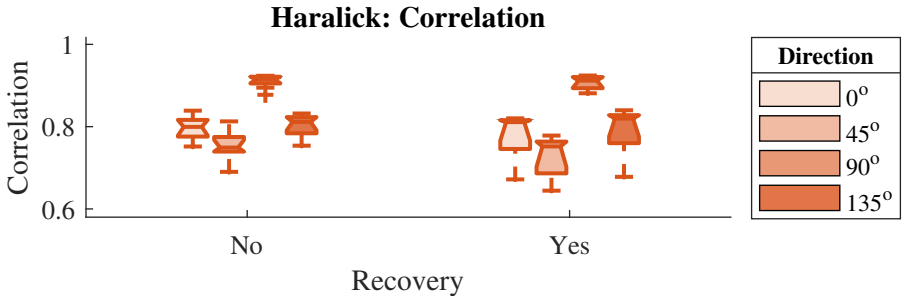

(b) Correlation

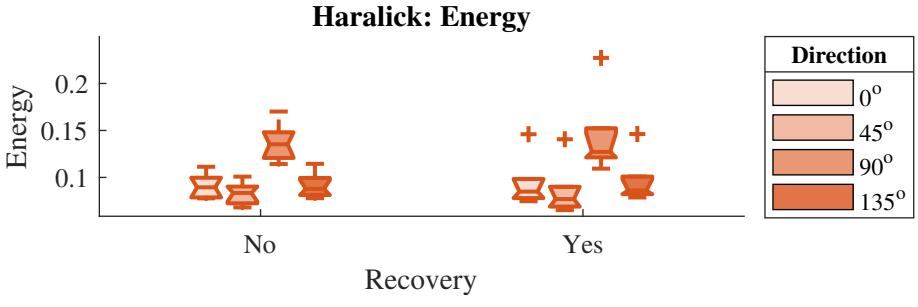

(c) Energy

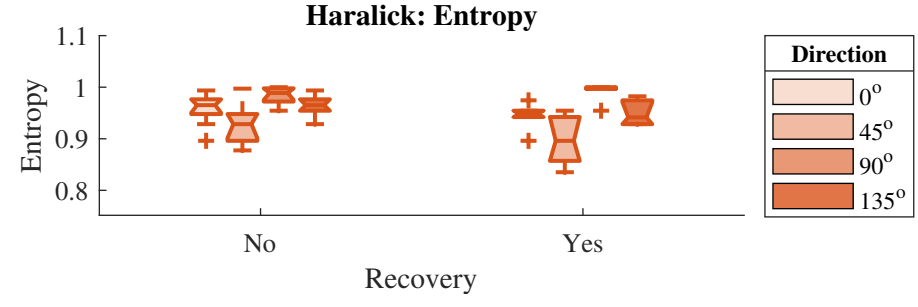

(d) Entropy

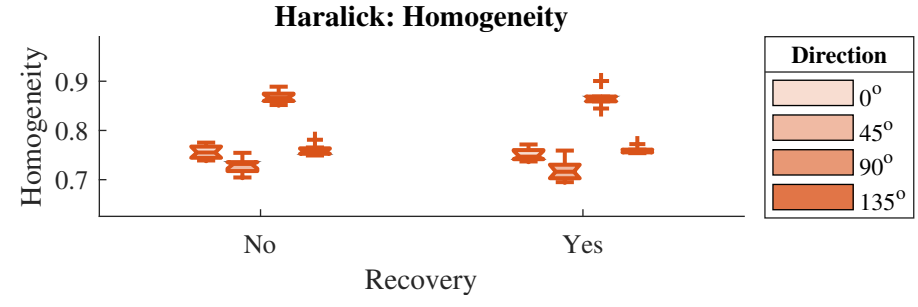

(e) Homogeneity

Figure 49: Boxplots of Haralick features describing muscle echotexture on the first session grouped according to whether participants showed significant recovery.

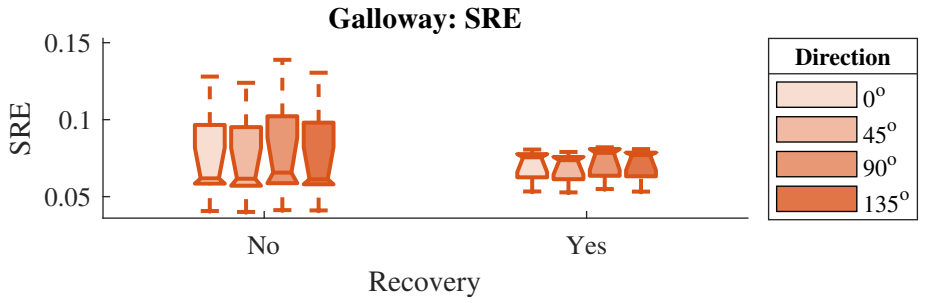

(a) SRE

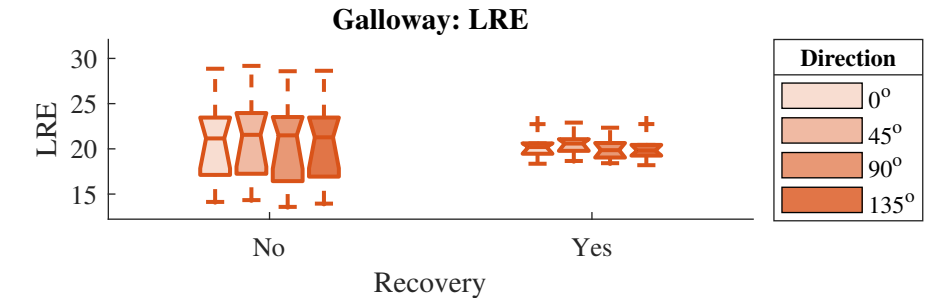

(b) LRE

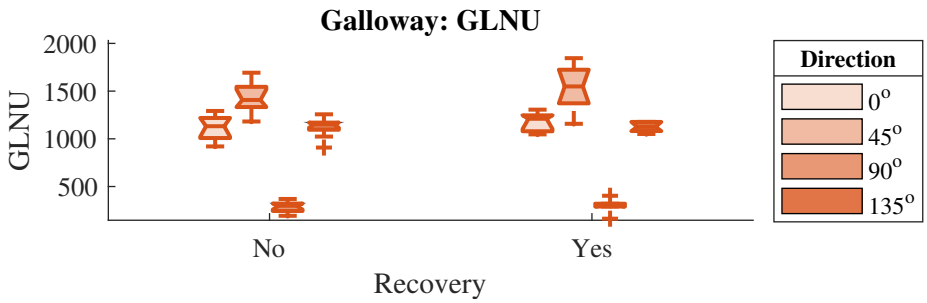

(c) GLNU

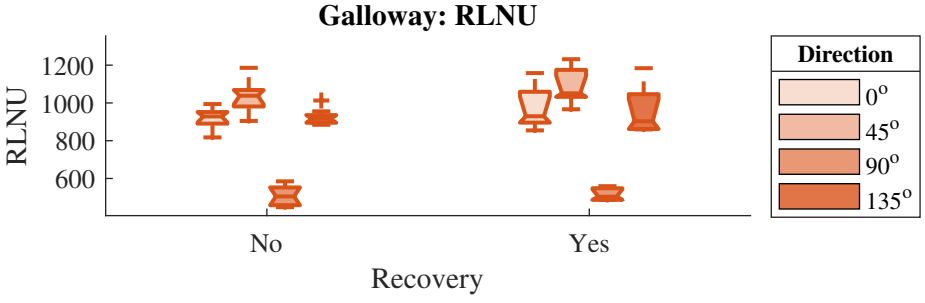

(d) RLNU

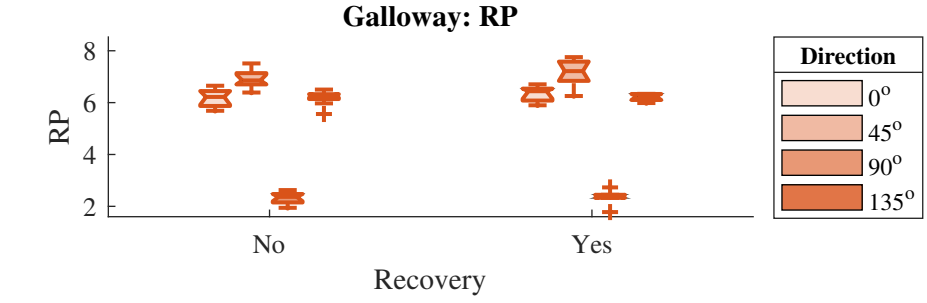

(e) Run Percentage

Figure 50: Boxplots of Galloway features describing muscle echotexture on the first session grouped according to whether participants showed significant recovery.

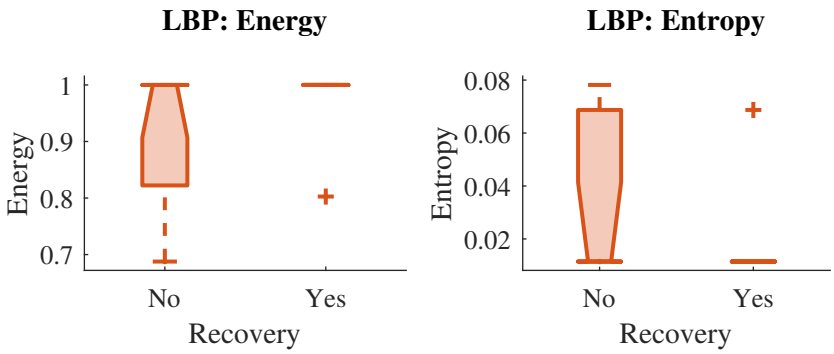

(a) Energy (b) Entropy

Figure 51: Boxplots of LBP features describing muscle echotexture on the first session grouped according to whether participants showed significant recovery.

Table 7: P-values and effect sizes for first-order descriptors of muscle echogenicity on the first session grouped according to whether participants showed significant recovery.

First order-descriptors		
	P-Value	*Effect Size*
Mean	0.61	0.13
Variance	0.78	0.04
Skewness	0.78	0.23
Kurtosis	0.39	0.67
Energy	0.53	0.19
IOD	0.69	0.08

Table 8: P-values and effect sizes for Haralick features on the first session grouped according to recovery.

Contrast		
	P-Value	*Effect Size*
0 °	0.53	0.39
45 °	0.33	0.51
90 °	0.78	0.06
135 °	0.61	0.10
Correlation		
	P-Value	*Effect Size*
0 °	0.95	0.40
45 °	0.61	0.57
90 °	0.78	0.21
135 °	0.78	0.24
Energy		
	P-Value	*Effect Size*
0 °	0.69	0.21
45 °	0.69	0.19
90 °	0.78	0.27
135 °	0.95	0.30
Entropy		
	P-Value	*Effect Size*
0 °	0.19	0.54
45 °	0.29	0.71
90 °	0.32	0.36
135 °	0.28	0.71
Homogeneity		
	P-Value	*Effect Size*
0 °	0.53	0.39
45 °	0.27	0.42
90 °	0.78	0.04
135 °	0.61	0.06

Table 9: P-values and effect sizes for changes in Galloway features on the first session grouped according to recovery.

SRE		
	P-Value	*Effect Size*
0 °	0.78	0.16
45 °	0.86	0.17
90 °	0.78	0.17
135 °	0.78	0.14
LRE		
	P-Value	*Effect Size*
0 °	0.53	0.20
45 °	0.53	0.18
90 °	0.69	0.18
135 °	0.53	0.23
GLNU		
	P-Value	*Effect Size*
0 °	0.33	0.53
45 °	0.33	0.49
90 °	0.95	0.17
135 °	0.78	0.02
RLNU		
	P-Value	*Effect Size*
0 °	0.78	0.63
45 °	0.46	0.58
90 °	0.61	0.23
135 °	0.78	0.43
RP		
	P-Value	*Effect Size*
0 °	0.33	0.51
45 °	0.39	0.47
90 °	0.95	0.09
135 °	1.00	0.08

Table 10: P-values and effect sizes for changes in LBP features on the first session grouped according to whether participants showed significant recovery.

LBP features		
	P-Value	*Effect Size*
Energy	0.55	0.42
Entropy	0.74	0.39

B.4 Measurements of muscle function to predict recovery

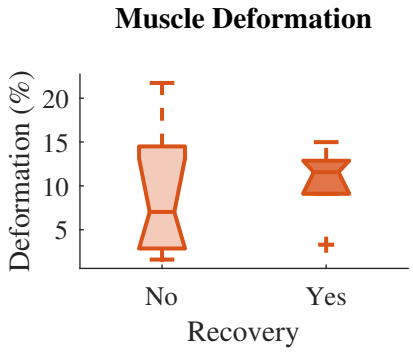

Figure 52: Boxplots of muscle deformation during attempted MVC on the first session grouped according to whether participants showed significant recovery.

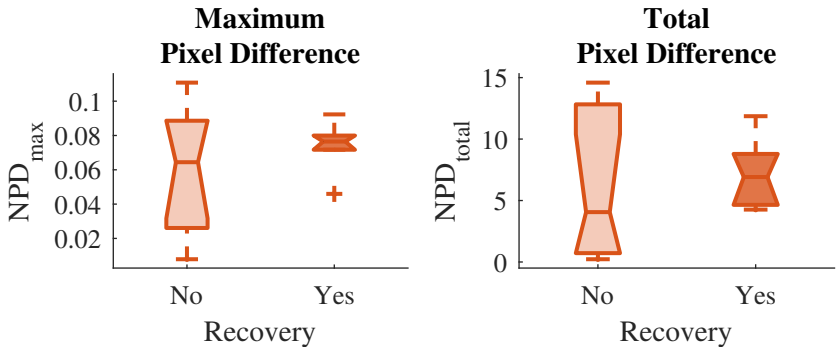

(a) Maximum (b) Total

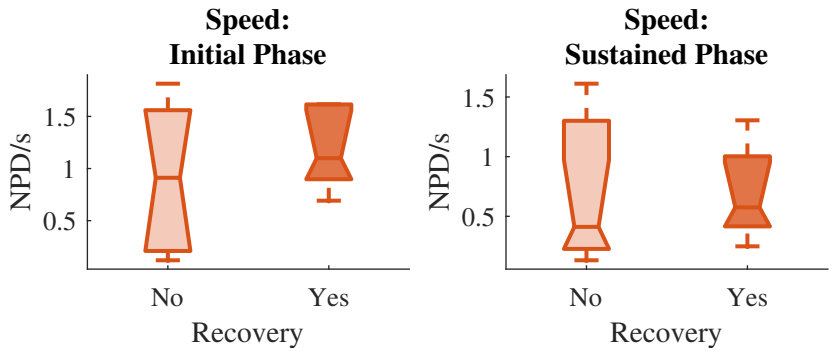

(c) Speed: Initial Phase (d) Speed: Sustained Phase

Figure 53: Boxplots of pixel difference measurements during attempted MVC on the first session grouped according to whether participants showed significant recovery ($*-p<0.05$, the black colour represents a significant difference between two groups).

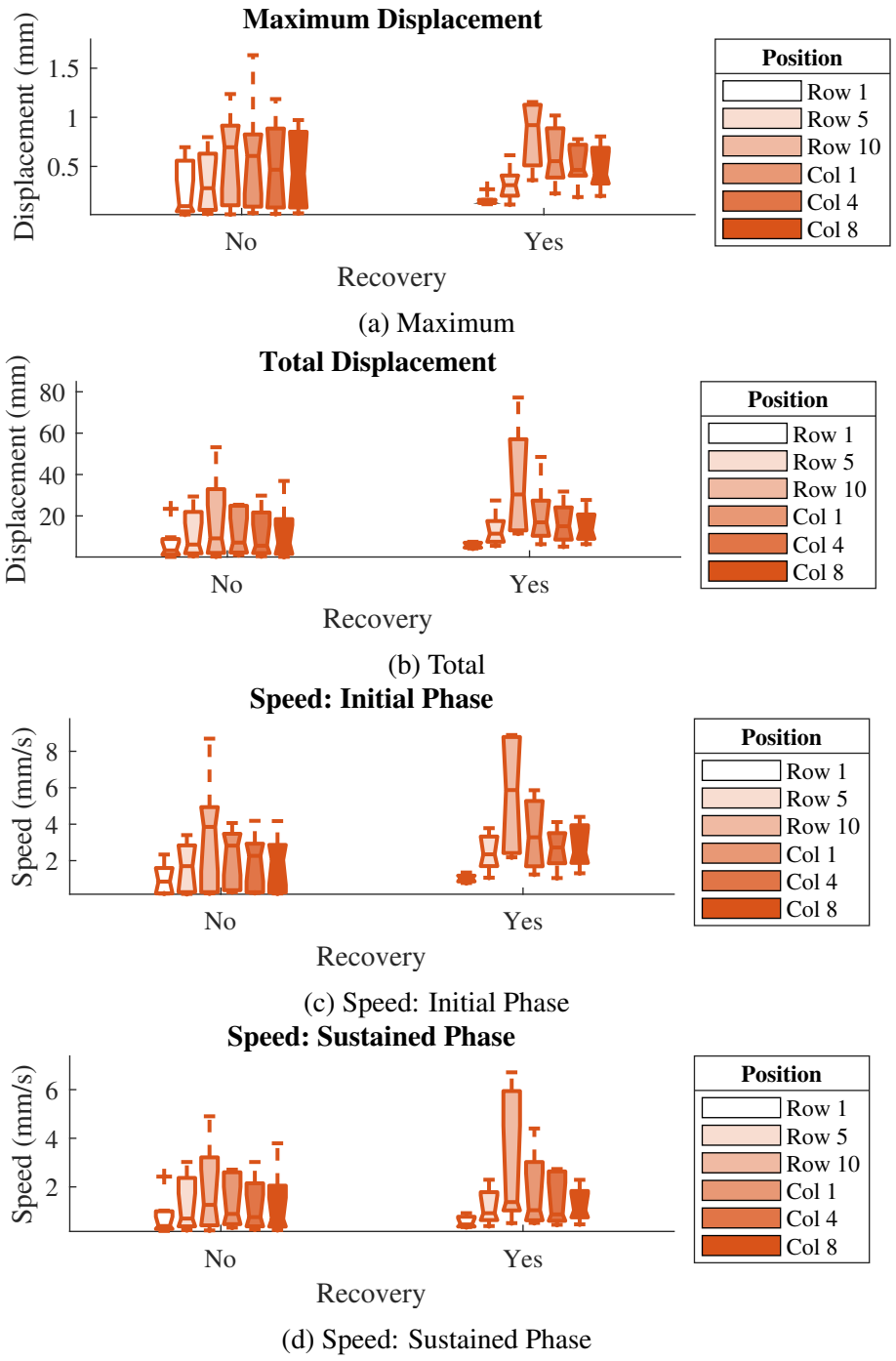

(a) Maximum

(b) Total

(c) Speed: Initial Phase

(d) Speed: Sustained Phase

Figure 54: Boxplots of muscle displacement measurements during attempted MVC on the first session grouped according to whether participants showed significant recovery.

Table 11: P-values and effect sizes for measurements of muscle movement calculated from the pixel difference during the first session between participants who did and did not show recovery.

Pixel difference measurements		
	P-Value	*Effect Size*
Maximum	0.61	0.45
Total	0.46	0.25
Speed (initial)	0.39	0.52
Speed (sustained)	0.61	0.01

Table 12: P-values and effect sizes for measurements of muscle movement calculated from the displacement during the first session between participants who did and did not show recovery.

Maximum displacement		
	P-Value	*Effect Size*
row 1	0.61	0.45
row 5	0.95	0.08
row 10	0.33	0.60
column 1	0.53	0.17
column 4	0.78	0.09
column 8	0.95	0.12
Total displacement		
	P-Value	*Effect Size*
row 1	0.53	0.06
row 5	0.39	0.27
row 10	0.11	0.77
column 1	0.22	0.69
column 4	0.27	0.49
column 8	0.27	0.37
Speed: initial (displacement)		
	P-Value	*Effect Size*
row 1	0.78	0.09
row 5	0.22	0.60
row 10	0.22	0.76
column 1	0.18	0.74
column 4	0.33	0.58
column 8	0.27	0.65
Speed: sustained (displacement)		
	P-Value	*Effect Size*
row 1	0.61	0.25
row 5	0.95	0.04
row 10	0.39	0.44
column 1	0.39	0.38
column 4	0.69	0.15
column 8	0.53	0.01

C Comparison of different NMES conditions

C.1 Stimulation parameters

Table 13: P-values and effect sizes for muscle deformation during different combinations of stimulation parameters. Values indicating a greater than medium effect size are shown in bold.

	Deformation	
	P-Value	*Effect Size*
I_{min} & I_{max}:		
PW_1, 50ms	0.05	0.66
PW_2, 50ms	0.08	0.59
PW_3, 50ms	0.50	0.21
PW_1, 25ms	0.01	**0.94**
PW_2, 25ms	0.11	0.53
PW_3, 25ms	0.51	0.20
50ms & 25ms:		
I_{min}, PW_1	0.44	0.24
I_{min}, PW_2	0.22	0.39
I_{min}, PW_3	0.10	0.55
I_{max}, PW_1	0.05	0.68
I_{max}, PW_2	0.51	0.21
I_{max}, PW_3	0.11	0.53
PW_1 & PW_2:		
I_{min}, 50ms	0.06	0.63
I_{max}, 50ms	0.57	0.18
I_{min}, 25ms	0.02	0.79
I_{max}, 25ms	0.56	0.18
PW_1 & PW_3:		
I_{min}, 50ms	0.04	0.73
I_{max}, 50ms	0.38	0.28
I_{min}, 25ms	0.03	0.75
I_{max}, 25ms	0.49	0.22
PW_2 & PW_3:		
I_{min}, 50ms	0.09	0.56
I_{max}, 50ms	0.20	0.28
I_{min}, 25ms	0.20	0.41
I_{max}, 25ms	0.80	0.08

Table 14: Statistical values reported as p-value [effect size] for total muscle displacement during the constant phase of different combinations of stimulation parameters. Values indicating a significant difference or a greater than medium effect size are shown in bold.

	Total displacement during constant phase					
	Row 1	*Row 5*	*Row 10*	*Col. 1*	*Col. 4*	*Col. 8*
I_{min} vs. I_{max}						
PW_1, 50ms	0.05 [0.68]	0.01 **[0.91]**	0.02 **[0.80]**	0.04 [0.69]	0.01 **[0.91]**	0.01**[1.07]**
PW_2, 50ms	0.19 [0.43]	0.77 [0.09]	0.17 [0.44]	0.12 [0.51]	0.40 [0.26]	0.18 [0.44]
PW_3, 50ms	0.39 [0.27]	0.93 [0.03]	0.56 [0.18]	0.83 [0.15]	0.87 [0.05]	0.68 [0.13]
PW_1, 25ms	0.20 [0.42]	0.58 [0.20]	0.08 [0.58]	0.24 [0.38]	0.19 [0.42]	0.46 [0.33]
PW_2, 25ms	0.64 [0.11]	0.18 [0.43]	0.51 [0.20]	0.83 [0.07]	0.24 [0.38]	0.11 [0.52]
PW_3, 25ms	0.17 [0.39]	0.10 [0.54]	0.11 [0.52]	0.46 [0.23]	0.09 [0.56]	0.08 [0.60]
50ms vs. 25ms						
I_{min}, PW_1	0.95 [0.02]	0.83 [0.23]	0.62 [0.15]	0.64 [0.15]	0.65 [0.14]	0.70 [0.27]
I_{min}, PW_2	0.16 [0.46]	0.16 [0.46]	0.75 [0.10]	0.61 [0.16]	0.80 [0.08]	0.70 [0.12]
I_{min}, PW_3	0.21 [0.18]	0.41 [0.26]	0.59 [0.17]	0.17 [0.46]	0.60 [0.16]	0.41 [0.26]
I_{max}, PW_1	0.81 [0.08]	0.73 [0.11]	0.68 [0.13]	0.96 [0.02]	0.83 [0.07]	0.94 [0.02]
I_{max}, PW_2	0.01 [0.96]	0.01 **[0.96]**	0.02 **[0.84]**	0.03 [0.74]	0.02 **[0.86]**	0.004 **[1.13]**
I_{max}, PW_3	0.07 [0.60]	0.09 [0.56]	0.21 [0.41]	0.35 [0.30]	0.11 [0.53]	0.05 [0.67]
PW_1 vs. PW_2						
I_{min}, 50ms	0.33 [0.31]	0.04 [0.73]	0.07 [0.62]	0.22 [0.40]	0.09 [0.56]	0.03 [0.76]
I_{max}, 50ms	0.81 [0.07]	0.34 [0.30]	0.92 [0.03]	0.59 [0.17]	0.84 [0.06]	0.73 [0.11]
I_{min}, 25ms	0.76 [0.09]	0.83 [0.09]	0.24 [0.38]	0.77 [0.09]	0.52 [0.20]	1.00 [0.10]
I_{max}, 25ms	0.03 **[0.80]**	0.01 **[0.93]**	0.05 [0.67]	0.09 [0.57]	0.02 [0.86]	0.01 **[1.06]**
PW_1 vs. PW_3						
I_{min}, 50ms	0.64 [0.14]	0.13 [0.50]	0.01 **[0.94]**	0.04 [0.78]	0.14 [0.48]	0.01 **[0.94]**
I_{max}, 50ms	0.19 [0.42]	0.19 [0.43]	0.23 [0.39]	0.18 [0.43]	0.20 [0.41]	0.51 [0.20]
I_{min}, 25ms	0.83 [0.05]	0.97 [0.12]	0.33 [0.31]	0.83 [0.07]	0.78 [0.09]	0.97 [0.05]
I_{max}, 25ms	0.01 **[0.99]**	0.01 **[1.00]**	0.02 **[0.89]**	0.01 **[0.97]**	0.01 **[1.06]**	0.01 **[1.08]**
PW_2 vs. PW_3						
I_{min}, 50ms	0.56 [0.18]	0.50 [0.21]	0.21 [0.40]	0.41 [0.32]	0.76 [0.10]	0.62 [0.16]
I_{max}, 50ms	0.30 [0.33]	0.42 [0.25]	0.19 [0.43]	0.17 [0.45]	0.22 [0.39]	0.47 [0.27]
I_{min}, 25ms	0.90 [0.07]	0.73 [0.11]	0.71 [0.11]	0.90 [0.04]	0.55 [0.18]	0.43 [0.25]
I_{max}, 25ms	0.03 [0.63]	0.11 [0.53]	0.01 **[1.02]**	0.01 **[0.94]**	0.09 [0.56]	0.15 [0.47]

C.2 Spatially distributed patterns of stimulation

Table 15: P-values and effect sizes for measurements of muscle movement at the start and end of different stimulation patterns.

Muscle deformation		
	P-Value	*Effect Size*
$CSS_{start\&end}$	0.15	0.37
$AsynS_{start\&end}$	0.55	0.31
$AsynR_{start\&end}$	0.55	0.37
$Start_{CSS\&AsynS}$	0.31	0.45
$Start_{CSS\&AsynR}$	0.25	0.45
$Start_{AsynS\&AsynR}$	0.55	0.19
$End_{CSS\&AsynS}$	0.46	0.45
$End_{CSS\&AsynR}$	0.55	0.39
$End_{AsynS\&AsynR}$	0.84	0.18
Maximum pixel difference		
	P-Value	*Effect Size*
$CSS_{start\&end}$	0.02	**1.17**
$AsynS_{start\&end}$	0.55	0.34
$AsynR_{start\&end}$	0.46	0.43
$Start_{CSS\&AsynS}$	0.11	0.66
$Start_{CSS\&AsynR}$	0.38	0.30
$Start_{AsynS\&AsynR}$	0.74	0.25
$End_{CSS\&AsynS}$	0.55	0.31
$End_{CSS\&AsynR}$	0.64	0.21
$End_{AsynS\&AsynR}$	0.74	0.12
Total pixel difference		
	P-Value	*Effect Size*
$CSS_{start\&end}$	0.20	0.59
$AsynS_{start\&end}$	0.15	0.67
$AsynR_{start\&end}$	0.05	0.67
$Start_{CSS\&AsynS}$	0.31	0.30
$Start_{CSS\&AsynR}$	0.64	0.25
$Start_{AsynS\&AsynR}$	0.46	0.40
$End_{CSS\&AsynS}$	0.31	0.42
$End_{CSS\&AsynR}$	0.74	0.10
$End_{AsynS\&AsynR}$	0.55	0.32

Table 16: P-values and effect sizes for measurements describing the timing of contractions at the start and end of different stimulation patterns.

Contraction time		
	P-Value	*Effect Size*
$CSS_{start\&end}$	0.08	0.71
$AsynS_{start\&end}$	0.15	0.67
$AsynR_{start\&end}$	0.64	0.24
$Start_{CSS\&AsynS}$	0.95	0.13
$Start_{CSS\&AsynR}$	0.64	0.20
$Start_{AsynS\&AsynR}$	0.95	0.04
$End_{CSS\&AsynS}$	0.64	0.26
$End_{CSS\&AsynR}$	0.64	0.17
$End_{AsynS\&AsynR}$	0.64	0.17
Half-relaxation time		
	P-Value	*Effect Size*
$CSS_{start\&end}$	0.15	0.58
$AsynS_{start\&end}$	0.74	0.18
$AsynR_{start\&end}$	0.81	0.24
$Start_{CSS\&AsynS}$	0.55	0.20
$Start_{CSS\&AsynR}$	1	0.02
$Start_{AsynS\&AsynR}$	0.38	0.29
$End_{CSS\&AsynS}$	0.25	0.51
$End_{CSS\&AsynR}$	0.95	0.09
$End_{AsynS\&AsynR}$	0.46	0.26
Peak-to-peak time		
	P-Value	*Effect Size*
$CSS_{start\&end}$	0.2	**0.99**
$AsynS_{start\&end}$	0.95	0.12
$AsynR_{start\&end}$	0.55	0.31
$Start_{CSS\&AsynS}$	0.08	0.79
$Start_{CSS\&AsynR}$	0.46	0.16
$Start_{AsynS\&AsynR}$	0.84	0.20
$End_{CSS\&AsynS}$	0.37	0.34
$End_{CSS\&AsynR}$	0.08	0.64
$End_{AsynS\&AsynR}$	0.84	0.15